UNIVERSITY OF CALIFORNIA, SAN DIEGO

Performance Analysis and Enhancement of OFDM-based WLAN Systems in the Presence of Nonlinear HPAs and Narrowband Interference for Single and Multiple Transmit Antennas

A dissertation submitted in partial satisfaction of the
requirements for the degree
Doctor of Philosophy

in

Electrical Engineering
(Communication Theory and Systems)

by

David Wei-Ting Chi

Committee in charge:

Professor Pankaj Das, Chair
Professor Rene L. Cruz, Co-Chair
Professor Chung-Kuan Cheng
Professor Laurence B. Milstein
Professor Tajana S. Rosing

2008

The dissertation of David Wei-Ting Chi is approved, and it is acceptable in quality and form for publication on microfilm:

Co-Chair

Chair

University of California, San Diego

2008

To my entire family

TABLE OF CONTENTS

LIST OF FIGURES

LIST OF TABLES

ACKNOWLEDGEMENTS

If you were to tell me ten-plus years ago that I would spend countless hours each day working on practical engineering problems and publishing research findings in conferences ten years later, I would say you were out of your mind. Yet, here I am, ten years later, a Ph.D. candidate, who is trying to put together a thesis and at the same time, thinking about how I was pulling my hair out for each project. It has been a particular long journey for me since I switched my research topics. No doubt, it is a journey that is full of joy and sadly it is coming to an end. In my journey of becoming a Ph.D., I have met quite a lot of people who had helped me along the way. Some helped me academically while some helped me in my private life. Now, I would like to thank them individually.

First and foremost, I would like to thank my family for supporting me through out my quest for the Ph.D. degree. They have always been there for me to support and to motivate me through out the years. More importantly, they allow me to fully concentrate in my research without worrying about anything. I also want to thank my girlfriend, Fonda Su, who lend me her supports along the way and let me fulfill my dream.

I also like to thank my advisor, Professor Pankaj Das, for his supports and encouragement. In addition, I want to thank him for the opportunity of working as a researcher with him. His precise criticism and professional comments about each presentation that I have done in the meetings have led to several interesting and practical projects which have turned into publications for conferences. Besides the gain in technical field, he has also shown me what a research is. Often in time, he would comment on how we should define a problem and through a rigorous studying process, we could resolve the problem. Those research skills that I acquire from him will definitely serve me well in my career. I thank you, Professor Das, from bottom of my heart.

I like to thank my co-advisor, Professor Rene Cruz who has also given me his supports in the time of need. I also like to thank Professor Laurence Milstein for his technical guidance. Whenever I am lost and confused about wireless communication theories, Professor Milstein never refuses to help me for any reasons. He has always been more than generous and kind and most importantly, patient with me when I come to seek his advice in countless times. I will not forget the generosity and kindness that I received from him. From the bottom of my heart, I thank you, Professor Milstein.

I also want to thank Mohammed Jalloh and Mishal Al-Gharabally for their friendships. Not only friendships, I like to thank them for the help I receive from them whenever I am stuck in my research. I will not forget the time we had together. I also want to thank my roommate, Shinko Cheng, who I think I might have spent more time than with my family. On numerous occasions,

he has taught me several things such as C++ and offers his friendship and supports throughout undergraduate and graduate schools.

Los Angeles *David W. Chi*
May 3, 2008

The text in Chapter 4 is based on the material as it appears in:

David W. Chi and Pankaj Das, "Effect of Jammer on the Performance of OFDM In the Presence of Nonlinearity In Rayleigh Fading channel with Application to 802.11n WLAN", IEEE Military Communications Conference, October 2006, pp. 1-7.

The text in Chapter 5 is based on the material as it appears in:

David W. Chi and Pankaj Das, "Effects of Nonlinear Amplifier and Partial Band Jammer in OFDM with Application to 802.11n WLAN", IEEE Military Communications Conference, October 2007, pp. 1-8.

The text in Chapter 6 is based on the material as it appears in:

David W. Chi, Mishal Al-Gharabally and Pankaj Das, "Effects of Channel Estimation Error and Nonlinear HPA on the Performance of OFDM in Rayleigh Channels with Application to 802.11n WLAN", IEEE Wireless Communications & Networking Conference, April 2008, pp. 852-857.

The text in Chapter 8 is based on the material as it appears in:

David W. Chi and Pankaj Das, "Effects of Nonlinear Amplifiers and Narrowband Interference in MIMO-OFDM with Application to 802.11n WLAN", 2008 IEEE Global Communications Conference (Submitted).

The text in Chapter 9 is based on the material as it appears in:

David W. Chi and Pankaj Das, "Effects of Jammer and Nonlinear Amplifiers in MIMO-OFDM with Application to 802.11n WLAN", 2008 IEEE Military Communications Conference (Submitted).

The text in Chapter 11 is a based on the material as it appears in:

David W. Chi and Pankaj Das, "Effects of Narrowband Interference and Nonlinear Amplifier in

Companded OFDM with Application to 802.11n WLAN", 2009 IEEE International Conference on Communications (Submitted).

The dissertation author was the primary researcher and author, and the co-authors listed in these publications directed and supervised the research which forms the basis for these chapters.

VITA

2001	B.S., University of California - San Diego, Electrical Engineering Department
2003	M.S., University of California - San Diego, Electrical Engineering Department
2008	Ph.D, University of California - San Diego, Electrical Engineering Department

PUBLICATIONS

David W. Chi and Pankaj Das, "Effect of Jammer on the Performance of OFDM in the Presence of Nonlinearity in Rayleigh Fading Channel with Application to 802.11n WLAN", *IEEE Military Communications Conference*, October 2006, pp. 1-7.

David W. Chi and Pankaj Das, "Effects of Nonlinear Amplifier and Partial Band Jammer in OFDM with Application to 802.11n WLAN", Proc. *IEEE Military Communications Conference*, October 2007, pp. 1-8.

David W. Chi, Mishal Al-Gharabally and Pankaj Das, "Effects of Channel Estimation Error and Nonlinear HPA on the Performance of OFDM in Rayleigh Channels with Application to 802.11n WLAN", *IEEE Wireless Communications & Networking Conference*, April 2008, pp. 852-857.

David W. Chi and Pankaj Das, "Effects of Nonlinear Amplifiers and Narrowband Interference in MIMO-OFDM with Application to 802.11n WLAN", *IEEE Global Communications Conference 2008* (Submitted).

David W. Chi and Pankaj Das, "Effects of Jammer and Nonlinear Amplifiers in MIMO-OFDM with Application to 802.11n WLAN", *IEEE Military Communications Conference 2008* (Submitted).

David W. Chi and Pankaj Das, "Effects of Narrowband Interference and Nonlinear Amplifier in Companded OFDM with Application to 802.11n WLAN", *IEEE International Conference on Communications 2009* (Submitted).

David W. Chi and Pankaj Das, "Effects of Narrowband Interference and Nonlinear HPA in OFDM with Application to 802.11n WLAN", *IEEE Transactions on Wireless Communications* (Submitted).

David W. Chi and Pankaj Das, "Effects of Narrowband Interference and HPAs in MIMO-OFDM with Application to 802.11n WLAN", *IEEE Transactions on Wireless Communications* (Submitted).

ABSTRACT OF THE DISSERTATION

Performance Analysis and Enhancement of OFDM-based WLAN Systems in the Presence of Nonlinear HPAs and Narrowband Interference for Single and Multiple Transmit Antennas

by

David Wei-Ting Chi
Doctor of Philosophy in Electrical Engineering
(Communication Theory and Systems)

University of California San Diego, 2008

Professor Pankaj Das, Chair
Professor Rene L. Cruz, Co-Chair

This dissertation addresses the performance issue of Orthogonal Frequency Division Multiplexing (OFDM) based WLANs operating in the presence of nonlinear high power amplifiers (HPAs), narrowband interference (NBI) or jammer and channel estimation error in Rayleigh fading channels for Single Input Single Output (SISO) and Multiple Input Multiple Output (MIMO) antennas configurations. Furthermore, to loosen the design criteria of practical HPAs, a novel PAPR reduction algorithm and receiver structure are proposed in the dissertation to improve the system performance.

In the first part of the thesis, we analyze the performance of a M-ary Quadrature Amplitude Modulation (M-QAM) SISO-OFDM system that is impaired by nonlinear HPAs, jammer and channel estimation error. We also present a more practical jammer model in this part of analysis. Next, we will consider a M-QAM SISO-OFDM system that is subject to nonlinear HPAs and channel estimation error in fading channels. In this case, we utilize the channel estimation error model[1] to significantly reduce the complexity of the bit error rate (BER) expression. For the third part of thesis, we extend the work presented in part one to include the scenario where the system has multiple transmit antennas while it is still impaired by nonlinear HPAs, NBI and channel estimation error. Finally, we propose a new algorithm to minimize the nonlinear distortion introduced by nonlinear HPAs and a new receiver structure that offers superior performance in fading channels. The performance of a SISO-OFDM system which is impaired by nonlinear HPAs, NBI and channel

[1]The model was proposed by M. Al-Gharabally in his work, M. Al-Gharabally and P. Das, "On the Performance of OFDM Systems in Time Varying Channels with Channel Estimation Error", IEEE ICC, 2006, pp. 5180-5185

estimation error is significantly improved when the proposed scheme is deployed. In addition to the improvement in the system performance, our proposed scheme also loosens the design criteria of practical HPAs and enables the practical HPAs to operate more efficiently in mobile situations. For the purpose of simulation, we extend the analytical models that are under study to an IEEE 802.11n WALN system and present both theoretical and simulation results.

1

Introduction

The root of Orthogonal Frequency Division Multiplexing (OFDM) scheme can be traced back to 1960's when it was first proposed by Chang in 1968 [1]. Since then, there has been a vigorous research effort in developing OFDM-based wireless communication systems. Over the years, OFDM has become to be the most popular transmission scheme for broadband communication systems that require high-speed communication. Its increasing popularity is mostly due to its spectral efficiency and inherent robustness to channel impairments. In addition, the OFDM waveforms offer substantial improvements in performance over traditional single carrier approaches.

For those technical advantages mentioned previously, OFDM had become a part of standards such as the European digital audio broadcast (DAB) and digital video broadcast (DVB) schemes. Besides the television broadcasting standards, OFDM has also been adapted as a part of IEEE 802.11 Wireless Local Area Network (WLAN) standards such as IEEE 802.11a, IEEE 802.11g, and IEEE 802.11n standards [2–4]. Currently, OFDM is under consideration for the Fourth Generation (4G) WLAN systems. As mentioned already, OFDM has been adapted in many wireless communication applications which make research topics related to OFDM technologies more critical. The chapter is organized as follows. In Section 1.1, a brief review of OFDM systems is presented for the purpose of completeness. Section 1.2 outlines the organization of the thesis.

1.1 OFDM Review

OFDM can be considered as a special case of Frequency Division Multiplexing (FDM) which has been used for a long time to carry more than one signal over a telephone line. FDM is a technique that uses different frequency channels to carry the information of different users. Each channel is identified by the center frequency of its transmission. To ensure that the signal of one channel does not overlap with the signal from an adjacent one, guard intervals were added between two different channels. Like FDM, OFDM uses different frequency channels to carry information. To

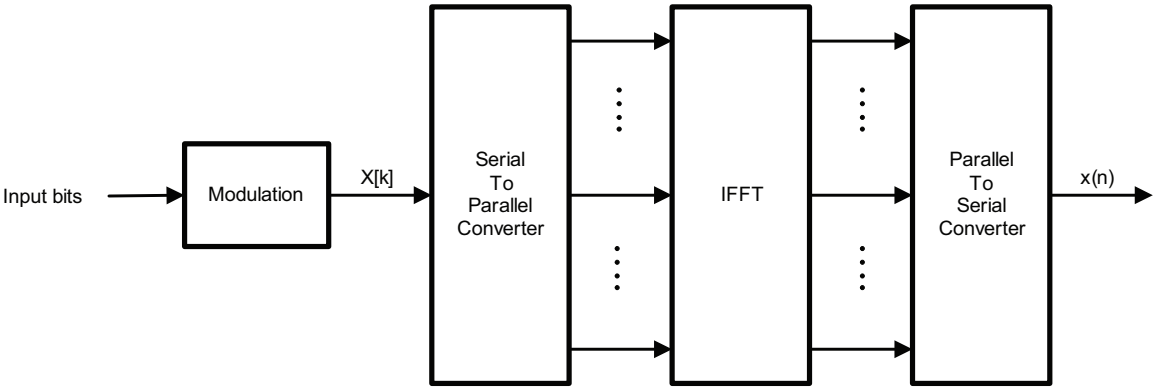

Figure 1.1 Simplified OFDM transmitter

understand how an OFDM-based wireless communication system operates, one can imagine that the bandwidth of the traditional broadband channel is divided into several orthogonal and narrowband subchannels which are typically referred to as subcarriers in literature. In the frequency spectrum, signals in subcarriers overlap on top of one another in a fashion that when one signal is at its peak value, the values for the other signals in the subcarriers are zero. The data symbols are modulated onto those orthogonal subcarriers. Then, those modulated signals are multiplexed together and sent through the transmitter. At the receiver end, the receiver will reverse the modulation process in the transmitter to extract the data symbols. In this section, a simple OFDM transmitter and receiver are described in Subsection 1.1.1. Subsection 1.1.2 briefly discusses the advantages and disadvantages associated with OFDM systems.

1.1.1 OFDM Transmitter and Receiver Structures

A simplified version of the OFDM transmitter and receiver are presented for the purpose of describing the basic structure of an OFDM system. The OFDM transmitter is shown in Fig. 1.1 and consists of a modulator, serial to parallel converter, Inverse Fast Fourier Transform (IFFT), and parallel to serial converter. Each block will be discussed in the following paragraph.

Assuming the input bits are equiprobable and independent, they are grouped into blocks of the size $log_2 M$ where M is the signal constellation size. The modulation scheme is usually chosen by the system designers or based on the requirements of the wireless communication systems. Each block of bits is mapped into a modulated symbol, denoted as $X[k]$, using the chosen modulation scheme or based on the signal constellation. The output signal is then converted from serial order to parallel order before IFFT and is converted back to serial order again. The mathematical representation for the transmitted signal, $x(n)$, is

$$x(n) = \frac{1}{N} \sum_{k=0}^{N-1} X[k] e^{j\frac{2\pi nk}{N}} \qquad 0 \leq n \leq N-1 \tag{1.1}$$

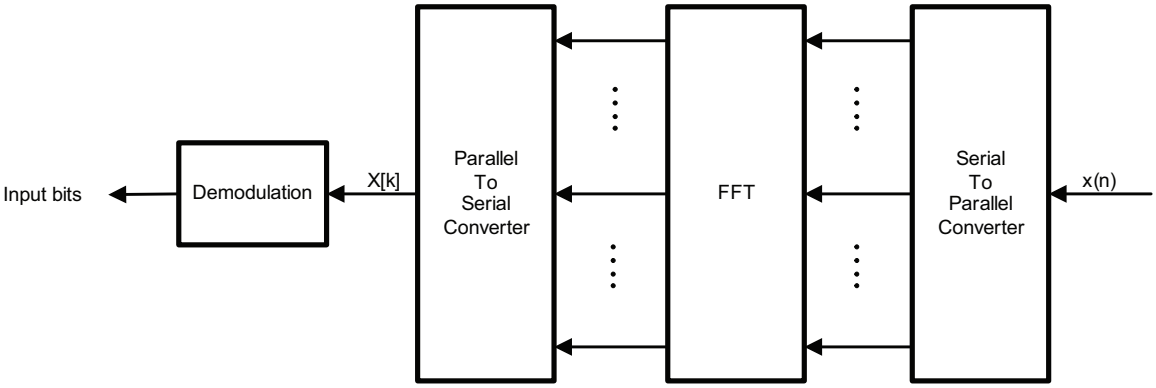

Figure 1.2 Simplified OFDM receiver

where N is the total number of subcarriers.

The channel model is omitted for now and it will be discussed in more detail later. The receiver which is composed of a serial to parallel converter, Fast Fourier Transform (FFT), parallel to serial converter and demodulation, is shown in Fig. 1.2. In the absence of the channel, the received signal is what it is being transmitted, namely $x(n)$. After receiving $x(n)$, the signal is converted into parallel order and processed by FFT. Then it is converted back to serial order. The FFT process is represented as

$$X[k] = \sum_{n=0}^{N-1} x(n) e^{-j\frac{2\pi nk}{N}} \tag{1.2}$$

The demodulation process maps the symbols back to bits based on the same mapping that the modulation uses. Assuming there is no noise or distortion imposed on the transmitted signal, the receiver is then able to recover the data perfectly. In most literature, the conversions between serial and parallel formats are often missing from the system block diagrams. The serial and parallel conversion blocks in the system block diagrams within this document will also be omitted and only represented by just a single IFFT or FFT blocks.

1.1.2 OFDM Advantages and Disadvantages

OFDM has two main advantages over its competitors. One of which is the high bandwidth efficiency. Fig. 1.3 illustrates the difference in the bandwidth usage between conventional multi-carrier systems and OFDM systems. In the conventional mutilcarrier system, each nonoverlapping tone presents user information that is being transmitted at a particular frequency. To ensure that signals are not interfering each other, there is a gap between two adjacent tones which potentially could be used for transmitting additional data. Fig. 1.4 shows the frequency spectrum of an OFDM system where the blue dotted lines represent the signals in the subcarriers and the black solid line

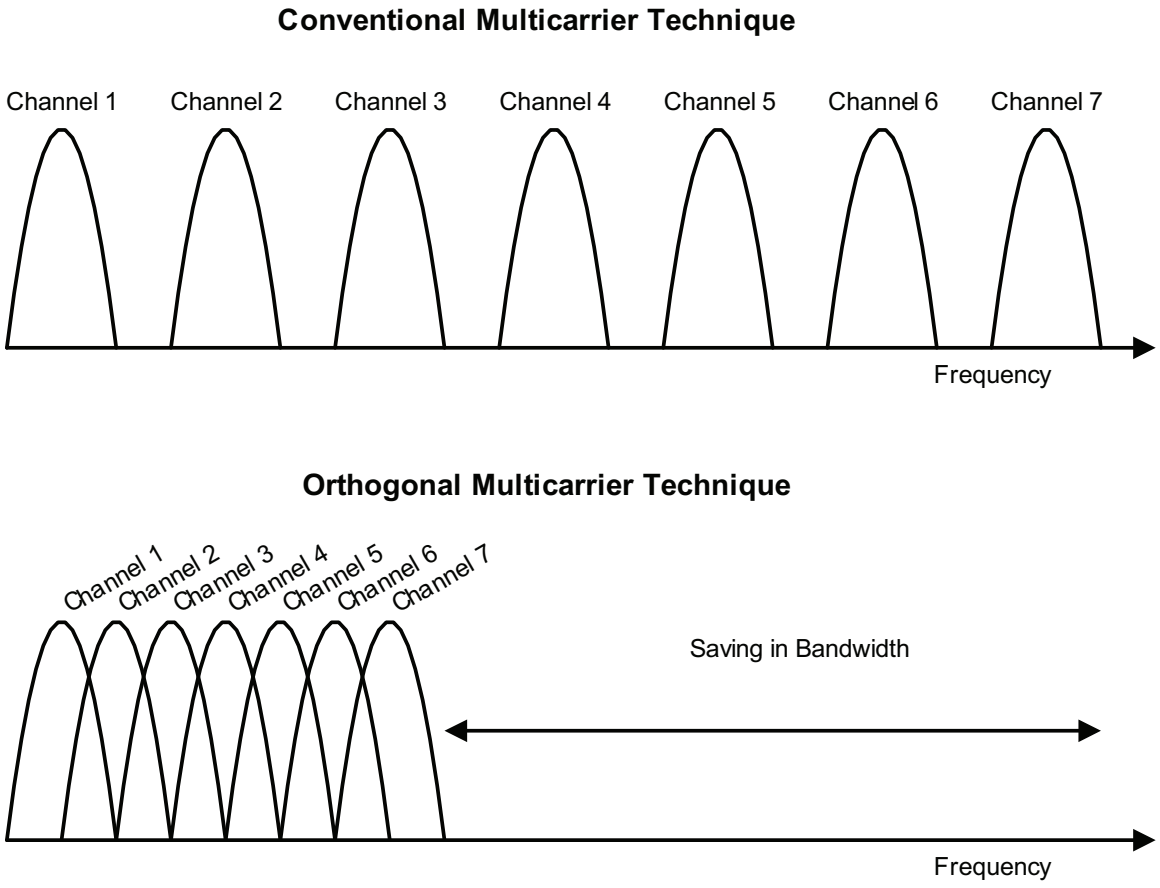

Figure 1.3 An illustration of the bandwidth efficiency in OFDM signals

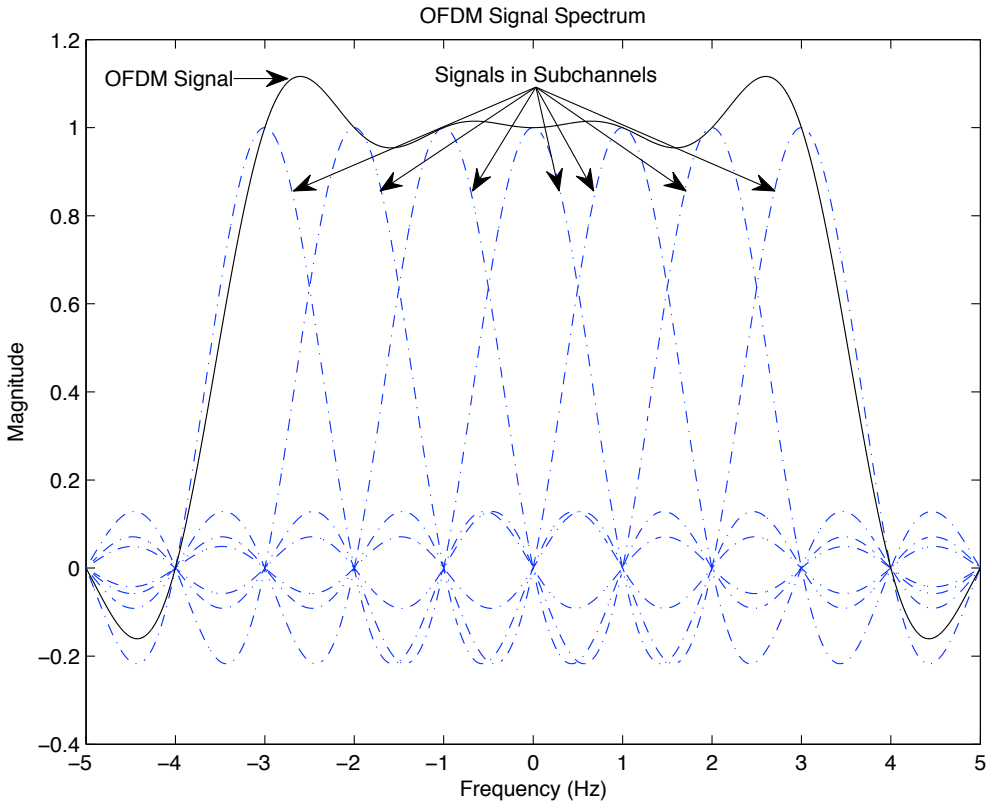

Figure 1.4 A depiction of OFDM Frequency Spectrum

represents the OFDM signal. As one can observe from Fig. 1.4, in OFDM systems, the signals in the subcarriers are orthogonal to each other. Even though signals are overlapping, they are not interfering each other due to the reason that wherever there is a peak in the subcarrier, the magnitudes of the signals from all the other subcarriers are zero. Since the signals are orthogonal to each other, the OFDM signals can placed on top of each other without interference. As a consequence, it leads to a significant saving in the usage of bandwidth compared to the conventional multicarrier systems which is illustrated in Fig. 1.3.

Another advantage that OFDM has is its robustness against the channel impulse response. In a typical wireless communication system, the transmitted signal is often severely degraded by the channel response. For a traditional single carrier system, the transmitted symbol usually occupies the bandwidth that is almost wide as the channel bandwidth. Within this channel bandwidth, both the magnitude and the phase of the channel impulse response can vary as a function of time depending on the environment. This would create problems since each part of the symbol experiences different gain and phase introduced by the channel response. To recover the transmitted symbol

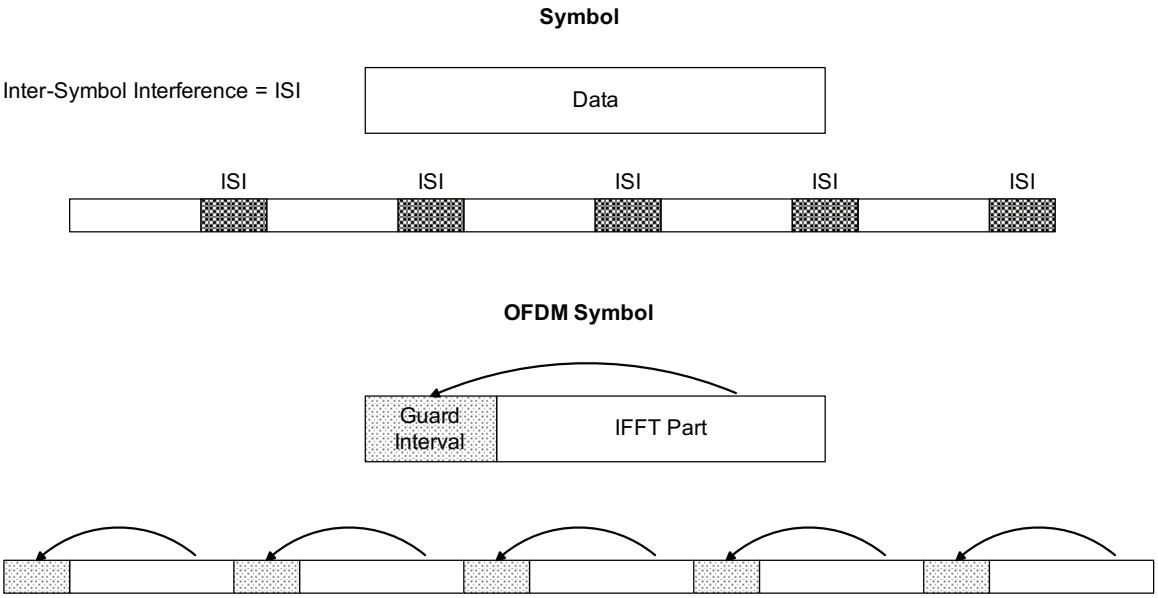

Figure 1.5 An illustration of the compositions of conventional symbols and OFDM symbols

accurately, the receiver has to be able to track the channel response properly and uses the estimated channel response to equalize the signal before the demodulation process. Consequently, in order to maintain a reasonable performance, the complexity in the design of the receiver has to increase in order to handle the extra workload.

In a multicarrier system such as an OFDM system, the channel bandwidth is split into N subchannels whose bandwidth are relatively small compared to the channel bandwidth. The symbol in each subchannel is still degraded by the channel like in the case of a single carrier system. However, the effect that the channel response has on the transmitted symbol in an OFDM system is different from a single carrier system. In OFDM systems, since each subchannel has a much smaller bandwidth compared to the channel bandwidth, the channel response that the subchannel experiences is relatively flat across the bandwidth of the subchannel. Due to this reason, better quality channel estimation can be obtained and used to remove the channel response that is imposed on the transmitted symbol. Subsequently, the performance of the system can be improved.

In addition to the reduction in the complexity of the receiver structure, the composition of OFDM symbols is also different from the conventional symbols. Fig. 1.5 shows the compositions of conventional symbols and OFDM symbols. In the conventional wireless communication systems, the modulated symbols often contains pure data bits. Upon receiving the transmitted signals, the received symbols at the receiver are most likely overlapping each other due to the characteristics of the wireless channels. This leads to the occurrence of interference which is due to the adjacent symbols, a phenomenon that is known as inter-symbol interference (ISI). Due to the ISI in the received

symbols, the system performance will degrade.

In the case of OFDM systems, each OFDM symbol is composed of an IFFT part and a guard interval as shown in Fig. 1.5. The IFFT part represents the signals in the time domain. Before transmission, a exact copy of the information in the last few samples in the time domain signals are then inserted at the beginning of the time domain signals to create a guard interval. At the receiver, even though, OFDM symbols can overlap each other like in the case of conventional wireless communication systems. However, as long as the duration of the channel impulse response is shorter than the duration of the guard interval, the overlapping will only occur within the guard interval. Since guard intervals only contains the copies of the information in the last few samples, they can be discarded in the receiver which leaves the IFFT part undistorted by the channel response. Notice in some literature, the guard intervals are also referred to as cyclic prefixes. In this thesis, we will assume those two terms are interchangeable.

One of the disadvantages that OFDM has is high sensitivity to frequency offset and phase noise. The frequency offset is generally due to the frequency deviation between the transmitter and receiver or by Doppler Shift. As for phase noise, it is often caused by the fluctuation of oscillators in the system. Fig. 1.6 shows the effect of frequency offset on the OFDM signals. The blue dotted lines in Fig. 1.6 represent the signals in the subcarriers while the black solid line implies the signal of a particular subcarrier after experiencing frequency offset. As one can observe, the signals in the subcarriers are orthogonal to each other when there is no frequency offset. However, when either frequency offset or phase noise is present in an OFDM system, the subcarriers are no longer orthogonal to each other. As shown in Fig. 1.6, wherever there is a peak in the subcarriers, the magnitude of the black line is no longer zero. As a result, inter-carrier interference (ICI) will occur [5–7] and the performance of the system will degrade. Another major disadvantage that most multicarrier systems have including OFDM systems is high peak to average power ratio (PAPR) which will be discussed in more detail in Chapter 2.

1.2 Thesis Organization

In this section, the outline of the dissertation is discussed and a brief description for each chapter will be given. The main contributions of this dissertation are contained in Chapters 4, 5, 6, 8, 9, and 11.

In Chapter 2, the concept of high PAPR and how signals that have high PAPR can cause nonlinearity through nonlinear HPAs are discussed. Two of nonlinear HPA models that are most widely used are also presented. In addition, a description of the input and output relationships of those two HPA models is given in the chapter. To illustrate the effect of nonlinear distortion

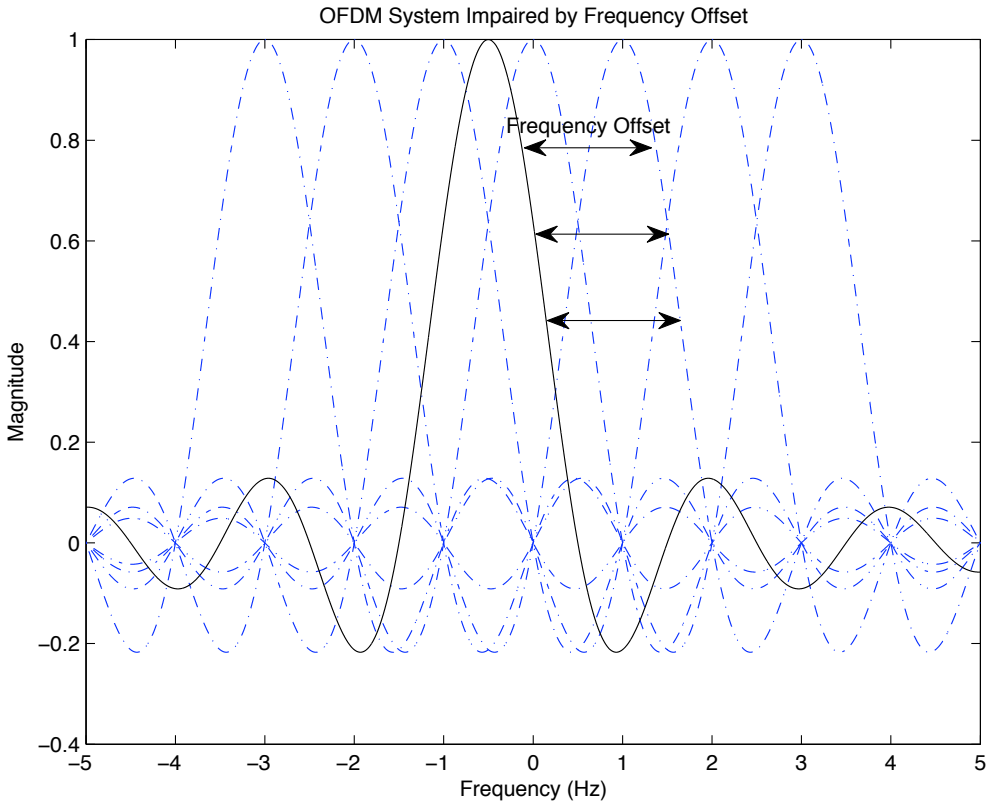

Figure 1.6 An illustration of the effect of frequency offset on the OFDM signals

produced by nonlinear HPAs on the performance of a system, we present the performance analysis of a BPSK OFDM system which is impaired by a nonlinear HPA in Additive White Gaussian Noise (AWGN) channel. Finally, since the bit error rate (BER) contains the variance of the nonlinear distortion and finding a numerical value of the variance is often difficult, we discuss the procedures of one method which is proposed by Banelli *et al.* as a way to obtain the variance of nonlinear distortion.

In Chapter 3, we present the IEEE 802.11n standard that is based on the Worldwide Spectrum Efficiency's (WWiSE) proposal. There are two operation modes, NTX-SDM and NTX-STBC modes, that the IEEE 802.11n standard operates on. In addition, the transceivers for both NTX-SDM and NTX-STBC modes are presented. The functionality of each block in both transceivers is also discussed in detail.

In Chapter 4, we present the performance analysis of a M-ary Quadrature Amplitude Modulation (M-QAM) OFDM system that is subject to nonlinear distortion provided by nonlinear high power amplifiers (HPAs), channel estimation error and jammer in Rayleigh fading channels.

The nonlinear HPA is modeled after the Saleh model. In addition, different from the conventional jammer model which was presented in literature, we propose a more realistic jammer model by introducing a separate Rayleigh fading channel between the source of jammer and the receiver. Due to the reason that not all the subcarriers are affected by the jammer, we derive the BER expression for the case where the subcarriers are under the influence of the jammer. Then, we show that the BER for the case where the subcarriers are free from jammer can be obtained from the case where the jammer is interfering the subcarriers by setting the jamming power to zero. The final BER expression for the system that is impaired by nonlinear HPA, channel estimation error and jammer is also presented for various sets of degradation. For the purpose of simulation, the analytical model is extended to a WLAN system based on IEEE 802.11n standard. The theoretical and simulation results are also presented with and without channel estimation error.

In Chapter 5, we analyze the performance of a M-QAM OFDM system which is impaired by nonlinear HPAs, partial band jammer, and channel estimation error in Rayleigh fading channels. In Chapter 4, we introduce a more realistic jammer model by proposing a separate channel response for the jamming signals. In this chapter, we extend the jammer model proposed in Chapter 4 to include the situations where there is a frequency offset between jamming and transmitted signals. When jammer transmits signals at a frequency that is slightly offset from the subcarrier frequency that the receiver has locked onto, an additional interference which behaves like ICI is produced by the jammer and leads to further degradation in the system performance. For the purpose of simulation, we extend the analytical model to be in compliance with IEEE 802.11n standard. The theoretical and simulation results are presented for different combinations of impairments with and without channel estimation error. Finally, based on the theoretical and simulation results, a discussion about the effectiveness of a jammer and how its bandwidth affects the performance if the total jamming power is one of the design criteria.

In Chapter 6, we present the performance analysis of a M-QAM OFDM system that is subject to a nonlinear HPA and channel estimation error in a Rayleigh fading channel. The conventional approach of analyzing a wireless communication system such as the one we present in this chapter always requires solving a triple integral due to the integration of the conditional BER over the joint probability density function (PDF) of the channel response and its estimate. In addition, solving a triple integral can sometimes be a very difficult task as Chapters 4 and 5 has shown in the section of performance analysis. In this chapter, we will make use of the channel estimation error model which was proposed previously[1] to simplify and reduce the complexity in the process of average BER calculation. In addition, the analytical model is extended to be in compliance with the IEEE 802.11n standard for the purpose of simulation. We also present simulation results along

[1]This particular channel estimation error model was first proposed by Al-Gharabally *et al.* in his work, "On the Performance of OFDM Systems in Time Varying Channels with Channel Estimation Error", IEEE International Conference on Communications, vol. 11, June 2006, pp. 5180-5185.

with theoretical values for various cases of channel estimation error and nonlinear distortion.

Chapter 7 presents performance analysis of OFDM systems with more than one transmit antennas in Rayleigh fading channels. In the first case, we analyze the performance of a M-QAM Multiple Input Multiple Output (MIMO) OFDM system with the Alamouti code, two transmit antennas and one receive antenna in Rayleigh fading channels. Furthermore, the performance of the M-QAM MIMO-OFDM system with two transmit antennas and one receive antenna is presented with and without the normalization in the transmit power. Next, we analyzed another M-QAM MIMO-OFDM system which has four transmit antennas and one receive antenna in Rayleigh fading channels. In this case, the performance analysis is also presented with and without the transmit power being normalized by the number of transmit antennas. In all cases, we simply the BER expressions by rewriting the conventional $Q(\cdot)$ function in its alternate form. Simulation and theoretical results for each case are also presented. In addition, we briefly discuss the advantages and disadvantages of using more than one transmit antenna in the chapter.

In Chapter 8, we analyze the performance of a M-QAM MIMO-OFDM system that is subject to nonlinear HPAs, a NBI and channel estimation error in Rayleigh fading channels. The nonlinear HPA model utilized in the chapter follows closely after the Saleh model. The Alamouti code is implemented in the Space Time Block Code (STBC) encoder to encode OFDM symbols and to take the advantages of diversity. In addition, we present a more realistic NBI model than the proposed models in previous studies by introducing a separate channel impulse response between the source of NBI and the receiver. Since only some of the data subcarriers are affected by the NBI, we present the BER derivation for two different cases. One of two cases represents the situation where the subcarriers are free from the NBI interference. The other case denotes the scenario where subcarriers are affected by NBI. We will also point out that the similarity between those two BER expressions for the two cases and how one can be obtained from the other. A brief discussion of effectiveness of NBI with various bandwidth on the performance of the MIMO-OFDM system under the assumption that the total power of NBI is held constant is also given. Finally, we will present simulation and theoretical results of the performance of the MIMO-OFDM system that is subject to various combinations of impairments with and without channel estimation error.

In Chapter 9, the performance analysis of a M-QAM MIMO-OFDM system that is subject to nonlinear HPAs, jamming and channel estimation error in Rayleigh fading channels. The Saleh model is utilized in the nonlinear HPA model. For the STBC encoder, the Alamouti code is used to encode OFDM symbols. Different from the jammer models presented in Chapter 8 or in literature, we present a more realistic jammer model by making two distinct assumptions in the chapter. The first assumption is we assume that the jammer experiences an additional channel impulse response that is statistically different from the channels that the transmitted signal experiences. This as-

sumption is based on the fact that the source of jammer usually locates at a far distance, therefore, the jamming signal must experience a different channel impulse response than the transmitted signal does. The second assumption that we make is we assume that the jammer has an offset in frequency with respect to the transmitted signal. This assumption is often valid since the jammer does not have priori knowledge about the center frequency of the transmitted signal. With those two assumptions, we are able to present some useful insights about the performance of a M-QAM MIMO-OFDM system that is under those impairments. In the chapter, an analytical BER expression is presented. For the purpose of simulation, we extend the analytical model to be in compliance with IEEE 802.11n standard. We also briefly discuss the advantages and disadvantages of a jammer with various number of frequency tones on the system performance under the assumption that the total jamming power is held constant and the most design criterion is the effectiveness of the jammer. Finally, we presented the theoretical and simulation results for different scenarios such as under the influence of nonlinear distortion or effect of jamming tones with the condition of constant jamming power with and without channel estimation error.

Chapter 10 presents the concepts of PAPR and OFDM signal distribution and a review of PAPR reduction techniques. We first discuss the PAPR by defining PAPR for the continuous time OFDM signals. As for the discrete case, we introduce the idea of oversampling factor. This is due to the fact that some of peaks in OFDM signals in continuous time may not get picked up when the sampling rate is at the Nyquist sampling rate. Next, we quantify the distribution of OFDM signals by using the complementary cumulative distribution function (CCDF). The CCDFs are also given with and without the oversampling factor. To avoid nonlinearity in practical HPAs, several algorithms that are the most popular for PAPR reduction in literature are also presented in the chapter. A detail description for each PAPR reduction technique is given along with the discussion for its technical advantages and disadvantages.

In Chapter 11, we analyze the performance of a M-QAM OFDM system with a compander that is subject to nonlinear HPAs, a NBI and channel estimation error in a Rayleigh fading channel. The nonlinear HPA is modeled as a Saleh model. Different from the NBI model which is previously proposed in literature, we propose a more realistic NBI model by introducing another separate channel between the source of NBI and the receiver. Simulating an OFDM system with the proposed NBI model would provide more useful insights to the performance of OFDM systems that operate in coexistence with a NBI. In previous chapters, we have shown the effects of nonlinear distortion on the system performance. To reduce the amount of nonlinear distortion introduced by the HPAs, we propose a new companding technique that would reduce the PAPR of OFDM signals and avoid the situations where the HPAs are operating at the nonlinear region. Since the decompanded signal is highly dependent on the input signal to the decompander, we also propose a novel receiver structure which would minimize the degradation effects due to the decompression

in the decompander when the OFDM systems are operating in a Rayleigh fading channel. For the purpose of simulation, we extend analytical model to an 802.11n WALN system based on the IEEE 802.11n specification. We will also show the effect of the proposed companding algorithm on the performance of an OFDM system that is subject to nonlinear HPAs. The simulation results show that the proposed companding technique is highly effective in reducing PAPR and can be used to loosen the design criteria for the HPA and the cost of production. Finally, theoretical and simulation results are presented for various combined sources of impairments with and without channel estimation error.

Finally, Chapter 12 summarizes the thesis. In addition, it discusses the contributions of the thesis.

2

Nonlinear High Power Amplifiers (HPAs)

2.1 Introduction

High peak to average power ratio (PAPR) is a common problem among multicarrier systems and it is no exception in OFDM systems. In OFDM systems, high PAPR is due to the nature of the Inverse Fast Fourier Transform (IFFT)/Fast Fourier Transform (FFT) operations. When L number of signals are added coherently, it produces a peak power that is L times larger than the average power. To demonstrate the concept of PAPR, Fig. 2.1 shows the PAPR of an all one vector whose length is six. As one can see from Fig. 2.1, this hypothetically signal vector produces a peak power that is six times larger than the average power. This implies that the peak power of OFDM signals can be as much as N time larger than the average power where N is the total number of subcarriers.

Due to the characteristic of high PAPR in OFDM signals, the system would require the digital/analog (D/A) and analog/digital (A/D) converters to be highly linear, which leads to an increase in the complexity of the high power amplifier's (HPA) design and the cost of implementing them. Often in time, backoff schemes can be applied to ensure that the HPAs operate in the linear range. However, the backoff scheme dramatically reduces the power efficiency of RF transmitters. This may have deleterious effects on battery lifetime in mobile systems and could outweigh all potential benefits that OFDM could offer.

In practice, nonlinear HPAs are used in implementation in order to lower the cost of production. When high PAPR signals such as OFDM signals are amplified by nonlinear HPAs, the signals will force the nonlinear HPAs to operate at their nonlinear region. Subsequently, the nonlinear HPAs introduce nonlinear distortion to the system and system performance will degrade.

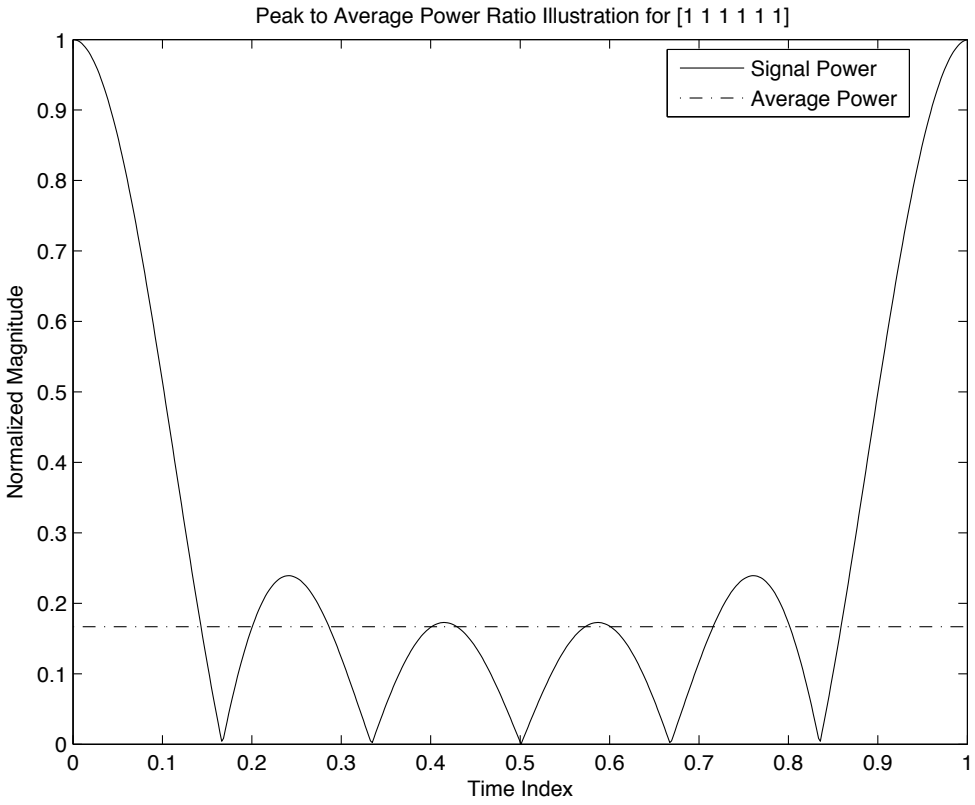

Figure 2.1 An illustration of peak to average power ratio (PAPR) for [1 1 1 1 1 1]

Over the years, several methods for nonlinearity suppression have been proposed and results have been presented in the literature [8–13]. In addition, those methods will be discussed in more detail in Chapter 10. In this chapter, we will present the effect of nonlinear distortion produced by the high PAPR signals through nonlinear HPAs on the system performance by analyzing a Binary Phase Shift Keying (BPSK) OFDM system which is impaired by the nonlinear HPA in Additive White Gaussian Noise (AWGN) channel. Two of most popular nonlinear HPA models are also presented as well.

The chapter is organized as follows. In Section 2.2, an analytical mode is presented and each block is discussed. Section 2.3 presents the two popular nonlinear HPA models that are often utilized in literature. Section 2.4 contains the performance analysis of the analytical model which is presented in Section 2.2. Finally, Section 2.5 summarizes the chapter.

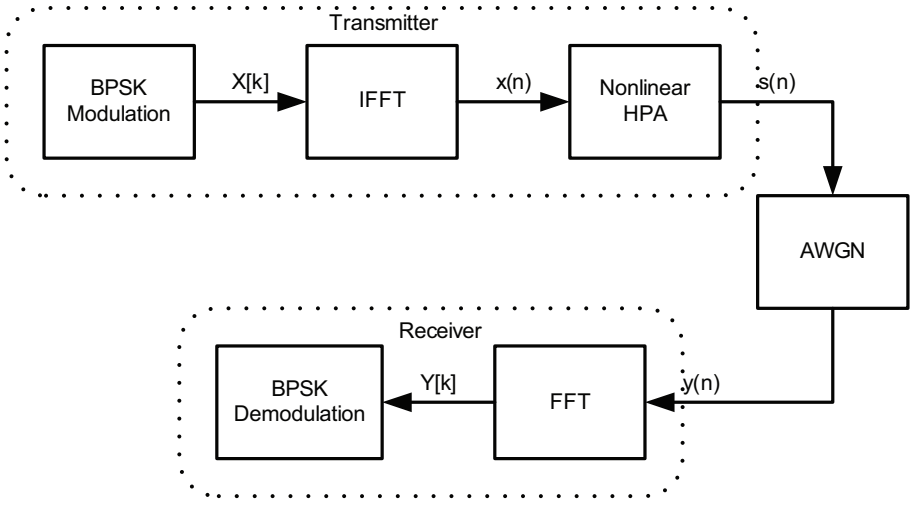

Figure 2.2 A system block diagram of a BPSK OFDM system that is impaired by a nonlinear HPA in Additive White Gaussian Noise (AWGN) channel.

2.2 System Description

Fig. 2.2 shows the block diagram of the analytical model and each block will be discussed in the following sections.

2.2.1 Transmitter

The transmitter consists of a BPSK modulator, IFFT and a nonlinear HPA. It is a fair assumption that the input bits to the modulation block are equiprobable and independent of each other. The BPSK modulator maps binary 0 and 1 to -1 and $+1$, respectively, and produces BPSK symbols, denoted as $X[k]$. The BPSK symbols are then processed by IFFT to yield the corresponding time domain signal, denoted as $x(n)$. Then, $x(n)$ is given by

$$x(n) = \frac{1}{N} \sum_{k=0}^{N-1} X[k] e^{j\frac{2\pi nk}{N}} \qquad 0 \leq n \leq N-1 \tag{2.1}$$

where N is the total number of subcarriers. The discussion about the output signal at the nonlinear HPA, denoted as $s(n)$, and its statistical property is given in more detail in Section 2.3.

2.2.2 AWAGN Model

The AWGN block, denoted as $w(n)$, represents the thermal noise within the circuits. It is modeled as a complex Gaussian random process with zero mean and $2\sigma_w^2$ variance.

2.2.3 Receiver

Upon receiving, $y(n)$, the time domain received signal, is then fed into FFT. The output of FFT which is the received signal in frequency domain and is denoted as $Y[k]$, is expressed as

$$\begin{aligned} Y[k] &= \sum_{n=0}^{N-1} y(n) e^{-j\frac{2\pi nk}{N}} \\ &= \sum_{n=0}^{N-1} \left[s(n) + w(n) \right] e^{-j\frac{2\pi nk}{N}} \\ &= S[k] + W[k] \end{aligned} \tag{2.2}$$

where $S[k]$ and $W[k]$ are FFT of $s(n)$ and $w(n)$, respectively. Next, the BPSK demodulator will yield an estimated transmitted bits by determining which region $Y[k]$ falls onto.

2.3 Nonlinear HPA Models

The nonlinear HPA in the transmitter shown in Fig. 2.2 represents the nonlinear distortion imposed on the baseband signal. There are two popular, yet accurate, nonlinear HPA models in the literature. One of the two models is the Solid State Power Amplifier (SSPA) model which was first proposed by *Rapp* [14] and was later widely accepted in literature [15,16]. When utilizing the SSPA model, the transmitted signal, $s(n)$, can be expressed as

$$\begin{aligned} s(n) &= x(n) \frac{f(r)}{r} \\ &= x(n) \frac{A(r) e^{j\Phi(r)}}{r} \end{aligned} \tag{2.3}$$

where $r = |x(n)|$ and $|\cdot|$ represents the magnitude of the signal. In addition, $f(r)$ denotes the nonlinear distorting function. $A(r)$ and $\Phi(r)$ in (2.3) are typically known as amplitude modulation/amplitude modulation (AM/AM) and amplitude modulation/phase modulation (AM/PM) conversions, respectively. The AM/AM and AM/PM conversions in the SSPA nonlinear HPA model are defined as

$$A(r) = \frac{\alpha_{AM} r}{\left[1 + (\frac{\alpha_{AM} r}{A_O})^{2p} \right]^{\frac{1}{2p}}} \quad , \quad \Phi(r) = \alpha_{PM} \left(\frac{\alpha_{AM} r}{A_O} \right)^4 \tag{2.4}$$

where α_{AM} is the small signal gain and A_O is the saturating amplitude. p represents a parameter which controls the smoothness of the transmission from the linear region to the saturation region [16]. Typically, α_{PM} is set to zero and this implies that there is no phase distortion imposed on the baseband signal. If p is increased, $A(r)$ in (2.4) would produce a curve that is quite similar to the ideal soft limiter nonlinear transformation which is given as [15]

$$A(r) = \begin{cases} \alpha_{AM} r, & 0 \le r \le \frac{1}{\sqrt{\beta_{AM}}} \\ A_O, & r \ge \frac{1}{\sqrt{\beta_{AM}}} \end{cases} \tag{2.5}$$

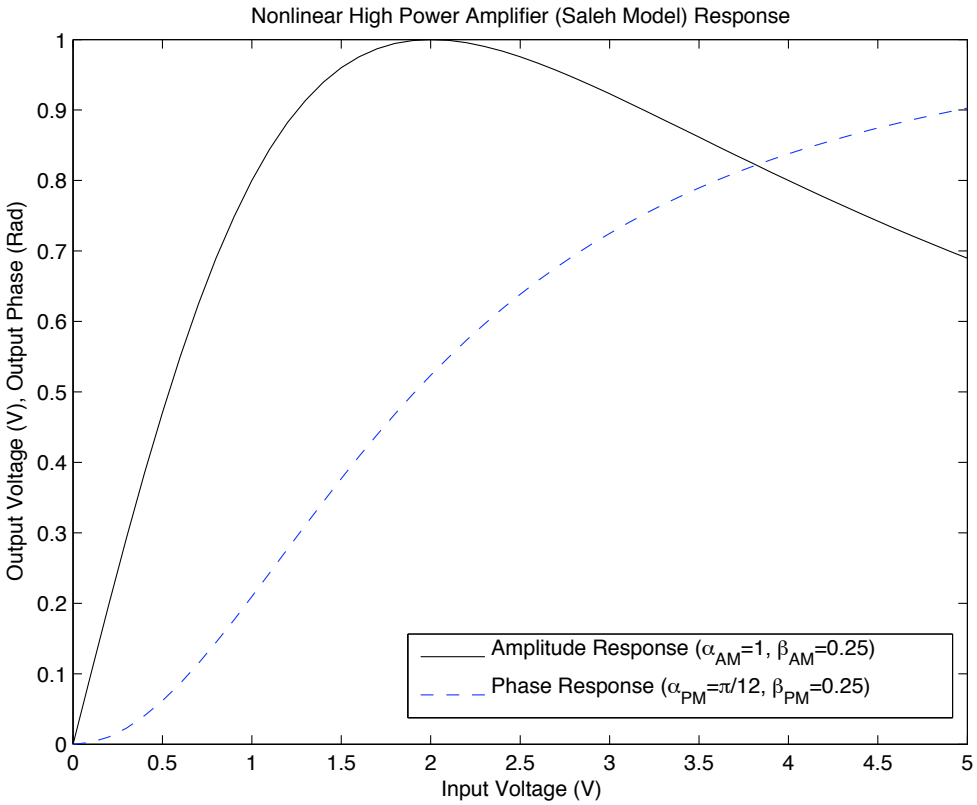

Figure 2.3 The Input and Output Relationship for Nonlinear HPA which is based on the Saleh Model. In this case, the α_{AM} and β_{AM} are set to 1 and 0.25, respectively. α_{PM} and β_{PM} are $\frac{\pi}{12}$ and 0.25.

Another popular model is the traveling wave tube amplifier (TWTA) nonlinear HPA model, proposed by *Saleh* [17], which is also known as the Saleh TWT model in some literature [15,18]. The relationship between the input and output signals is defined as (2.3). However, the characteristic functions, namely AM/AM and AM/PM conversions, are defined differently. In this nonlinear HPA model, $A(r)$ and $\Phi(r)$ are defined as

$$A(r) = \frac{\alpha_{AM} r}{1 + \beta_{AM} r^2} \quad , \quad \Phi(r) = \frac{\alpha_{PM} r^2}{1 + \beta_{PM} r^2} \tag{2.6}$$

where α_{AM}, α_{PM}, β_{AM} and β_{PM} are the parameters that are used to model the actual HPA. To illustrate the input and output signals relationship based on the Saleh nonlinear HPA model, two examples are provided and are shown in Fig. 2.3 and Fig. 2.4. For example, as one can see from Fig. 2.3 that the input voltage is not linearly amplified, especially when the input voltage is greater than 2 Volts (V). In addition to the nonlinear relationship between the magnitudes of input and output, the phase distortion is also added onto the phase of the signal. Hence, one can think of

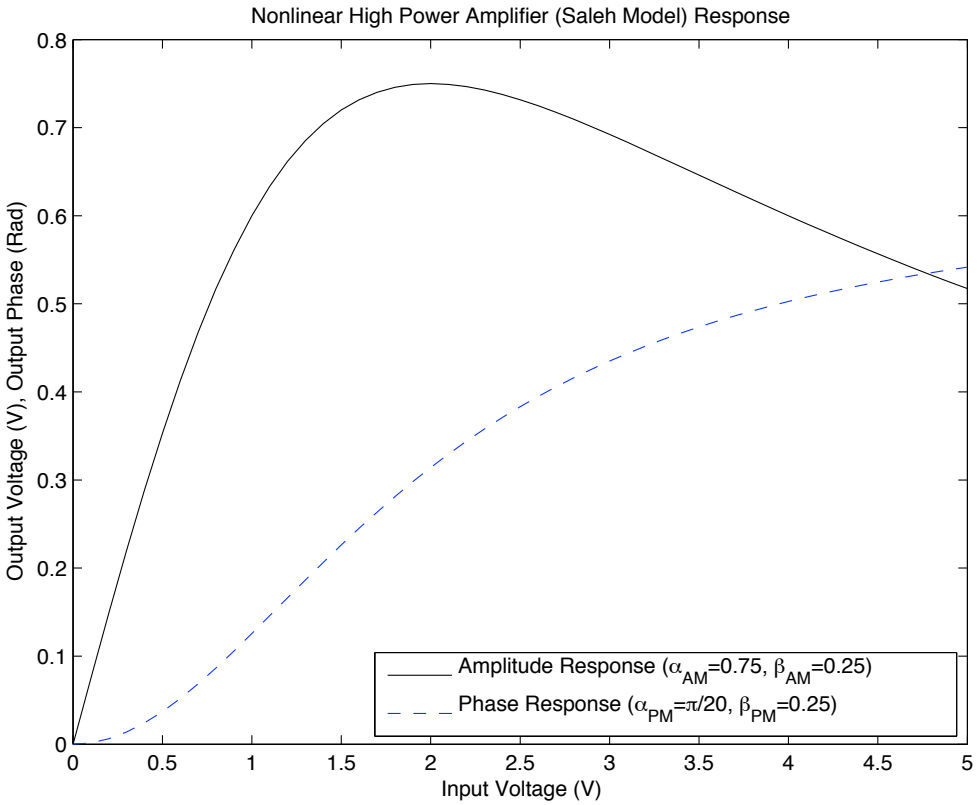

Figure 2.4 The Input and Output Relationship for Nonlinear HPA which is based on the Saleh Model. In this case, the α_{AM} and β_{AM} are set to 0.75 and 0.25, respectively, while α_{PM} and β_{PM} are $\frac{\pi}{20}$ and 0.25.

the nonlinear distortion is a combination of nonlinearly amplified input signal with additional phase distortion being added onto the signal itself. In the rest of thesis, the Saleh nonlinear HPA model is chosen and adapted for the purposes of performance analysis and simulation.

2.4 Performance Analysis

In this section, we will present the derivation of the bit error rate (BER) of the system which is later used as a measure of the system performance. To analyze the performance of the system shown in Fig. 2.2, the characterization of $x(n)$ has to be determined first. Under the assumption that N is large, by the *Central Limit Theorem*, $x(n)$ can be considered as a zero mean Gaussian process [19]. With that assumption of $x(n)$ being a zero mean Gaussian bandpass process, the output signal of the nonlinear HPA and its corresponding frequency domain signal are given as

$$s(n) = \alpha_G x(n) + d_G(n) \overset{FFT}{\longleftrightarrow} S[k] = \alpha_G X[k] + D_G[k] \tag{2.7}$$

where α_G is the complex gain. In addition, $D_G[k]$ represents the distortion noise introduced by the nonlinear HPA and is said to be a complex Gaussian random variable with zero mean and $2\sigma_D^2$ variance [20]. For two different subcarriers, k_1 and k_2, $D_G[k_1]$ and $D_G[k_2]$ are shown to be mutually independent. Furthermore, the in-phase and quadrature phase components of $D_G[k]$ are shown to be mutually independent and identically distributed (i.i.d.) [15]. The multiplicative coefficient, α_G, in (2.7) is given by

$$\begin{aligned}\alpha_G =& \frac{E\{s(n)^* x(n)\}}{2\sigma_{x(n)}^2} \\ =& \frac{E\{f(r)r\}}{2\sigma_{x(n)}^2} \\ =& \frac{1}{2\sigma_{x(n)}^2}\int_0^\infty f(r)\ r\ p(r)dr \end{aligned} \tag{2.8}$$

where $f(r)$ is defined in (2.3) and $2\sigma_{x(n)}^2$ represents the input signal power. $E\{\cdot\}$ is the expected value and $(\cdot)^*$ represents the complex conjugate operation. In additional, $p(r)$ is the probability density function (PDF) of the input envelope which is Rayleigh distributed [20].

For simplicity of the mathematical notations, the subcarrier indices will be dropped in the rest of the derivation. By substituting $S[k]$ which is defined in (2.7) into (2.2), the received signal in frequency domain, $Y[k]$, is

$$Y = \alpha_G X + D_G + W \tag{2.9}$$

where D_G is the FFT of d_G. Based on the decision boundary for the BPSK modulation and assuming $X = +1$ is transmitted, the BER, denoted P_{BER}, is

$$\begin{aligned} P_{BER} =& P\left(\alpha_G X + D_G + W < 0\right) \\ =& Q\left(\sqrt{\frac{|\alpha_G|^2 E_b}{\sigma^2}}\right) \end{aligned} \tag{2.10}$$

where E_b is the energy per bit and $Q(\nu)$ is defined as

$$Q(\nu) = \frac{1}{\sqrt{2\pi}}\int_\nu^\infty e^{-t^2/2}dt, \qquad \nu \geq 0 \tag{2.11}$$

Furthermore, σ^2 represents the variance of the noise component of the signal. Since the mean of noise component is zero, σ^2 in (2.10) is found to be

$$\begin{aligned}\sigma^2 =& E\{(D_G + W)(D_G + W)^*\} \\ =& \sigma_D^2 + \sigma_w^2 \end{aligned} \tag{2.12}$$

The calculation for obtaining σ_D^2 is usually a difficult task because the numerical value of σ_D^2 depends on the parameters that are used in the nonlinear HPA model. To find the numerical value for σ_D^2, Banelli, *et al.* [20] proposed the following steps.

1. Express the autocorrelation function of the output signal as a function of autocorrelation function of the input signal to the nonlinear HPA.
2. Represent $f(r)$, the nonlinear distortion function, as Bessel series expansion.
3. Obtain the power spectral density (PSD) function of the signal at the output of the nonlinear HPA.
4. Integrating the PSD function of nonlinear distortion over the subcarrier's bandwidth.

For the purpose of completeness, we will briefly show the procedures as outlined in [20] for obtaining the numerical value of σ_D^2. By the definition of autocorrelation function and denoting $R_{ss}(\tau)$ as the autocorrelation function of output signal which is defined in (2.7), $R_{ss}(\tau)$ is found to be

$$\begin{aligned} R_{ss}(\tau) =& E\left\{s(n+\tau)s(n)^*\right\} \\ =& E\left\{\left[\alpha_G x(n+\tau) + d_G(n+\tau)\right]\left[\alpha_G^* x(n)^* + d_G(n)^*\right]\right\} \\ =& \left|\alpha_G\right|^2 E\left\{x(n+\tau)x(n)^*\right\} + E\left\{d_G(n+\tau)d_G(n)^*\right\} \\ =& \left|\alpha_G\right|^2 R_{xx}(\tau) + R_{dd}(\tau) \end{aligned} \tag{2.13}$$

where $R_{xx}(\tau)$ and $R_{dd}(\tau)$ are the autocorrelation functions of $x(n)$ and $d_G(n)$, respectively. (2.13) can also be expressed only as a function of autocorrelation function of the input signal [20], namely,

$$\begin{aligned} R_{ss}(\tau) =& \sum_{i=0}^{\infty} c_i \left[\frac{R_{xx}(\tau)}{2\sigma_{x(n)}^2}\right]^{2i+1} \\ =& \frac{c_0}{2\sigma_{x(n)}^2} R_{xx}(\tau) + \sum_{i=1}^{\infty} c_i \left[\frac{R_{xx}(\tau)}{2\sigma_{x(n)}^2}\right]^{2i+1} \end{aligned} \tag{2.14}$$

where c_i, the coefficients, are given as

$$c_i = \frac{1}{2\sigma_{x(n)}^2 (i+1)} \left| \int_0^{\infty} f(r) \frac{r^2}{\sigma_{x(n)}^2} e^{-r^2/2\sigma_{x(n)}^2} L_i^{(1)}\left(\frac{r^2}{2\sigma_{x(n)}^2}\right) dr \right|^2 \tag{2.15}$$

while $L_i^{(1)}\left(\frac{r^2}{2\sigma_{x(n)}^2}\right)$ can be obtained by evaluating the Laguerre function, which is given as (2.16),

$$L_i^{(k)}(\nu) = \frac{\nu^{-k} e^{\nu}}{i!} \left(\frac{d}{d\nu}\right)^i \left(\nu^{i+k} e^{-\nu}\right) \tag{2.16}$$

with $k = 1$ and $\nu = \frac{r^2}{2\sigma_{x(n)}^2}$.

Comparing (2.13) and (2.14), $R_{dd}(\tau)$ is then given by

$$R_{dd}(\tau) = \sum_{i=1}^{\infty} c_i \left[\frac{R_{xx}(\tau)}{2\sigma_{x(n)}^2}\right]^{2i+1} \tag{2.17}$$

To further reduce (2.15), the nonlinear distortion function can be represented by the Bessel series expansion and is given by

$$f(r) = \sum_{m=0}^{L} b_m J_1\left(\frac{(2m-1)\pi}{R_{max}} r\right) \tag{2.18}$$

where R_{max} is a normalization factor and $J_1(\cdot)$ is the Bessel function of the first kind of order 1 [20]. L in this case represents the number of terms that is required to sufficiently represent the nonlinear function. Subsequently, the coefficients, c_i, are

$$c_i = \frac{1}{i!(i+1)!}\left|\sum_{m=0}^{L} b_m \left(\frac{\beta}{2}\right)^{2i+1} e^{(\frac{-\beta}{2})^2}\right|^2 \tag{2.19}$$

where β is defined as

$$\beta = \frac{(2m-1)\pi}{R_{max}}\sqrt{2\sigma^2_{x(n)}} \tag{2.20}$$

and b_m is found to be

$$b_m = \frac{2\int_0^{R_{max}} r f(r) J_1\left(\frac{(2m-1)\pi}{R_{max}} r\right) dr}{R^2_{max}\left[J_2\left(\frac{(2m-1)\pi}{R_{max}} r\right)\right]^2} \tag{2.21}$$

Furthermore, the derivation of b_m is presented in Appendix 13.1. In practice, the output response of a practical HPA can be obtained by sending an input signal with various amount of voltage. Subsequently, one can plot the input and output relationship of a practical HPA such as the one that is shown in Fig. 2.3 or 2.4. Utilizing both (2.18) and (2.21), one can try to find b_m that would best represent the nonlinear distortion function with the minimum error.

To find the PSD function of $d_g(n)$, one can take the FFT of (2.17). Denote the PSD function for $d_G(n)$ as $S_{dd}(f)$, then $S_{dd}(f)$ is found to be

$$\begin{aligned} &S_{dd}(f) \overset{FFT}{\longleftrightarrow} R_{dd}(\tau) \\ &\qquad = \sum_{i=1}^{\infty} \frac{c_i}{(2\sigma^2_{x(n)})^{2i+1}} \left[\underbrace{S_{xx}(f) \otimes S_{xx}(f) \otimes \cdots \otimes S_{xx}(f)}_{(2i+1)\ \ times}\right] \end{aligned} \tag{2.22}$$

where $\otimes$ represents convolution operation and $S_{xx}(f)$ represents the PSD function of the input signal, $x(n)$. Finally, the variance, σ^2_D, is obtained by integrating (2.22) over the subcarrier's bandwidth, namely,

$$\sigma^2_D = \int_B S_{dd}(f) df \approx S_{dd}(f) B \tag{2.23}$$

where B is the bandwidth of the subcarrier. Notice that the last approximation in (2.23), this approximation is only valid if and only if the PSD function of $d_G(n)$ is relatively flat across the

subcarrier's bandwidth. By observing the result in (2.23), one can see that this procedure proposed by Banelli *et al* is not limited to just BPSK modulation scheme due to the reason that the variance only depends on the power of the input signal to the nonlinear HPAs and parameters used in the nonlinear HPA model. In fact, for the same set of parameters used in the nonlinear HPA model, the only thing needs to be recalculated is the input signal power when the modulation scheme is switched from BPSK to Quadrature Phase Shift Keying (QPSK) or Quadrature Amplitude Modulation (QAM).

2.5 Conclusion

In this chapter, we first discussed the concept of high PAPR. Next, we presented the two most popular, yet practical, nonlinear HPA models used in literature. The input and output relationships of those nonlinear HPA models were also described. To see the effect of the nonlinear distortion caused by high PAPR signals through HPAs, we analyzed the performance of a BPSK OFDM system that is impaired by a nonlinear HPA in AWGN channel. Since obtaining the variance of nonlinear distortion, σ_D^2, is often a complicated task due to its strong dependency on the nonlinear HPA model, we presented one method which was outlined by Banelli *et al.* for obtaining a numerical value for σ_D^2. In addition, the advantage of this particular method is also discussed.

3

IEEE 802.11n Review

3.1 Introduction

Recent advances in wireless digital communication technology have made the hardware equipment, used to access WLANs, widely available and more affordable to the general public. Recently, WLANs that are implemented based on IEEE 802.11b standard are most popular and widely deployed in the market. Unlike the most common IEEE 802.11b standard, there are WLAN hardware that utilize the IEEE 802.11a and 802.11g standards which operate on OFDM technique.

Since OFDM is a multicarrier system, OFDM has become a popular technique for transmission of signals over wireless channels due to its superior performance in fading channels. OFDM modulation converts the signal from the frequency domain to the time domain before transmission; and upon receiving, it converts the signal from the time domain back to the frequency domain in the receiver by using Inverse Fast Fourier Transform (IFFT) and Fast Fourier Transform (FFT), respectively. Through this process, OFDM modulation also transforms a frequency-selective channel into a parallel collection of frequency flat subchannels which makes the system more robust against known conventional signal degradations which are due to the effects of frequency selectivity. In addition, in the case of single carrier systems, the structure of an equalizer in the receiver is normally complicated since the channel frequency response varies within a symbol duration. However, in the case of a multicarrier system such as OFDM, the frequency flatness in the subchannels makes the structure of the equalizer in the receiver simpler. In most cases, an one-tap equalizer is sufficient to remove channel frequency response.

Until recently, Single Input Single Output (SISO) has been the main type of antenna configuration in wireless communication systems. In literature, OFDM systems with the SISO antenna configuration are typically known as SISO-OFDM. In SISO-OFDM systems, modulated OFDM symbols are transmitted or received sequentially. To increase the data rate of the systems,

Multiple Input Multiple Output (MIMO) antennas configuration and Space Time Coding (STC) are implemented at the transmitter and receiver in systems. For OFDM systems which are equipped with MIMO and STC, they are widely known as MIMO-OFDM in literature. During operation, the multiple modulated OFDM symbols are transmitted or received through multiple antennas in a single time slot. Comparing with SISO-OFDM, MIMO-OFDM yields better performance since it takes advantage of spatial diversity. Furthermore, MIMO antenna configuration works as a tool that explores the spatial diversity, therefore, it can be adapted in wireless communication systems with any signal modulation scheme to enhance the system performance. The topics related to MIMO will be discussed in more detail in Chapter 7.

In this chapter, we will present the physical layers of the transmitter and receiver that are implemented based on the Worldwide Spectrum Efficiency's (WWiSE) proposal to IEEE 802.11n standard. The IEEE 802.11n will use a combination of MIMO and OFDM to improve the performance. In IEEE 802.11n, there are two modes, NTX-SDM (Spatial Data Multiplexing) and NTX-STBC (Space Time Block Coding) modes [4]. In NTX-SDM mode, all the transmission rates for 2 transmit antennas (TX) in 20 MHz mode are mandatory and supports for 3 TX and 4 TX modes in 20 MHz; 1 TX, 2 TX, 3 TX and 4 TX in 40 MHz are all optional. Transmission supports described in NTX-STBC mode are all optional in IEEE 802.11n [4]. In this chapter, we will only focus on the physical layer configurations for 2 TX in 20 MHz in NTX-SDM and NTX-STBC modes since they are used in simulations in later chapters.

The chapter is organized as follows. Section 3.2 describes the structure of the transmitter in NTX-SDM mode. In Section 3.3, the structure of the receiver in NTX-SDM mode is discussed. Next, the physical layer of the transmitter and receiver for the NTX-STBC mode are described in Sections 3.4 and 3.5, respectively. Finally, Section 3.6 summarizes this chapter.

3.2 Transmitter (NTX-SDM mode)

The physical layer of the transmitter for 2 TX mandatory transmission mode is shown in Fig. 3.1. Since both spatial streams, denoted as TX Spatial Stream 1 and TX Spatial Stream 2 in Fig. 3.1, are identical in design, only one of them is shown in Fig. 3.2. Each block is discussed in more detail in the following sections.

3.2.1 Service Field Insertion

The Service field which is composed of 16 bits is preappended in front of user's data. The 0^{th} to 6^{th} bits of the Service field have the values zero and are used to synchronize the descrambler at the receiver. The remaining 9 bits are reserved for future uses and they are all set to zero.

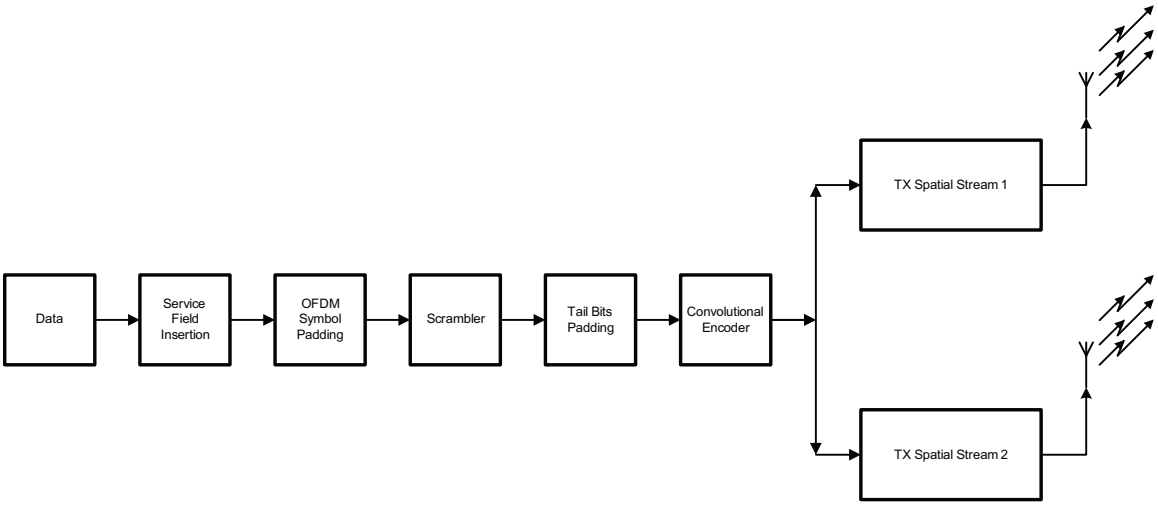

Figure 3.1 A block diagram of the physical layer of 2 TX transmitter in NTX-SDM mode.

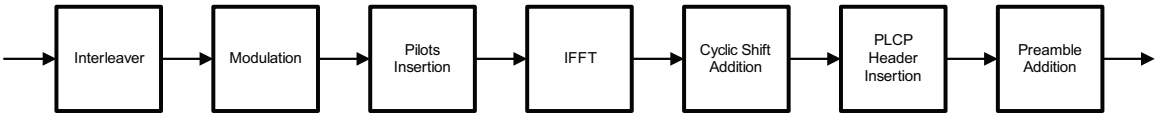

Figure 3.2 A block diagram of the physical layer of the TX spatial stream as shown in Fig. 3.1

3.2.2 OFDM Symbol Padding

Padding is done in such a fashion that ensures the number of bits in the DATA field in the Physical Layer Convergence Procedure (PLCP) protocol data unit (PPDU) is a multiple of number of coded bits per OFDM symbol, denoted as N_{CBPS}. To determine how many padded bits are required, the number of OFDM symbols has to be determined first. Let N_{SYM} be the number of OFDM symbols, then N_{SYM} is given as

$$N_{SYM} = \left\lceil \frac{16 + 8L + 6N_{ES}}{N_{DBPS}} \right\rceil \tag{3.1}$$

where $\lceil \cdot \rceil$ is the ceiling function and L is the length of the data sequence. N_{ES} represents the number of encoding streams. The number of data bits per OFDM symbol is denoted as N_{DBPS}.

After N_{SYM} is determined, the required number of bits in the data filed, denoted as N_{DATA}, for a multiple of N_{CBPS} is

$$N_{DATA} = N_{SYM} N_{DBPS} \tag{3.2}$$

where N_{DBPS} represents the number of data bits per OFDM symbol. The number of padding bits, denoted as N_{PAD}, is just the difference between N_{DATA} and the length of actual data sequence,

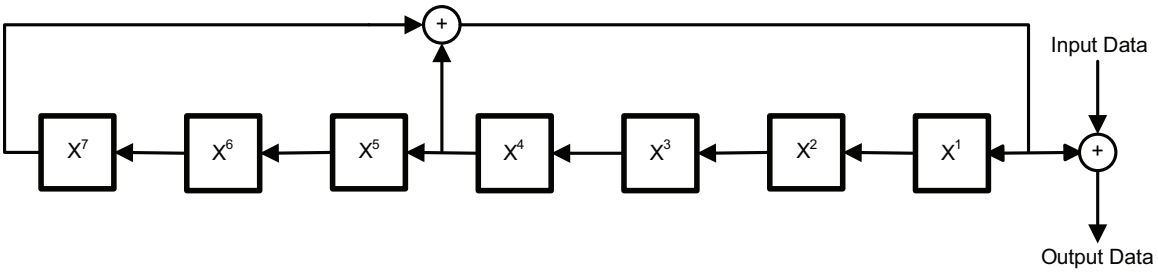

Figure 3.3 A delay box block diagram of the polynomial equation, (3.4)

namely

$$N_{PAD} = N_{DATA} - (16 + 8L + 6N_{ES}) \tag{3.3}$$

The numerical values of padding bits are set to zero and they should be removed from the signal before calculating the bit error rate (BER). In addition, the numerical values for N_{CBPS}, N_{ES} and N_{DBPS} are different depending what error correction coding rate, data rate and data modulation scheme are used in the transmission.

3.2.3 Scrambler

After the padding, the data is scrambled using (3.4) which can also be expressed in terms of delay boxes. Its structure is shown in Fig. 3.3.

$$S(x) = x^7 + x^4 + 1 \tag{3.4}$$

3.2.4 Tail Bits Padding

The purpose of tail bits padding is to force the convolutional encoder to end at the zero state. Since the convolutional encoder ends up at the zero state, the decoder can exploit this information in its algorithm and enhance the system performance. In this case, six zeros are appended to each set of data to force the convolutional encoder to end at the zero state.

3.2.5 Convolutional Encoder

The purpose of utilizing the convolution code is to take an advantage of error correction capability that coding has to offer to enhance BER. The convolutional encoder will encode the DATA field which contains Service field, Physical Sublayer Service Data Units (PSDUs), Tail and Pad bits. The polynomials for encoding generators are $[g_0 = 133_8, g_1 = 171_8]$ in octave notation. Fig. 3.4 shows the corresponding encoding generator with coding rate, $R = \frac{1}{2}$.

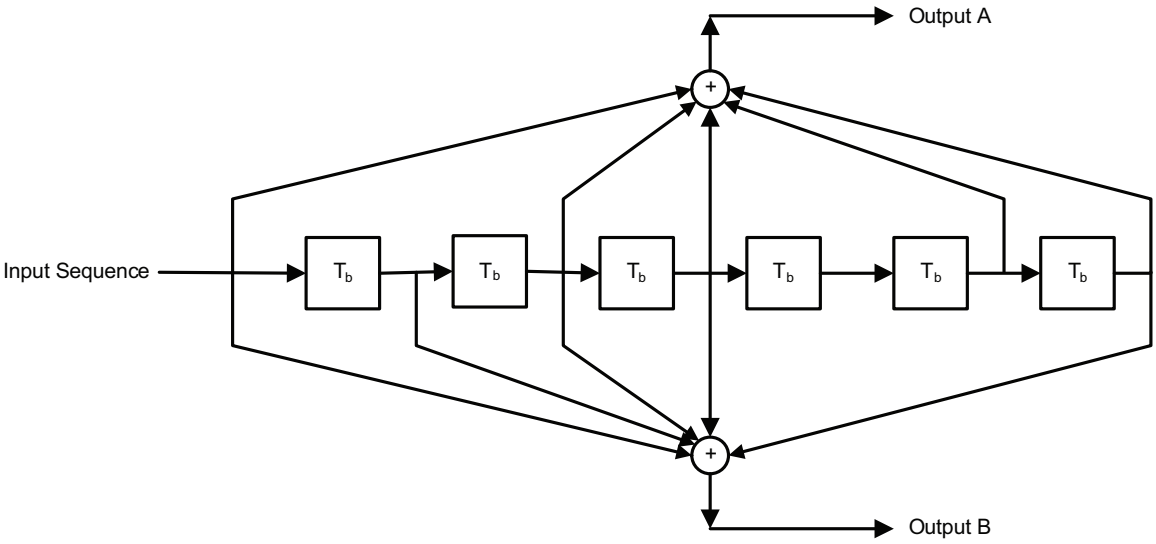

Figure 3.4 A delay box block diagram of a convolutional encoder with the encoding generator polynomials, $[g_0 = 133_8, g_1 = 171_8]$, and $R = \frac{1}{2}$

In Fig. 3.4, T_b denotes the period of the bit. The bit comes out from Output A should be before the bit from Output B in the encoding process. The convolutional encoder will provide encoding rates at $R = \frac{1}{2}, \frac{2}{3}, \frac{3}{4}$, and $\frac{5}{6}$. In addition, depending on the performance requirements, a different encoding rate can be chosen to enhance the performance. Puncturing is required when higher code rate is desired. To demonstrate puncturing, an example of $R = \frac{5}{6}$ is illustrated in Fig. 3.5. At the output of the convolutional encoder, the coded data sequence is then assigned alternately across the spatial streams, with bit 0 assigned to the TX Spatial Stream 1.

3.2.6 Interleaver

After a convolutional encoder, interleavers are applied to rearrange coded data bits in a deterministic fashion. Interleavers are generally used in digital data transmission technology such as magnetic recording or wireless communication. Its purpose is to protect data against burst errors which often overwrite many data bits in a row, but fortunately, the occurrence is rare. Since the burst errors often change a lot of bits in a row, they can be prevented from affecting the BER by interleaving the data sequences. In general, coded data is transmitted with parity bits that would enable decoders to correct some correctable errors. When a burst error occurs and changes a lot of bits in the data sequence which has been rearranged by the interleaver, the altered bits are no longer grouped together after deinterleaving. This will enable the decoder to decode codewords correctly since now, altered bits are only in part of a codeword.

The input coded sequence is interleaved in the following fashion. Let k be the index of the coded bits before interleaving and $k = 0, 1, ..., (N_{CBPS} - 1)$, where N_{CBPS} denotes the num-

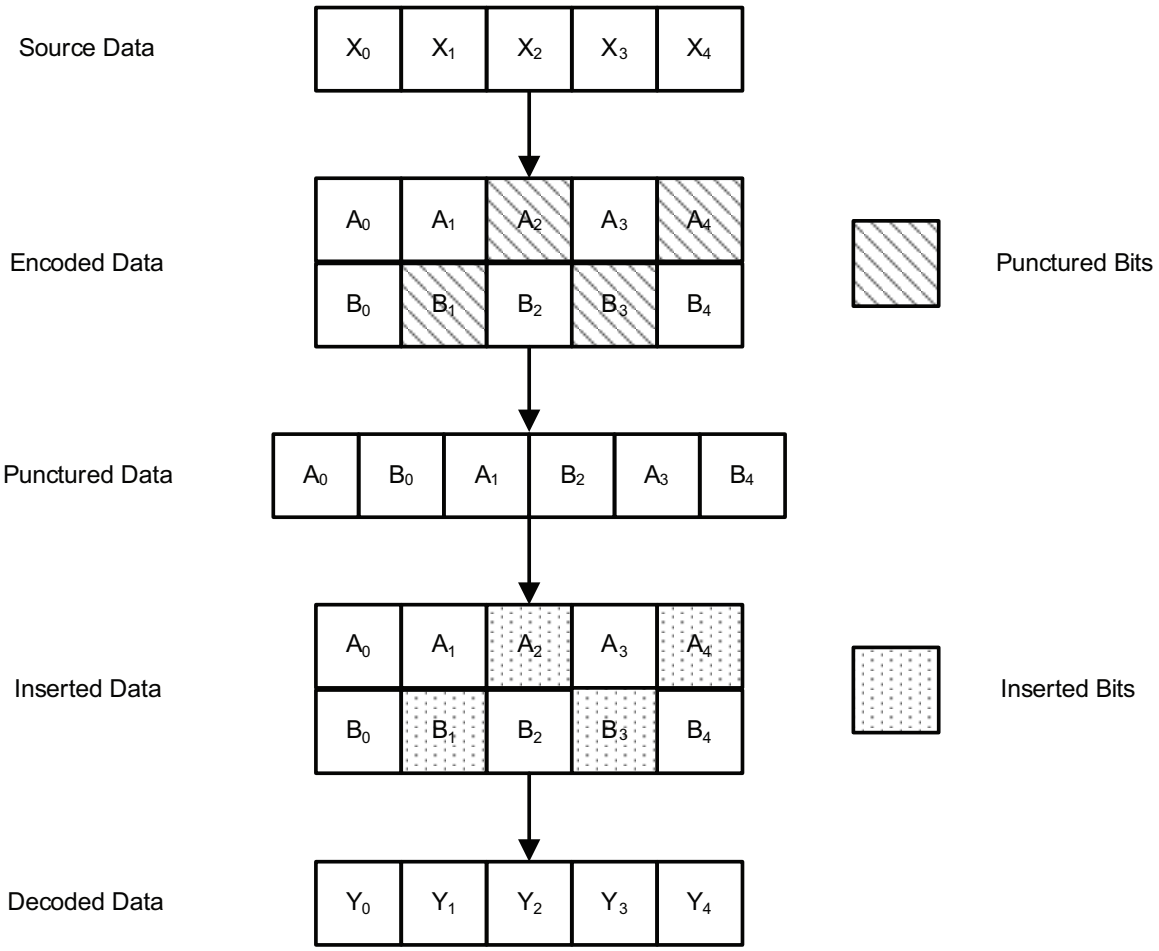

Figure 3.5 The Puncturing Example for $R = \frac{5}{6}$

ber of coded bits per MIMO-OFDM symbol. In addition, let n be the index of spatial stream and $n = 0, 1, \ldots, N_{SS} - 1$, where N_{SS} represents the number of spatial streams. First, the coded bits are cycled through N_{SS} based on (3.5).

$$k = k_n \cdot N_{SS} + n \tag{3.5}$$

where k_n is defined as $k_n = 0, 1, \ldots, \left(\frac{N_{CBPS}}{N_{SS}} - 1\right)$. Then, the input sequences to the interleavers should have a block size of (N_{CBPS}/N_{SS}) bits.

Let i and j be the indices for the k_n^{th} coded data bit after the first and second intermediate interleaving processes, respectively. After the first intermediate interleaving process, the k_n^{th} coded data bit will be mapped to the i^{th} place where the value for i is given by

$$i = \frac{N_{CBPS}/N_{SS}}{I_{DEPTH}} \left(k_n \, mod \, I_{DEPTH}\right) + \left\lfloor \frac{k_n}{I_{DEPATH}} \right\rfloor \tag{3.6}$$

Table 3.1 Numerical Values of I_{DEPTH}, N_{SS} and N_{SD}

N_{SS}	N_{SD}	I_{DEPTH}
1, 2, 3, 4	54	6
2, 3, 4	108	6
1	108	12

where $\lfloor \cdot \rfloor$ represents the floor function. I_{DEPTH} denotes the interleaving depth. In addition, the value for I_{DEPTH} depends on the numerical value of N_{SS} and the number of data subcarriers per OFDM symbol, N_{SD}. The numerical values for N_{SS}, N_{SD} and I_{DEPTH} are listed in the Table 3.1.

After the first interleaving process, the second intermediate process will map the i^{th} coded data bit to j^{th} location in the sequence. The mapping between i^{th} coded data bit to the j^{th} location is governed by

$$j = s \cdot \left\lfloor \frac{i}{s} \right\rfloor + \left(i + \frac{N_{CBPS}}{N_{SS}} - floor\left(\frac{i \cdot I_{DEPATH}}{N_{CBPS}/N_{SS}} \right) \right) \ mod\, s \tag{3.7}$$

where *mod* is the modulo operation. Furthermore, s is found to be

$$s = max\left(\frac{N_{BPSC}}{2}, 1 \right) \tag{3.8}$$

where N_{BPSC} is the number of bits in each OFDM subcarrier per antenna and $max(\cdot, \cdot)$ is the maximum value of the two arguments.

After the second intermediate interleaving process, the sequence will be passed through the final interleaving process. This process will rearrange the order of the sequence by mapping the j^{th} coded data to the j_n^{th} location in the sequence according to (3.9)

$$j_n = \left(j + \frac{N_{CBPS}}{N_{SS}} - N_{BPSC} D_n \right) \ mod \ \left(\frac{N_{CBPS}}{N_{SS}} \right) \tag{3.9}$$

where D_n is denoted as the shift in subcarriers for spatial stream n and it is defined as

$$D_n = 5n \tag{3.10}$$

3.2.7 Modulation

The modulation schemes for the IEEE 802.11n follow closely with the modulations used in the 802.11a standard. The possible modulation schemes are four types of Gray-coded signal constellations: Binary Phase Shift Keying (BPSK), Quadrature Phase Shift Keying (QPSK), 16 Quadrature Amplitude Modulation (QAM) and 64 QAM. For the purpose of illustration, the 16 QAM and 64 QAM signal constellations are shown in Fig. 3.6 and 3.7, respectively.

In the case of M-QAM, the input coded bits are first grouped into blocks size of $log_2 M$,

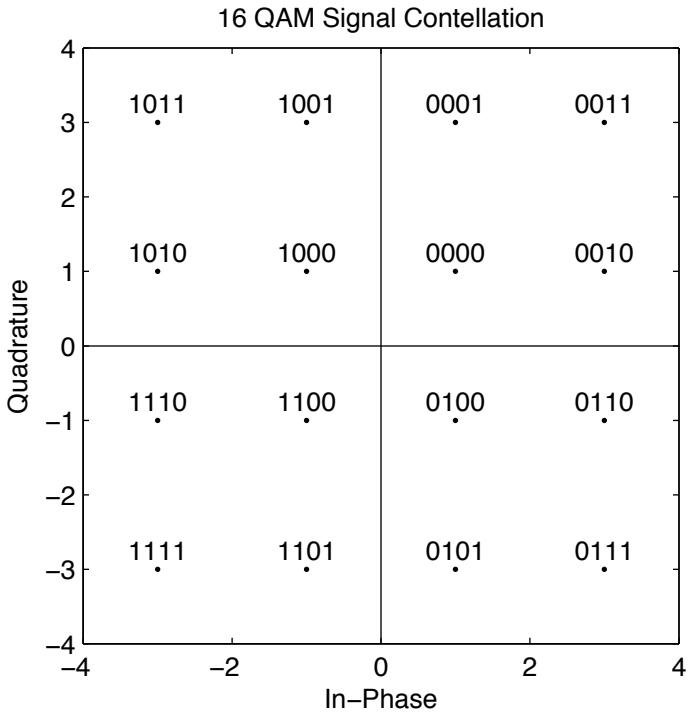

Figure 3.6 The Gray-coded signal constellation map for 16 QAM modulation.

Table 3.2 Normalization Factor for Modulations

Modulation	Normalization Factor
BPSK	1
QPSK	$\frac{1}{\sqrt{2}}$
16 QAM	$\frac{1}{\sqrt{10}}$
64 QAM	$\frac{1}{\sqrt{42}}$

where M is the constellation size. Next, each block of bits is mapped according to the alphabet, $A = \{(2m - 1 - \sqrt{M}) + j(2n - 1 - \sqrt{M})\}$ where $\{m, n = 1, 2, ..., \sqrt{M}\}$. The signal at the output of the modulator will be scaled by a normalization factor which is listed in Table 3.2. By multiplying the output signal at the modulator with the normalization factor, the same average power for all signal mappings are achieved. However, in practices, an approximation of the normalization factor is often used if the result of modulation is within the acceptable modulation accuracy.

3.2.8 Pilot Insertion

Before applying the IFFT to transform the signal from frequency domain to time domain, pilots are inserted in the designated subcarriers for each transmit antenna. The purpose of pilots insertion is to aid the receiver in estimating the channel response. For all 20 MHz NTX-SDM modes, the subcarriers, -21 and $+21$, are dedicated for transmitting pilot signal for each OFDM symbol.

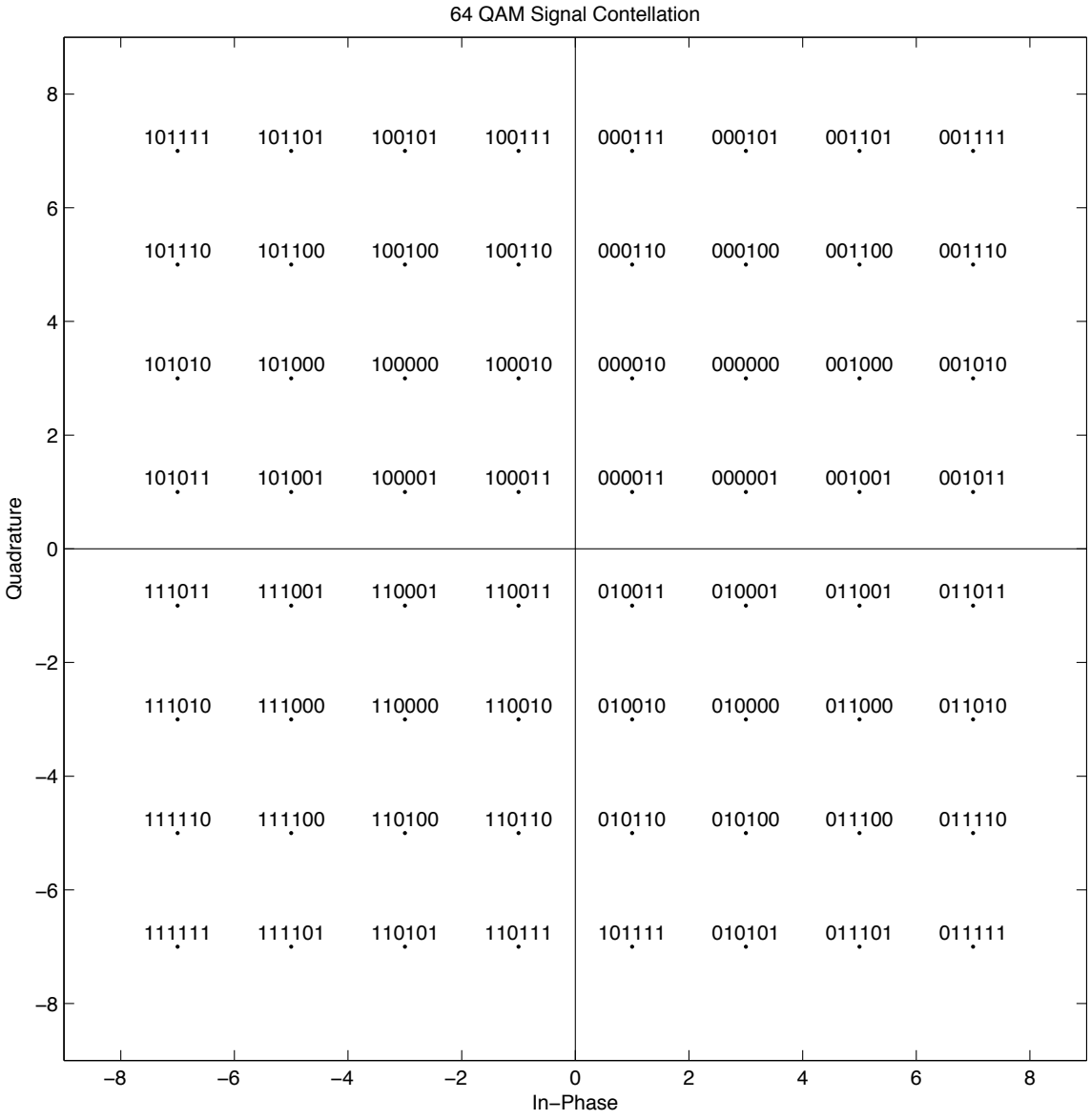

Figure 3.7 The Gray-coded signal constellation map for 64 QAM modulation.

Table 3.3 Pilot Values for 20 MHz NTX-SDM Modes

Subcarrier index, k	2 TX-SDM	3 TX-SDM	4 TX-SDM
-21	$a_{m-1,\, n \bmod 2}$	$b_{m-1,\, f(n \bmod 4)}$	$c_{m-1,\, f(n \bmod 4)}$
+21	$a_{m-1,\, (n+1) \bmod 2}$	$b_{m-1,\, f((n+2) \bmod 4)}$	$c_{m-1,\, f((n+2) \bmod 4)}$

As for all 40 MHz modes, the subcarriers -42, -14, $+14$ and $+42$ are designated for pilot signal transmission.

Define $a_{i,j}$, $b_{i,j}$, and $c_{i,j}$ as the elements on the i^{th} row and j^{th} column of the matrices, A, B and C, respectively, which are defined as

$$A = \begin{bmatrix} +1 & +1 & +1 & -1 \\ +1 & -1 & +1 & +1 \end{bmatrix} \tag{3.11}$$

$$B = \begin{bmatrix} +1 & +1 & -1 & -1 \\ +1 & -1 & +1 & -1 \\ -1 & +1 & +1 & -1 \end{bmatrix} \tag{3.12}$$

$$C = \begin{bmatrix} +1 & +1 & +1 & -1 \\ +1 & +1 & -1 & +1 \\ +1 & -1 & +1 & +1 \\ -1 & +1 & +1 & +1 \end{bmatrix} \tag{3.13}$$

For transmitting the n^{th} OFDM symbol from the m^{th} antenna, the numerical value of the pilot signal is chosen according to Table 3.3 for all 20 MHz modes. In addition, the function $f(\cdot)$ is defined as $f(0) = 0$, $f(1) = 2$, $f(2) = 1$ and $f(3) = 3$. After the numerical values are chosen from the matrices, the values of pilots are then multiplied with the polarity sequence, denoted as $p_{n \bmod 127}$, and is defined as

$$\begin{aligned} p_{n \bmod 127} = \{&1,1,1,1,-1,-1,-1,1,-1,-1,-1,-1,1,1,-1,1,-1,-1,1, \\ &1,-1,1,1,-1,1,1,1,1,1,1,-1,1,1,1,-1,1,1,-1,-1,1,1,1, \\ &-1,1,-1,-1,-1,1,-1,1,-1,-1,1,-1,-1,1,1,1,1,1,-1, \\ &-1,1,1,-1,-1,1,-1,1,-1,1,1,-1,-1,-1,1,1,-1,-1,-1, \\ &-1,1,-1,-1,1,-1,1,1,1,1,-1,1,-1,1,-1,1,-1,-1,-1, \\ &-1,-1,1,-1,1,1,-1,1,-1,1,1,1,-1,-1,1,-1,-1,-1,1, \\ &1,1,-1,-1,-1,-1,-1,-1,-1\} \end{aligned} \tag{3.14}$$

For the transmission of the n^{th} OFDM symbol from the m^{th} antenna in the 40 MHz modes, the values for the pilot signal are chosen according to Table 3.4. Then, the signal values are also multiplied by the polarity sequence before the insertion.

Table 3.4 Pilot Values for 40 MHz NTX-SDM Modes

Subcarrier index, k	1 TX-SDM	2 TX-SDM	3 TX-SDM	4 TX-SDM
-42	+1	$a_{m-1,\, n \bmod 4}$	$b_{m-1,\, n \bmod 4}$	$c_{m-1,\, n \bmod 4}$
-14	+1	$a_{m-1,\, (n+1) \bmod 4}$	$b_{m-1,\, (n+1) \bmod 4}$	$c_{m-1,\, (n+1) \bmod 4}$
+14	+1	$a_{m-1,\, (n+2) \bmod 4}$	$b_{m-1,\, (n+2) \bmod 4}$	$c_{m-1,\, (n+2) \bmod 4}$
+42	-1	$a_{m-1,\, (n+3) \bmod 4}$	$b_{m-1,\, (n+3) \bmod 4}$	$c_{m-1,\, (n+3) \bmod 4}$

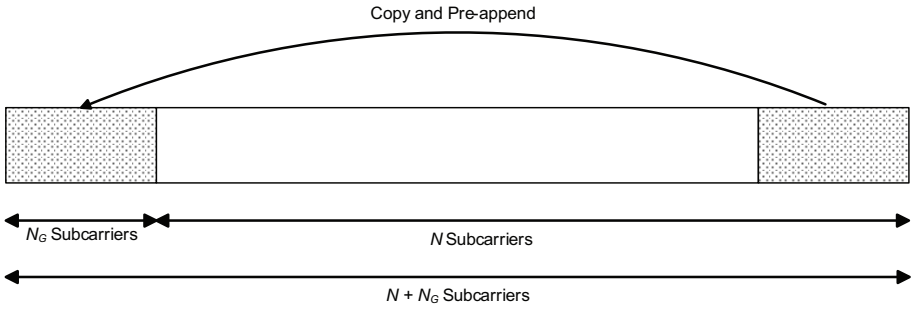

Figure 3.8 An illustration of creating cyclic shift in OFDM system.

3.2.9 IFFT

The IFFT operation on the signal has already been described in Section 1.1 of Chapter 1.

3.2.10 Cyclic Shift

In practical situations, the received signal will experience the channel response which includes signal distortions such as delays in receiving time. The cyclic shift or Guard Interval (GI) is designed to help minimize the Intersymbol Interference (ISI) which is one of the effects from time dispersive channels. By copying the information in the last few samples, denoted as N_G, in the OFDM symbol and placing them in front of the entire time domain signal, a guard interval is created. Fig. 3.8 illustrates the creation of cyclic shift. Since the received symbols are delayed, they often overlap a part of previous symbol. In the case where the GIs are not inserted, the result of overlapping usually leads to performance degradation. If the signal overlapping occurs in the guard interval, the ISI does not degrade the performance because the guard interval only contains the duplicated data and will be removed in the receiver.

3.2.11 PLCP Header Insertion

The Physical Layer Convergence Procedure (PLCP) header is composed of two fields. One of the fields is SIGNL-N (SIG-N) and the other one is SERVICE field which has been discussed in this chapter, Section 3.2.1. The main functionality that SIG-N field provides for MIMO-OFDM stations is the signal configuration information such as N_{SS}, N_{TX} and R, etc. How SIGNAL-N is defined depends on which configuration that the station operates in. The SIG-N field is composed

Table 3.5 SIG-N Field Bit Assignment

Bits	Field	Subfield	Parameter	Values
B0 to B5	RSVD		Reserved bits	111111, Bits shall be ignored at the receiver
B6 to B21	CONFIG		Configuration	
B6 to B8		N_{SS}	Number of spatial streams	000→1, 001→2, 010→3, 011→4
B9 to B11		N_{TX}	Number of transmit antennas	000→1, 001→2, 010→3, 011→4
B12 to B13		BW	Bandwidth	00→20 MHz, 01→40 MHz
B14 to B16		R	Code rate	000→ $\frac{1}{2}$, 001→ $\frac{2}{3}$, 010→ $\frac{3}{4}$, 011→ $\frac{5}{6}$
B17 to B18		CT	ECC type	00→ Convolutional, 01→ LDPC
B19 to B21		CON	Constellation type	000→ BPSK, 001→ QPSK, 010→ 16 QAM, 011→ 64 QAM
B22 to B24	LEN		Length	Number of bytes in the payload
B35	LPI		Last PSDU indicator	1 indicates that this is the last PSDU to be aggregated into the current PPDU
B36	REXT		Standard or extended communication range configuration	0→ Standard configuration, 1→ Extended Communication Range Configuration
B37 to B43	RSVD		Reserved	0000000, Bits shall be ignored at the receiver
B44 to B47	CRC		Cyclic Redundancy Check	CRC calculated on bits 0-43 using generator polynomial $x^4 + x + 1$
B48 to B53	TAIL			000000

of 54 bits and the assignment is listed in Table 3.5. In all 20 MHz operations, the SIG-N field should be modulated into QPSK signals and encoded with a R=1/2 convolutional encoder. One single OFDM symbol is produced after the SIG-N is padded and transformed by IFFT. For the second configuration, extended communication range, the SIG-N is duplicated and total of two OFDM symbols are used. In addition, the latter configuration is only used when systems are operating in NTX-STBC mode. In all 40 MHz operations, BPSK modulation is used to modulate the SIGN-N instead of QPSK modulation. In addition, for both transmission modes in mandatory configuration, the SIG-N field should not be scrambled. Refer to ([4], pp. 52-54) for the values of cyclic shifts in each operation mode.

3.2.12 Preamble Addition

The PLCP preamble is used for synchronization purpose. It is composed of two training sequences, short and long sequences. Depending on which transmission mode is being used, the designs of short and long sequences are different. For example, the short and long sequences for 20 MHz for greenfield 2 TX mode are defined as

$$\begin{aligned} SS_{20}[-28,28] = \sqrt{\left(\frac{7}{3}\right)}\{&0,0,0,0,1+j,0,0,0,-1-j,0,0,0,1+j,0,0,0,-1-j,0,0,0,-1-j,\\ &0,0,0,1+j,0,0,0,0,0,0,0,-1-j,0,0,0,-1-j,0,0,0,1+j,0,0,0,\\ &1+j,0,0,0,1+j,0,0,0,1+j,0,0,0,0\} \end{aligned} \tag{3.15}$$

$$\begin{aligned} LS_{20}[-28,28] =\{&1,1,1,1,-1,-1,1,1,-1,1,-1,1,1,1,1,1,1,-1,-1,1,1,-1,1,-1,1,1,1,1,\\ &0,1,-1,-1,1,1,-1,1,-1,1,-1,-1,-1,-1,-1,1,1,-1,-1,1,-1,1,-1,1,1,\\ &1,1,-1,-1\} \end{aligned} \tag{3.16}$$

The second antenna will transmit a cyclically shifted version of the same sequences with respect to the first antenna. In this case, the second antenna will transmit the short and long sequences that are shifted by 400 and 1600 nsec, respectively. In addition, the delays are with respect to the transmission time of the first antenna. For readers who are interested in other transmission modes, a description of numerical values of training sequences and time parameters is given in ([4], pp. 50-54).

3.3 Receiver (NTX-SDM mode)

In many communication systems, the receiver is always designed to recover the user's data by reversing what has been done on the data at the transmitter. In this case, the block diagram of the corresponding receiver is shown in Fig. 3.9. Since the spatial streams in the transmitter are identical in design, the spatial streams, denoted as RX Spatial Stream 1 and RX Spatial Stream 2, are the same as well. The block diagram of the spatial stream in the receiver is shown in Fig. 3.10. Each block in both figures is discussed in detail in the following sections.

3.3.1 Preamble Removal

The first process that the receiver performs is to initialize the synchronization process. The synchronization is achieved by locking onto the Preamble sequence, more specifically, the short and long training sequences as defined in Section 3.2.12. Once the synchronization has been established, the received signal is decomposed into two parts, PLCP header and PSDU. The Preamble is simply removed from the received signal and discarded since it does not have any desired data. In addition, the removal of the Preamble does not affect the system performance.

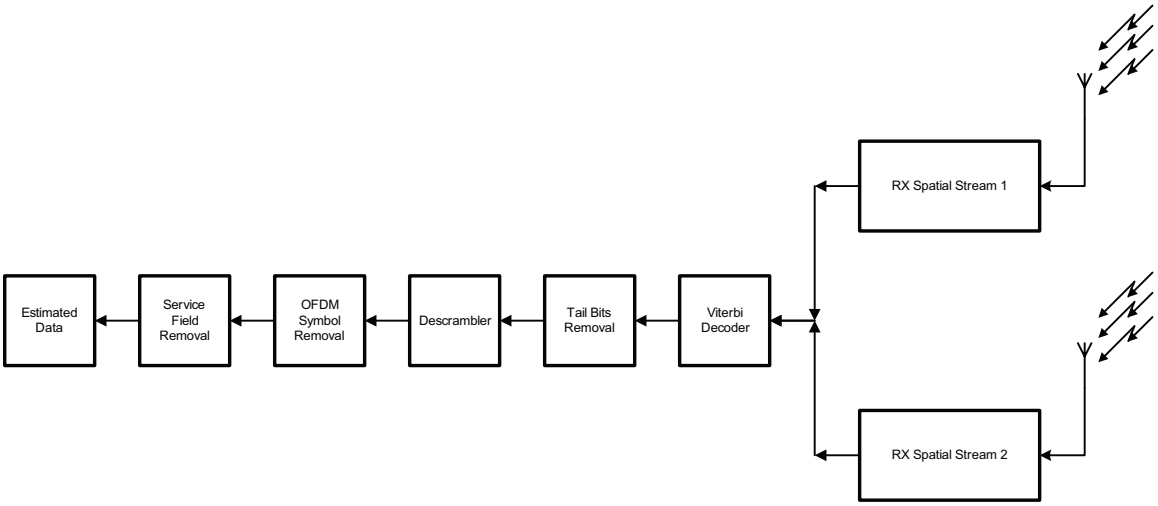

Figure 3.9 A block diagram of the physical layer of 2 TX receiver in NTX-SDM mode.

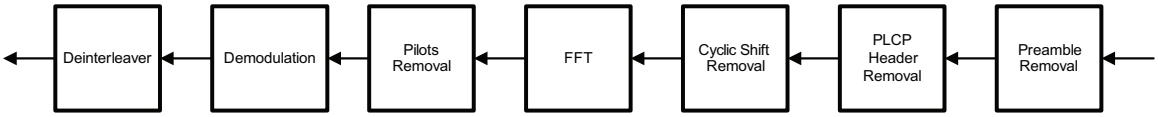

Figure 3.10 A block diagram of the physical layer of the RX spatial stream as shown in Fig. 3.9

3.3.2 PLCP Header Removal

After the removal of Preamble, the receiver then retrieves information such as length of user's data and any configuration related parameters from the PLCP header from SIG-N field. The information contained in the field is crucial because the receiver needs it for configuring itself to decode the received signal properly. Once the information is retrieved, the PLCP header is also discarded for the same reason as removing Preamble.

3.3.3 Cyclic Shift Removal

The cyclic shift is also removed from the signal since its purpose is to prevent ISI and does not contain additional user's data. The removal of cyclic shift will not affect the system performance.

3.3.4 FFT

The FFT operation on the signal has already been described in Section 1.1 of Chapter 1.

3.3.5 Pilot Removal

Once the signal has been transformed back to frequency domain, Pilots can be used to estimate the channel impulse response. The channel estimate is then passed onto the equalizer where

the channel impulse response can be equalized or removed from the signal. Before demodulating the signal, the Pilots are then removed from the sequence.

3.3.6 Demodulation

Before the demodulation, the signal has to be renormalized by dividing the symbols by the normalization factor listed in Table 3.2 in this chapter, Section 3.2.7. Depending on what modulation is utilized in the transmitter, the same scheme is used to map the symbols back to bits based on Gray-coded signal constellations. For example, if 16 QAM modulation is used in the transmitter, then each 16 QAM symbol, ranging from 0 to 15, is mapped to its corresponding 4 binary bits. At the end, the output of the demodulation contains only 0's and 1's and its length is four times longer than the input sequence.

3.3.7 Deinterleaver

The deinterleavers implemented at the receiver will perform the reverse processes and they will also perform three deinterleaving processes to obtain the non-interleaved version. Let k_d and i_d be the indices for the first and second intermediate deinterleaving processes. Then, the first intermediate deinterleaving process maps the k_n^{th} bit to the k_d^{th} location according to (3.17)

$$k_d = \left(k_n + \frac{N_{CBPS}}{N_{SS}} + 2sD_n\right) \; mod \; \left(\frac{N_{CBPS}}{N_{SS}}\right) \tag{3.17}$$

where s and D_n are defined in this chapter, Section 3.2.6. After the first intermediate deinterleaving process, the second process maps the k_d^{th} data bit to the i_d^{th} place in the sequence. Furthermore, the numerical value for the i_d^{th} location is defined as

$$i_d = \left\lfloor \frac{k_d}{s} \right\rfloor s + \left(k_d + \left\lfloor \frac{I_{DEPTH} k_d}{N_{CBPS}/N_{SS}} \right\rfloor\right) \; mod\,(s) \tag{3.18}$$

where the values for I_{DEPTH} is listed in Table 3.1 along with the numerical values for N_{SS} and N_{SD}. Finally, to obtain the non-interleaved version, the third deinterleaving process rearranges the order of the sequence by mapping the i_d^{th} data bit to the j_{dn}^{th} data location where the value of j_{dn} is given by

$$j_{dn} = I_{DEPTH} i_d \left(\frac{N_{CBPS}}{N_{SS}} - 1\right) \left\lfloor \frac{I_{DEPTH} i_d}{N_{CBPS}/N_{SS}} \right\rfloor \tag{3.19}$$

3.3.8 Viterbi Decoder

At the outputs of the spatial streams, the sequences are multiplexed alternately across the streams to produce a single sequence which contains encoded information. To decode the encoded information, a Viterbi decoder with the same generator polynomials, $[g_0 = 133_8,\ g_1 = 171_8]$, is implemented. The Viterbi algorithm essentially performs maximum likelihood decoding while reducing the computational load by taking advantage of the trellis structure. The trellis diagram is created

based on the finite state diagram which can be derived from the encoding generator polynomials. The algorithm calculates the Euclidian distance between the received signal, at time t_i, and all the trellis paths entering each state at time t_i. Next, the result is added to the results obtained from previous states. The decoder then removes those branches that could not possibly be candidates for the maximum likelihood choice. When two paths enter the same state, the one having the best metric is chosen. This particular path is called surviving path. This selection of survival paths is performed for all the states. The decoder functions in this way as time progresses and makes decisions by eliminating the least likely paths. Finally, by tracing along the surviving path, the uncoded bits can be determined.

3.3.9 Tail Bits Removal

The purpose of tail bits is to force the encoder to state zero, hence, it does not contain any data nor serves any further purpose after the encoder is forced to state zero. The tale bits are removed from the signal before the next stage.

3.3.10 Descrambler

Before descrambling, it is necessary to establish synchronization in the descrambler. This can be achieved by using the 0^{th} to 6^{th} bits in the Service field. Once the descrambler declares that it is in sync, it can start the descrambling process. The same polynomial which is defined as (3.4) is used to descramble the bits.

3.3.11 OFDM Symbol Padding Removal

The padding bits are removed from the signal as it should be since its purpose to ensure the transmissions from each antenna are multiples of whole OFDM symbols.

3.3.12 Service Field Removal

As mentioned in this chapter, Section 3.2.1, the sole purpose of the Service field is for synchronization at the descrambler. After removing the Service field, the estimated data is obtained.

3.4 Transmitter (NTX-STBC mode)

The physical layer for the transmitter in the NTX-STBC mode is shown in Fig. 3.11. In addition, Fig. 3.12 shows the block diagram of TX Spatial Stream in detail.

Since the majority of the blocks in the diagram have been already discussed in Section 3.2 of this chapter. In this section, we will only focus on the differences in the system when the WLAN system is operating in the NTX-STBC mode. One of the differences in operating in the

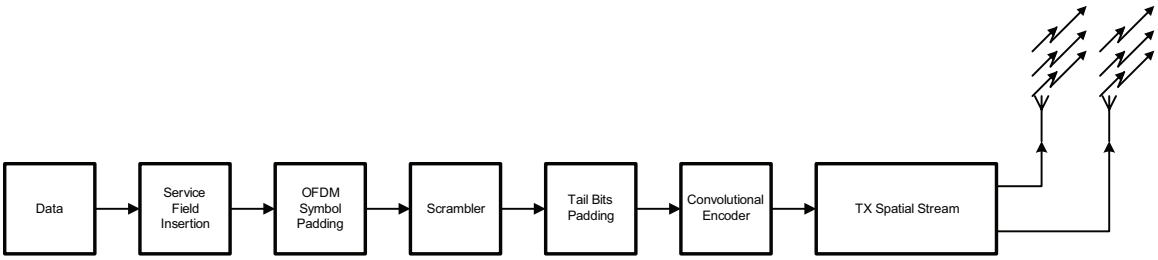

Figure 3.11 A block diagram of the physical layer of 2 TX transmitter in NTX-STBC mode.

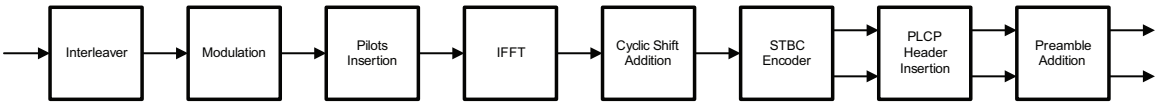

Figure 3.12 A block diagram of the physical layer of the TX spatial stream as shown in Fig. 3.11.

NTX-STBC mode is the number of OFDM symbols which are generated in the multiples of two OFDM symbols in each time instance. The reason behind generating multiples of two OFDM symbols is through STBC encoding process, two OFDM symbols are transmitted from two different antennas in each OFDM symbol duration. The STBC encoding process will be discussed in more detail in Section 3.4.1 in this chapter. In addition, the process of generating two OFDM symbols should be conformed to descriptions given in subsections in Section 3.2 of this chapter.

3.4.1 Space Time Block Code (STBC) Encoder

As mentioned already, the signal at the input to the STBC encoder contains the multiples of two OFDM symbols. The STBC encoder encodes the input signal in the following fashion. Let $s_o(n)$ and $s_e(n)$ be the odd and even number of two OFDM symbols. At time $2t$, $s_o(n)$ and $s_e(n)$ are transmitted separately from the first and second antennas, respectively. At time $2t+1$, $-s_e^*(n)$ is transmitted from the first antenna while $s_o^*(n)$ is transmitted from the second antenna. This encoding process can be described in a matrix and is given by

$$\mathcal{G}_2 = \begin{bmatrix} s_o(n) & s_e(n) \\ -s_e^*(n) & s_o^*(n) \end{bmatrix} \tag{3.20}$$

where the subscript 2 represents the total number of transmitted antennas [21]. $(\cdot)^*$ implies the complex conjugation operation. Furthermore, the same encoding process will be applied to the next set of two OFDM symbols. Chapter 7 discusses the STBC code and the BER performance in more detail.

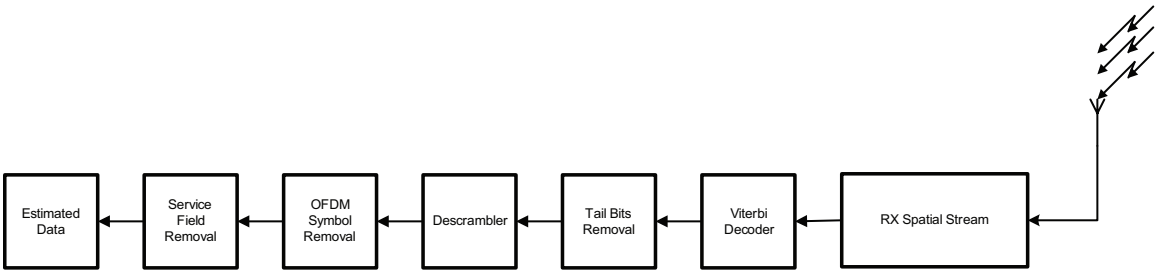

Figure 3.13 A block diagram of the physical layer of 2 TX receiver in NTX-STBC mode.

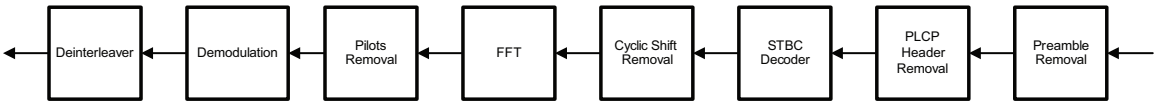

Figure 3.14 A block diagram of the physical layer of the RX spatial stream as shown in Fig. 3.13.

3.5 Receiver (NTX-STBC mode)

Fig. 3.13 shows the corresponding receiver which operates in the NTX-STBC mode. In addition, the RX spatial stream is shown in detail in Fig. 3.14. Since STBC decoder is the new block in the system, we will focus on describing the new STBC decoder block in the next section.

3.5.1 Space Time Block Code (STBC) Decoder

After two OFDM symbols transmissions, the received signal in frequency domain is

$$\begin{bmatrix} Y_o[k] \\ Y_e^*[k] \end{bmatrix} = \underbrace{\begin{bmatrix} H_1[k] & H_2[k] \\ H_2^*[k] & -H_1^*[k] \end{bmatrix}}_{\mathbf{H}} \begin{bmatrix} S_o[k] \\ S_e[k] \end{bmatrix} + \begin{bmatrix} W_o[k] \\ W_e^*[k] \end{bmatrix} \tag{3.21}$$

where $H_1[k]$ and $H_2[k]$ are the frequency responses for channel one and two, respectively. In addition, $S_o[k]$ and $S_e[k]$ are FFT of $s_o(n)$ and $s_e(n)$, respectively. $W_o[k]$ represents Additive White Gaussian Noise (AWGN) at time $2t$ while $W_e[k]$ implies AWGN at time $2t+1$. In (3.21), $\mathbf{H}$ represents the matrix. To decouple the signal, i.e. obtaining only $S_o[k]$ or $S_e[k]$, the pseudo inverse of $\mathbf{H}$ is multiplied to the received signal. Chapter 7 gives more details about the decoupling process and the BER performance of the STBC coding.

3.6 Conclusion

In this chapter, we presented a detailed description of two transceivers, one was for operating in NTX-SDM mode while the other transceiver was operating in NTX-STBC mode. In both cases, the transceivers were implemented based on the WWiSE proposal to IEEE 802.11n standard. In addition, we also discussed the functionality for each block in both transceivers.

4

Effects of Nonlinear High Power Amplifier (HPA) and Jammer on the Performance of OFDM

4.1 Introduction

Orthogonal Frequency Division Multiplexing (OFDM) has several technical advantages such as the ability of delivering high data rate, high bandwidth efficiency and outstanding performance in fading channels over its technical competitors. In addition, OFDM is currently being considered for the fourth generation (4G) mobile and Wireless Local Area Network (WLAN) communication system. Different from Single Input Single Output (SISO) antenna configuration, Multiple Input Multiple Output (MIMO) antenna implementations can be employed to further increase the data rate of the system by utilizing more than one antenna for data transmissions and receptions. The IEEE 802.11n incorporates both OFDM and MIMO technologies to achieve better performance [4].

Even though OFDM has some advantages over its competitors, by itself it presents technical challenges such as high sensitivity to frequency offsets, phase noise [22, 23] and high peak to average power ratio (PAPR) to engineers. The property of orthogonality between subcarriers is the foundation of OFDM systems and because of this property, the processes of synchronization and data extraction are straightforward. However, if the orthogonality between subcarriers is lost due to the presence of either or both frequency offset and phase noise in the communication chain, inter-carrier interference (ICI) will occur and the system performance degrades [5]. Another disadvantage that is associated with OFDM systems is its high PAPR which is due to the nature of Fast Fourier Transform (FFT) and Inverse Fast Fourier Transform (IFFT) operations. When L number of sig-

nals are being added coherently, IFFT/FFT produces a peak power that is L times larger than the average power. Practical amplifiers have difficulty reproducing such high PAPR signals and often introduce clipping and spectral regrowth [24, 25].

Although some papers dealt with the performance of OFDM systems that were impaired by nonlinear high power amplifiers (HPAs) in the additive white Gaussian noise (AWGN) channel, very few of them adequately addressed the effects of nonlinearity on the performance of equalized OFDM systems in the Rayleigh flat fading channel. Even fewer discussed the problem of narrowband interference or jamming with the combination of nonlinear HPAs in OFDM systems through the Rayleigh flat fading channel. In [15], the authors presented the performance analysis of an M-ary Quadrature Amplitude Modulation (M-QAM) OFDM system with a nonlinear HPA and phase noise in AWGN channel only. Chang, *et al.* [26] showed the performance of an equalized OFDM system in Rayleigh flat fading channel for various modulations such as Binary Phase Shift Keying (BPSK), Quadrature Phase Shift Keying (QPSK), Differential Phase Shift Keying (DPSK) and QAM; however, the effects of nonlinearity from a HPA and narrowband interference on the system performance were not considered in the paper.

In [27], the performance of an OFDM system with carrier interferometry spreading codes and narrowband interference in the Rayleigh fading channel was presented without considering the nonlinear distortion from HPAs. In addition, the authors assumed that the source of narrowband interference or jammer was very close to the receiver; hence, the narrowband interference did not experience any channel effects. This particular approach does not fit many situations where in general, the jamming sources are usually located in remote areas such as satellites in orbit or battleships in sea. Therefore, it is reasonable and practical to assume that the jammer experiences another separate channel which is different from the channel for the transmitted signal. In this chapter, we analyze the performance of an equalized M-QAM OFDM system that is subject to a nonlinear HPA, channel estimation error, and jamming in the Rayleigh fading channel. On the contrary to the jamming model presented in [27], the jammer by itself will experience a separate channel impulse response. This analytical model is then extended in compliance with the IEEE 802.11n standard for the purpose of simulation. The simulation results of the extended model are presented and compared with theoretical results.

The chapter is organized as follows. In Section 4.2, the system model under study is described in detail. Section 4.3 contains the performance analysis of the analytical model. Section 4.4 describes the simulation setup for the extended model. Section 4.5 provides simulation results of the model described in Section 4.4. Finally, Section 4.6 summarizes the chapter.

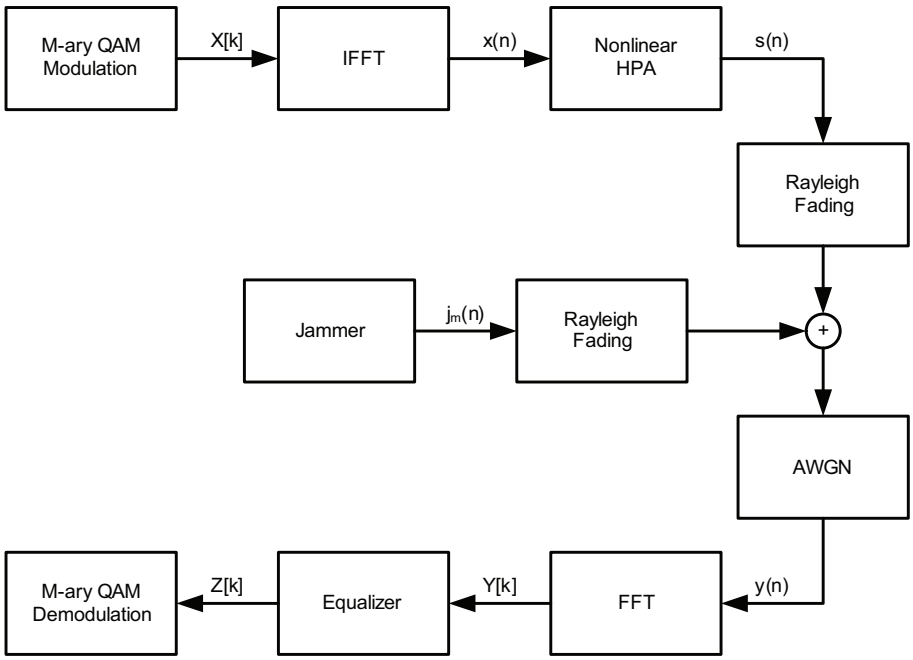

Figure 4.1 The block diagram of an equalized M-ary QAM OFDM system impaired by a nonlinear HPA, channel estimation error, and jamming in the Rayleigh fading channel.

4.2 System Description

The analytical system diagram is shown in Fig. 4.1 and is discussed in the following subsections.

4.2.1 Transmitter

The transmitter consists of a M-QAM modulator, an IFFT, and a nonlinear HPA. In addition, each block is discussed in detail in following subsections. Assuming binary data bits for the input to the M-QAM modulator are equiprobable and independent, they are grouped into blocks of $log_2 M$ and mapped into M-QAM symbols, $X[k]$, according to alphabet, $A = \{(2m - 1 - \sqrt{M}) + j(2n - 1 - \sqrt{M})\}$ where $\{m, n = 1, 2, ...\sqrt{M}\}$ and M is the signal constellation size. At appropriate sampling time, the signal at the output of the IFFT, $x(n)$, is

$$x(n) = \frac{1}{N} \sum_{k=0}^{N-1} X[k] e^{j\frac{2\pi nk}{N}} \qquad 0 \leq n \leq N-1 \tag{4.1}$$

where N is the number of subcarriers.

4.2.2 HPA Model

The nonlinear HPA model in the transmitter represents the nonlinear distortion imposed on the signal. In this chapter, the nonlinear HPA model follows the Saleh model which has been

described in Chapter 2, Section 2.3.

4.2.3 Jammer Model, Channel Model and AWGN

The jammer is modeled as a complex Gaussian random process which has zero mean and $2\sigma_{J_m}^2$ variance. The jamming signal in time domain, denoted as $j_m(n)$, is expressed as

$$j_m(n) = \frac{1}{N}\sum_{k=0}^{N-1} J_m[k]e^{j\frac{2\pi nk}{N}} \tag{4.2}$$

where $J_m[k]$ represents the jamming signal for the k^{th} subcarrier in the frequency domain.

Let $h_1(n)$ be the impulse response of the Rayleigh fading channels between the transmitter and the receiver. The in-phase and quadrature components of $h_1(n)$ are Gaussian random variables with zero mean and $\sigma_{H_1}^2$ variance. In addition, the in-phase and quadrature components of $h_1(n)$ are assumed to be statistically independent of each other. Denote $h_2(n)$ as the Rayleigh fading channel between the jammer and the receiver, $h_2(n)$ is then modeled as a complex Gaussian random process with zero mean and $2\sigma_{H_2}^2$ variance. In addition, it is assumed that the in-phase and quadrature components of $h_2(n)$ are statistically independent of each other. The thermal noise which is denoted as $w(n)$ is an independent additive white Gaussian noise process which has zero mean and $2\sigma_w^2$ variance.

4.2.4 Receiver

Assuming perfect synchronization and there is no time delay introduced by the path to the transmitted signal, the received signal, denoted as $y(n)$, with the jammer interference is given by

$$y(n) = h_1(n)s(n) + h_2(n)j_m(n) + w(n) \tag{4.3}$$

Fig. 4.2 shows the effect of a single tone jamming on the OFDM signals. As one can observe, the jammer is only present in one particular subcarrier and it has no effects on the other subcarriers since its magnitude at the other subcarriers are zero. This implies, unless the jamming signal is present in all subcarriers, the received signal in frequency domain can be separated into two cases. One case represents the scenario where the jamming signal is present in the subcarriers while the other case denotes the situation where the data subcarriers in the received signal are free from jamming. Let $Y[k]$ be the received signal in frequency domain, then $Y[k]$ is expressed as

$$\begin{aligned} Y[k] &= \sum_{n=0}^{N-1} y(n)e^{-j\frac{2\pi kn}{N}} \\ &= \begin{cases} H_1[k]S[k] + H_2[k]J_m[k] + W[k] & \text{Jamming} \\ H_1[k]S[k] + W[k] & \text{Otherwise} \end{cases} \end{aligned} \tag{4.4}$$

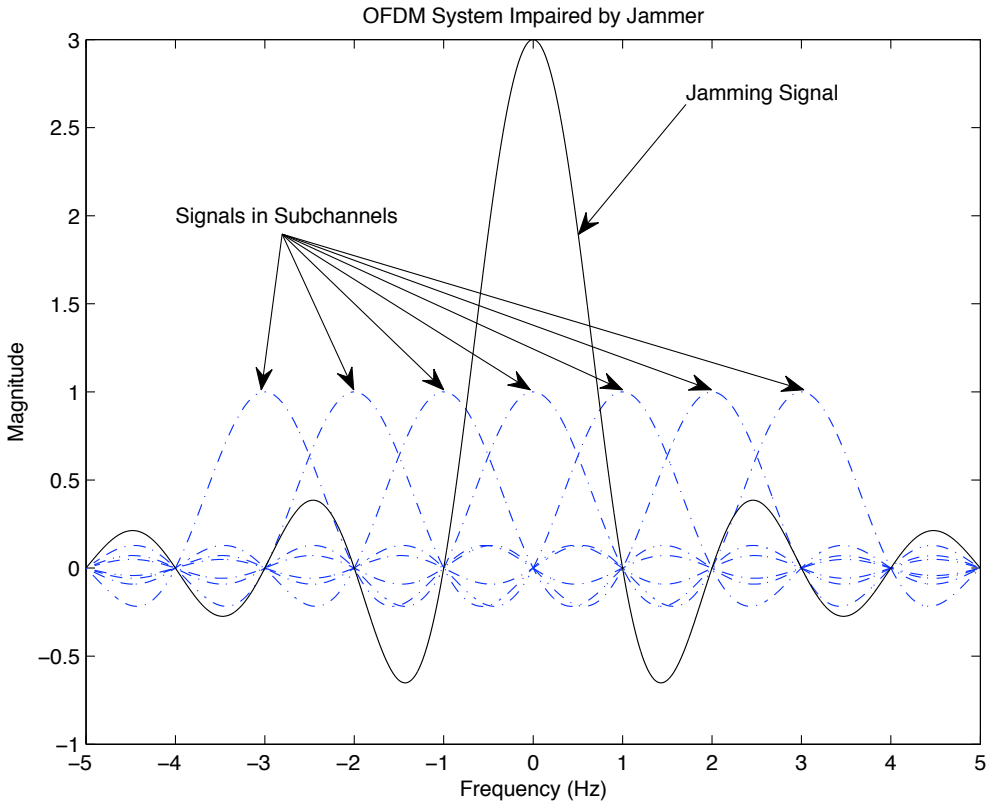

Figure 4.2 An illustration of the effect of jammer in the OFDM signals

where $H_1[k]$, $S[k]$, $H_2[k]$, $J_m[k]$ and $W[k]$ are FFT of $h_1(n)$, $s(n)$, $h_2(n)$, $j_m(n)$, and $w(n)$, respectively. One can observe from (4.4) that the received signal for the case where the subcarriers which are not interfered by the jammer can be obtained from the other case by setting $J_m[k]$ to zero.

4.2.5 Equalizer Model

One of the most attractive features of OFDM systems is the simplicity in the equalization process which is adequately done by using a one-tap equalizer in the frequency domain. Among many available algorithms, we choose the Zero Forcing algorithm because of its simplicity in implementation.

Before the equalization process, estimating the channel response is necessary and can be obtained with the aid of pilots. Let $X[P_1], X[P_2], ..., X[P_p]$ be the pilot symbols modulated onto the subcarriers, $P_1, P_2, ..., P_p$, where p is the total number of pilots. Using Least Squares, the estimated

channel response at the pilot subcarriers is found to be

$$\hat{H}[P_i] = \frac{Y[P_i]}{X[P_i]} \qquad i = 1, 2, ..., p \tag{4.5}$$

where $Y[P_i]$ is the received signal at the pilot subcarrier, P_i. Once the estimated channel responses at the pilot subcarriers are found, the estimated channel response at the data subcarriers can be obtained by interpolating between two consecutive pilots.

After obtaining the estimate, the equalized signal, denoted as $Z[k]$, is given by

$$\begin{aligned} Z[k] =& \frac{Y[k]}{\hat{H}_1[k]} \\ =& \begin{cases} \frac{H_1[k]S[k]+H_2[k]J_m[k]+W[k]}{\hat{H}_1[k]} & \text{Jamming} \\ \frac{H_1[k]S[k]+W[k]}{\hat{H}_1[k]} & \text{Otherwise} \end{cases} \end{aligned} \tag{4.6}$$

where $\hat{H}_1[k]$ is the estimate of the channel, $H_1[k]$ and is defined as

$$\hat{H}_1[k] = H_1[k] + \epsilon[k] \tag{4.7}$$

where $\epsilon[k]$ represents the error in estimating channel, $H_1[k]$, and is modeled as a complex Gaussian random process with zero mean and $2\sigma_\epsilon^2$ variance.

4.3 Performance Analysis

In this section, we will present the derivation of bit error rate (BER) which is used later as a measure of system performance. The performance analysis of the system which is shown in Fig. 4.1, starts with the characterization of $x(n)$. Under the assumption that N is large and by the *Central Limit Theorem*, $x(n)$ is said to be Gaussian distributed with zero mean [19]. With that assumption, Benelli, *et al.* had shown that $s(n)$ can be written as a product of a complex gain, α_G, and the input signal, $x(n)$, added with noise distortion $d_G(n)$. $s(n)$ and its FFT are expressed as

$$s(n) = \alpha_G x(n) + d_G(n) \overset{FFT}{\longleftrightarrow} S[k] = \alpha_G X[k] + D_G[k] \tag{4.8}$$

where $D_G[k]$ is shown to be a complex Gaussian random variable with zero mean and $2\sigma_D^2$ variance [20]. The numerical value of σ_D^2 can be obtained by following steps outlined in Section 2.4 of Chapter 2. For two different subcarriers, k_1 and k_2, $D_G[k_1]$ and $D_G[k_2]$ are mutually independent. Furthermore, the in-phase and quadrature phase components of $D_G[k]$ are shown to be mutually independent and identically distributed (i.i.d) [15]. The multiplicative coefficient α_G in (4.8) is given by

$$\alpha_G = \frac{E\{s(n)^* x(n)\}}{2\sigma_{x(n)}^2} = \alpha_{G_I} + j\alpha_{G_Q} \tag{4.9}$$

where $(\cdot)^*$ denotes the complex conjugate operation and $2\sigma^2_{x(n)}$ represents the power of $x(n)$ [20]. $E\{\cdot\}$ is the expected value. The subscripts, I and Q, implies the in-phase and quadrature components, respectively.

For the simplicity of mathematical notations, we will drop the subcarrier indices in the rest of the derivation. As it has been shown in (4.4), the expression of the received signal in frequency domain depends on whether the subcarrier is affected by the jammer and this difference in the expression of the received signal will yield a different BER expression. Since the theoretical result for the case where the jammer interference is absent in the subcarrier can be derived from the case where the subcarrier suffers from jammer interference by setting appropriate terms to zero, we will continue the derivation of BER expression for the case where the jammer interference is present in the subcarriers.

Assuming perfect synchronization and after the removal of the preamble sequences and cyclic prefix, the equalized signal for the case where the jammer is present in the subcarrier, denoted as Z^J, is given by

$$\begin{aligned} Z^J =& \frac{H_1(\alpha_G X + D_G) + H_2 J_m + W}{\hat{H}_1} \\ =& \frac{\alpha_1}{\hat{\alpha}_1} e^{j\theta}\left(\alpha_G X + D_G\right) + \frac{\alpha_2}{\hat{\alpha}_1} e^{j\phi} J_m + \frac{W e^{-j\angle \hat{H}_1}}{\hat{\alpha}_1} \\ =& \frac{\alpha_1}{\hat{\alpha}_1} e^{j\theta}\alpha_G X + \underbrace{\frac{\alpha_1}{\hat{\alpha}_1} e^{j\theta} D_G}_{\zeta} + \underbrace{\frac{\alpha_2}{\hat{\alpha}_1} e^{j\phi} J_m}_{\xi} + \underbrace{\frac{W}{\hat{\alpha}_1} e^{-j\angle \hat{H}_1}}_{\upsilon} \\ =& \frac{\alpha_1}{\hat{\alpha}_1} e^{j\theta}\alpha_G X + \zeta + \xi + \upsilon \end{aligned} \tag{4.10}$$

where

$$\begin{aligned} &\alpha_1 = |H_1|, \quad \hat{\alpha}_1 = |\hat{H}_1|, \quad \alpha_2 = |H_2| \\ &\theta = \angle H_1 - \angle \hat{H}_1, \quad \phi = \angle H_2 - \angle \hat{H}_1 \end{aligned} \tag{4.11}$$

α_1 and $\hat{\alpha}_1$ are Rayleigh distributed and the phase error is uniformly distributed in $[-\pi, \pi]$. The joint probability density function (PDF) of α_1, $\hat{\alpha}_1$, and θ is given by [28] as

$$p(\alpha_1, \hat{\alpha}_1, \theta) = \frac{\alpha_1 \hat{\alpha}_1}{2\pi |\Delta|^{\frac{1}{2}}} exp\left\{ -\frac{[\sigma^2_{\hat{H}_1}\alpha_1^2 + \sigma^2_{H_1}\hat{\alpha}_1^2 - 2R_c\alpha_1\hat{\alpha}_1\cos\theta - 2R_{cs}\alpha_1\hat{\alpha}_1\sin\theta]}{2|\Delta|^{\frac{1}{2}}} \right\} \tag{4.12}$$

where

$$\begin{aligned} &\sigma^2_{H_1} = E\{H^2_{1_I}\} = E\{H^2_{1_Q}\}, \qquad R_c = E\{H_{1_I}\hat{H}_{1_I}\} = E\{H_{1_Q}\hat{H}_{1_Q}\} \\ &\sigma^2_{\hat{H}_1} = E\{\hat{H}^2_{1_I}\} = E\{\hat{H}^2_{1_Q}\}, \qquad R_{cs} = E\{H_{1_I}\hat{H}_{1_Q}\} = -E\{H_{1_Q}\hat{H}_{1_I}\} \\ &|\Delta| = \left[\sigma^2_{H_1}\sigma^2_{\hat{H}_1} - R_c^2 - R_{cs}^2\right]^2 \end{aligned} \tag{4.13}$$

Since H_1 and H_2 are independent of each other, the PDF of α_2 is

$$p(\alpha_2) = \frac{\alpha_2}{\sigma_{H_2}^2} e^{\frac{-\alpha_2^2}{2\sigma_{H_2}^2}} \tag{4.14}$$

Since ζ, ξ and υ in (4.10) are noise terms with zero mean, their variances are required in deriving the BER expression. Let σ_ζ^2 be variance for the in-phase and quadrature components of ζ, then σ_ζ^2 is found as

$$\sigma_\zeta^2 = E\{\zeta\zeta^*\} = E\left\{\left(\frac{\alpha_1}{\hat{\alpha}_1} e^{j\theta} D_G\right)\left(\frac{\alpha_1^*}{\hat{\alpha}_1^*} e^{-j\theta} D_G^*\right)\right\} = \frac{\alpha_1^2}{\hat{\alpha}_1^2}\sigma_D^2 \tag{4.15}$$

Denote σ_ξ^2 as the variance for the in-phase and quadrature components of ξ, then σ_ξ^2 is given by

$$\sigma_\xi^2 = E\{\xi\xi^*\} = E\left\{\left(\frac{\alpha_2}{\hat{\alpha}_1} e^{j\phi} J_m\right)\left(\frac{\alpha_2^*}{\hat{\alpha}_1^*} e^{-j\phi} J_m^*\right)\right\} = \frac{\alpha_1^2}{\hat{\alpha}_1^2}\sigma_{J_m}^2 \tag{4.16}$$

Finally, let σ_υ^2 be the variance of in-phase or quadrature component of υ, then σ_υ^2 is expressed as

$$\sigma_\upsilon^2 = E\{\upsilon\upsilon^*\} = E\left\{\left(\frac{W}{\hat{\alpha}_1} e^{-j\angle\hat{H}_1}\right)\left(\frac{W^*}{\hat{\alpha}_1^*} e^{j\angle\hat{H}_1}\right)\right\} = \frac{\sigma_w^2}{\hat{\alpha}_1^2} \tag{4.17}$$

Further expanding Z_J into in-phase and quadrature components, Z^J becomes

$$\begin{aligned}
Z^J =& \frac{\alpha_1}{\hat{\alpha}_1}(\cos\theta + j\sin\theta)(\alpha_{G_I} + j\alpha_{G_Q})(X_I + jX_Q) + \zeta + \xi + \upsilon \\
=& \underbrace{\left\{\frac{\alpha_1}{\hat{\alpha}_1}[\cos\theta\alpha_{G_I}X_I - \cos\theta\alpha_{G_Q}X_Q - \sin\theta\alpha_{G_I}X_Q - \sin\theta\alpha_{G_Q}X_I] + \zeta_I + \xi_I + \upsilon_I\right\}}_{Z_I^J} \\
&+ j\underbrace{\left\{\frac{\alpha_1}{\hat{\alpha}_1}[\cos\theta\alpha_{G_I}X_Q + \cos\theta\alpha_{G_Q}X_I + \sin\theta\alpha_{G_I}X_I - \sin\theta\alpha_{G_Q}X_Q] + \zeta_Q + \xi_Q + \upsilon_Q\right\}}_{Z_Q^J} \\
=& Z_I^J + jZ_Q^J
\end{aligned} \tag{4.18}$$

To continue the derivation, we assume that 16-QAM modulation is utilized in the system. Nevertheless, the BER expression can be derived in the similar fashion if other rectangular QAM constellations were chosen to modulate signals. The conditional BER of 16-QAM conditioned on α_1, α_2, $\hat{\alpha}_1$, and θ for the case that the jammer exists in the subcarriers is defined as

$$P_{BER|\alpha_1,\alpha_2,\hat{\alpha}_1,\theta}^J = \frac{1}{2}\left(P_{MSB}^J + P_{LSB}^J\right) \tag{4.19}$$

where P_{MSB}^J and P_{LSB}^J are the conditional BER of most significant bits (MSB) and least significant bits (LSB) of 16-QAM symbols conditioned on α_1, α_2, $\hat{\alpha}_1$, and θ. Based on the decision boundaries given in [28], the conditional BER of MSB for the case where the jammer is present is given by

$$\begin{aligned}
P_{MSB}^J =& P(Z_I^J < 0|\alpha_1, \hat{\alpha_1}, \theta, \alpha_2) \\
=& \frac{1}{8}\sum_{i=1}^{8} Q\left(\sqrt{\frac{(\Upsilon_i)^2}{\sigma_\zeta^2 + \sigma_\xi^2 + \sigma_\upsilon^2}}\right)
\end{aligned} \tag{4.20}$$

Table 4.1 Numerical Values of Variables in Conditional BER for MSB

Index i	X_{I_i}	X_{Q_i}	Index i	X_{I_i}	X_{Q_i}
1	d	$3d$	5	$3d$	$3d$
2	d	d	6	$3d$	d
3	d	$-d$	7	$3d$	$-d$
4	d	$-3d$	8	$3d$	$-3d$

Table 4.2 Numerical Values and Signs of Variables in Conditional BER for LSB

Index i	λ_i	κ_i	ζ_i	X_{I_i}	X_{Q_i}	Index i	λ_i	κ_i	ζ_i	X_{I_i}	X_{Q_i}
1	+	+	+	d	$3d$	9	+	-	-	$-3d$	$3d$
2	+	+	-	d	$3d$	10	-	+	-	$-3d$	$3d$
3	+	+	+	d	d	11	+	-	-	$-3d$	d
4	+	+	-	d	d	12	-	+	-	$-3d$	d
5	+	+	+	d	$-d$	13	+	-	-	$-3d$	$-d$
6	+	+	-	d	$-d$	14	-	+	-	$-3d$	$-d$
7	+	+	+	d	$-3d$	15	+	-	-	$-3d$	$-3d$
8	+	+	-	d	$-3d$	16	-	+	-	$-3d$	$-3d$

where $\Upsilon_i = \frac{\alpha_1}{\hat{\alpha}_1}[\cos\theta\alpha_{G_I}X_{I_i} - \cos\theta\alpha_{G_Q}X_{Q_i} - \sin\theta\alpha_{G_I}X_{Q_i} - \sin\theta\alpha_{G_Q}X_{I_i}]$ and $Q(\nu) = \int_\nu^\infty \frac{1}{\sqrt{2\pi}} e^{\frac{-t^2}{2}} dt, \nu \geq 0$. In addition, σ_ζ^2, σ_ξ^2 and σ_υ^2 are defined as (4.15), (4.16) and (4.17), respectively. The numerical values for X_{I_i} and X_{Q_i} in (4.20) are listed in Table 4.1. The conditional BER of LSB can be found in the similar way. Based on the decision boundaries, it is given by

$$\begin{aligned} P_{LSB}^J =& \{P(Z_I^J < -2d|\alpha_1, \hat{\alpha_1}, \theta, \alpha_2) + P(Z_I^J > 2d|\alpha_1, \hat{\alpha_1}, \theta, \alpha_2)\}|_{_{LSB=0}} \\ &+ \left\{P(-2d < Z_I^J < 2d|\alpha_1, \hat{\alpha_1}, \theta, \alpha_2)\right\}|_{_{LSB=1}} \end{aligned} \tag{4.21}$$

where $|_{LSB=0}$ and $|_{LSB=1}$ represent the boundaries for LSB is zero and one, respectively. The conditional BER of LSB is then given by

$$P_{LSB}^J = \frac{1}{8}\sum_{i=1}^{16} \lambda_i Q\left(\sqrt{\frac{(\kappa_i 2d + \zeta_i \Upsilon_i)^2}{\sigma_\zeta^2 + \sigma_\xi^2 + \sigma_\upsilon^2}}\right) \tag{4.22}$$

where λ_i, κ_i, and ζ_i are signs of the value for i^{th} quantity and are listed along with values for X_{I_i} and X_{Q_i} in Table 4.2. Finally, in both Tables 4.1 and 4.2, $d^2 = \frac{2E_b}{5}$ where E_b is the energy per bit.

As mentioned already, we can obtain the theoretical BER expression for the case where the jammer does not affect the subcarriers from the case where the subcarriers are under the influence of jammer by setting $\sigma_{J_m}^2$ to zero. Denote $P_{BER|\alpha_1,\hat{\alpha}_1,\theta}^F$ as the conditional BER for the case where the subcarriers are free from jamming, then $P_{BER|\alpha_1,\hat{\alpha}_1,\theta}^F$ is expressed as

$$P_{BER|\alpha_1,\hat{\alpha}_1,\theta}^F = \frac{1}{2}\left(P_{MSB}^F + P_{LSB}^F\right) \tag{4.23}$$

where P^F_{MSB} and P^F_{LSB} are the conditional BER for MSB and LSB for 16-QAM symbols and are given by

$$\begin{aligned} P^F_{MSB} =& \frac{1}{8}\sum_{i=1}^{8} Q\left(\sqrt{\frac{(\Upsilon_i)^2}{\sigma^2_\zeta + \sigma^2_v}}\right) \\ P^F_{LSB} =& \frac{1}{8}\sum_{i=1}^{16} \lambda_i Q\left(\sqrt{\frac{(\kappa_i 2d + \zeta_i \Upsilon_i)^2}{\sigma^2_\zeta + \sigma^2_v}}\right) \end{aligned} \tag{4.24}$$

In addition, $\Upsilon_i = \frac{\alpha_1}{\hat{\alpha}_1}[\cos\theta\alpha_{G_I}X_{I_i} - \cos\theta\alpha_{G_Q}X_{Q_i} - \sin\theta\alpha_{G_I}X_{Q_i} - \sin\theta\alpha_{G_Q}X_{I_i}]$ and σ^2_ζ and σ^2_v are defined as (4.15) and (4.17), respectively. The signs and numerical values for X_{I_i} and X_{Q_i} defined in both P^F_{MSB} and P^F_{LSB} are also listed in Table 4.1 and 4.2.

The overall conditional BER of 16-QAM depends on how many subcarriers are affected by the jammer and how many of them are not. Let N^J be the number of subcarriers that are interfered by the jammer and $N^F = N - N^J$ be the number of subcarriers that are free from the jammer interference. The overall conditional BER is given by

$$P_{BER|\alpha_1,\alpha_2,\hat{\alpha}_1,\theta} = \frac{N^J}{N}\left\{P^J_{BER|\alpha_1,\alpha_2,\hat{\alpha}_1,\theta}\right\} + \frac{N^F}{N}\left\{P^F_{BER|\alpha_1,\hat{\alpha}_1,\theta}\right\} \tag{4.25}$$

Finally, the unconditional BER for 16-QAM is found by averaging (4.25) over the two PDFs (4.12) and (4.14), namely

$$\begin{aligned} P_{BER} =& \frac{N^J}{N}\int_0^\infty\int_0^\infty\int_0^\infty\int_{-\pi}^{\pi} P^J_{BER|\alpha_1,\alpha_2,\hat{\alpha}_1,\theta} p(\alpha_2)p(\alpha_1,\hat{\alpha}_1,\theta)d\alpha_1 d\hat{\alpha}_1 d\alpha_2 d\theta \\ &+ \frac{N^F}{N}\int_0^\infty\int_0^\infty\int_{-\pi}^{\pi} P^F_{BER|\alpha_1,\hat{\alpha}_1,\theta} p(\alpha_1,\hat{\alpha}_1,\theta)d\alpha_1 d\hat{\alpha}_1 d\theta \end{aligned} \tag{4.26}$$

where the first term shows the BER contribution from all the subcarriers that are interfered by the jammer and the second term represents the BER contribution from subcarriers which are free from the jamming effect. For the case where the transmitted signal only suffers from nonlinearity introduced by the HPA and channel estimation error, i.e. $N_J = 0$ and $N_F = N$, only the second term in (4.26) contributes to unconditional BER.

For the perfect channel estimation, i.e. $H_1 = \hat{H}_1$, (4.26) becomes only a function of α_1 and α_2 and (4.26) is reduced to

$$P_{BER} = \int_0^\infty\int_0^\infty \frac{N^J}{N} P^J_{BER|\alpha_1,\alpha_2} p(\alpha_1)p(\alpha_2)d\alpha_1 d\alpha_2 + \int_0^\infty \frac{N^F}{N} P^F_{BER|\alpha_1} p(\alpha_1)d\alpha_1 \tag{4.27}$$

where $p(\alpha_1)$ is obtained by substituting α_2 and $\sigma^2_{H_2}$ in (4.14) for α_1 and $\sigma^2_{H_1}$. If we further assume that the jammer does not exist in the channel, the unconditional BER for 16-QAM becomes

$$P_{BER} = \int_0^\infty P^F_{BER|\alpha_1} p(\alpha_1)d\alpha_1 \tag{4.28}$$

Finally, in the case where the HPA is ideal, i.e. $\alpha_G = 1$ and $\sigma^2_D = 0$, and perfect channel estimation is achieved, (4.28) is further reduced to a known result ([26], Eq:69).

Table 4.3 Summary of Simulation Cases

Case Number	Jammer Power	Nonlinear HPA	Number of Subcarriers	$2\sigma_\epsilon^2$
1	0.1	Constant	Varying	0
2	Varying	Constant	1	0
3	No	Varying	No	0
4	0.1	Constant	1	Varying
5	0.1	Constant	3	Varying
6	No	Constant	No	Varying

4.4 Simulation Model and Parameters

The simulation model is an extension of the analytical model described in Section 4.2 in compliance with the IEEE 802.11n standard ([4], Clause 10.4.4.2 rate code 73); except the convolutional encoder, interleaver/deinterleaver and Viterbi decoder are omitted. After pre-appending 16-bit Service Field and padding enough bits to ensure the transmission from each antenna are multiples of whole OFDM symbols, the resulting signal is scrambled with a scrambler that is based on the IEEE 802.11a standard and subsequently demultiplexed alternately across the transmitter spatial streams. In each spatial stream, the data is modulated with the 16-QAM modulation and processed with the 64-point IFFT, of which subcarriers, $\pm$ 21, are designated for pilots. The OFDM symbol is then cyclically extended and pre-appended with the preamble sequences as specified in [4] before transmission. To recover the data, the corresponding receiver reverses the encoding procedure in the transmitter.

The channel, jammer and the equalizer are modeled as described in Section 4.2.3 and Section 4.2.5, respectively. Without loss of generality, the statistical mean and variance of fading channels, H_1 and H_2, are set to 0 and 1, respectively. The simulations are performed based on the extended model for several cases which are summarized in Table 4.3. In the first case, the jammer power in the jammed subcarrier is set to a constant value, 0.1, while the number of subcarriers affected by the jammer varies. In case 2, the jamming power varies while we assume that there is only one subcarrier that is jammed. In both cases, the α_{AM} and β_{AM} are set to 1 and 0.25, and the α_{PM} and β_{PM} are 1.2π and 0.01, respectively. For case 3, the narrowband interference is removed and leaving only the influence of the nonlinear HPA, aside from AWGN, in the system. The nonlinear HPA is varied based on the parameters in the HPA model, described in Section 4.2.2, and the numerical values for those parameters are listed in Table 4.4. Note that in Case 3.1 where α_{AM} is set to unity and the other parameters for the HPA model are set to zero, the nonlinear HPA becomes an ideal amplifier which has an unity gain with no phase distortion.

In the first three cases, the channel estimation is assumed to be perfect. For cases 4 and 5, the jammer power in the subcarriers is set to 0.1 and the number of affected subcarriers are

Table 4.4 Simulation Parameters for Nonlinear HPA Model

Case Number	α_{AM}	β_{AM}	α_{PM}	β_{PM}
3.1	1	0	0	0
3.2	1	0.25	π	0.25
3.3	1	0.25	1.2π	0.01
3.4	1	0.25	1.5π	0.01

set to 1 and 3, respectively. On the contrary to cases 4 and 5, case 6 presents the situation where the jammer is not present in the system. In addition, the parameters used in the nonlinear HPA for case 6 is the same as the one used in cases 1 and 2. In addition, the simulations are performed based on the settings mentioned for various values of $2\sigma_\epsilon^2$.

4.5 Simulation Results

In case 1 where we assume perfect channel estimation, the number of jammed subcarriers varies from 0, 1, 3, and 5, the simulation results are plotted against the theoretical results obtained from (4.27) and are shown in Fig. 4.3. Then, instead of varying the number of subcarriers that are affected by jammer, the jammer power for the subcarrier is increased from 0, 0.1, 0.3 to 0.5 in case 2. The results of simulation are shown along with the theoretical results in Fig. 4.4. For case 3 where besides the AWGN, the only noisy interference is the nonlinear distortion from the HPA, the simulation results are compared with theoretical values acquired by using (4.28) and shown in Fig. 4.5.

In all three cases, the sign of error floor in the performance occurs at around 30 dB. In addition, the sign of error floor can be explained by examining signal to noise ratio (SNR) either for MSB or LSB probabilities. At high SNR, the effect of σ_w^2 is negligible compared to σ_D^2 and $\sigma_{J_m}^2$. As a consequence, the SNR for MSB and LSB probabilities in the presence of jammer, denoted as γ_{MSB}^J and γ_{LSB}^J, are

$$\begin{aligned}\gamma_{MSB}^J &\simeq \frac{[\alpha_{G_I} X_{I_i} - \alpha_{G_Q} X_{Q_i}]^2}{\sigma_D^2 + \frac{\alpha_2^2}{\alpha_1^2}\sigma_{J_m}^2} \\ \gamma_{LSB}^J &\simeq \frac{\left(\kappa_i 2d + \zeta_i[\alpha_{G_I} X_{I_i} - \alpha_{G_Q} X_{Q_i}]\right)^2}{\sigma_D^2 + \frac{\alpha_2^2}{\alpha_1^2}\sigma_{J_m}^2}\end{aligned} \tag{4.29}$$

where γ_{MSB}^J and γ_{LSB}^J are only a function of X_{I_i}, X_{Q_i}, σ_D^2, and $\sigma_{J_m}^2$, of which σ_D^2 is a constant for a given set of parameters used in the HPA model and $\sigma_{J_m}^2$ only depends on the values of jammer power for each subcarrier. In addition, X_{I_i} and X_{Q_i} are constants which are multiplied by E_b. Therefore, at high SNR, the system still sees the same amount of degradation and subsequently produces an error floor. The same conclusion can be drawn for the case where the subcarrier is free from jammer.

When the channel response is not completely known, the phase error between the true

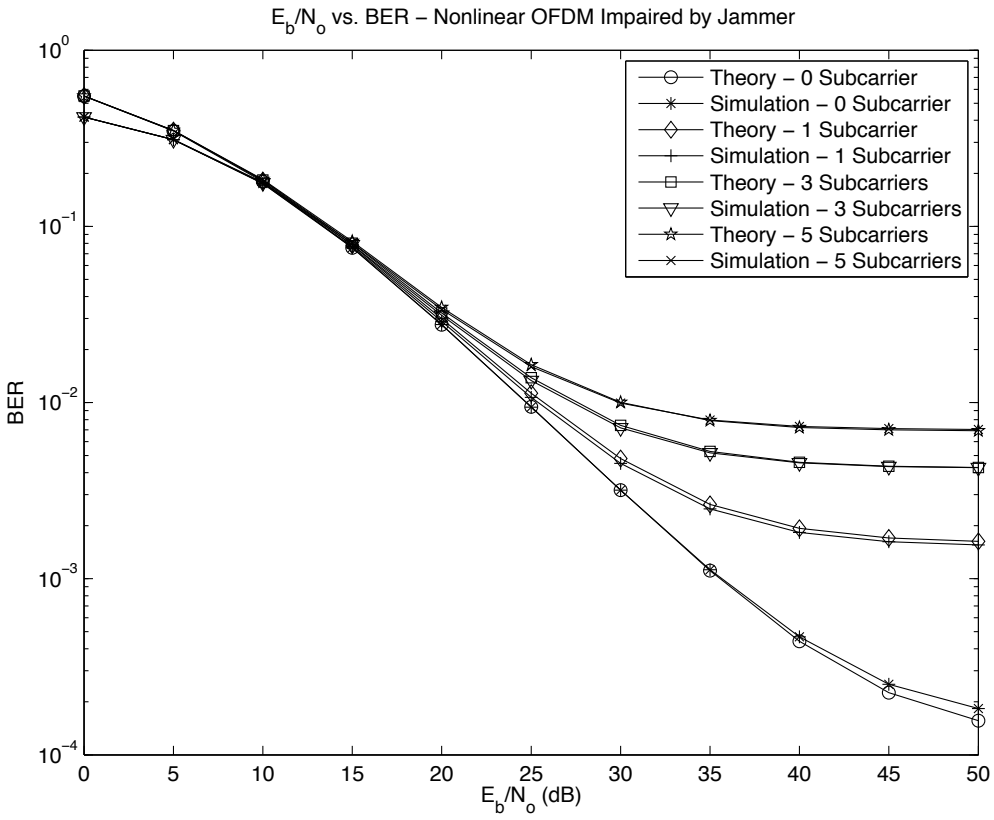

Figure 4.3 BER performance of the equalized 16-QAM OFDM system impaired by a nonlinear HPA and a jammer in the Rayleigh flat fading channel for various number of jammed subcarriers.

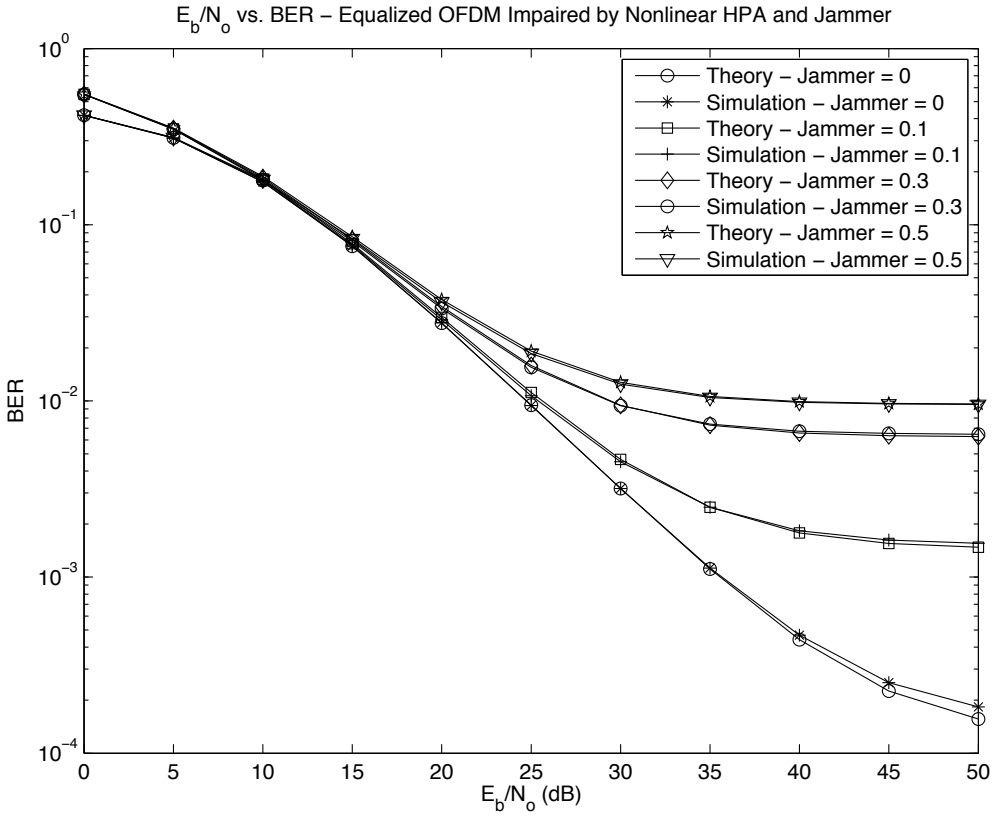

Figure 4.4 BER performance of the equalized 16-QAM OFDM system impaired by a nonlinear HPA and a jammer in the Rayleigh flat fading channel for various values of jamming power. The jammer is assumed to be present only in one of data subcarriers.

channel response and estimate introduces more degradation to the system. Fig. 4.6, 4.7 and 4.8 show the effect of channel estimation error on the performance of the system modeled based on the parameters of cases 4, 5, and 6.

4.6 Conclusion

In this chapter, we analyzed the performance of an equalized 16-QAM OFDM system which was impaired by a nonlinear HPA, channel estimation error and jammer through a Rayleigh fading channel. In addition, we proposed a more realistic jammer model by introducing a separate Rayleigh channel for the jammer. Due to the reason that not all the subcarriers are affected by the jammer, we derived the BER expression for the case where the subcarriers were under the influence of the jammer. Then, we showed that the BER for the case where the subcarriers were free from jammer can be obtained from the case where the jammer was interfering the subcarriers. The final BER expression for the system that was impaired by nonlinear HPA, channel estimation error and jammer

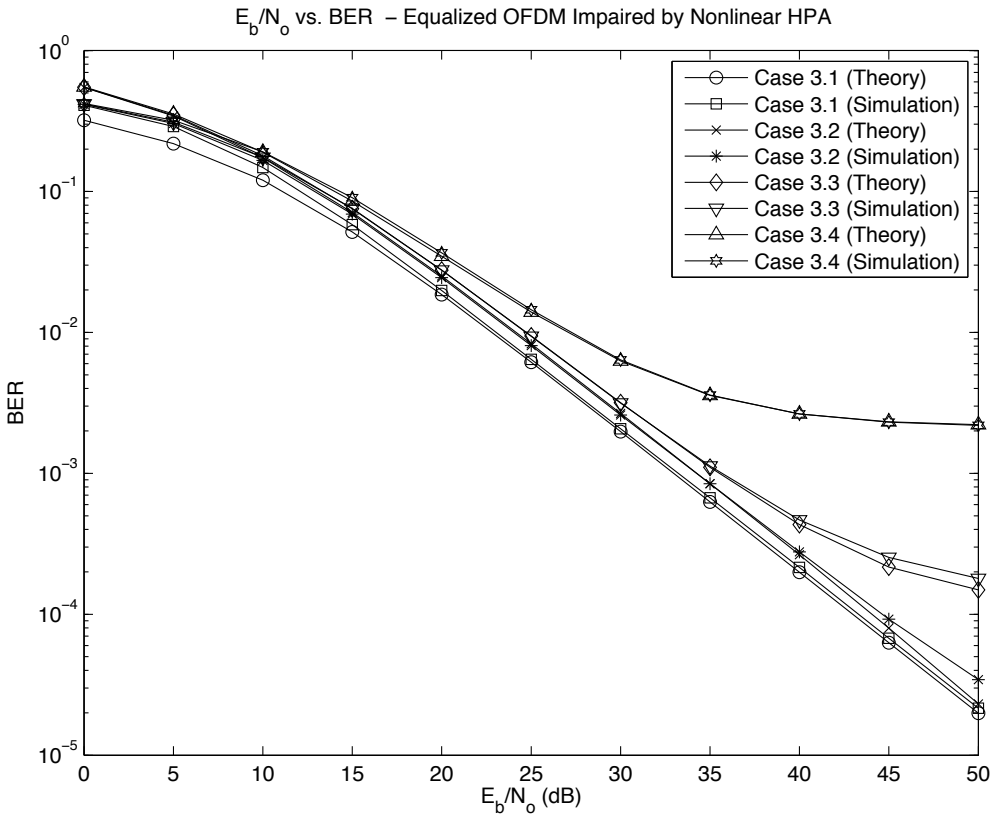

Figure 4.5 BER performance of the equalized 16-QAM OFDM system in the Rayleigh flat fading channel for various levels of degradation introduced by nonlinear HPAs.

was also presented for various sets of degradation. Based on the WLAN system in compliance with IEEE 802.11n standard, we presented simulation results along with theoretical values for various sets of parameters used in the system with and without channel estimation error.

The text in Chapter 4 is based on the material as it appears in:

David W. Chi and Pankaj Das, "Effect of Jammer on the Performance of OFDM In the Presence of Nonlinearity In Rayleigh Fading channel with Application to 802.11n WLAN", IEEE Military Communications Conference, October 2006, pp. 1-7.

The dissertation author was the primary researcher and author, and the co-author listed in the publication directed and supervised the research which forms the basis for this chapter.

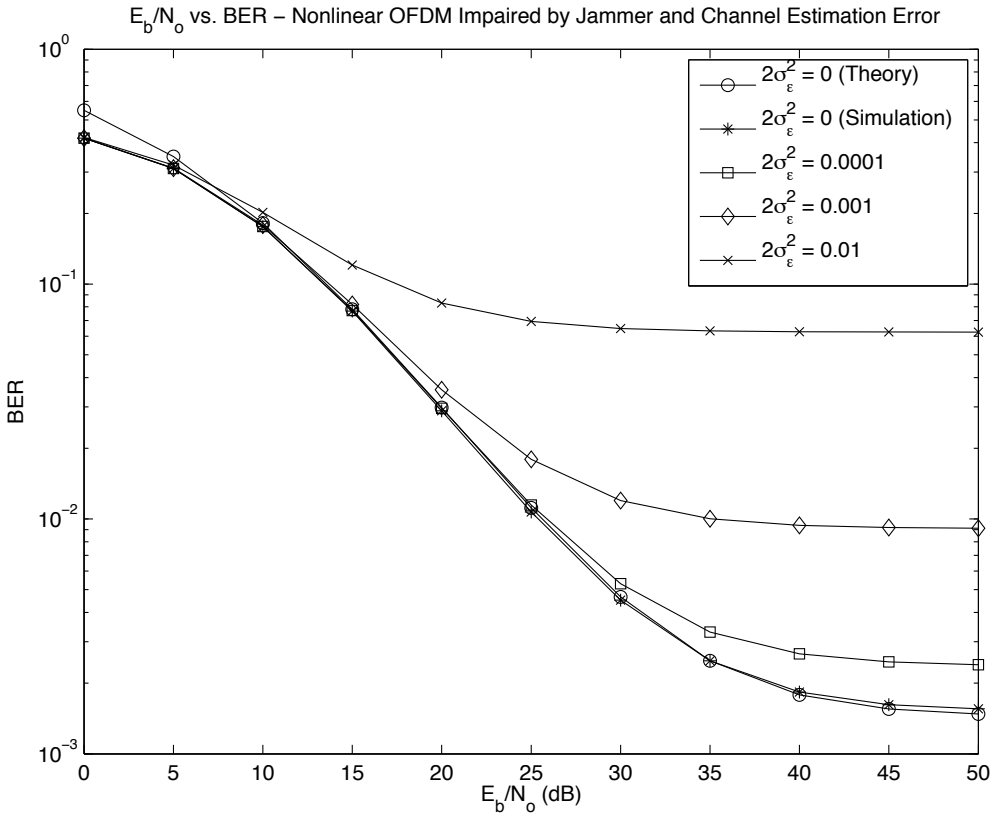

Figure 4.6 BER performance of an equalized 16-QAM OFDM system impaired by a nonlinear HPA, channel estimation error and jamming interference in 1 subcarrier in the Rayleigh flat fading channel for various values of $2\sigma_\epsilon^2$.

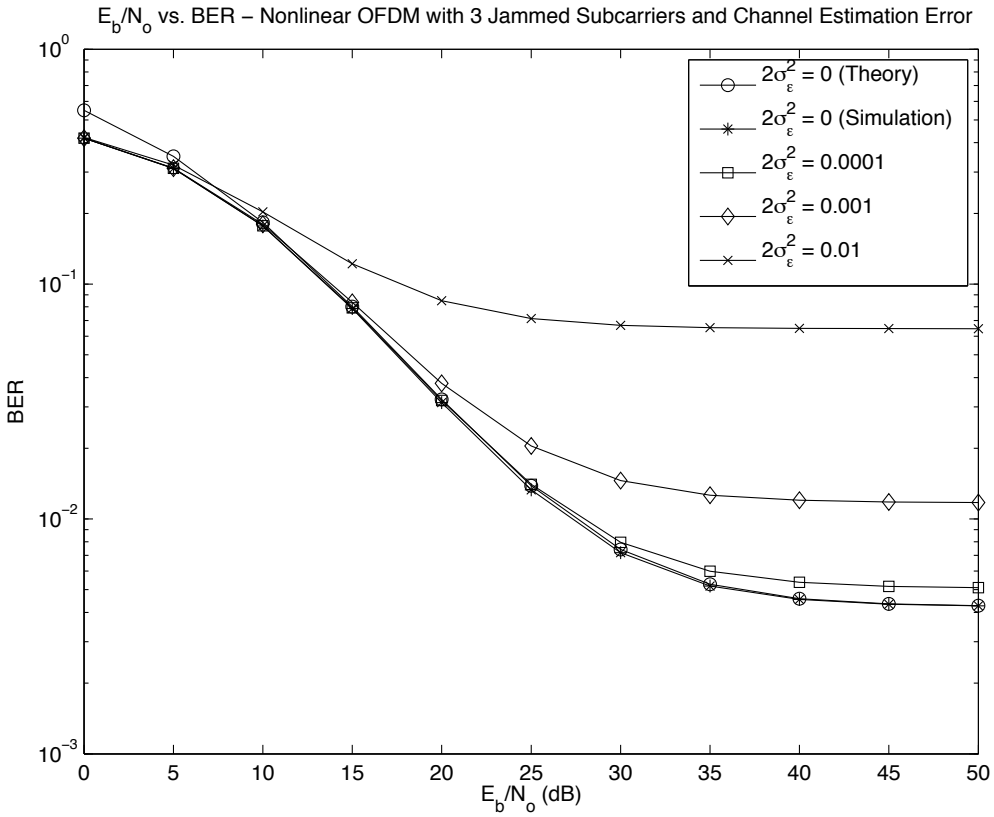

Figure 4.7 BER performance of an equalized 16-QAM OFDM system impaired by a nonlinear HPA, channel estimation error and jamming interference in 3 subcarriers in the Rayleigh flat fading channel for various values of $2\sigma_\epsilon^2$.

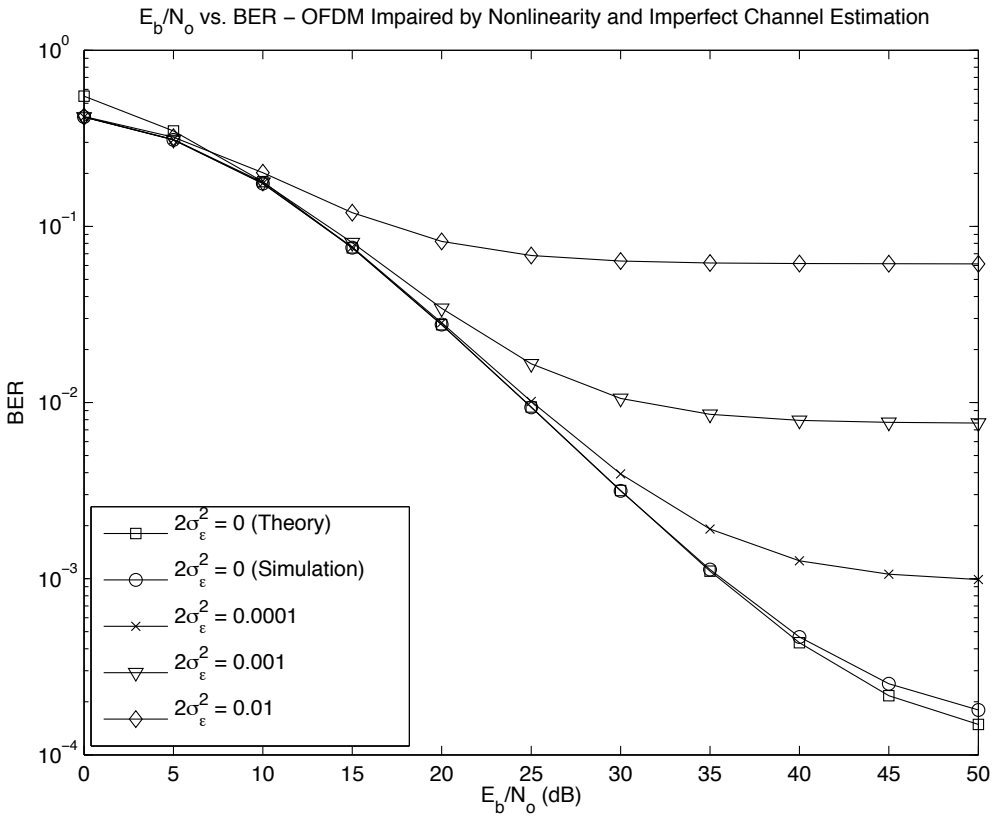

Figure 4.8 BER performance of an equalized 16-QAM OFDM system impaired by a nonlinear HPA and channel estimation error in the Rayleigh flat fading channel for various values of $2\sigma_\epsilon^2$.

5

Effects of Nonlinear Amplifier and Partial Band Jammer with Normalized Frequency Offset on the Performance of OFDM

5.1 Introduction

Over the years, Orthogonal Frequency Division Multiplexing (OFDM) has gained its popularity mainly due to its ability to deliver high data rate, high bandwidth efficiency and robustness in performance in fading channels. It has been chosen as a part of IEEE 802.11a and 802.11g standards [2, 3] and is currently being considered for the fourth generation (4G) mobile and Wireless Local Area Network (WLAN) communication systems. Different from the traditional Single Input Single Output (SISO) antenna configuration, Multiple Input Multiple Output (MIMO) antenna implementation provides an additional tool to further enhance the system's performance by utilizing more than one antenna for signal transmission and reception. The IEEE 802.11n incorporates both OFDM and MIMO technologies to improve the system's performance [4].

Although, OFDM can offer several technical advantages such as superior performance in fading channels and high data rate capability, by itself, it also has some design challenges such as sensitivity to phase noise or frequency offset [22, 23] and high peak to average power ratio (PAPR). The phenomenon of frequency offset is, in general, caused by the frequency deviation between the transmitter and receiver, or by Doppler shift. Unlike the frequency offset, the phase noise is usually a random process because the phase noise is often caused by the fluctuation of the receiver

and transmitter oscillators. When either the phase noise or the frequency offset is present in the system, the orthogonality between subcarriers is no longer valid. Subsequently, the inter-carrier interference (ICI) will occur and the system performance degrades [5]. Another disadvantage associated with OFDM is high PAPR which is due to the nature of Fast Fourier Transform (FFT) and Inverse Fast Fourier Transform (IFFT) operations. When L number of signals that have the same amplitude are added coherently in the IFFT and FFT processes, those processes produce a peak power that is L times larger than the average power as demonstrated in Fig. 2.1 in Section 2.1 of Chapter 2. The high magnitude in the signal forces practical amplifiers to operate at their nonlinear regions and subsequently, introduces clipping and spectral regrowth to the systems [24,25].

While there are some papers dealing with the effect of nonlinear distortion due to the high power amplifier (HPA) in OFDM systems in the additive white Gaussian noise (AWGN) channel, few of them adequately address the performance of an OFDM system in the presence of a nonlinear HPA through a Rayleigh fading channel. Even fewer analyze the combined effects of partial band jammer and nonlinear HPAs in OFDM systems through the Rayleigh fading channels. Costa, *et al.* [15] presented the performance analysis of an M-ary quadrature amplitude modulation (M-QAM) OFDM system with impairments from a nonlinear HPA and phase noise in AWGN channel only. In [26], the authors analyzed an equalized OFDM system in a Rayleigh fading channel for various modulations such as Binary Phase Shift Keying (BPSK), Quadrature Phase Shift Keying (QPSK), Differential Phase Shift Keying (DPSK) and QAM; however, the nonlinear distortion caused by a HPA and partial band jammer were not included in the performance analysis. In [27], an OFDM system with carrier interferometry spreading codes and narrowband interference in a Rayleigh fading channel was analyzed without considering the effect of nonlinear distortion. In addition, in the paper, the authors assumed that the source of jamming signal was very close to the receiver; hence, the jamming signal did not experience any channel effects. This particular assumption does not provide useful insights to the performance of an OFDM system in the presence of jammer because in many cases, the jamming sources are usually located in remote areas such as satellites in orbit or battleships at sea. Therefore, it is more reasonable and practical to assume that the jamming signal experiences another separate channel.

In Chapter 4, we analyzed the performance of an equalized M-QAM OFDM system that was subject to a nonlinear HPA, channel estimation error, and jamming in a Rayleigh flat fading channel. In contrast to the jammer model presented in [27] and to simulate a more realistic situation, we assumed that the jammer by itself experienced a separate channel response. In this chapter, we extend the jamming model that was presented in Chapter 4 to include the situations where the jamming signal is a collection of single tone signals which have an offset in frequency with respect to the desired signal. This assumption is generally valid because the jammer usually does not have knowledge of which frequency the desired signal is being transmitted. As a result, the jammer often

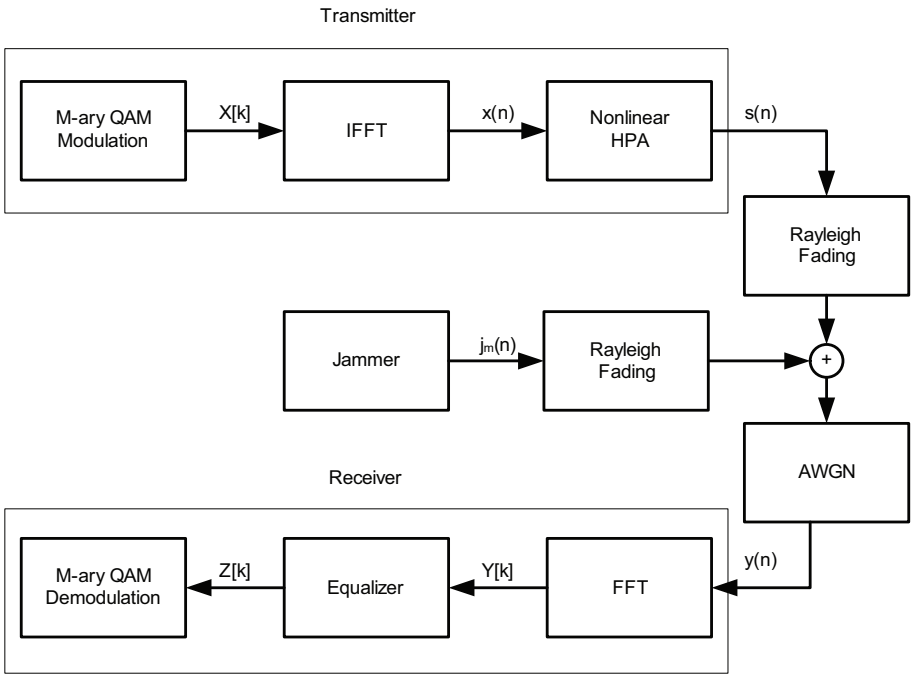

Figure 5.1 The block diagram of an equalized M-ary QAM (M-QAM) OFDM system which is impaired by a nonlinear HPA, channel estimation error and jamming in the Rayleigh fading channels.

transmits at a frequency that is slightly offset from the frequency that the receiver has locked onto and introduces varying amounts of interference to the system.

The chapter is organized as follows. In Section 5.2, the analytical model is presented and each component within is discussed in detail. Section 5.3 contains the performance analysis of the analytical model. Section 5.4 discusses the simulation setup for the extended model. Section 5.5 provides simulation results of the model described in Section 5.4. Finally, Section 5.6 summarizes the chapter.

5.2 System Description

The block diagram of the analytical model which consists of a transmitter, a wireless channel and a receiver is shown in Fig. 5.1. In addition, each component in the model is discussed in the following subsections.

5.2.1 Transmitter

The transmitter which is shown in Fig. 5.1 consists of a M-QAM modulator, IFFT and a nonlinear HPA. The input to the M-QAM modulator is assumed to be binary data bits which are equiprobable and statistically independent from each other. The stream of binary data bits are

grouped into blocks of size $log_2 M$. Each block is then mapped into M-QAM symbols, denoted as $X[k]$, according to the alphabet, $A = \{(2m-1-\sqrt{M})+j(2n-1-\sqrt{M})\}$ where $\{m, n = 1, 2, ...\sqrt{M}\}$ and M is the size of constellation. The output of the modulator is subsequently fed into and processed by IFFT. At appropriate sampling time, the signal at the output of the IFFT, denoted as $x(n)$, is

$$x(n) = \frac{1}{N}\sum_{k=0}^{N-1} X[k]e^{j\frac{2\pi nk}{N}} \qquad 0 \leq n \leq N-1 \tag{5.1}$$

where N is the number of subcarriers.

5.2.2 HPA Model

The nonlinear HPA model in the transmitter represents the nonlinear distortion imposed on the signal. In this chapter, the nonlinear HPA at the transmitter is modeled based on the Saleh model which has been described in Chapter 2, Section 2.3.

5.2.3 Jammer Model, Channel Model and AWGN

$j_m(n)$ represents the jamming signal in time domain and is expressed as

$$j_m(n) = \frac{1}{N}\sum_{k=0}^{N-1} J_m[k]e^{j\frac{2\pi n(k+\Delta k)}{N}} \tag{5.2}$$

where $J_m[k]$ represents the jamming signal for the k^{th} subcarrier and has power equal to $\frac{|J_m[k]|^2}{2}$. Furthermore, Δk represents the constant offset in frequency between the transmitted signal and the jamming signal.

The channel impulse response for the desired signal, $s(n)$, is a Rayleigh flat fading channel which is denoted as $h_1(n)$. The in-phase and quadrature components of $h_1(n)$ are modeled as zero mean and $\sigma^2_{H_1}$ variance Gaussian random variables. In addition, in-phase and quadrature components are assumed to be statistically independent of each other. Let $h_2(n)$ be the channel impulse response between the jammer and the receiver and is assumed to be another Rayleigh fading channel with zero mean and $2\sigma^2_{H_2}$ variance. Furthermore, the in-phase and quadrature components of the channel impulse response, $h_2(n)$, are assumed to be independent of each other. The thermal noise, denoted as $w(n)$, is modeled as an independent additive white Gaussian noise (AWGN) process which has zero mean and $2\sigma^2_w$ variance.

5.2.4 Receiver

The receiver is composed of a FFT, an equalizer and a M-QAM demodulator. Denote $y(n)$ as the received signal in time domain and assuming perfect synchronization, $y(n)$ is given by

$$y(n) = h_1(n)s(n) + h_2(n)j_m(n) + w(n) \tag{5.3}$$

After the FFT block, the received signal in frequency domain, denoted as $Y[k]$ in Fig. 5.1, is given by

$$\begin{aligned} Y[k] &= \sum_{n=0}^{N-1} y(n) e^{-j\frac{2\pi kn}{N}} \\ &= H_1[k]S[k] + H_2[k]J_m[k]\frac{1}{N}\sum_{n=0}^{N-1} e^{j\frac{2\pi\Delta kn}{N}} \\ &\quad + \sum_{n=0}^{N-1}\frac{1}{N}\sum_{\substack{l=0 \\ l\neq k}}^{N-1} J_m[l]H_2[l]e^{j\frac{2\pi(l+\Delta k-k)n}{N}} + W[k] \end{aligned} \tag{5.4}$$

where $H_1[k]$, $S[k]$, $H_2[k]$ and $W[k]$ are the FFT of $h_1(n)$, $s(n)$, $h_2(n)$ and $w(n)$, respectively. In the case where there is only a single tone jammer present in the channel, $Y[k]$ can be simplified further and becomes

$$Y[i] = \begin{cases} H_1[k]S[k] + H_2[k]J_m[k]\frac{1}{N}\sum_{n=0}^{N-1} e^{j\frac{2\pi\Delta kn}{N}} + W[k] & \text{if i=k} \\ H_1[l]S[l] + \sum_{n=0}^{N-1}\frac{1}{N}J_m[k]H_2[k]e^{j\frac{2\pi(k+\Delta k-l)n}{N}} + W[l] & \text{if i}\neq\text{k} \end{cases} \tag{5.5}$$

where i represents the subcarrier index.

5.2.5 Equalizer Model

One of the most attractive features of OFDM systems is the simplicity in the equalization process which is adequately done by using a one-tap equalizer in the frequency domain. Among many available algorithms, we choose the Zero Forcing algorithm because of its simplicity in implementation.

Before the equalizing the received signal, estimating the channel response is necessary. The estimate can be obtained with the aid of pilots. Let $X[P_1], X[P_2], ..., X[P_p]$ be the pilot symbols modulated onto the subcarriers, $P_1, P_2, ..., P_p$, where p is the total number of pilots. Using Least Squares, the estimated channel response at the pilot subcarriers is

$$\hat{H}[P_i] = \frac{Y[P_i]}{X[P_i]} \qquad i = 1, 2, ..., p \tag{5.6}$$

where $Y[P_i]$ is the received signal at the pilot subcarrier, P_i. Afterward, the estimated channel response at the data subcarriers is obtained by interpolating between two consecutive pilots.

After obtaining the estimate, the equalized signal which is represented by $Z[k]$ is given

by

$$\begin{aligned} Z[k] =& \frac{Y[k]}{\hat{H}_1[k]} \\ =& \frac{H_1[k]}{\hat{H}_1[k]} S[k] + \frac{H_2[k]}{\hat{H}_1[k]} J_m[k] \frac{1}{N} \sum_{n=0}^{N-1} e^{j\frac{2\pi\Delta kn}{N}} \\ &+ \frac{1}{\hat{H}_1[k]} \sum_{n=0}^{N-1} \frac{1}{N} \sum_{\substack{l=0 \\ l\neq k}}^{N-1} J_m[l] H_2[l] e^{j\frac{2\pi(l+\Delta k-k)n}{N}} + \frac{W[k]}{\hat{H}_1[k]} \end{aligned} \tag{5.7}$$

where $\hat{H}_1[k]$ is the estimate of the channel, $H_1[k]$ and is defined as

$$\hat{H}_1[k] = H_1[k] + \epsilon_1[k] \tag{5.8}$$

In addition, the variable $\epsilon_1[k]$ is modeled as a complex Gaussian random process with zero mean and $2\sigma_\epsilon^2$ variance.

5.3 Performance Analysis

In this section, we will present the derivation of the bit error rate (BER) expression. In addition, the BER will later be used as a measure of system performance. The performance analysis of the system, shown in Fig. 5.1, starts with the characterization of $x(n)$. Under the assumption that N is large and applying the *Central Limit Theorem*, $x(n)$ is said to be Gaussian distributed with zero mean [19]. With that assumption, Banelli, *et al.* [20] had shown that $s(n)$ can be written as a product of a complex gain, α_G, and the input signal, $x(n)$, added with noise distortion $d_G(n)$. The transmitted signal, denoted as $s(n)$, and its FFT are given by

$$s(n) = \alpha_G x(n) + d_G(n) \overset{FFT}{\longleftrightarrow} S[k] = \alpha_G X[k] + D_G[k] \tag{5.9}$$

where $D_G[k]$ was shown to be a complex Gaussian random variable with zero mean and $2\sigma_{D_G}^2$ variance. In addition, the numerical value of σ_D^2 can be obtained by following steps outlined in Section 2.4 of Chapter 2. For two different subcarriers, k_1 and k_2, $D_G[k_1]$ and $D_G[k_2]$ are mutually independent. Furthermore, the in-phase and quadrature phase components of $D_G[k]$ were shown to be mutually independent and identically distributed (i.i.d) [15]. The multiplicative coefficient α_G in (5.9) is given by

$$\alpha_G = \frac{E\{s(n)^* x(n)\}}{2\sigma_{x(n)}^2} = \alpha_{G_I} + j\alpha_{G_Q} \tag{5.10}$$

where $(\cdot)^*$ denotes the complex conjugate operation [20] and $E\{\cdot\}$ is the expected value. The subscripts I and Q represent the in-phase and quadrature components of the signal.

Under the assumption of perfect synchronization and after removing the preamble sequences and cyclic prefix, the equalized signal can be obtained by substituting (5.9) into (5.7). With

the substitution and mathematical simplification, the equalized signal, $Z[k]$, is found as

$$\begin{aligned} Z[k] =& \frac{\alpha_1}{\hat{\alpha}_1} e^{j\theta} \alpha_G X[k] + \underbrace{\frac{\alpha_1}{\hat{\alpha}_1} e^{j\theta} D_G[k]}_{\Psi_{HPA}[k]} + \underbrace{\frac{\alpha_2}{\hat{\alpha}_1} e^{j\phi} J_m[k] \frac{1}{N} \sum_{n=0}^{N-1} e^{j\frac{2\pi\Delta kn}{N}}}_{J_D[k]} \\ &+ \underbrace{\frac{1}{\hat{H}_1[k]} \sum_{n=0}^{N-1} \frac{1}{N} \sum_{\substack{l=0 \\ l\neq k}}^{N-1} J_m[l] H_2[l] e^{j\frac{2\pi(l+\Delta k-k)n}{N}}}_{J_o[k]} + \frac{W[k] e^{-j\angle \hat{H}_1[k]}}{\hat{\alpha}_1} \\ =& \frac{\alpha_1}{\hat{\alpha}_1} e^{j\theta} \alpha_G X[k] + \Xi[k] \end{aligned} \tag{5.11}$$

where

$$\begin{aligned} &\alpha_1 = |H_1|, \quad \hat{\alpha}_1 = |\hat{H}_1|, \quad \alpha_2 = |H_2| \\ &\theta = \angle H_1 - \angle \hat{H}_1, \quad \phi = \angle H_2 - \angle \hat{H}_1 \end{aligned} \tag{5.12}$$

and $\Xi[k]$ is defined as

$$\Xi[k] = \Psi_{HPA}[k] + J_D[k] + J_o[k] + \frac{W[k] e^{-j\angle \hat{H}_1[k]}}{\hat{\alpha}_1} \tag{5.13}$$

In addition, the terms $\Psi_{HPA}[k]$, $J_D[k]$ and $J_o[k]$ are defined as shown in (5.11).

Fig. 5.2 shows the effect of a single tone jammer on the OFDM signals for the case where the normalized frequency offset is nonzero. For the purpose of a comparison, Fig. 4.2 in Section 4.2.4 of Chapter 4 shows the situation where the normalized frequency offset is zero. In this particular case, the jamming signal only has impact on the BER of the subcarriers that it is present. When the normalized frequency offset is nonzero, the orthogonality between the subcarriers in the jamming signal is no longer valid. This leads to the situation where the jamming signal is slightly offset from the frequencies of the subcarriers. As a consequence, all the subcarriers are affected with the varying amount of jamming power because the magnitude of the jamming signal is nonzero at all subcarriers.

The same conclusion can be drawn by looking at (5.11). One can observe the effect of the normalized frequency offset that is due to the mismatch between the frequencies of jamming and desired signals. When the jammer has prior knowledge about the frequency of the desired signal, i.e. the frequency offset is zero, $J_D[k]$ which is due to the jammer is the only source of jamming interference present in the received signal aside from nonlinear distortion and AWGN. In the case where the jammer does not have knowledge about the frequency of desired signal and the frequency offset is nonzero, not only is $J_D[k]$ present in the system, but the jammer produces an additional interference, denoted as $J_o[k]$ in (5.11), which behaves like ICI and causes further degradation in the BER performance.

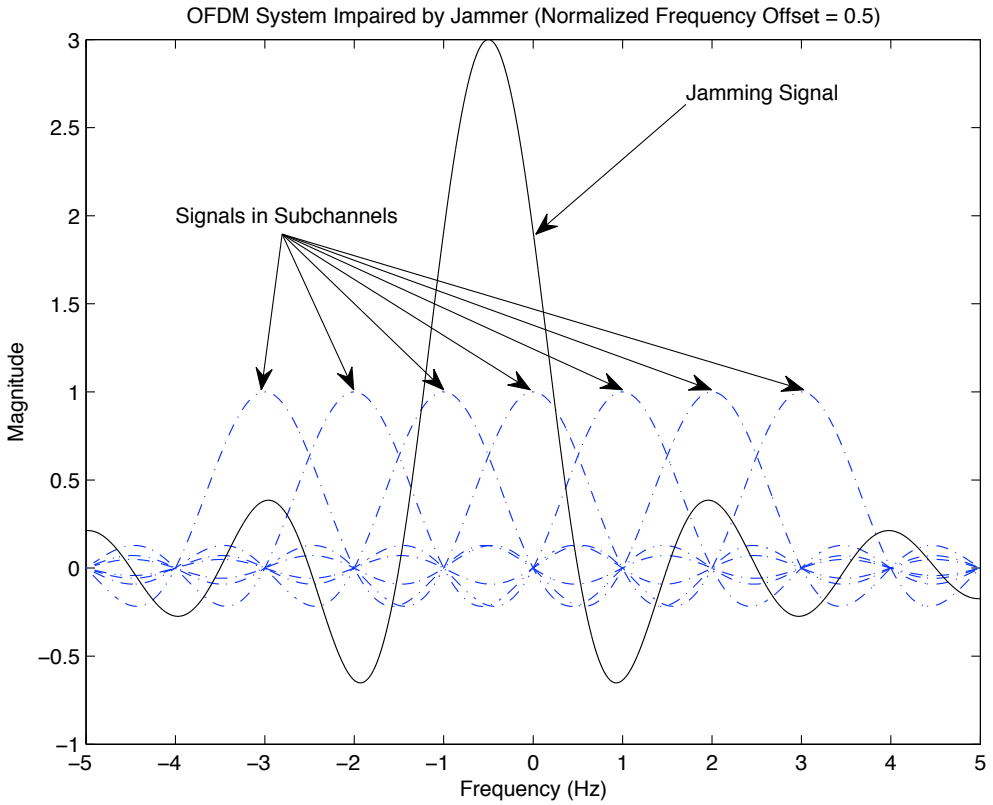

Figure 5.2 An illustration of the effect of a single tone jammer with the normalized frequency offset = 0.5 on the OFDM signals

In order to calculate the BER of the system, it is necessary to find the means and the variances of the noise, $\Xi[k]$,which is a sum of $\Psi_{HPA}[k]$, $J_D[k]$, $J_o[k]$ and $\frac{W[k]e^{-j\angle\hat{H}_1[k]}}{\hat{\alpha}_1}$. The mean for each term, conditioned on H_1, $\hat{H}_1$ and H_2, is zero based on the model. Let σ^2_Ψ be the variance of the in-phase or the quadrature components of $\Psi_{HPA}[k]$, then conditioned on the channel responses, σ^2_Ψ is found to be

$$\sigma^2_\Psi = E\left\{\Psi_{HPA}[k]\Psi^*_{HPA}[k]\right\} = E\left\{\left(\frac{\alpha_1}{\hat{\alpha}_1}e^{j\theta}D_G[k]\right)\left(\frac{\alpha_1^*}{\hat{\alpha}_1^*}e^{-j\theta}D^*_G[k]\right)\right\} = \frac{\alpha_1^2}{\hat{\alpha}_1^2}\sigma^2_{D_G} \tag{5.14}$$

Before calculating the variance of J_D, we need to simplify the expression of J_D further by utilizing the Geometric series. By definition, the Geometric series is given by [29]

$$\sum_{i=0}^{N-1}\alpha^i = \frac{1-\alpha^N}{1-\alpha} \qquad |\alpha| < 1 \tag{5.15}$$

Applying (5.15), J_D becomes

$$\begin{aligned}
J_D[k] =& \frac{\alpha_2}{\hat{\alpha}_1} e^{j\phi} J_m[k] \frac{1}{N} \left(\frac{1 - e^{j\frac{2\pi\Delta k}{N} N}}{1 - e^{j\frac{2\pi\Delta k}{N}}} \right) \\
=& \frac{\alpha_2}{\hat{\alpha}_1} e^{j\phi} J_m[k] \frac{1}{N} \left[\frac{e^{j\pi\Delta k}(e^{-j\pi\Delta k} - e^{j\pi\Delta k})}{e^{j\frac{\pi\Delta k}{N}}(e^{-j\frac{\pi\Delta k}{N}} - e^{j\frac{\pi\Delta k}{N}})} \right] \\
=& \frac{\alpha_2}{\hat{\alpha}_1} e^{j\phi} J_m[k] \frac{1}{N} e^{j\pi\Delta k\left(1-\frac{1}{N}\right)} \frac{\sin(\pi\Delta k)}{\sin\left(\frac{\pi\Delta k}{N}\right)}
\end{aligned} \tag{5.16}$$

Denote $\sigma^2_{J_D}$ as the variance for the in-phase or the quadrature component of J_D conditioned on the channel responses. The variance, $\sigma^2_{J_D}$, is expressed as

$$\begin{aligned}
\sigma^2_{J_D} =& E\left\{ J_D[k] J_D^*[k] \right\} \\
=& E\left\{ \left[\frac{\alpha_2}{\hat{\alpha}_1} e^{j\phi} J_m[k] \frac{1}{N} e^{j\pi\Delta k\left(1-\frac{1}{N}\right)} \frac{\sin(\pi\Delta k)}{\sin\left(\frac{\pi\Delta k}{N}\right)} \right] \left[\frac{\alpha_2^*}{\hat{\alpha}_1^*} e^{-j\phi} J_m^*[k] \frac{1}{N} e^{-j\pi\Delta k\left(1-\frac{1}{N}\right)} \frac{\sin(\pi\Delta k)}{\sin\left(\frac{\pi\Delta k}{N}\right)} \right] \right\} \\
=& \frac{\alpha_2^2}{\hat{\alpha}_1^2} \frac{1}{N^2} \left[\frac{\sin^2(\pi\Delta k)}{\sin^2(\frac{\pi\Delta k}{N})} \right] \frac{|J_m[k]|^2}{2}
\end{aligned} \tag{5.17}$$

The ICI-like interference, $J_o[k]$, which is due to the jammer can also be expanded by using the Geometric series. Subsequently, $J_o[k]$ becomes

$$\begin{aligned}
J_o[k] =& \frac{1}{\hat{H}_1[k]} \frac{1}{N} \sum_{\substack{l=0 \\ l \neq k}}^{N-1} J_m[l] H_2[l] e^{j\pi(l+\Delta k-k)\left(1-\frac{1}{N}\right)} \left[\frac{\sin\left(\pi(l+\Delta k-k)\right)}{\sin\left(\frac{\pi(l+\Delta k-k)}{N}\right)} \right] \\
=& \frac{1}{\hat{H}_1[k]} \frac{1}{N} \sum_{l=0}^{N-1} J_m[l] H_2[l] e^{j\pi(l+\Delta k-k)\left(1-\frac{1}{N}\right)} \left[\frac{\sin\left(\pi(l+\Delta k-k)\right)}{\sin\left(\frac{\pi(l+\Delta k-k)}{N}\right)} \right] \\
& - \frac{1}{\hat{H}_1[k]} \frac{1}{N} J_m[k] H_2[k] e^{j\pi\Delta k\left(1-\frac{1}{N}\right)} \left[\frac{\sin\left(\pi\Delta k\right)}{\sin\left(\frac{\pi\Delta k}{N}\right)} \right]
\end{aligned} \tag{5.18}$$

Let $\sigma^2_{J_o}$ be the variance for in-phase or quadrature component of (5.18) conditioned on the channel responses, then $\sigma^2_{J_o}$ is found to be

$$\begin{aligned}
\sigma^2_{J_o} =& E\left\{ J_o[k] J_o^*[k] \right\} \\
=& \frac{1}{\hat{\alpha}_1^2} \frac{1}{N^2} \sum_{l=0}^{N-1} \frac{|J_m[l]|^2}{2} \alpha_2^2 \left[\frac{\sin^2\left(\pi(l+\Delta k-k)\right)}{\sin^2\left(\frac{\pi(l+\Delta k-k)}{N}\right)} \right] \\
& - \frac{1}{\hat{\alpha}_1^2} \frac{1}{N^2} \left[\frac{\sin\left(\pi\Delta k\right)}{\sin\left(\frac{\pi\Delta k}{N}\right)} \right] \sum_{l=0}^{N-1} E\{ J_m[l] J_m^*[k] \} \alpha_2^2 e^{j\pi(l-k)\left(1-\frac{1}{N}\right)} \left[\frac{\sin\left(\pi(l+\Delta k-k)\right)}{\sin\left(\frac{\pi(l+\Delta k-k)}{N}\right)} \right] \\
& - \frac{1}{\hat{\alpha}_1^2} \frac{1}{N^2} \left[\frac{\sin\left(\pi\Delta k\right)}{\sin\left(\frac{\pi\Delta k}{N}\right)} \right] \sum_{l=0}^{N-1} E\{ J_m^*[l] J_m[k] \} \alpha_2^2 e^{-j\pi(l-k)\left(1-\frac{1}{N}\right)} \left[\frac{\sin\left(\pi(l+\Delta k-k)\right)}{\sin\left(\frac{\pi(l+\Delta k-k)}{N}\right)} \right] \\
& + \frac{\alpha_2^2}{\hat{\alpha}_1^2} \frac{1}{N^2} \frac{|J_m[k]|^2}{2} \left[\frac{\sin^2\left(\pi\Delta k\right)}{\sin^2\left(\frac{\pi\Delta k}{N}\right)} \right]
\end{aligned} \tag{5.19}$$

Finally, the conditional variance for $\frac{W[k]e^{-j\angle\hat{H}_1[k]}}{\hat{\alpha}_1}$, denoted as σ^2, is given by

$$\sigma^2 = E\left\{\left[\frac{W[k]e^{-j\angle\hat{H}_1[k]}}{\hat{\alpha}_1}\right]\left[\frac{W^*[k]e^{j\angle\hat{H}_1[k]}}{\hat{\alpha}_1}\right]\right\} = \frac{\sigma_w^2}{\hat{\alpha}_1^2} \tag{5.20}$$

Further expanding $Z[k]$ into its in-phase and quadrature components, then $Z[k]$ becomes

$$\begin{aligned} Z[k] =& \frac{\alpha_1}{\hat{\alpha}_1}(\cos\theta + j\sin\theta)(\alpha_{G_I} + j\alpha_{G_Q})(X_I[k] + jX_Q[k]) + \Xi[k] \\ =& Z_I + jZ_Q \end{aligned} \tag{5.21}$$

where $Z_I[k]$ and $Z_Q[k]$ are defined as

$$\begin{aligned} Z_I[k] =& \frac{\alpha_1}{\hat{\alpha}_1}[\cos\theta\alpha_{G_I}X_I[k] - \cos\theta\alpha_{G_Q}X_Q[k] - \sin\theta\alpha_{G_I}X_Q[k] - \sin\theta\alpha_{G_Q}X_I[k]] + \Xi_I[k] \\ Z_Q[k] =& \frac{\alpha_1}{\hat{\alpha}_1}[\cos\theta\alpha_{G_I}X_Q[k] + \cos\theta\alpha_{G_Q}X_I[k] + \sin\theta\alpha_{G_I}X_I[k] - \sin\theta\alpha_{G_Q}X_Q[k]] + \Xi_Q[k] \end{aligned} \tag{5.22}$$

To continue the derivation, we assume that 16-QAM modulation is utilized in the system. Nevertheless, the BER expression for other rectangular QAM constellations can be derived in the similar fashion. It has been mentioned already that all the subcarriers are affected with varying amount of jamming power due to the nonzero normalized frequency offset that is between the jamming and desired signals. To obtain the unconditional BER, one needs to first calculate the conditional BER for each subcarrier and then take an average of the BER contributions over all subcarriers.

Let $P^k_{BER|\alpha_1,\alpha_2,\hat{\alpha}_1,\theta}$ be the conditional BER of 16-QAM conditioned on α_1, α_2, $\hat{\alpha}_1$, and θ for the k^{th} subcarrier, then $P^k_{BER|\alpha_1,\alpha_2,\hat{\alpha}_1,\theta}$ is given by

$$P^k_{BER|\alpha_1,\alpha_2,\hat{\alpha}_1,\theta} = \frac{1}{2}\left(P^k_{MSB} + P^k_{LSB}\right) \tag{5.23}$$

where P^k_{MSB} and P^k_{LSB} are the conditional BER of most significant bits (MSB) and least significant bits (LSB) of 16-QAM symbols conditioned on α_1, α_2, $\hat{\alpha}_1$, and θ for the k^{th} subcarrier. Based on the decision boundaries given in [28], the conditional BER of MSB for the k^{th} subcarrier is given by

$$P^k_{MSB} = P(Z_I < 0|\alpha_1, \hat{\alpha_1}, \theta, \alpha_2) = \frac{1}{8}\sum_{i=1}^{8} Q\left(\sqrt{\frac{(\Upsilon_i)^2}{\sigma^2_\Xi}}\right) \tag{5.24}$$

where $\Upsilon_i = \frac{\alpha_1}{\hat{\alpha}_1}[\cos\theta\alpha_{G_I}X_{I_i} - \cos\theta\alpha_{G_Q}X_{Q_i} - \sin\theta\alpha_{G_I}X_{Q_i} - \sin\theta\alpha_{G_Q}X_{I_i}]$ and $\sigma^2_\Xi = (\sigma^2_\Psi + \sigma^2_{J_D} + \sigma^2_{J_o} + \sigma^2)$. In addition, $Q(\nu) = \int_\nu^\infty \frac{1}{\sqrt{2\pi}}e^{\frac{-t^2}{2}}dt, \nu \geq 0$. The numerical values for X_{I_i} and X_{Q_i} in (5.24) are listed in Table 5.1. The conditional BER of LSB can be found in the similar way. Based on the decision boundaries, P^k_{LSB} is given by

$$\begin{aligned} P^k_{LSB} =& \{P(Z_I < -2d|\alpha_1, \hat{\alpha_1}, \theta, \alpha_2) + P(Z_I > 2d|\alpha_1, \hat{\alpha_1}, \theta, \alpha_2)\}|_{LSB=0} \\ &+ \{P(-2d < Z_I < 2d|\alpha_1, \hat{\alpha_1}, \theta, \alpha_2)\}|_{LSB=1} \\ =& \frac{1}{8}\sum_{i=1}^{16}\lambda_i Q\left(\sqrt{\frac{(\kappa_i 2d + \zeta_i\Upsilon_i)^2}{\sigma^2_\Xi}}\right) \end{aligned} \tag{5.25}$$

Table 5.1 Numerical Values of Variables in Conditional BER for MSB

Index i	X_{I_i}	X_{Q_i}	Index i	X_{I_i}	X_{Q_i}
1	d	$3d$	5	$3d$	$3d$
2	d	d	6	$3d$	d
3	d	$-d$	7	$3d$	$-d$
4	d	$-3d$	8	$3d$	$-3d$

Table 5.2 Numerical Values and Signs of Variables in Conditional BER for LSB

Index i	λ_i	κ_i	ζ_i	X_{I_i}	X_{Q_i}	Index i	λ_i	κ_i	ζ_i	X_{I_i}	X_{Q_i}
1	+	+	+	d	$3d$	9	+	-	-	$-3d$	$3d$
2	+	+	-	d	$3d$	10	-	+	-	$-3d$	$3d$
3	+	+	+	d	d	11	+	-	-	$-3d$	d
4	+	+	-	d	d	12	-	+	-	$-3d$	d
5	+	+	+	d	$-d$	13	+	-	-	$-3d$	$-d$
6	+	+	-	d	$-d$	14	-	+	-	$-3d$	$-d$
7	+	+	+	d	$-3d$	15	+	-	-	$-3d$	$-3d$
8	+	+	-	d	$-3d$	16	-	+	-	$-3d$	$-3d$

where $|_{LSB=0}$ and $|_{LSB=1}$ denote the boundaries for LSB is zero and one, respectively. In (5.25), λ_i, κ_i, and ζ_i are signs of the values for i^{th} quantity and are listed along with values for X_{I_i} and X_{Q_i} in Table 5.2. Finally, in both Tables 5.1 and 5.2, $d^2 = \frac{2E_b}{5}$ where E_b is the energy per bit.

To obtain the unconditional BER, we first need to average the conditional BER over the probability density functions (PDFs) of α_1, $\hat{\alpha}_1$, θ and α_2 for each subcarrier. Next, we average the result over all the subcarriers to obtain the final result. Denote P_{BER} as the unconditional BER, then P_{BER} is found as

$$P_{BER} = \frac{1}{N}\sum_{k=0}^{N-1}\int_0^\infty\int_0^\infty\int_0^\infty\int_{-\pi}^{\pi} P^k_{BER|\alpha_1,\alpha_2,\hat{\alpha}_1,\theta} p(\alpha_1,\hat{\alpha}_1,\theta)p(\alpha_2)d\alpha_1 d\hat{\alpha}_1 d\theta d\alpha_2 \tag{5.26}$$

where $p(\alpha_1,\hat{\alpha}_1,\theta)$ denotes the joint PDF of α_1, $\hat{\alpha}_1$ and θ and is defined as

$$p(\alpha_1,\hat{\alpha}_1,\theta) = \frac{\alpha_1\hat{\alpha}_1}{2\pi|\Delta|^{\frac{1}{2}}} exp\left\{-\frac{[\sigma^2_{\hat{H}_1}\alpha_1^2 + \sigma^2_{H_1}\hat{\alpha}_1^2 - 2R_c\alpha_1\hat{\alpha}_1\cos\theta - 2R_{cs}\alpha_1\hat{\alpha}_1\sin\theta]}{2|\Delta|^{\frac{1}{2}}}\right\} \tag{5.27}$$

where

$$\begin{aligned}
&\sigma^2_{H_1} = E\{H^2_{1_I}\} = E\{H^2_{1_Q}\}, \qquad R_c = E\{H_{1_I}\hat{H}_{1_I}\} = E\{H_{1_Q}\hat{H}_{1_Q}\}\\
&\sigma^2_{\hat{H}_1} = E\{\hat{H}^2_{1_I}\} = E\{\hat{H}^2_{1_Q}\}, \qquad R_{cs} = E\{H_{1_I}\hat{H}_{1_Q}\} = -E\{H_{1_Q}\hat{H}_{1_I}\}\\
&|\Delta| = \left[\sigma^2_{H_1}\sigma^2_{\hat{H}_1} - R_c^2 - R_{cs}^2\right]^2
\end{aligned} \tag{5.28}$$

In addition, $p(\alpha_2)$ is the PDF of α_2 and is defined as

$$p(\alpha_2) = \frac{\alpha_2}{\sigma^2_{H_2}} e^{\frac{-\alpha_2^2}{2\sigma^2_{H_2}}} \tag{5.29}$$

Table 5.3 Summary of Simulation Cases

Case	$\|J_m\|$	HPA	Jamming Tones	Δk	$2\sigma_\epsilon^2$
1	Varying	Linear	1	Varying	0
2	0	Varying	0	0	0
3	Varying	Constant	1	0.5	0
4	0.5	Constant	Varying	0.5	0
5	0.1	Constant	1	0.5	Varying

For perfect channel estimation, i.e. $H_1 = \hat{H}_1$, (5.26) is reduced to a double integral, namely

$$P_{BER} = \frac{1}{N}\sum_{k=0}^{N-1}\int_0^\infty\int_0^\infty P^k_{BER|\alpha_1,\alpha_2}p(\alpha_2)p(\alpha_1)d\alpha_1 d\alpha_2 \tag{5.30}$$

where $p(\alpha_1)$ can be obtained by substituting α_2 and $\sigma^2_{H_2}$ in (5.29) for α_1 and $\sigma^2_{H_1}$, respectively. If we further assume that the jammer does not exist in the channel, the unconditional BER for 16-QAM reduces to

$$P_{BER} = \frac{1}{N}\sum_{k=0}^{N-1}\int_0^\infty P^k_{BER|\alpha_1}p(\alpha_1)d\alpha_1 \tag{5.31}$$

Finally, in the case where the HPA is ideal, i.e. $\alpha_G = 1$ and $D_G = 0$, and perfect channel estimation is achieved, (5.31) is further reduced to the known result ([26], Eq:69).

5.4 Simulation Model and Parameters

The simulation model, programmed using Matlab Simulink, is an extension of the analytical model described in Section 5.2 in compliance with the IEEE 802.11n standard ([4], Clause 10.4.4.2 rate code 73); except the convolutional encoder, interleaver/deinterleaver and Viterbi decoder are omitted. After pre-appending 16-bit Service Field and padding enough bits to ensure the transmission from each antenna are multiples of whole OFDM symbols, the resulting signal is scrambled with a scrambler that is based on the IEEE 802.11a standard and subsequently demultiplexed alternately across the transmitter spatial streams. In each spatial stream, the data is modulated with the 16-QAM modulation and processed with the 64-point IFFT, of which subcarriers, $\pm$ 21, are designated for pilots. The OFDM symbol is then cyclically extended and pre-appended with the preamble sequences as specified in [4] before transmission. To recover the data, the corresponding receiver reverses the encoding procedure in the transmitter.

The channel, jammer and the equalizer are modeled as described in Section 5.2.3 and Section 5.2.5, respectively. Without loss of generality, the statistical means and variances are set to 0 and 1, respectively, in both Rayleigh fading channels. The simulations are performed for several cases and the parameters used for all cases are summarized in Table 5.3. In case 1, it is assumed that there is only a single tone jammer whose jamming amplitude is set to 1, 3 and 5 while Δk

Table 5.4 Simulation Parameters for Nonlinear HPA Model

Case	α_{AM}	β_{AM}	α_{PM}	β_{PM}
2.1	1	0	0	0
2.2	1	0.25	π	0.25
2.3	1	0.25	1.2π	0.01
2.4	1	0.25	1.5π	0.01

for each amplitude varies from 0 to 1 with 0.1 increment. In addition, the HPA is assumed to be linear. In case 2, the jammer is removed to consider only the influence from the nonlinear HPA in the system. The level of nonlinear distortion is varied based on the parameters in the HPA model which is described in Section 5.2.2 and the numerical values of those parameters are listed in Table 5.4. Note that in Case 2.1, when α_{AM} is set to unity and the other parameters in the model are zero, the nonlinear HPA becomes a linear amplifier which has an unity gain with no phase distortion.

For case 3, the number of jamming tones in the jammer is assumed to be one and the jamming amplitude is set to 0, 0.1, 0.3 and 0.5 while Δk is set to a constant value of 0.5. In case 4, the jamming amplitude and frequency offset, Δk, are both set to 0.5 and 0.5, respectively, while the number of jamming tones in the jammer varies. In the first four cases, it is assumed that there is no error in estimating the channel response. For the last case, the system is subject to a nonlinear HPA and a single tone jammer whose amplitude is 0.1 and is transmitted with the frequency offset that is equal to 0.5. In this case, it is assumed that the error is present in the channel estimation. Finally, in cases 3, 4 and 5, the HPA is assumed to be nonlinear. For those cases, the α_{AM} and β_{AM} are 1 and 0.25, and α_{PM} and β_{PM} are 1.2π and 0.01, respectively.

5.5 Simulation Results

In the first case where we assume the frequency offset, Δk, varies from 0 to 1 with 0.1 increment for three different values of jamming amplitude, the simulation results are plotted against the theoretical results in Fig. 5.3. The theoretical results for case 1 are obtained from (5.30) with $\sigma^2_{D_G}$ equals 0. As one can observe, for a given jamming amplitude, the BER performance becomes worse as Δk increases. However, once Δk is greater than 0.5, the BER performance starts to improve again. This is due to the fact that the orthogonality between subcarriers is lost when Δk is not zero. Subsequently, the magnitude due to the jamming signal at the k^{th} frequency is nonzero at the other subcarriers. As Δk increases, the magnitude at all subcarriers, other than the k^{th} subcarrier, increases since the jammer in time domain is a sinc function. Furthermore, the magnitude is at the highest when Δk is 0.5 and starts to decrease once Δk is greater than 0.5. Hence, for a given jamming amplitude, the BER of the system is at the worst when Δk equals 0.5.

Fig. 5.4 shows the simulation and theoretical results for the second case where the jammer

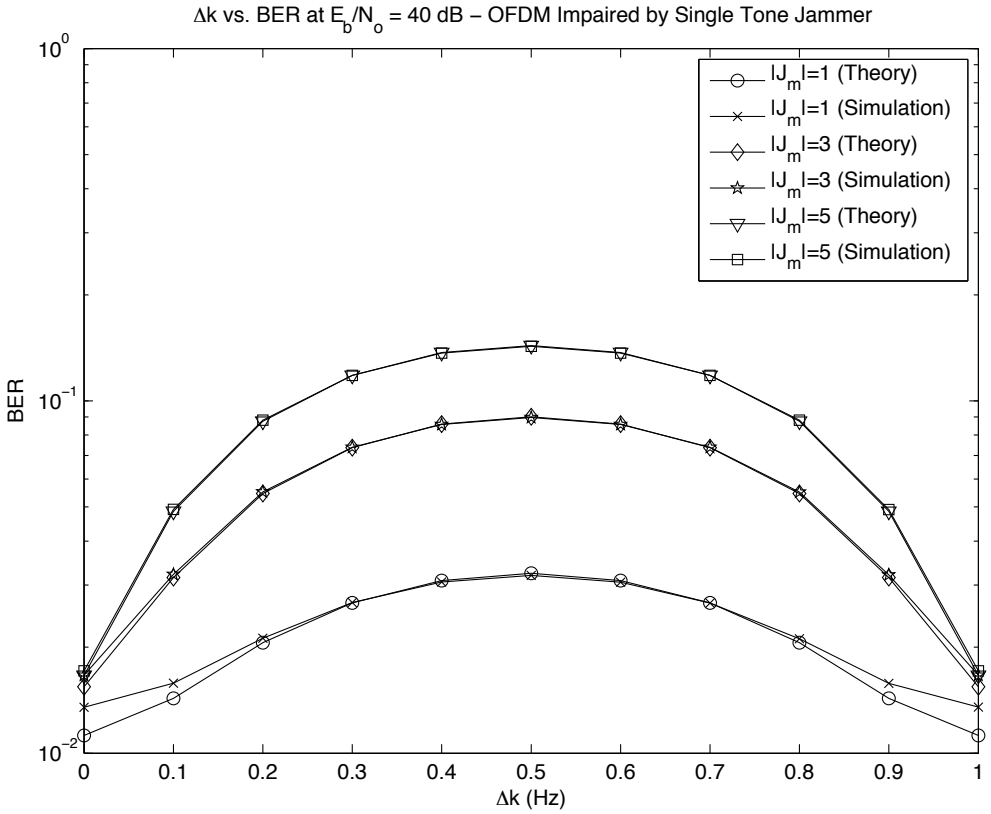

Figure 5.3 The effect of Δk on the BER performance of a 16-QAM OFDM system impaired by a single tone jammer for various jamming amplitudes at $E_b/N_o = 40$ (dB).

does not exist and the only nonlinear distortion introduced by a nonlinear HPA is present in the system besides AWGN. Instead of varying frequency offset or the severity level of nonlinear distortion, in case 3, the amplitude of jamming signal is set t0 0, 0.1, 0.3 and 0.5 while the system is still subject to nonlinear distortion. The results of the simulation are shown in Fig. 5.5 along with the theoretical results obtained by using (5.30). In cases 3 and 4, the occurrence of error floor in the performance occurs at around 30 dB. The occurrence of the error floor can be explained by examining signal to noise ratio (SNR) for MSB or LSB probabilities. For example, at high SNR, the effect of σ_w^2 is negligible compared to σ_Ψ^2, $\sigma_{J_D}^2$ and $\sigma_{J_o}^2$. As a consequence, the SNR for MSB probability, denoted as SNR_{MSB}, becomes

$$SNR_{MSB} \simeq \frac{\Upsilon_i}{\sigma_\Psi^2 + \sigma_{J_D}^2 + \sigma_{J_o}^2} \tag{5.32}$$

where Υ_i is defined in (5.24). Furthermore, SNR_{MSB} is only a function of Υ_i, σ_Ψ^2, $\sigma_{J_D}^2$ and $\sigma_{J_o}^2$ of which σ_Ψ^2 is a constant for a given set of parameters used in the HPA model. As for $\sigma_{J_D}^2$ and $\sigma_{J_o}^2$, they both only depend on the amplitude of jammer. Therefore, at high SNR, the system is still being affected by the same amount of degradation and subsequently produces an error floor. The

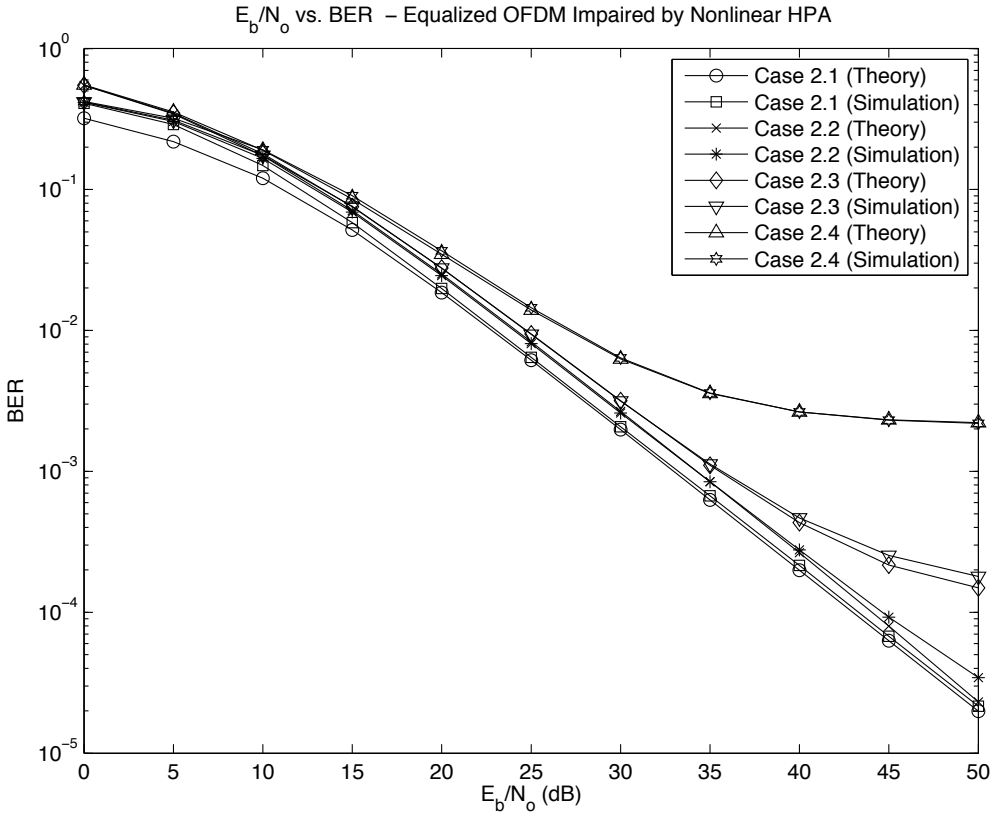

Figure 5.4 BER performance of a 16-QAM OFDM system in the Rayleigh fading channel for various levels of degradation introduced by nonlinear HPAs in the absence of the jammer.

same conclusion can be drawn if one examines the SNR for LSB probability.

In case 4, the amplitude of the jammer or the total of jamming power is held constant while we vary the number of jamming tones in the jammer. In addition, the simulation and theoretical results for this case are shown in Fig. 5.6. As one can see from Fig. 5.6, a jammer that has a single tone causes the most degradation in the system performance as compared to other cases where the jammer has more than one frequency tones. This is because as the number of jamming tones in the jammer model increases, the jamming power in each frequency tone has to decrease in order to preserve the condition that the total jamming power is held constant. As a result, $\sigma^2_{J_D}$ and $\sigma^2_{J_o}$ become smaller in values and have less impact in the system performance.

By looking at results in Fig. 5.6, one might be inclined to use a single tone jammer when it comes to designing a jammer. Even though, a single tone jammer causes the most degradation, it is not practical in real situations for two reasons. The first reason is the jammer does not usually have the perfect knowledge of the center frequency of the desired signal. When that is the case, the jam-

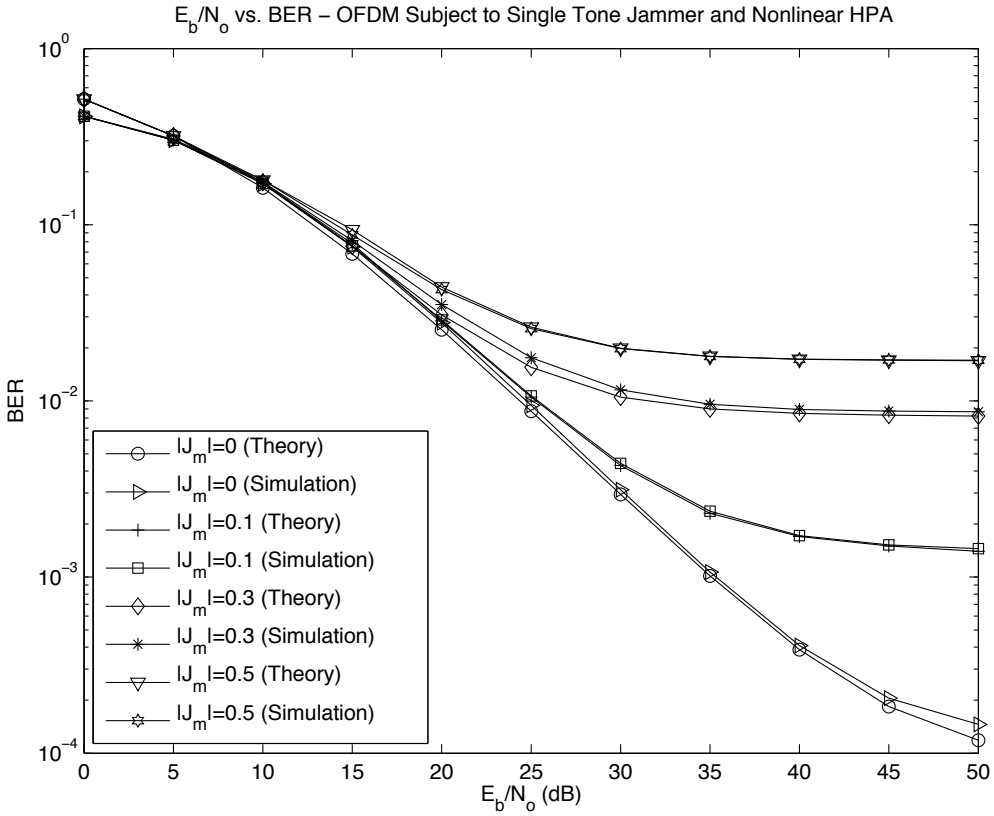

Figure 5.5 BER performance of a 16-QAM OFDM system impaired by a single tone jammer and nonlinear HPA in the Rayleigh fading channels for various values of jamming amplitude. In all four cases, the frequency offset, Δk, is set to 0.5.

mer often appears at the outside of the frequency spectrum of the transmitted signal and introduces an ICI-like interference to the system as illustrated in both Fig. 5.7 and 5.8. Even though, the center frequency of the jamming signal does not overlap with the desired signal spectrum, the right tail of the jamming signal still appears within the spectrum of the transmitted signal. As a consequence, the right tail of the jammer which is referred to as the ICI-like interference causes degradation in performance. Furthermore, as one can observe by comparing Fig. 5.7 with Fig. 5.8, the effect of the ICI-like interference on the performance strongly depends on the distance of the jammer's location in the frequency spectrum with respect to the desired signal. The further away the jamming signal is in the frequency spectrum, the smaller magnitude that ICI-like interference has and the less impact that it has on the system performance. Another reason is that the OFDM system can simply turn off the subcarrier's frequency at which the jammer interferes. By doing so, the BER performance can improve since only the ICI-like interference which is due to the jammer is present in the received signal. However, the cost of not utilizing a particular subcarrier's frequency is the decrease in data rate.

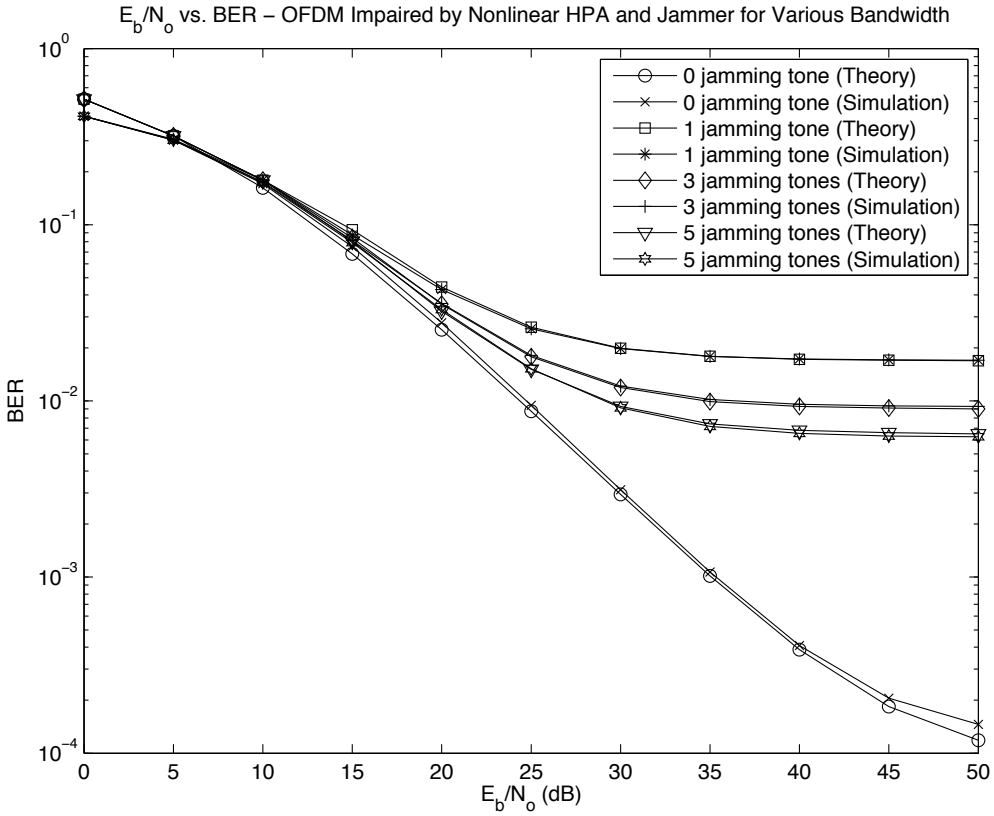

Figure 5.6 BER performance of a 16-QAM OFDM system impaired by a single tone jammer and nonlinear HPA in the Rayleigh fading channel for various number of jamming tones in the jammer. In addition, the total power of the jamming signal in each case is held constant.

Finally, when the channel response is not perfectly known at the receiver, the error between the estimate and the true channel response further degrades the performance. Fig. 5.9 shows the effect of channel estimation error on the performance of a system modeled based on the parameters of case 5.

5.6 Conclusion

In this chapter, we presented the performance analysis of an M-QAM OFDM system which had a nonlinear HPA in the transmitter and was subject to jamming and channel estimation error in a Rayleigh fading channel. The model for the jammer presented in this chapter was more realistic compared to models in previous studies because not only did the jamming signals experience a separate Rayleigh fading channel, the proposed model incorporated the possibility that the jammer transmitted jamming signals at a frequency that was offset from the frequency of the desired signal. By introducing a constant frequency offset between jamming and transmitted signals, the jammer

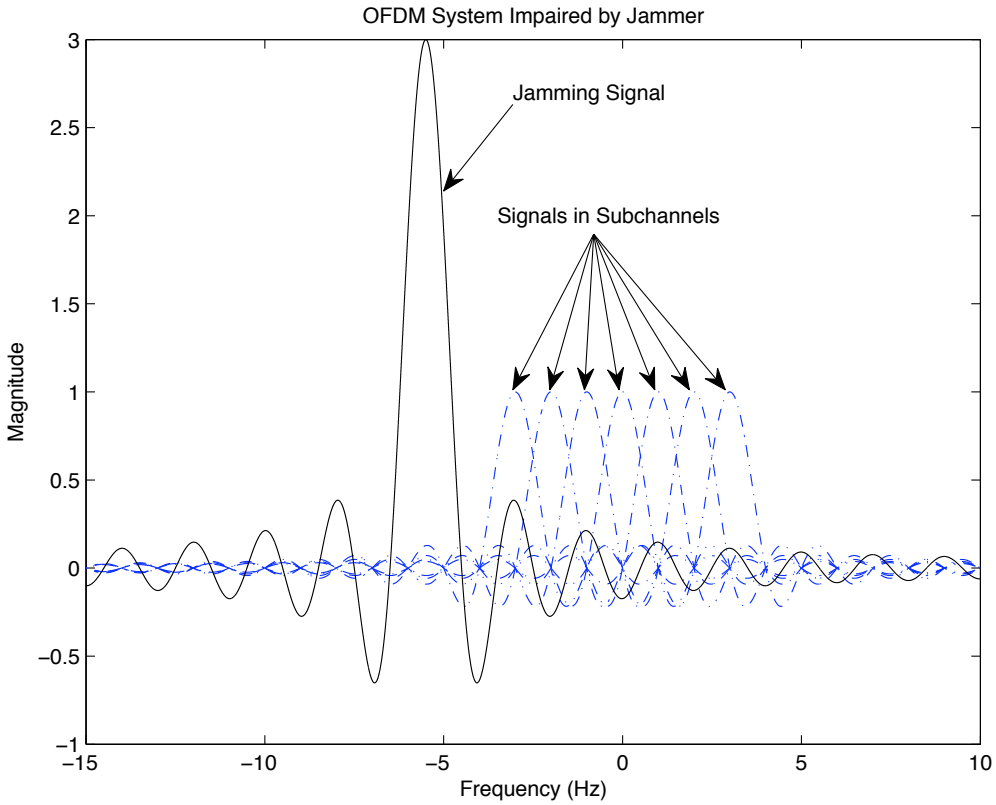

Figure 5.7 An illustration of the effect of the center frequency location of the jamming signal with respect to the center frequency location of the OFDM signals in frequency spectrum

produced an additional interference which behaves like ICI and caused more significant impact on the system performance compared to the scenario where the normalized frequency offset is zero. In addition, we simulated a IEEE 802.11n WLAN system that was extended from the analytical model and presented simulation results along with theoretical values for various sets of parameters used with and without channel estimation error. Based on the theoretical and simulation results, we also discussed the impact of a jammer on the performance of M-QAM OFDM systems and how the bandwidth of the jammer had an effect on the performance if the total jamming power is a design constraint.

The text in Chapter 5 is based on the material as it appears in:

David W. Chi and Pankaj Das, "Effects of Nonlinear Amplifier and Partial Band Jammer in OFDM with Application to 802.11n WLAN", IEEE Military Communications Conference, October 2007, pp. 1-8.

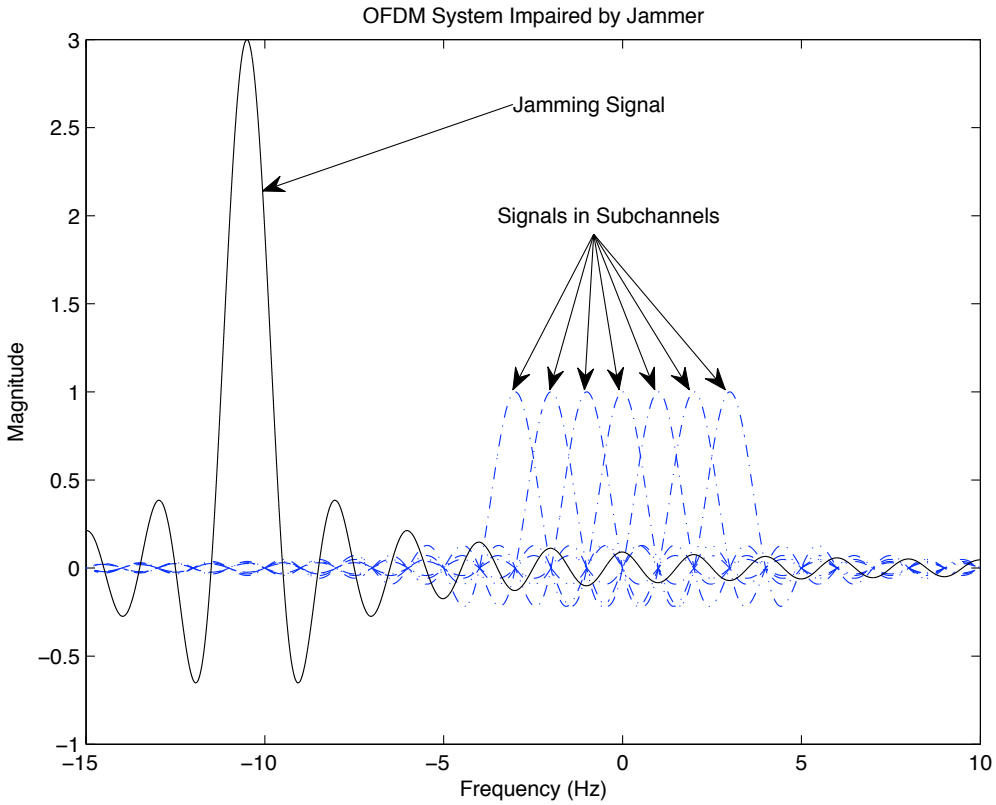

Figure 5.8 An illustration of the effect of the center frequency location of the jamming signal with respect to the location of center frequency of the OFDM signals in frequency spectrum. In this case, the center frequency of the jamming signal is located further away in frequency from the OFDM signals when compared to the one that is shown in Fig. 5.7.

The dissertation author was the primary researcher and author, and the co-author listed in the publication directed and supervised the research which forms the basis for this chapter.

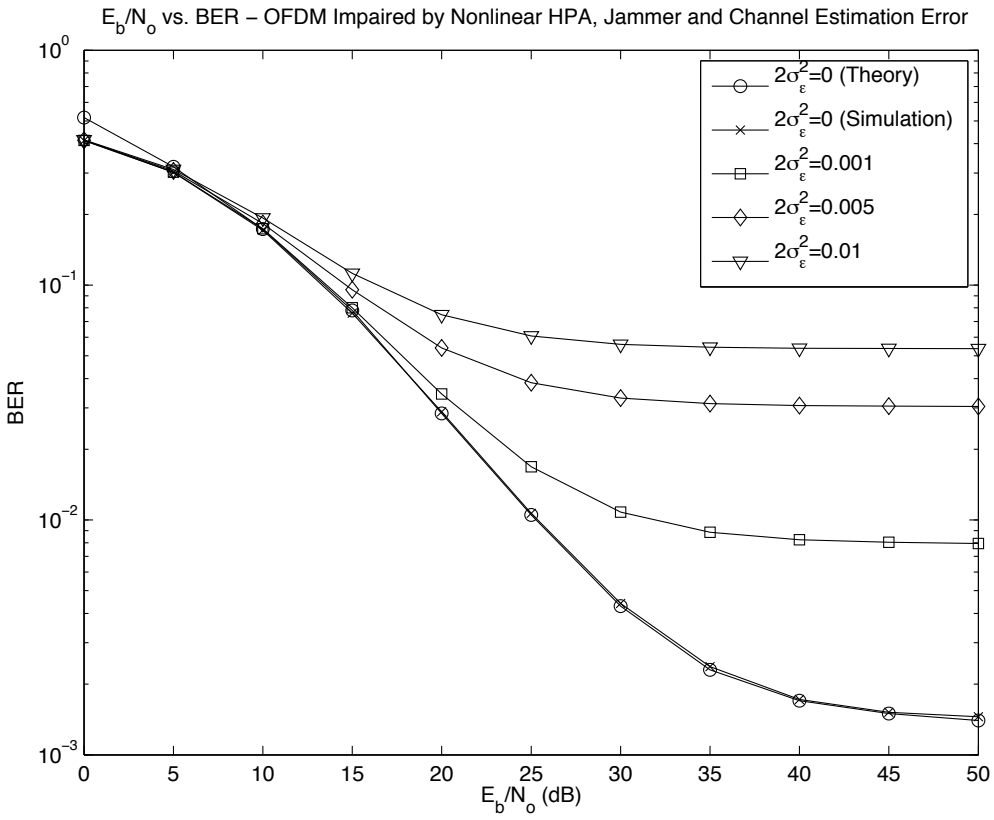

Figure 5.9 BER performance of a 16-QAM OFDM system impaired by a single tone jammer whose frequency offset is 0.5 and a nonlinear HPA in the Rayleigh fading channel for various values of $2\sigma_\epsilon^2$.

6

Effect of Channel Estimation Error and Nonlinear High Power Amplifier (HPA) on the Performance of OFDM

6.1 Introduction

Orthogonal Frequency Division Multiplexing (OFDM) is a promising technology for wireless communication applications that require high data rate transmission [30]. Due to its technical advantages, OFDM is currently being considered for the fourth generation (4G) mobile and Wireless Local Area Networks (WLAN) communication systems. One way to increase the data rate of wireless communication systems is to employ multiple antennas for data transmission and reception. These types of systems are also known as Multiple Input Multiple Output (MIMO) systems in literature. The IEEE 802.11n standard incorporates both OFDM and MIMO technologies to achieve better performance [4].

In OFDM, the broadband channel is divided into several orthogonal and narrowband subchannels which are known as subcarriers. The bandwidth of a subcarrier is usually smaller than the channel coherence bandwidth; therefore, OFDM systems are able to deliver high data rates with high bandwidth efficiency and low receiver complexity. However, OFDM is known to be sensitive to frequency offsets, phase noise [22, 23] and high peak to average power ratio (PAPR). Frequency offsets are, in general, caused by the frequency deviation between the transmitter and receiver, or by Doppler shift. Unlike the frequency offset, the phase noise is usually a random process because the

phase noise is often caused by the fluctuation of the receiver and transmitter oscillators. When either frequency offset or phase noise is present in the system, the orthogonality among the subcarriers is lost. As a result, inter-carrier interference (ICI) occurs and the system performance degrades [5]. Another problem often associated with multicarrier modulations such as OFDM is the high PAPR. This particular phenomenon is a direct consequence of using Fast Fourier Transform (FFT) and Inverse Fast Fourier Transform (IFFT) operations. When L number of signals of the same amplitude are being added coherently, IFFT/FFT produces a peak power that is L times larger than the average power. Practical high power amplifiers (HPAs) have difficulty reproducing such high PAPR signals and often introduce nonlinear distortion such as clipping and spectral regrowth [24, 25]. As a result of inefficient HPAs, the performance is further degraded due to nonlinear distortion.

Although there are some papers dealing with the performance of OFDM systems that are impaired by nonlinear HPAs in the additive white Gaussian noise (AWGN) channel, few of them adequately address the effects of nonlinearity in OFDM systems in the Rayleigh fading channel. In [15], the authors presented the performance analysis of an M-ary Quadrature Amplitude Modulation (M-QAM) OFDM system which is impaired by a nonlinear HPA and phase noise in the AWGN channel only. Chang, *et al.* [26] showed the performance of an equalized OFDM system in a Rayleigh flat fading channel for various modulations with and without channel estimation error. However, the effect of nonlinear distortion introduced by a HPA on the system performance was not considered in the paper. The conventional approach for analyzing the performance of an OFDM system which is subject to channel estimation error in Rayleigh fading channels requires integrating the conditional bit error rate (BER) over the joint probability density function of the channel impulse response and its estimate. Subsequently, this approach leads to solving a triple integral which can be a difficult task to do. In this chapter, we analyze the performance of a M-QAM OFDM system that is subject to distortion from a nonlinear HPA, and channel estimation error in the Rayleigh fading channel. Different from the channel estimation error model presented in [26], we make use of the model that is proposed previously in [31] to help facilitate the derivation of a closed form BER expression.

The chapter is organized as follows. In Section 6.2, the analytical system under study is described in detail. Section 6.3 contains the performance analysis of the analytical model. Section 6.4 describes the simulation setup for the extended model. Section 6.5 provides simulation results of the model described in Section 6.4. Finally, Section 6.6 summarizes the chapter.

6.2 System Description

Fig. 6.1 shows the block diagram of the system under study. Each block is discussed in the following subsections.

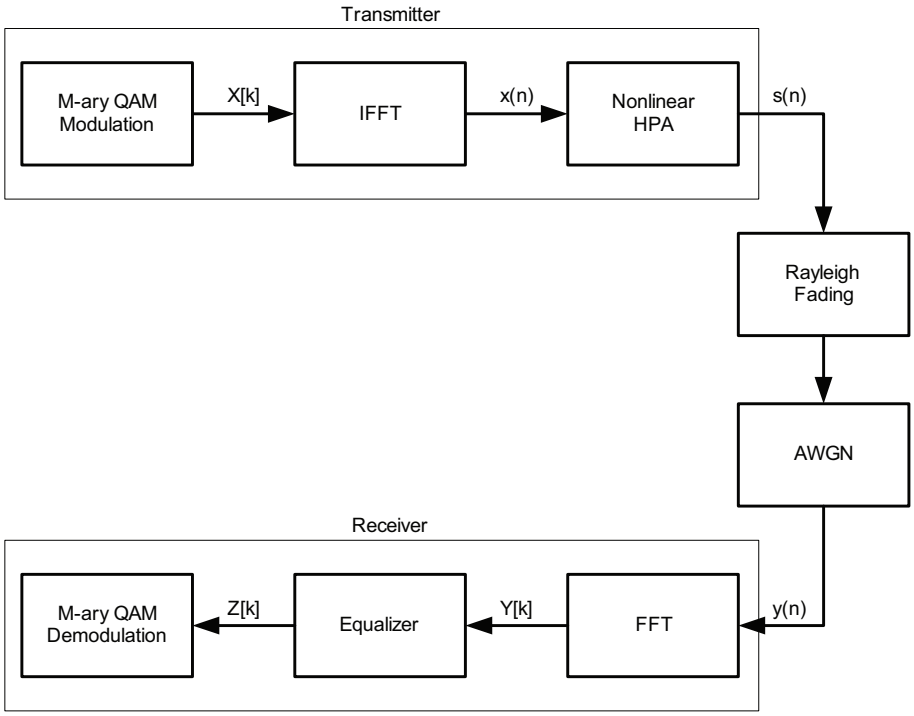

Figure 6.1 The system block diagram of an equalized M-ary QAM OFDM system which is impaired by a nonlinear HPA, and channel estimation error in the Rayleigh fading channel.

6.2.1 Transmitter

The transmitter is consisted of a M-QAM signal modulator, an IFFT and a nonlinear HPA. The binary input to the M-QAM modulator is assumed to be equiprobable and independent. They are subsequently grouped into a block size of $log_2 M$ and mapped into M-QAM symbols, $X[k]$, according to alphabet, $A = \{(2m-1-\sqrt{M})+j(2n-1-\sqrt{M})\}$ where $\{m, n = 1, 2, ...\sqrt{M}\}$ and M is the signal constellation size. At appropriate sampling time, the signal at the output of the IFFT, $x(n)$, is

$$x(n) = \frac{1}{N}\sum_{k=0}^{N-1} X[k]e^{j\frac{2\pi nk}{N}} \qquad 0 \le n \le N-1 \tag{6.1}$$

where N is the number of subcarriers.

6.2.2 HPA Model

The nonlinear HPA model in the transmitter represents the nonlinear distortion imposed on the signal. In this chapter, the nonlinear HPA modeled proposed by Saleh is utilized in the system. The detail about the Saleh HPA model can be found in Chapter 2, Section 2.3.

6.2.3 Channel Model and AWGN

Let $h(n)$ be the impulse response of the Rayleigh fading channel between the transmitter and the receiver. The in-phase and quadrature components of $h(n)$ are both Gaussian random variables with zero mean and σ_H^2 variance. In addition, each component is statistically independent of the other. The thermal noise, denoted as $w(n)$, is an independent AWGN process which has zero mean and $2\sigma_w^2$ variance.

6.2.4 Receiver

Let $y(n)$ be the received signal in time domain and assuming perfect synchronization, $y(n)$ is given by

$$y(n) = h(n)s(n) + w(n) \tag{6.2}$$

The received signal is then fed to the FFT block and consequently, the received signal in frequency domain, $Y[k]$, is

$$\begin{aligned} Y[k] &= \sum_{n=0}^{N-1} y(n)e^{-j\frac{2\pi kn}{N}} \\ &= H[k]S[k] + W[k] \end{aligned} \tag{6.3}$$

where $H[k]$, $S[k]$, and $W[k]$ are FFT of $h(n)$, $s(n)$, and $w(n)$, respectively.

6.2.5 Equalizer Model

Since the bandwidth of a subcarrier in OFDM signals is usually much smaller than the channel coherence bandwidth. The equalization process becomes one of the most attractive features of OFDM systems and can be adequately done by using an one-tap equalizer in the frequency domain. Among many available algorithms, we choose the Zero Forcing algorithm because of its simplicity in implementation and mathematical tractability.

Before equalization, estimating the channel response is necessary and can be obtained with the aid of pilots. Let $X[P_1], X[P_2], ..., X[P_p]$ be the pilot symbols modulated onto the subcarriers, $P_1, P_2, ..., P_p$, where p is the total number of pilots. Using Least Squares, the estimated channel response at the pilot subcarriers is given by

$$\hat{H}[P_i] = \frac{Y[P_i]}{X[P_i]} \qquad i = 1, 2, ..., p \tag{6.4}$$

where $Y[P_i]$ is the received signal at the pilot subcarrier, P_i. The estimated channel response at the data subcarriers can be obtained by interpolating between two consecutive pilots [32].

After obtaining the channel estimate, an estimate of the transmitted signal on the k^{th} subcarrier, denoted as $Z[k]$, is then given by

$$\begin{aligned} Z[k] =& \frac{\hat{H}^*[k]Y[k]}{|\hat{H}[k]|^2} \\ =& \frac{\hat{H}^*[k]H[k]S[k] + \hat{H}^*[k]W[k]}{|\hat{H}[k]|^2} \end{aligned} \tag{6.5}$$

where $\hat{H}[k]$ is the estimate of the channel, $H[k]$, and is a complex Gaussian random process with zero mean and $2\sigma^2_{\hat{H}}$ variance. In addition, $(\cdot)^*$ denotes the complex conjugate operation.

6.3 Performance Analysis

In this section, we will derive the BER of the system which will be used later as a measure of system performance. The performance analysis of the system which is shown in Fig. 6.1 starts with the characterization of $x(n)$. Under the assumption that N is large, by the *Central Limit Theorem*, $x(n)$ is said to be Gaussian distributed with zero mean [19]. With that assumption, Banelli, *et al.* had shown that $s(n)$ can be written as a product of a complex gain, α_G, and the input signal, $x(n)$, added with noise distortion $d_G(n)$, namely,

$$s(n) = \alpha_G x(n) + d_G(n) \overset{FFT}{\longleftrightarrow} S[k] = \alpha_G X[k] + D_G[k] \tag{6.6}$$

where $D_G[k]$ was shown to be a complex Gaussian random variable with zero mean and $2\sigma^2_D$ variance. Furthermore, one can follow the steps outlined in Section 2.4 of Chapter 2 to obtain the numerical value of σ^2_D. For two different subcarriers, k_1 and k_2, $D_G[k_1]$ and $D_G[k_2]$ are independently distributed. Furthermore, the in-phase and quadrature components of $D_G[k]$ were shown to be mutually independent and identically distributed (i.i.d) [15]. The multiplicative coefficient α_G is given by

$$\alpha_G = \frac{E\{s(n)^* x(n)\}}{2\sigma^2_{x(n)}} = \alpha_{G_I} + j\alpha_{G_Q} \tag{6.7}$$

where $E\{\cdot\}$ is the expected value [20]. The subscripts, I and Q, represent in-phase and quadrature components of a signal, respectively.

For simplicity of notations, we will drop the subcarrier index in the rest of the derivation. After synchronization and the removal of the preamble sequences and cyclic prefix, the estimate of the transmitted signal on the k^{th} subcarrier, Z, can be obtained by substituting (6.6) into (6.5) and becomes

$$\begin{aligned} Z =& \frac{\hat{H}^* H(\alpha_G X + D_G) + \hat{H}^* W}{|\hat{H}|^2} \\ =& \frac{\hat{H}^* H}{|\hat{H}|^2}\alpha_G X + \frac{\hat{H}^* H}{|\hat{H}|^2} D_G + \frac{\hat{H}^* W}{|\hat{H}|^2} \end{aligned} \tag{6.8}$$

In [33], authors analyzed the performance of the estimate of transmitted signal which is defined as (6.8). In addition, authors assumed that the magnitudes of H and $\hat{H}$ are independent of the phase difference between H and $\hat{H}$. Therefore, the average BER was obtained by first integrating the conditional BER over the joint probability density function (PDF) of the magnitudes of H and $\hat{H}$. The integration result is then integrated over the PDF of the phase difference. However, Cao, *et al.* [28] argued that the performance analysis presented in [33] was only an approximation because the magnitudes of H and $\hat{H}$ and the phase difference between them statistically depends on each other. As a result, it is required to solve a triple integral in order to obtain the exact average BER. Nonetheless, it is sometimes a difficult task to evaluate the triple integral due to the integrand is a Q function. Here, by making use of the channel estimation error model proposed in the previous paper [31], we express the channel response as a function of its estimate. This approach greatly reduces the complexity of performance analysis by avoiding the triple integral calculation and facilitates the derivation of a closed form BER expression.

Since H and $\hat{H}$ are jointly Gaussian, conditioned on $\hat{H}$, we may write the channel as [31]

$$H = \rho \frac{\sigma_H}{\sigma_{\hat{H}}} \hat{H} + U \tag{6.9}$$

where U represents the channel estimation error and is modeled as a complex Gaussian random variable with zero mean and $2\sigma_U^2$ variance. In addition, $2\sigma_U^2$ is given by

$$2\sigma_U^2 = 2\sigma_H^2(1 - |\rho|^2) \tag{6.10}$$

ρ in (6.9) represents the quality of the channel estimate and is measured by the complex correlation coefficient between the channel, H, and its estimate, $\hat{H}$. Furthermore, ρ can take on any values between 1 and 0. For perfect channel estimation, i.e. ρ is 1, U is subsequently reduced to zero due to its variance is also reduced to zero and $\sigma_H = \sigma_{\hat{H}}$. Hence, (6.9) yields $H = \hat{H}$ as expected.

Substituting (6.9) into (6.8), Z becomes

$$Z = \rho \frac{\sigma_H}{\sigma_{\hat{H}}} (\alpha_G X + D_G) + \frac{\hat{H}^*}{|\hat{H}|^2} U (\alpha_G X + D_G) + \frac{\hat{H}^*}{|\hat{H}|^2} W \tag{6.11}$$

After expanding U and W into in-phase and quadrature components, the estimate of the transmitted signal on the k^{th} subcarrier, Z, is given by

$$\begin{aligned} Z =& \rho \frac{\sigma_H}{\sigma_{\hat{H}}} (\alpha_G X + D_G) + \underbrace{\frac{\hat{H}^*}{|\hat{H}|^2} [U_I (\alpha_G X + D_G) + W_I]}_{\eta_1} + j \underbrace{\frac{\hat{H}^*}{|\hat{H}|^2} [U_Q (\alpha_G X + D_G) + W_Q]}_{\eta_2} \\ =& \rho \frac{\sigma_H}{\sigma_{\hat{H}}} (\alpha_G X + D_G) + \eta_1 + j\eta_2 \end{aligned} \tag{6.12}$$

From (6.12), η_1 and η_2 are both zero mean Gaussian random variables since they are sums of several zero mean Gaussian random variables namely, U, D_G and W. Denote σ_η^2 as the variance of η_1

conditioned on $\hat{H}$, then σ_η^2 is found to be

$$\begin{aligned}
\sigma_\eta^2 =& E\{\eta_1\eta_1^*\} \\
=& E\left\{\left(\frac{\hat{H}^*}{|\hat{H}|^2}\left[U_I\left(\alpha_G X + D_G\right) + W_I\right]\right)\left(\frac{\hat{H}^*}{|\hat{H}|^2}\left[U_I\left(\alpha_G X + D_G\right) + W_I\right]\right)^*\right\} \\
=& E\left\{\frac{1}{|\hat{H}|^2}\left[U_I^2\alpha_G^2X^2 + 2U_I^2\alpha_G X D_G + U_I^2 D_G^2 + W_I^2\right]\right\} \\
=& \frac{1}{|\hat{H}|^2}\left(\sigma_H^2\alpha_G^2 E\{|X|^2\}(1-|\rho|^2) + 2\sigma_H^2\sigma_D^2(1-|\rho|^2) + \sigma_w^2\right)
\end{aligned} \tag{6.13}$$

The variance of η_2 conditioned on $\hat{H}$ can easily be shown to be the same as the variance of η_1. As one can notice, (6.13) is a function of modulated symbols, X. For the case where X represents a M-ary Phase Shift Keying (M-PSK) symbol, the numerical values for σ_η^2 are the same for all M-PSK symbols. However, in the situation where the signal constellation is rectangular instead of circular such as in the case of M-QAM modulation, the numerical values of σ_η^2 will highly depend on where the location of X is in the signal constellation. To avoid any confusion when one derives the BER expression, we will rewrite (6.13) in such a way that the expression of σ_η^2 explicitly shows the dependency on modulated symbols, namely

$$\sigma_{\eta_i}^2 = \frac{1}{|\hat{H}|^2}\left(\sigma_H^2\alpha_G^2 E\{|X_i|^2\}(1-|\rho|^2) + 2\sigma_H^2\sigma_D^2(1-|\rho|^2) + \sigma_w^2\right) \tag{6.14}$$

where the subscript i in X_i represents the i^{th} modulated symbol.

After expanding (6.12) by expressing α_G as $\alpha_{G_I} + j\alpha_{G_Q}$, X as $X_I + jX_Q$, and D_G as $D_{G_I} + jD_{G_Q}$, (6.12) is further reduced to

$$\begin{aligned}
Z =& \left\{\rho\frac{\sigma_H}{\sigma_{\hat{H}}}\left[\alpha_G X + D_{G_I}\right] + \eta_1\right\} + j\left\{\rho\frac{\sigma_H}{\sigma_{\hat{H}}}D_{G_Q} + \eta_2\right\} \\
=& \rho\frac{\sigma_H}{\sigma_{\hat{H}}}(\alpha_{G_I} + j\alpha_{G_Q})(X_I + jX_Q) + \beta_1 + j\beta_2 \\
=& \underbrace{\left(\rho\frac{\sigma_H}{\sigma_{\hat{H}}}(\alpha_{G_I}X_I - \alpha_{G_Q}X_Q) + \beta_1\right)}_{Z_I} + j\underbrace{\left(\rho\frac{\sigma_H}{\sigma_{\hat{H}}}(\alpha_{G_Q}X_I + \alpha_{G_I}X_Q) + \beta_2\right)}_{Z_Q} \\
=& Z_I + jZ_Q
\end{aligned} \tag{6.15}$$

where β_1 and β_2 are defined as

$$\beta_1 = \rho\frac{\sigma_H}{\sigma_{\hat{H}}}D_{G_I} + \eta_1 \qquad\qquad \beta_2 = \rho\frac{\sigma_H}{\sigma_{\hat{H}}}D_{G_Q} + \eta_2 \tag{6.16}$$

In addition, β_1 and β_2 are both zero mean Gaussian random variables due to the fact that D_G, η_1 and η_2 are zero mean Gaussian random variables. Since $\sigma_{\eta_i}^2$ is a function of modulated symbol, X, the variances of β_1 and β_2 will also be a function of X. Let $\sigma_{\beta_i}^2$ be the variance of β_1 conditioned

on $\hat{H}$ for the i^{th} modulated symbol, then $\sigma^2_{\beta_i}$ is found as

$$\sigma^2_{\beta_i} = E\left\{\left(\rho\frac{\sigma_H}{\sigma_{\hat{H}}}D_{G_I}+\eta_1\right)\left(\rho^*\frac{\sigma_H}{\sigma_{\hat{H}}}D^*_{G_I}+\eta^*_1\right)\right\} = \rho^2\frac{\sigma^2_H}{\sigma^2_{\hat{H}}}\sigma^2_D+\sigma^2_{\eta_i} \tag{6.17}$$

where $\sigma^2_{\eta_i}$ is defined as (6.14). Due to the fact that D_G has the same variance for its in-phase and quadrature components and both η_1 and η_2 have the same variances, consequently β_2 would have the same variance as β_1.

To continue the derivation, we assume that 16-QAM modulation is utilized for data modulation in the system. Nevertheless, the BER expression for other rectangular QAM constellations can be derived in the similar fashion if another modulation scheme is chosen. The BER of 16-QAM conditioned on $\hat{H}$ is given by

$$P_{BER|\hat{H}} = \frac{1}{2}\left(P_{MSB}+P_{LSB}\right) \tag{6.18}$$

where P_{MSB} and P_{LSB} denote as the conditional BER of most significant bits (MSB) and least significant bits (LSB) of 16-QAM symbols conditioned on $\hat{H}$. The average BER is then obtained by averaging (6.18) over the probability density function (PDF) of $|\hat{H}|$, namely

$$P_{BER} = \int_0^\infty P_{BER|\hat{H}}p(|\hat{H}|)d|\hat{H}| \tag{6.19}$$

where $p(|\hat{H}|)$ is defined as

$$p(|\hat{H}|) = \frac{|\hat{H}|}{\sigma^2_{\hat{H}}}e^{-\frac{|\hat{H}|^2}{2\sigma^2_{\hat{H}}}} \tag{6.20}$$

As one can observe from (6.19), the expression of the average BER is in the form of a single integral instead of a triple integral which is the common average BER expression for a system that is subject to channel estimation error in literature. This simplification in the complexity of average BER calculation can be achieved when (6.9) is utilized as the channel estimation model.

Based on the decision boundaries shown in Fig. 1 in [28], the conditional BER of MSB is found to be

$$\begin{aligned} P_{MSB} =& P\left(Z_I<0|\hat{H}\right) \\ =& \frac{1}{8}\sum_{i=1}^{8}P\left(\rho\frac{\sigma_H}{\sigma_{\hat{H}}}(\alpha_{G_I}X_{I_i}-\alpha_{G_Q}X_{Q_i})+\beta_1<0\right) \\ =& \frac{1}{8}\sum_{i=1}^{8}Q\left(\sqrt{\frac{\left(\rho\frac{\sigma_H}{\sigma_{\hat{H}}}\gamma_i\right)^2}{\sigma^2_{\beta_i}}}\right) \end{aligned} \tag{6.21}$$

where $\gamma_i = (\alpha_{G_I}X_{I_i}-\alpha_{G_Q}X_{Q_i})$ and $Q(\nu)=\int_\nu^\infty\frac{1}{\sqrt{2\pi}}e^{\frac{-t}{2}}dt, \nu\geq 0$. The variance $\sigma^2_{\beta_i}$ is defined as (6.17). In addition, the numerical values for X_{I_i}, X_{Q_i} and $E\{|X_i|^2\}$ in (6.21) are listed in Table

Table 6.1 Numerical Values of Variables in Conditional BER for MSB

Index i	X_{I_i}	X_{Q_i}	$E\{\|X_i\|^2\}$	Index i	X_{I_i}	X_{Q_i}	$E\{\|X_i\|^2\}$
1	d	$3d$	$10d^2$	5	$3d$	$3d$	$18d^2$
2	d	d	$2d^2$	6	$3d$	d	$10d^2$
3	d	$-d$	$2d^2$	7	$3d$	$-d$	$10d^2$
4	d	$-3d$	$10d^2$	8	$3d$	$-3d$	$18d^2$

Table 6.2 Numerical Values and Signs of Variables in Conditional BER for LSB

Index i	λ_i	κ_i	ζ_i	X_{I_i}	X_{Q_i}	$E\{\|X_i\|^2\}$
1	+	+	+	d	$3d$	$10d^2$
2	+	+	-	d	$3d$	$10d^2$
3	+	+	+	d	d	$2d^2$
4	+	+	-	d	d	$2d^2$
5	+	+	+	d	$-d$	$2d^2$
6	+	+	-	d	$-d$	$2d^2$
7	+	+	+	d	$-3d$	$10d^2$
8	+	+	-	d	$-3d$	$10d^2$
9	+	-	-	$-3d$	$3d$	$18d^2$
10	-	+	-	$-3d$	$3d$	$18d^2$
11	+	-	-	$-3d$	d	$10d^2$
12	-	+	-	$-3d$	d	$10d^2$
13	+	-	-	$-3d$	$-d$	$10d^2$
14	-	+	-	$-3d$	$-d$	$10d^2$
15	+	-	-	$-3d$	$-3d$	$18d^2$
16	-	+	-	$-3d$	$-3d$	$18d^2$

6.1. The conditional BER of LSB can be obtained in the similar way and based on the decision boundaries, it is given by

$$\begin{aligned} P_{LSB} =& \left\{ P(Z_I < -2d|\hat{H}) + P(Z_I > 2d|\hat{H}) \right\} |_{LSB=0} + \left\{ P(-2d < Z_I < 2d|\hat{H}) \right\} |_{LSB=1} \\ =& \frac{1}{8} \sum_{i=1}^{16} \lambda_i Q \left(\sqrt{\frac{\left(\kappa_i 2d + \zeta_i \rho \frac{\sigma_H}{\sigma_{\hat{H}}} \gamma_i \right)^2}{\sigma_{\beta_i}^2}} \right) \end{aligned} \tag{6.22}$$

where $|_{LSB=0}$ and $|_{LSB=1}$ imply the boundaries for LSB is zero and one, respectively. In (6.22), λ_i, κ_i, and ζ_i are signs of the values for i^{th} quantity and are listed along with numerical values for X_{I_i}, X_{Q_i} and $E\{|X_i|^2\}$ in Table 6.2. Finally, in both Tables 6.1 and 6.2, $d^2 = \frac{2E_b}{5}$ where E_b is the energy per bit.

If we assume that channel response is completely known to the receiver, i.e. $\rho = 1$ or $H = \hat{H}$, the average BER can be still obtained by evaluating (6.19). Finally, if we further assume that the HPA is ideal, i.e. $\alpha_G = 1$ and $D_G = 0$, in addition to having complete knowledge about channel response, (6.19) is further reduced to a known result ([26], Eq:69).

Table 6.3 Simulation Parameters for Case 1

Case Number	ρ	HPA	σ_H^2	$\sigma_{\hat{H}}^2$
1-A	1	Linear	0.5	0.5
1-B	0.9999	Linear	0.5	0.5
1-C	0.999	Linear	0.5	0.5
1-D	0.99	Linear	0.5	0.5

Table 6.4 Simulation Parameters for Case 2

Case Number	ρ	HPA	σ_H^2	$\sigma_{\hat{H}}^2$
2-A	1	Linear	0.5	0.5
2-B	1	Nonlinear	0.5	0.5
2-C	0.9999	Nonlinear	0.5	0.5
2-D	0.999	Nonlinear	0.5	0.5

6.4 Simulation Model and Parameters

The simulation model is an extension of the analytical model described in Section 6.2 in compliance with the IEEE 802.11n standard ([4], Clause 10.4.4.2 rate code 73); except the convolutional encoder, interleaver/deinterleaver and Viterbi decoder are omitted. After pre-appending 16-bit Service Field and padding enough bits to ensure the transmission from each antenna are multiples of whole OFDM symbols, the resulting signal is scrambled with a scrambler that is based on the IEEE 802.11a standard and subsequently demultiplexed alternately across the transmitter spatial streams. In each spatial stream, the data is modulated with the 16-QAM modulation and processed with the 64-point IFFT, of which subcarriers, $\pm$ 21, are designated for pilots. The OFDM symbol is then cyclically extended and pre-appended with the preamble sequences as specified in [4] before transmissions. To recover the data, the corresponding receiver reverses the encoding procedure in the transmitter.

The simulations are performed based on the extended model for three cases. The parameters used for each case are listed separately in Tables 6.3, 6.4, and 6.5. For all the subcases in Case 1 and subcase 2-A where the HPA is assumed to be linear, α_{AM} is set to one and the other parameters for the HPA model are set to zero. Note that if this is the case, the nonlinear HPA model reduces to unity gain and there is no phase distortion imposed on the signal, $x(n)$. As for subcases, 2-B, 2-C and 2-D where the nonlinear HPA is assumed to be present in the system, α_{AM} and β_{AM} are set to 1 and 0.25 while α_{PM} and β_{PM} are set to 1.2π and 0.01, respectively. For Case 3, ρ is set to one to simulate the situations where the only source of degradation aside from AWGN is the nonlinear distortion from the HPA. Furthermore, the means and variances for H and $\hat{H}$ are both set to 0 and 1, respectively.

Table 6.5 Simulation Parameters For Nonlinear HPA Model In Case 3

Case Number	α_{AM}	β_{AM}	α_{PM}	β_{PM}
3-A	1	0	0	0
3-B	1	0.25	π	0.25
3-C	1	0.25	1.2π	0.01
3-D	1	0.25	1.5π	0.01

6.5 Simulation Results

In case 1 where we assume the HPA is perfectly linear while varying ρ, the quality of the channel estimate, the simulation results are plotted against the theoretical values obtained from (6.19) and are shown in Fig. 6.2. As one can observe, as ρ decreases the BER performance worsens. This is because the value of ρ strongly depends on the accuracy of the channel estimation algorithm which one uses to estimate the true channel. Intuitively, when ρ or the accuracy of the channel estimation algorithm decreases, it implies that the power of channel estimation error increases. Therefore, Fig. 6.2 shows the trend of decrease in the BER performance as ρ decreases.

Next, not only the channel estimation error is present in the system, the distortion produced by the nonlinear HPA which is configured based on the parameters described in Case 2 is also applied to the system. The simulation results obtained for Case 2 are shown along with the theoretical values in Fig. 6.3. In Case 3 where we assume that the channel response is completely known to the receiver while we vary the degrees of nonlinear distortion caused by the HPA, the simulation results are shown in Fig. 6.4. In this case, the theoretical values are obtained by evaluating (6.19) with $\rho = 1$.

Depending on how much degradation there is in the system, the sign of error floor in the performance might occur at higher signal to noise ratio (SNR) than the other cases. In all three cases, the error floor generally occurs at around 35 dB. The occurrence of the error floor can be explained by the SNR of either the MSB or LSB probabilities. For example, at high SNR, the effect of σ_w^2 is negligible compared to σ_D^2 and σ_U^2. As a consequence, the SNR for MSB BER becomes

$$SNR_{MSB} \simeq \frac{\rho^2 \frac{\sigma_H^2}{\sigma_{\hat{H}}^2} (\alpha_{G_I} X_{I_i} - \alpha_{G_Q} X_{Q_i})^2}{\rho^2 \frac{\sigma_H^2}{\sigma_{\hat{H}}^2} \sigma_D^2 + \sigma_{\eta_i}^{2'}} \tag{6.23}$$

where

$$\sigma_{\eta_i}^{2'} \simeq \frac{\sigma_H^2 \alpha_G^2 E\{|X_i|^2\}(1-|\rho|^2) + 2\sigma_H^2 \sigma_D^2 (1-|\rho|^2)}{|\hat{H}|^2} \tag{6.24}$$

Furthermore, SNR_{MSB} is only a function of E_b, α_G, σ_D^2 and ρ, of which α_G and σ_D^2 are constants for a given set of parameters applied to the nonlinear HPA model and ρ only depends on the quality of the channel estimate which is controlled by the channel estimation algorithm that is used to obtain

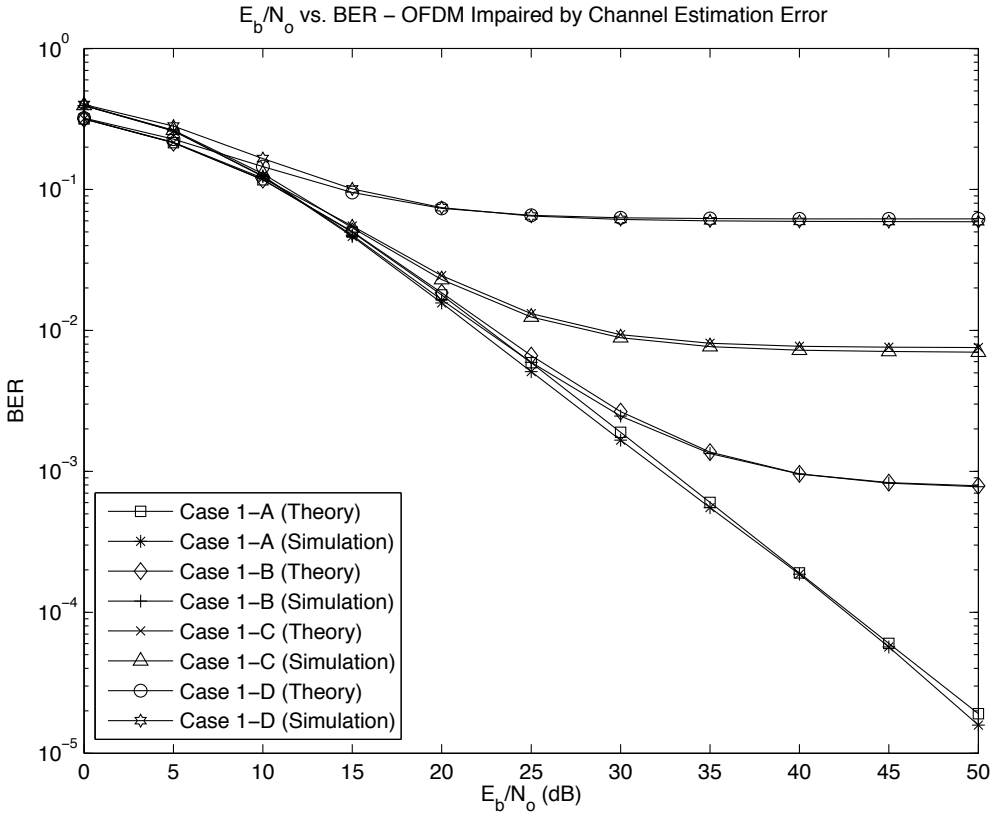

Figure 6.2 BER performance of a 16-QAM OFDM system with linear HPAs in the Rayleigh fading channel for various values of ρ.

the estimate. Therefore, at high SNR, the system would still have the same amount of degradation and subsequently produces an error floor.

6.6 Conclusion

In this chapter, we analyzed the performance of a M-QAM OFDM system which was impaired by nonlinear distortion produced by a nonlinear HPA located in the transmitter and channel estimation error in a Rayleigh fading channel. The traditional approach for analyzing the performance of such system under the same sources of impairments was to integrating the conditional BER expression over the joint PDF of the channel and its estimate to obtain the exact average BER. As a result, this approach led to solving a complicated triple integral. In this chapter, the channel estimation error model we utilized significantly reduced the complexity of the problem by simplifying the required triple integral down to a single integral. Furthermore, for the purpose of simulation, we extended the analytical model to be in compliance with the IEEE 802.11n standard. We then presented simulation results along with theoretical values obtained by using the proposed

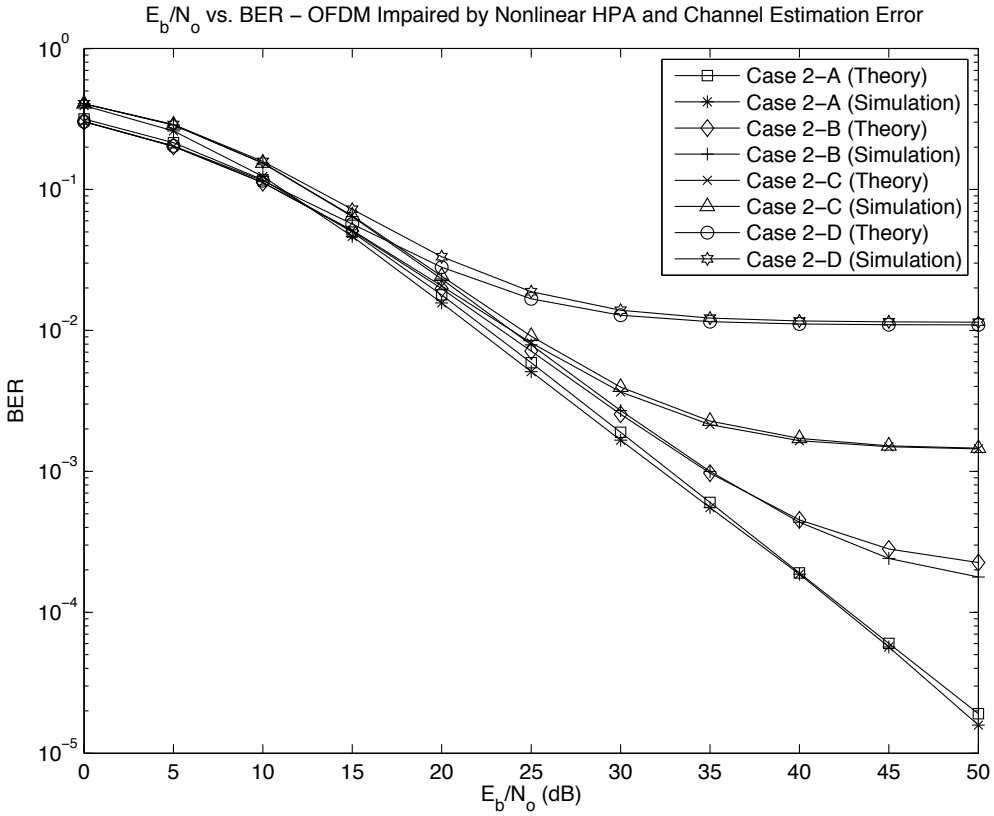

Figure 6.3 BER performance of a 16-QAM OFDM system which is impaired by a nonlinear HPA and channel estimation error in the Rayleigh fading channel for various values of ρ.

approach for various levels of channel estimation error and nonlinear distortion.

The text in Chapter 6 is based on the material as it appears in:

David W. Chi, Mishal Al-Gharabally and Pankaj Das, "Effects of Channel Estimation Error and Nonlinear HPA on the Performance of OFDM in Rayleigh Channels with Application to 802.11n WLAN", IEEE Wireless Communications & Networking Conference, April 2008, pp. 852-857.

The dissertation author was the primary researcher and author, and the co-authors listed in the publication directed and supervised the research which forms the basis for this chapter.

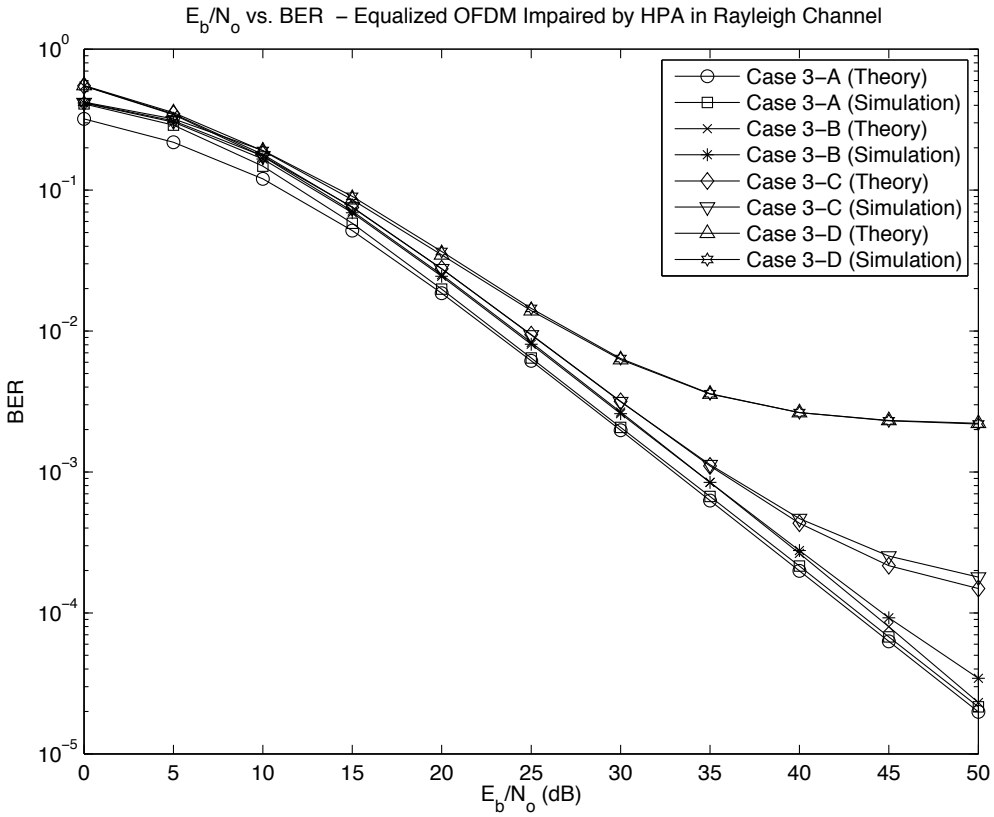

Figure 6.4 BER performance of a 16-QAM OFDM system which is subject to nonlinear distortion in the Rayleigh fading channel for various levels of nonlinear distortion under the assumption of perfect channel estimation.

7

Multiple Input Multiple Output (MIMO) Review

7.1 Introduction

Due to the increase in the demand for high data rate and superior performance as wireless communication systems become more popular and affordable to consumers, the desire for a technology that would satisfy the demand has forced research scientists to review and improve the existing technologies or simply invent a brand new system. Orthogonal Frequency Division Multiplexing (OFDM) whose root can be traced back to late 1950's is one of those existing technologies that gets the second look by research scientists. Even though, OFDM can offer several technical advantages which were already described in previous chapters, by itself, OFDM might not fully satisfy the increase in demand of higher data rate.

The Single Input Single Output (SISO) antenna implementation has always been the main type of antenna configuration for mobile or wireless local area network (WLAN) systems until recently. To further improve OFDM's capability of delivering high data rate, another antenna implementation called Multiple Input Multiple Output (MIMO) has been proposed. In addition, for those wireless communication systems that are equipped with multiple antennas, they are typically known as MIMO systems in literature. Fig. 7.1 shows two possible antenna configurations for MIMO systems. One of MIMO systems shown in Fig. 7.1 is Multiple Input Single Output (MISO) systems which have multiple transmit antennas and only a single receive antenna. Another MIMO system shown in the same figure has both multiple antennas at the transmitter and receiver. Despite the differences in system performance and hardware physical layer, MISO systems are sometimes referred as MIMO systems in literature. In this thesis, we will follow the conventional notation and refer MISO systems as MIMO systems. Furthermore, we will focus on the performance of a MISO

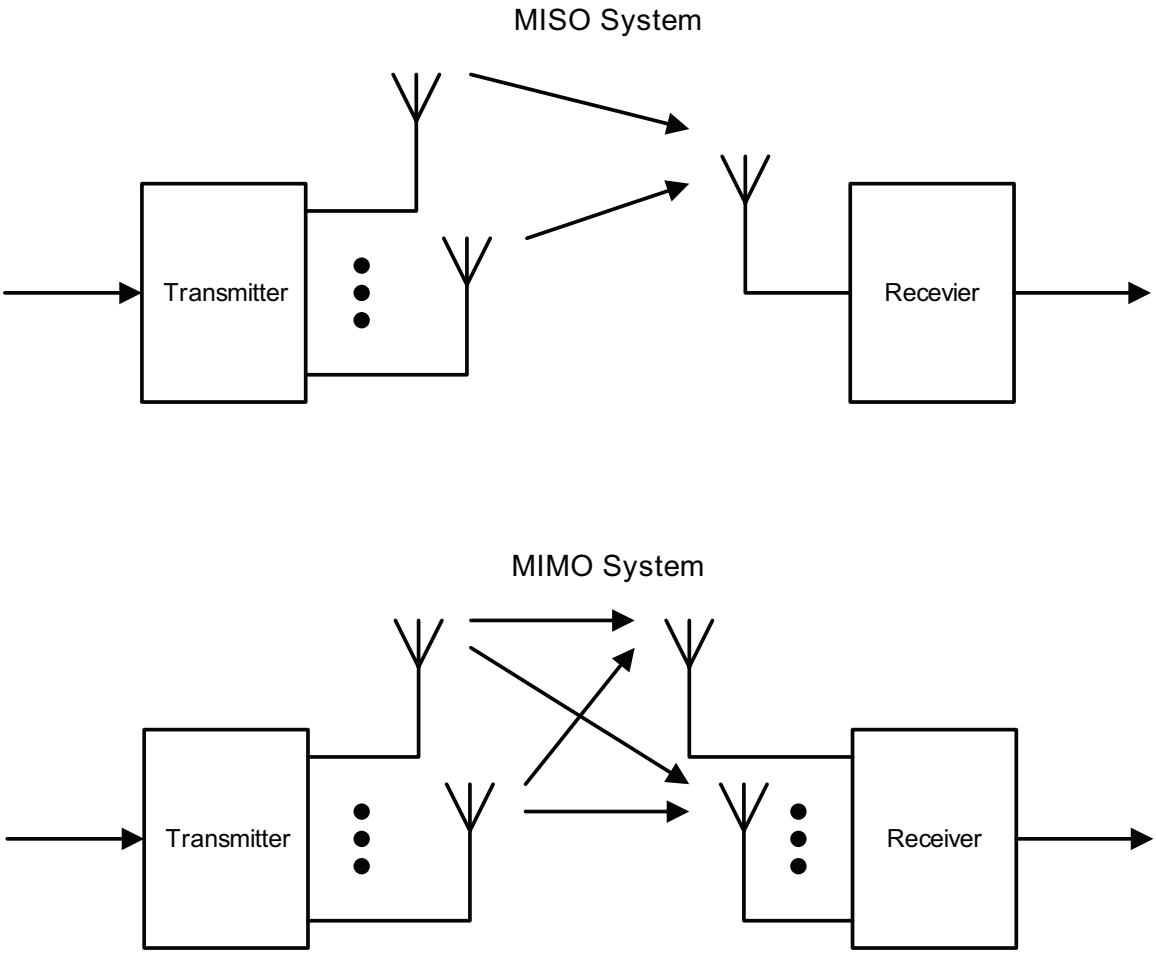

Figure 7.1 A depiction of MIMO systems with two different antenna configurations.

system in the thesis.

In 1998, Alamouti [21] presented a novel transmit diversity technique for a MISO system with two transmit antennas and one receive antenna which is shown in Fig. 7.2. The Alamouti code, proposed by Alamouti, [21] encodes modulated symbols across antennas and over time with the advantage of linear decoding. The improvement on system performance that the Alamouti code can offer is surprising. For example, it has been shown that a system with two transmit antennas and one receive antenna can provide the same diversity order as a system which has maximum ratio combining and is equipped with one transmit antenna and two receive antennas. Due to this reason, the Alamouti code has triggered a tremendous amount of research in coding schemes. Other codes were found for the cases where the systems have three or four transmit antennas and one receive antenna [34, 35]. Although the coding for three or four transmit antennas and one receive antenna can offer full diversity, however, they suffer from a loss in data rate since the number of modulated

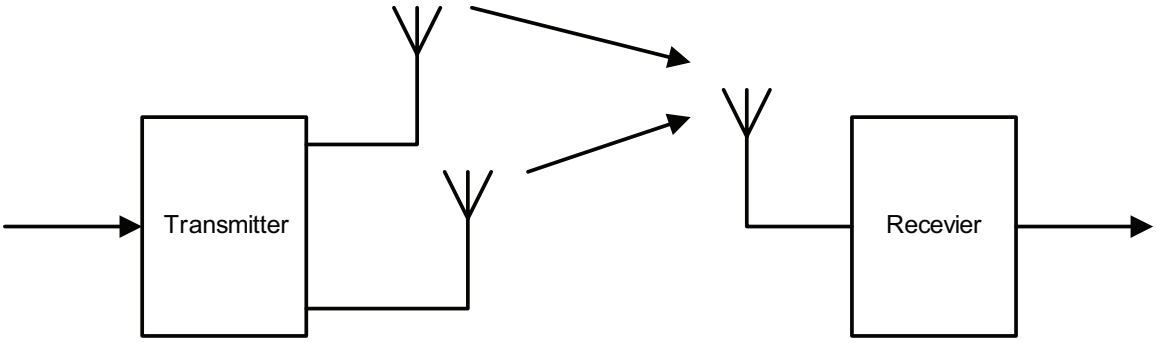

Figure 7.2 A depiction of a MISO system with two transmit antennas and one receive antenna.

symbols that are transmitted is less than the number of time slots that are used for transmissions. Since the coding schemes proposed in [21, 34, 35] encode modulated symbols across antennas and over time while providing the advantage of linear decoding, they are often referred to as Space Time Block Code (STBC) in literature. However, one should know that those coding schemes presented in [21, 34, 35] are only the subset of the STBC.

Since STBC can bring performance enhancement to wireless communication systems, it was soon adapted in OFDM systems. Lee *et al.* [36] presented the performance analysis of an OFDM system with two transmit antennas and a single receive antenna under the assumption of perfect channel estimation. In addition, the authors in [37] also presented a new application for STBC in OFDM. Instead of encoding OFDM symbols in time domain, the authors applied the Alamouti code to subcarriers of OFDM signals. Even though, both systems provide the same data rate, it has been shown that when the Alamouti code is applied to subcarriers, the performance is superior to the case where the Alamouti code is applied to OFDM symbols in time varying channels [37]. For the OFDM systems that have Alamouti code applied to OFDM symbols, those systems are typically known as STBC-OFDM or MIMO-OFDM. As for the case where the Alamouti code is applied to subcarriers, they are generally referred as Space Frequency Block Code (SFBC) OFDM. In this chapter, we will present the performance analysis of a M-ary Quadrature Amplitude Modulation (M-QAM) MIMO-OFDM with two or four transmit antennas and a single receive antenna in Rayleigh fading channels with and without the normalization in transmit power.

This chapter is organized as follows. Section 7.2 describes a MIMO-OFDM system with two transmit antennas and one receive antenna and Section 7.3 will present the MIMO-OFDM system with four transmit antennas and one receive antenna. In Section 7.4, we analyze the performance of the MIMO-OFDM system described in Section 7.2 with and without the normalization in transmit power. In Section 7.5, we will present the performance analysis for the other MIMO-OFDM system which is equipped with four transmit antennas instead of two. Simulation models and results

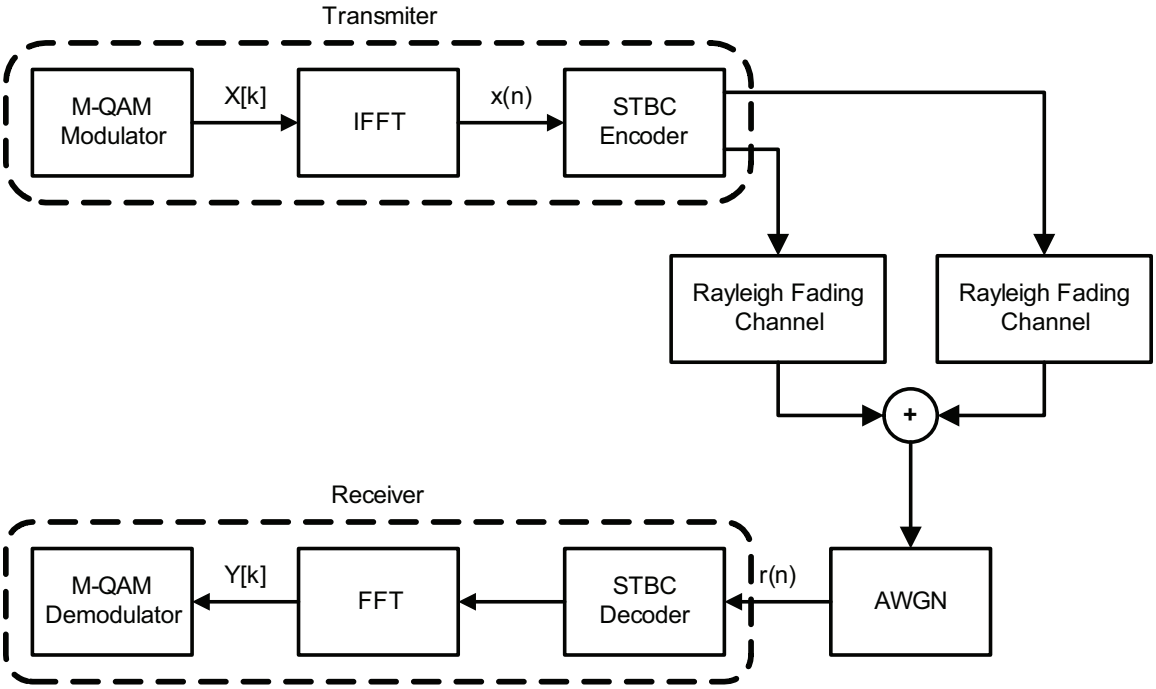

Figure 7.3 A system block diagram of a M-ary Quadrature Amplitude Modulation (M-QAM) MIMO-OFDM system with two transmit antennas and one receive antenna in Rayleigh fading channels.

along with theoretical values will be presented for both cases in Section 7.6. Finally, Section 7.7 summarizes the chapter.

7.2 System Description - Two Transmit Antennas

In this section, a description of a MIMO-OFDM system with two transmit antennas and one receive antenna will be presented and discussed first in detail, then followed by a discussion of a MIMO-OFDM system with four transmit antennas. Fig. 7.3 shows a MIMO-OFDM system with two transmit antennas. Each block is discussed in the following subsections.

7.2.1 Transmitter

The transmitter which is shown in Fig. 7.3 consists of a M-QAM modulator, IFFT and a STBC encoder. The input to the M-QAM modulator is assumed to be binary data bits which are equiprobable and statistically independent of each other. The stream of binary data bits are grouped into blocks of size $log_2 M$. They are subsequently mapped into M-QAM symbols, denoted as $X[k]$, according to the alphabet, $A = \{(2m-1-\sqrt{M})+j(2n-1-\sqrt{M})\}$ where $\{m, n = 1, 2, ...\sqrt{M}\}$ and M is the size of constellation. The output of the modulator is then fed into and processed by IFFT.

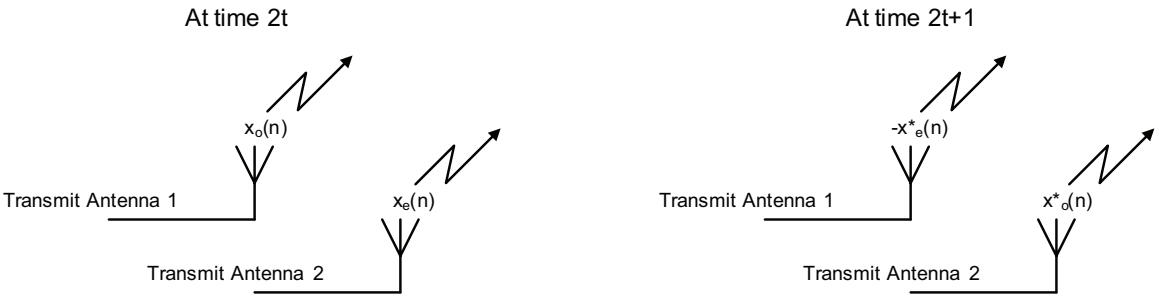

Figure 7.4 An illustration of the Alamouti coding scheme

At appropriate sampling time, the signal at the output of the IFFT, denoted as $x(n)$, is given by

$$x(n) = \frac{1}{N} \sum_{k=0}^{N-1} X[k] e^{j\frac{2\pi nk}{N}} \qquad 0 \leq n \leq N-1 \tag{7.1}$$

where N is the number of subcarriers.

7.2.2 STBC Encoder

For two transmit antennas, Fig. 7.4 illustrates how the STBC encoder which is implemented based on the Alamouti code encodes the OFDM symbols over time and across antennas. Let $x_o(n)$ and $x_e(n)$ be the odd and even number of OFDM symbols, respectively. At time $2t$, $x_o(n)$ and $x_e(n)$ are sent from transmit antenna one and transmit antenna two, respectively. At time $2t+1$, $-x_e^*(n)$ is transmitted from the first transmit antenna while x_o^* is transmitted from the second transmit antenna. Let $\mathcal{G}_2$ be the matrix that describes the coding scheme, then $\mathcal{G}_2$ is [21]

$$\mathcal{G}_2 = \begin{bmatrix} x_o(n) & x_e(n) \\ -x_e^*(n) & x_o^*(n) \end{bmatrix} \tag{7.2}$$

where $(\cdot)^*$ represents the complex conjugate operation and the subscript, 2, implies the number of transmit antennas.

7.2.3 Channel Model and AWGN

Denote $h_1(n)$ as the impulse response of the channel between the first transmit antenna and the receive antenna. The in-phase and quadrature components of $h_1(n)$ are assumed to be two independent Gaussian random variables with zero mean and $\sigma_{H_1}^2$ variance. Let $h_2(n)$ be the channel impulse response between the second transmit antenna and the receive antenna and its in-phase and quadrature components are assumed to be two independent Gaussian random variables with zero mean and $\sigma_{H_2}^2$ variance. Both Rayleigh fading channels are assumed to be statistically independent of each other and are static for the duration of two OFDM symbols transmissions. The additive white Gaussian noise (AWGN), denoted as $w(n)$, represents the thermal noise and is modeled as an independent AWGN process which has zero mean and $2\sigma_w^2$ variance.

7.2.4 Receiver

For the simplicity of notations, we will drop the time and frequency indices in the rest of chapter. Assuming perfect synchronization, $r_t(n)$, the received signal in time domain at time index t, is given by

$$r_t = \begin{cases} h_1 x_o + h_2 x_e + w_o & t = odd \\ -h_1 x_e^* + h_2 x_o^* + w_e & t = even \end{cases} \tag{7.3}$$

After rewriting (7.3) in the matrix format, $r_t(n)$ and its FFT are given by

$$\underbrace{\begin{bmatrix} r_o \\ r_e^* \end{bmatrix}}_{\mathbf{r}} = \underbrace{\begin{bmatrix} h_1 & h_2 \\ h_2^* & -h_1^* \end{bmatrix}}_{\mathbf{h}} \underbrace{\begin{bmatrix} x_o \\ x_e \end{bmatrix}}_{\mathbf{x}} + \underbrace{\begin{bmatrix} w_o \\ w_e^* \end{bmatrix}}_{\mathbf{w}}$$

$$\underbrace{\begin{bmatrix} R_o \\ R_e^* \end{bmatrix}}_{\mathbf{R}} = \underbrace{\begin{bmatrix} H_1 & H_2 \\ H_2^* & -H_1^* \end{bmatrix}}_{\mathbf{H}} \underbrace{\begin{bmatrix} X_o \\ X_e \end{bmatrix}}_{\mathbf{X}} + \underbrace{\begin{bmatrix} W_o \\ W_e^* \end{bmatrix}}_{\mathbf{W}}$$

$$\mathbf{r} = \mathbf{hx} + \mathbf{w} \overset{FFT}{\longleftrightarrow} \mathbf{R} = \mathbf{HX} + \mathbf{W} \tag{7.4}$$

where the bold face letters represent matrices or vectors. To accurately demodulate the received signal, estimating channel responses is necessary. In this chapter, we assume the channel impulse responses are known to the receiver. Denote the output of the FFT as $\mathbf{Y}$, then $\mathbf{Y}$ is found as

$$\begin{aligned} \mathbf{Y} =& \mathbf{H}^H \mathbf{R} \\ =& \mathbf{H}^H \mathbf{H} \mathbf{X} + \mathbf{H}^H \mathbf{W} \end{aligned} \tag{7.5}$$

where $(\cdot)^H$ is the Hermitian operation of matrix and $\mathbf{H}^H$ is given by

$$\mathbf{H}^H = \begin{bmatrix} H_1^* & H_2 \\ H_2^* & -H_1 \end{bmatrix} \tag{7.6}$$

Here, one can notice the advantage of the Alamouti code which is the linear decoding. By multiplying $\mathbf{H}$ with $\mathbf{H}^H$, the resulting matrix is an identity matrix with the channel gains, namely

$$\mathbf{H}^H \mathbf{H} = \begin{bmatrix} \alpha_1^2 + \alpha_2^2 & 0 \\ 0 & \alpha_1^2 + \alpha_2^2 \end{bmatrix} \tag{7.7}$$

where α_1 and α_2 are the magnitudes of the channels, H_1, and H_2, respectively. Since (7.7) is a matrix that has the nondiagonal elements being zero, this implies that X_o and X_e in (7.4) are decoupled after multiplying $\mathbf{R}$ in (7.4) with $\mathbf{H}^H$.

7.3 System Description - Four Transmit Antennas

Fig. 7.5 shows the MIMO-OFDM system with Four transmit antennas. Each block is discussed in the following subsections.

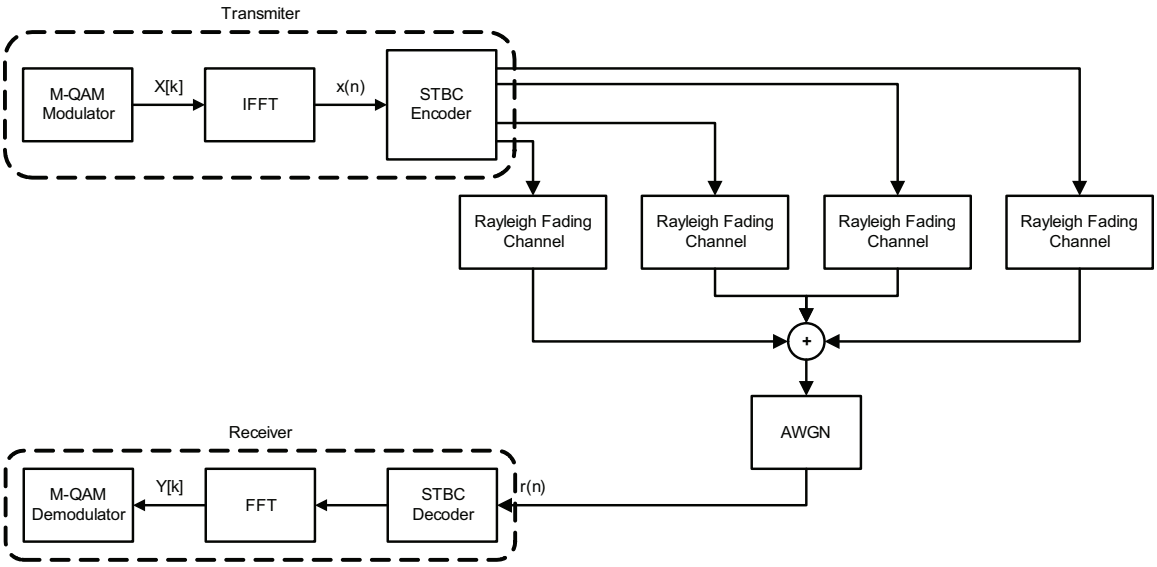

Figure 7.5 A system block diagram of a M-ary Quadrature Amplitude Modulation (M-QAM) MIMO-OFDM system with four transmit antennas and one receive antenna in Rayleigh fading channels.

7.3.1 Transmitter

Like in the case where there are two transmit antennas, the transmitter in this case is also composed of a M-QAM modulator, an IFFT and a STBC encoder. The assumption for the input signal to the M-QAM modulator is the same as for the case of two transmit antennas. In addition, the signal at the output of the IFFT, denoted as $x(n)$, has exactly the same expression as in the case of two transmit antennas and is defined as (7.1).

7.3.2 STBC Encoder

In the case of four transmit antennas, the STBC encoder which is implemented based on the code proposed by Tarokh *et al.* [34,35] encodes four OFDM symbols in each time slot and those four coded OFDM symbols are transmitted from four different transmit antennas in that time slot. The encoding process for the four transmit antennas is shown in Fig. 7.6. As it is shown in Fig. 7.6, the same four OFDM symbols are encoded differently by the STBC encoder and are transmitted from four different antennas in the second time slot. The encoding and transmission process continue until the transmitter has reached eight transmissions.

Let $x_1(n)$, $x_2(n)$, $x_3(n)$, and $x_4(n)$ be the first, second, third and fourth OFDM symbols, respectively. Denote $\mathcal{G}_4$ as the matrix that describes such STBC encoding process, then $\mathcal{G}_4$ is

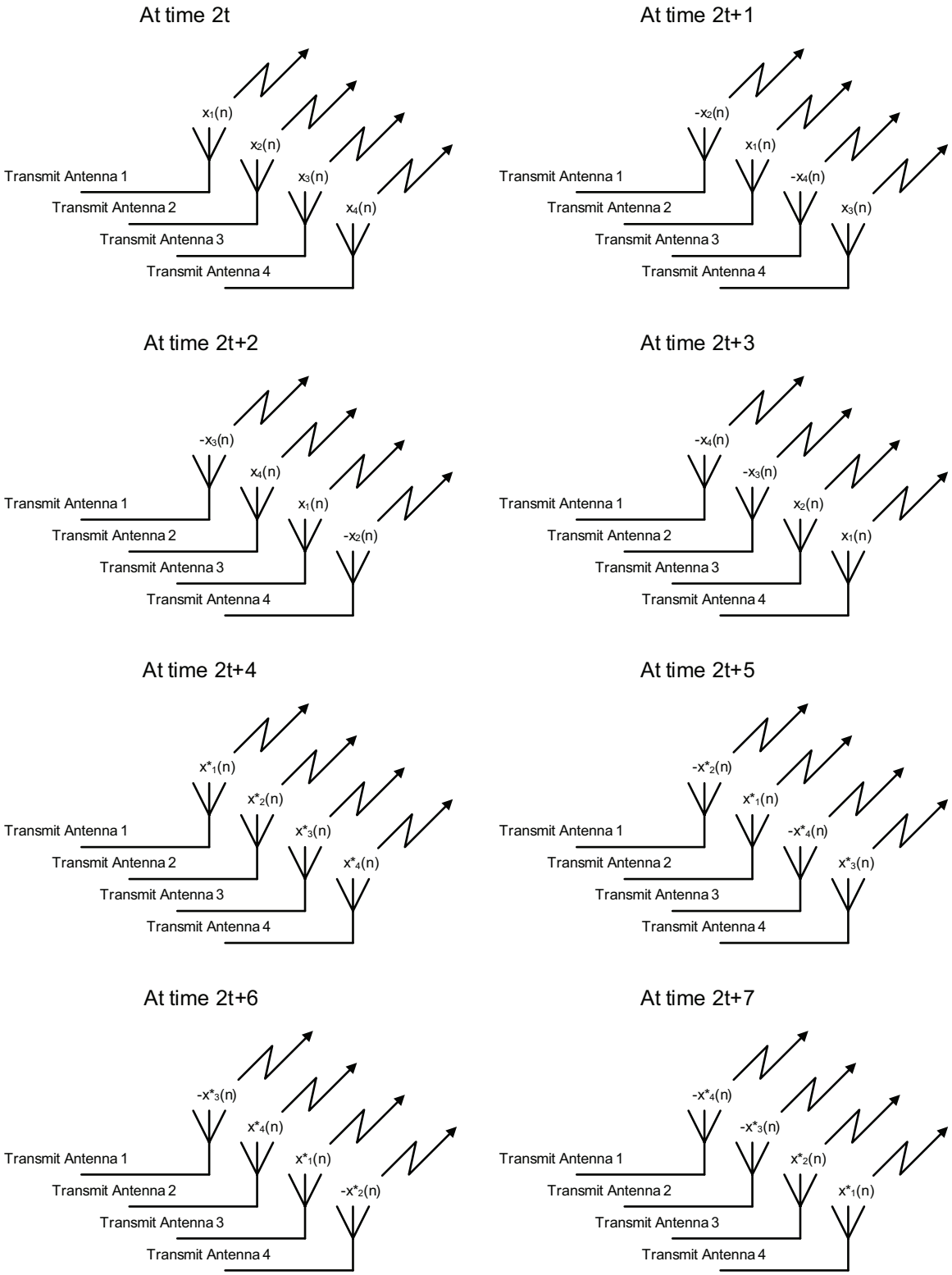

Figure 7.6 An illustration of the STBC coding process for four transmit antennas

given by [34, 35]

$$\mathcal{G}_4 = \begin{bmatrix} x_1(n) & x_2(n) & x_3(n) & x_4(n) \\ -x_2(n) & x_1(n) & -x_4(n) & x_3(n) \\ -x_3(n) & x_4(n) & x_1(n) & -x_2(n) \\ -x_4(n) & -x_3(n) & x_2(n) & x_1(n) \\ x_1^*(n) & x_2^*(n) & x_3^*(n) & x_4^*(n) \\ -x_2^*(n) & x_1^*(n) & -x_4^*(n) & x_3^*(n) \\ -x_3^*(n) & x_4^*(n) & x_1^*(n) & -x_2^*(n) \\ -x_4^*(n) & -x_3^*(n) & x_2^*(n) & x_1^*(n) \end{bmatrix} \tag{7.8}$$

7.3.3 Channel Model and AWGN

Let

- $h_1(n)$ be the channel impulse response between the first transmit antenna and the receive antenna. In addition, $h_1(n)$ is modeled as a complex Gaussian random process with zero mean and $2\sigma_{H_1}^2$ variance.
- $h_2(n)$ be the channel impulse response between the second transmit antenna and the receive antenna. $h_2(n)$ is also modeled as a complex Gaussian random process with zero mean and $2\sigma_{H_2}^2$ variance.
- $h_3(n)$ be the channel impulse response between the third transmit antenna and the receive antenna. Furthermore, the in-phase and quadrature components of $h_3(n)$ are Gaussian random variables with zero mean and $\sigma_{H_3}^2$ variance.
- $h_4(n)$ be the channel impulse response between the fourth transmit antenna and the receive antenna. In addition, $h_4(n)$ is modeled as a complex Gaussian random process with zero mean and $2\sigma_{H_4}^2$ variance.

All four channels and their in-phase and quadrature components are assumed to be statistically independent of each other and are static for the duration of eight OFDM transmissions. Denote $w(n)$ as the thermal noise, then $w(n)$ is modeled as an independent AWGN process with zero mean and $2\sigma_w^2$ variance.

7.3.4 Receiver

Assuming perfect synchronization, the received signal in time domain, denoted as $r_t(n)$, is given by

$$r_t(n) = \begin{cases} h_1x_1 + h_2x_2 + h_3x_3 + h_4x_4 + w_1 & t = 1 \\ -h_1x_2 + h_2x_1 - h_3x_4 + h_4x_3 + w_2 & t = 2 \\ -h_1x_3 + h_2x_4 + h_3x_1 - h_4x_2 + w_3 & t = 3 \\ -h_1x_4 - h_2x_3 + h_3x_2 + h_4x_1 + w_3 & t = 4 \\ h_1x_1^* + h_2x_2^* + h_3x_3^* + h_4x_4^* + w_5 & t = 5 \\ -h_1x_2^* + h_2x_1^* - h_3x_4^* + h_4x_3^* + w_6 & t = 6 \\ -h_1x_3^* + h_2x_4^* + h_3x_1^* - h_4x_2^* + w_7 & t = 7 \\ -h_1x_4^* - h_2x_3^* + h_3x_2^* + h_4x_1^* + w_8 & t = 8 \end{cases} \tag{7.9}$$

where t denotes the signal transmission at time index t.

After writing (7.9) in the matrix format, $r_t(n)$ is given by

$$\underbrace{\begin{bmatrix} r_1 \\ r_2 \\ r_3 \\ r_4 \\ r_5^* \\ r_6^* \\ r_7^* \\ r_8^* \end{bmatrix}}_{\mathbf{r}} = \underbrace{\begin{bmatrix} h_1(n) & h_2(n) & h_3(n) & h_4(n) \\ -h_2(n) & h_1(n) & -h_4(n) & h_3(n) \\ -h_3(n) & h_4(n) & h_1(n) & -h_2(n) \\ -h_4(n) & -h_3(n) & h_2(n) & h_1(n) \\ h_1^*(n) & h_2^*(n) & h_3^*(n) & h_4^*(n) \\ -h_2^*(n) & h_1^*(n) & -h_4^*(n) & h_3^*(n) \\ -h_3^*(n) & h_4^*(n) & h_1^*(n) & -h_2^*(n) \\ -h_4^*(n) & -h_3^*(n) & h_2^*(n) & h_1^*(n) \end{bmatrix}}_{\mathbf{h}} \underbrace{\begin{bmatrix} x_1 \\ x_2 \\ x_3 \\ x_4 \end{bmatrix}}_{\mathbf{x}} + \underbrace{\begin{bmatrix} w_1 \\ w_2 \\ w_3 \\ w_4 \\ w_5^* \\ w_6^* \\ w_7^* \\ w_8^* \end{bmatrix}}_{\mathbf{w}}$$

$$\mathbf{r} = \mathbf{hx} + \mathbf{w} \tag{7.10}$$

Consequently, the received signal in frequency domain, denote as $\mathbf{R}$, is given by

$$\underbrace{\begin{bmatrix} R_1 \\ R_2 \\ R_3 \\ R_4 \\ R_5^* \\ R_6^* \\ R_7^* \\ R_8^* \end{bmatrix}}_{\mathbf{R}} = \underbrace{\begin{bmatrix} H_1 & H_2 & H_3 & H_4 \\ -H_2 & H_1 & -H_4 & H_3 \\ -H_3 & H_4 & H_1 & -H_2 \\ -H_4 & -H_3 & H_2 & H_1 \\ H_1^* & H_2^* & H_3^* & H_4^* \\ -H_2^* & H_1^* & -H_4^* & H_3^* \\ -H_3^* & H_4^* & H_1^* & -H_2^* \\ -H_4^* & -H_3^* & H_2^* & H_1^* \end{bmatrix}}_{\mathbf{H}} \underbrace{\begin{bmatrix} X_1 \\ X_2 \\ X_3 \\ X_4 \end{bmatrix}}_{\mathbf{X}} + \underbrace{\begin{bmatrix} W_1 \\ W_2 \\ W_3 \\ W_4 \\ W_5^* \\ W_6^* \\ W_7^* \\ W_8^* \end{bmatrix}}_{\mathbf{W}}$$

$$\mathbf{R} = \mathbf{HX} + \mathbf{W} \tag{7.11}$$

Let $\mathbf{Y}$ be the signal at the output of the FFT. Then, under the assumption of perfect channel estimation, $\mathbf{Y}$ is given by

$$\begin{aligned}\mathbf{Y} =& \mathbf{H}^H \mathbf{R} \\ =& \mathbf{H}^H \mathbf{H}\mathbf{X} + \mathbf{H}^H \mathbf{W}\end{aligned} \tag{7.12}$$

where $\mathbf{H}^H$ in the case of four transmit antennas is given by

$$\mathbf{H}^H = \begin{bmatrix} H_1^* & -H_2^* & -H_3^* & -H_4^* & H_1 & -H_2 & -H_3 & -H_4 \\ H_2^* & H_1^* & H_4^* & -H_3^* & H_2 & H_1 & H_4 & -H_3 \\ H_3^* & -H_4^* & H_1^* & H_2^* & H_3 & -H_4 & H_1 & H_2 \\ H_4^* & H_3^* & -H_2^* & H_1^* & H_4 & H_3 & -H_2 & H_1 \end{bmatrix} \tag{7.13}$$

Here, in the case of four transmit antennas, the coding scheme has the same advantage that the Alamouti code offers. By taking the product of $\mathbf{H}^H$ and $\mathbf{H}$, the resulting matrix is given by

$$\mathbf{H}^H \mathbf{H} = 2(\alpha_1^2 + \alpha_2^2 + \alpha_3^2 + \alpha_4^2) \begin{bmatrix} 1 & 0 & 0 & 0 \\ 0 & 1 & 0 & 0 \\ 0 & 0 & 1 & 0 \\ 0 & 0 & 0 & 1 \end{bmatrix} \tag{7.14}$$

where α_1, α_2, α_3, and α_4 are the magnitudes of channels, H_1, H_2, H_3 and H_4, respectively. As one can see from (7.14), this leads to the decouplings of X_1, X_2, X_3 and X_4 because (7.14) is an identity matrix multiplied by a sum of four random variables.

7.4 Performance Analysis - Two Transmit Antennas

In this section, we will derive the bit error rate (BER) of the MIMO-OFDM system which is described in Section 7.2. In order to make a fair comparison with the performance of SISO-OFDM systems, we will also present the BER derivation of the MIMO-OFDM system with two transmit antennas and one receive antenna for the case where there is a constraint of normalization in transmit power. First, we will present the performance analysis of the system without the normalization in transmit power, followed by the performance analysis of the same system but with the normalization in transmit power.

7.4.1 No Normalization in Transmit Power

After some algebra, the output of FFT, $\mathbf{Y}$, is given by

$$\begin{aligned}\mathbf{Y} =& \mathbf{H}^H\mathbf{H}\mathbf{X} + \mathbf{H}^H\mathbf{W} \\ =& \left(\alpha_1^2+\alpha_2^2\right)\mathbb{I}_{2\times 2}\begin{bmatrix} X_o \\ X_e \end{bmatrix} + \begin{bmatrix} H_1^* & H_2 \\ H_2^* & -H_1 \end{bmatrix}\begin{bmatrix} W_o \\ W_e^* \end{bmatrix} \\ =& \left(\alpha_1^2+\alpha_2^2\right)\mathbb{I}_{2\times 2}\begin{bmatrix} X_o \\ X_e \end{bmatrix} + \underbrace{\begin{bmatrix} H_1^*W_o + H_2W_e^* \\ H_2^*W_o - H_1W_e^* \end{bmatrix}}_{\mathbf{W}'}\end{aligned} \tag{7.15}$$

where $\mathbb{I}_{2\times 2}$ implies the 2 by 2 identity matrix. $\mathbf{W}^{'}$ which has zero mean represents the noise component of the received signal in (7.15). To derive the BER, it is necessary to find the variance of $\mathbf{W}^{'}$. Denote $\sigma^2_{\mathbf{W}'}$ as the variance matrix for $\mathbf{W}^{'}$, then $\sigma^2_{\mathbf{W}'}$ is given by

$$\begin{aligned}\sigma^2_{\mathbf{W}'} =& E\left\{\mathbf{W}^{'}\mathbf{W}^{'H}\right\} \\ =& E\left\{\begin{bmatrix} H_1^*W_o + H_2W_e^* \\ H_2^*W_o - H_1W_e^* \end{bmatrix}\begin{bmatrix} H_1W_o^* + H_2^*W_e & H_2W_o^* - H_1^*W_e \end{bmatrix}\right\} \\ =& \left(\alpha_1^2+\alpha_2^2\right)\sigma_w^2\mathbb{I}_{2\times 2}\end{aligned} \tag{7.16}$$

To arrive the result in (7.16), we assume that the in-phase or quadrature components of W_o and W_e have the same variance which is equal to σ_w^2. In addition, we make no distinction between even and odd number of OFDM symbols and we assume that each OFDM symbol has the same average power, i.e. $E\{X_o^2\} = E\{X_e^2\} = E\{X^2\}$. (7.15) becomes

$$Y = \left(\alpha_1^2+\alpha_2^2\right)X + W^{'} \tag{7.17}$$

To continue derivation, we choose 16-QAM modulation as the modulation scheme. However, this derivation can be extended to any rectangular QAM modulation scheme. Denote $P_{BER|\alpha_1,\alpha_2}$ as the conditional BER of 16-QAM symbols conditioned on α_1 and α_2, then $P_{BER|\alpha_1,\alpha_2}$ is given by

$$\begin{aligned}P_{BER|\alpha_1,\alpha_2} =& \frac{1}{2}\left(P_{MSB} + P_{LSB}\right) \\ =& \frac{3}{4}Q\left(\sqrt{\frac{\left(\alpha_1^2+\alpha_2^2\right)d^2}{\sigma_w^2}}\right) + \frac{1}{2}Q\left(\sqrt{\frac{9\left(\alpha_1^2+\alpha_2^2\right)d^2}{\sigma_w^2}}\right) - \frac{1}{4}Q\left(\sqrt{\frac{25\left(\alpha_1^2+\alpha_2^2\right)d^2}{\sigma_w^2}}\right)\end{aligned} \tag{7.18}$$

where P_{MSB} and P_{LSB} are the conditional probabilities of most significant bits and least significant bits of 16-QAM symbols. $d^2 = \frac{2}{5}E_b$ and E_b is energy per bit. Subsequently, let P_{BER} be the unconditional BER of 16-QAM, then P_{BER} is found as

$$P_{BER} = \int_0^\infty \int_0^\infty P_{BER|\alpha_1,\alpha_2}p(\alpha_1)p(\alpha_2)d\alpha_1 d\alpha_2 \tag{7.19}$$

where $p(\alpha_1)$ and $p(\alpha_2)$ are probability density functions (PDFs) of α_1 and α_2, respectively. Both $p(\alpha_1)$ and $p(\alpha_2)$ are then given by

$$p(\alpha_1) = \frac{\alpha_1}{\sigma_{H_1}^2} e^{\frac{-\alpha_1^2}{2\sigma_{H_1}^2}} \qquad\qquad p(\alpha_2) = \frac{\alpha_2}{\sigma_{H_2}^2} e^{\frac{-\alpha_2^2}{2\sigma_{H_2}^2}} \tag{7.20}$$

In most literature [38–42], (7.19) would be the end result of performance analysis. However, (7.19) can be simplified further by rewriting the $Q(\cdot)$ function in its alternate form which is given by ([43], Eq:(4.2))

$$Q(x) = \frac{1}{\pi} \int_0^{\frac{\pi}{2}} exp\left(\frac{-x^2}{2\sin^2\theta}\right) d\theta \tag{7.21}$$

One observation about (7.21) is this alternate form of Q function provides the same exact numerical value if one evaluates using the conventional definition for the Q function. Substituting (7.20) and (7.21) into (7.19), P_{BER} then becomes

$$\begin{aligned} P_{BER} =& \frac{1}{\pi} \int_0^{\frac{\pi}{2}} \int_0^{\infty} \int_0^{\infty} \frac{3}{4} \frac{\alpha_1}{\sigma_{H_1}^2} \frac{\alpha_2}{\sigma_{H_2}^2} exp\left(\frac{-\left(\alpha_1^2+\alpha_2^2\right) d^2}{2\sigma_w^2 \sin^2\theta} - \frac{\alpha_1^2}{2\sigma_{H_1}^2} - \frac{\alpha_2^2}{2\sigma_{H_2}^2}\right) d\alpha_1 d\alpha_2 d\theta \\ &+ \frac{1}{\pi} \int_0^{\frac{\pi}{2}} \int_0^{\infty} \int_0^{\infty} \frac{1}{2} \frac{\alpha_1}{\sigma_{H_1}^2} \frac{\alpha_2}{\sigma_{H_2}^2} exp\left(\frac{-9\left(\alpha_1^2+\alpha_2^2\right) d^2}{2\sigma_w^2 \sin^2\theta} - \frac{\alpha_1^2}{2\sigma_{H_1}^2} - \frac{\alpha_2^2}{2\sigma_{H_2}^2}\right) d\alpha_1 d\alpha_2 d\theta \\ &- \frac{1}{\pi} \int_0^{\frac{\pi}{2}} \int_0^{\infty} \int_0^{\infty} \frac{1}{4} \frac{\alpha_1}{\sigma_{H_1}^2} \frac{\alpha_2}{\sigma_{H_2}^2} exp\left(\frac{-25\left(\alpha_1^2+\alpha_2^2\right) d^2}{2\sigma_w^2 \sin^2\theta} - \frac{\alpha_1^2}{2\sigma_{H_1}^2} - \frac{\alpha_2^2}{2\sigma_{H_2}^2}\right) d\alpha_1 d\alpha_2 d\theta \end{aligned} \tag{7.22}$$

Notice that (7.22) might seem to be more complicated than (7.19), however, (7.22) can be simplified further due to the reason that α_1 and α_2 are independent of each other. To demonstrate, we will use the first term in (7.22) as an example,

$$\begin{aligned} &\frac{1}{\pi} \int_0^{\frac{\pi}{2}} \int_0^{\infty} \int_0^{\infty} \frac{3}{4} \frac{\alpha_1}{\sigma_{H_1}^2} \frac{\alpha_2}{\sigma_{H_2}^2} exp\left(\frac{-\left(\alpha_1^2+\alpha_2^2\right) d^2}{2\sigma_w^2 \sin^2\theta} - \frac{\alpha_1^2}{2\sigma_{H_1}^2} - \frac{\alpha_2^2}{2\sigma_{H_2}^2}\right) d\alpha_1 d\alpha_2 d\theta \\ &= \frac{3}{4\pi} \int_0^{\frac{\pi}{2}} \int_0^{\infty} \frac{\alpha_2}{\sigma_{H_2}^2} \left[\int_0^{\infty} \frac{\alpha_1}{\sigma_{H_1}^2} exp\left(-\alpha_1^2\left(\frac{d^2}{2\sigma_w^2 \sin^2\theta} + \frac{1}{2\sigma_{H_1}^2}\right)\right) d\alpha_1\right] \\ &\qquad exp\left(-\alpha_2^2\left(\frac{d^2}{2\sigma_w^2 \sin^2\theta} + \frac{1}{2\sigma_{H_2}^2}\right)\right) d\alpha_2 d\theta \\ &= \frac{3}{4\pi} \int_0^{\frac{\pi}{2}} \frac{1}{\left[1 + \frac{\sigma_{H_1}^2 d^2}{\sigma_w^2 \sin^2\theta}\right]} \int_0^{\infty} \frac{\alpha_2}{\sigma_{H_2}^2} exp\left(-\alpha_2^2\left(\frac{d^2}{2\sigma_w^2 \sin^2\theta} + \frac{1}{2\sigma_{H_2}^2}\right)\right) d\alpha_2 d\theta \\ &= \frac{3}{4\pi} \int_0^{\frac{\pi}{2}} \left[1 + \frac{\sigma_{H_1}^2 d^2}{\sigma_w^2 \sin^2\theta}\right]^{-1} \left[1 + \frac{\sigma_{H_2}^2 d^2}{\sigma_w^2 \sin^2\theta}\right]^{-1} d\theta \end{aligned} \tag{7.23}$$

Applying the same procedure to the rest of terms in (7.22), P_{BER} is then expressed as

$$\begin{aligned} P_{BER} =& \frac{3}{4\pi}\int_0^{\frac{\pi}{2}} \left[1+\frac{\sigma_{H_1}^2 d^2}{\sigma_w^2 \sin^2\theta}\right]^{-1}\left[1+\frac{\sigma_{H_2}^2 d^2}{\sigma_w^2 \sin^2\theta}\right]^{-1} d\theta \\ &+ \frac{1}{2\pi}\int_0^{\frac{\pi}{2}} \left[1+\frac{9\sigma_{H_1}^2 d^2}{\sigma_w^2 \sin^2\theta}\right]^{-1}\left[1+\frac{9\sigma_{H_2}^2 d^2}{\sigma_w^2 \sin^2\theta}\right]^{-1} d\theta \\ &- \frac{1}{4\pi}\int_0^{\frac{\pi}{2}} \left[1+\frac{25\sigma_{H_1}^2 d^2}{\sigma_w^2 \sin^2\theta}\right]^{-1}\left[1+\frac{25\sigma_{H_2}^2 d^2}{\sigma_w^2 \sin^2\theta}\right]^{-1} d\theta \end{aligned} \tag{7.24}$$

Notice that compared to (7.19), (7.24) provides a much easier way to evaluate the same BER expression since P_{BER} now is equal to a sum of three single integrals instead of a sum of three double integrals. However, one can not apply this simplifying approach to the performance analysis of a system which has the nonlinear high power amplifiers (HPAs) in the transmitter. This is due to the reason that when the nonlinear HPAs are present in the transmitter, the integration variable would appear in both the numerator and denominator of the Q function's argument which prevents further mathematical simplification.

7.4.2 Normalization in Transmit Power

In this section, we will derive the BER for the MIMO-System which is shown in Fig. 7.3 for the case where the transmit power is normalized by the number of transmit antennas. With the transmit power normalized by the number of transmit antennas, the received signal, denoted as $r_t(n)$, and its FFT are given by

$$\begin{aligned} \underbrace{\begin{bmatrix} r_o \\ r_e^* \end{bmatrix}}_{\mathbf{r}} =& \frac{1}{\sqrt{2}} \underbrace{\begin{bmatrix} h_1 & h_2 \\ h_2^* & -h_1^* \end{bmatrix}}_{\mathbf{h}} \underbrace{\begin{bmatrix} x_o \\ x_e \end{bmatrix}}_{\mathbf{x}} + \underbrace{\begin{bmatrix} w_o \\ w_e^* \end{bmatrix}}_{\mathbf{w}} \\ \underbrace{\begin{bmatrix} R_o \\ R_e^* \end{bmatrix}}_{\mathbf{R}} =& \frac{1}{\sqrt{2}} \underbrace{\begin{bmatrix} H_1 & H_2 \\ H_2^* & -H_1^* \end{bmatrix}}_{\mathbf{H}} \underbrace{\begin{bmatrix} X_o \\ X_e \end{bmatrix}}_{\mathbf{X}} + \underbrace{\begin{bmatrix} W_o \\ W_e^* \end{bmatrix}}_{\mathbf{W}} \\ \mathbf{r} =& \frac{1}{\sqrt{2}}\mathbf{h}\mathbf{x} + \mathbf{w} \overset{FFT}{\longleftrightarrow} \mathbf{R} = \frac{1}{\sqrt{2}}\mathbf{H}\mathbf{X} + \mathbf{W} \end{aligned} \tag{7.25}$$

At the output of FFT, $\mathbf{Y}$ is expressed as

$$\begin{aligned} \mathbf{Y} =& \frac{(\alpha_1^2+\alpha_2^2)}{\sqrt{2}}\mathbb{I}_{2\times 2}\begin{bmatrix} X_o \\ X_e \end{bmatrix} + \begin{bmatrix} H_1^* & H_2 \\ H_2^* & -H_1 \end{bmatrix}\begin{bmatrix} W_o \\ W_e^* \end{bmatrix} \\ =& \frac{(\alpha_1^2+\alpha_2^2)}{\sqrt{2}}\mathbb{I}_{2\times 2}\begin{bmatrix} X_o \\ X_e \end{bmatrix} + \begin{bmatrix} H_1^* W_o + H_2 W_e^* \\ H_2^* W_o - H_1 W_e^* \end{bmatrix} \end{aligned} \tag{7.26}$$

In addition, the variance for the noise matrix in (7.26) can be obtained by following the procedure described in the case where the transmit power is not normalized and is found as (7.16). In this case, we also assume that 16-QAM modulation is utilized to modulate signals. Denote $P_{BER|\alpha_1,\alpha_2}^N$ as the

conditional BER for 16-QAM symbols conditioned on α_1 and α_2 for the case where the transmit power is normalized by the number of transmit antennas, then $P^N_{BER|\alpha_1,\alpha_2}$ is given by

$$\begin{aligned} P^N_{BER|\alpha_1,\alpha_2} =& \frac{1}{2}\left(P_{MSB} + P_{LSB}\right) \\ =& \frac{3}{4}Q\left(\sqrt{\frac{\left(\alpha_1^2+\alpha_2^2\right)d^2}{2\sigma_w^2}}\right) + \frac{1}{2}Q\left(\sqrt{\frac{9\left(\alpha_1^2+\alpha_2^2\right)d^2}{2\sigma_w^2}}\right) - \frac{1}{4}Q\left(\sqrt{\frac{25\left(\alpha_1^2+\alpha_2^2\right)d^2}{2\sigma_w^2}}\right) \end{aligned} \tag{7.27}$$

In addition, let P^N_{BER} be the unconditional BER for 16-QAM for the case where the transmit power is normalized by the number of transmit antennas, then P^N_{BER} is

$$P^N_{BER} = \int_0^\infty \int_0^\infty P^N_{BER|\alpha_1,\alpha_2} p(\alpha_1) p(\alpha_2) d\alpha_1 d\alpha_2 \tag{7.28}$$

where $p(\alpha_1)$ and $p(\alpha_2)$ are defined as (7.20). By writing $Q(\cdot)$ function as its alternate form, (7.28) is given by

$$\begin{aligned} P^N_{BER} =& \frac{3}{4\pi}\int_0^{\frac{\pi}{2}} \left[1+\frac{\sigma_{H_1}^2 d^2}{2\sigma_w^2\sin^2\theta}\right]^{-1}\left[1+\frac{\sigma_{H_2}^2 d^2}{2\sigma_w^2\sin^2\theta}\right]^{-1} d\theta \\ &+ \frac{1}{2\pi}\int_0^{\frac{\pi}{2}} \left[1+\frac{9\sigma_{H_1}^2 d^2}{2\sigma_w^2\sin^2\theta}\right]^{-1}\left[1+\frac{9\sigma_{H_2}^2 d^2}{2\sigma_w^2\sin^2\theta}\right]^{-1} d\theta \\ &- \frac{1}{4\pi}\int_0^{\frac{\pi}{2}} \left[1+\frac{25\sigma_{H_1}^2 d^2}{2\sigma_w^2\sin^2\theta}\right]^{-1}\left[1+\frac{25\sigma_{H_2}^2 d^2}{2\sigma_w^2\sin^2\theta}\right]^{-1} d\theta \end{aligned} \tag{7.29}$$

7.5 Performance Analysis - Four Transmit Antennas

In this section, we will derive the BER of the MIMO-OFDM system which is described in Section 7.3 with and without the constraint of normalization in transmit power. We will first derive the performance of the system when total transmit power is not normalized, followed by the derivation of the performance of the same system when the normalization is applied to the transmit power.

7.5.1 No Normalization in Transmit Power

Recall that the output signal at the FFT is given by

$$\begin{aligned} \mathbf{Y} =& \mathbf{H}^H\mathbf{H}\mathbf{X} + \mathbf{H}^H\mathbf{W} \\ =& 2\left(\alpha_1^2+\alpha_2^2+\alpha_3^2+\alpha_4^2\right)\mathbb{I}_{4\times 4}\mathbf{X} + \mathbf{W}'' \end{aligned} \tag{7.30}$$

where

$$\mathbf{W}'' = \begin{bmatrix} H_1^* & -H_2^* & -H_3^* & -H_4^* & H_1 & -H_2 & -H_3 & -H_4 \\ H_2^* & H_1^* & H_4^* & -H_3^* & H_2 & H_1 & H_4 & -H_3 \\ H_3^* & -H_4^* & H_1^* & H_2^* & H_3 & -H_4 & H_1 & H_2 \\ H_4^* & H_3^* & -H_2^* & H_1^* & H_4 & H_3 & -H_2 & H_1 \end{bmatrix} \begin{bmatrix} W_1 \\ W_2 \\ W_3 \\ W_4 \\ W_5^* \\ W_6^* \\ W_7^* \\ W_8^* \end{bmatrix} \tag{7.31}$$

Since $\mathbf{W}''$ is the noise component of (7.30). We need to find its mean and variance. The mean of $\mathbf{W}''$ is zero and the variance, denoted as $\sigma^2_{\mathbf{W}''}$, is found as

$$\begin{aligned} \sigma^2_{\mathbf{W}''} =& E\left\{\mathbf{W}''\mathbf{W}''^H\right\} \\ =& E\left\{(\mathbf{H}^H\mathbf{W})(\mathbf{W}^H\mathbf{H})\right\} \\ =& 2\left(\alpha_1^2+\alpha_2^2+\alpha_3^2+\alpha_4^2\right)\sigma_w^2\mathbb{I}_{4\times 4} \end{aligned} \tag{7.32}$$

To arrive the result in (7.32), we assume that the in-phase and quadrature components of W_t where $t = 1, 2, ...8$ have the same variance which equals σ_w^2. To make a fair comparison, we will also assume that the 16-QAM modulation is used to modulate signals, however, the derivation presented here can be extended to other rectangular QAM modulation schemes. Furthermore, we make no distinction between the first, the second, the third and the fourth OFDM symbols. We also assume that the average power of X_1, X_2, X_3 and X_4 are the same, namely $E\{X_1^2\} = E\{X_2^2\} = E\{X_3^2\} = E\{X_4^2\} = E\{X^2\}$. Denote $P_{BER|\alpha_1,\alpha_2,\alpha_3,\alpha_4}$ as the conditional BER for 16-QAM conditioned on α_1, α_2, α_3 and α_4, then $P_{BER|\alpha_1,\alpha_2,\alpha_3,\alpha_4}$ is expressed as

$$\begin{aligned} P_{BER|\alpha_1,\alpha_2,\alpha_3,\alpha_4} =& \frac{1}{2}\left(P_{MSB}+P_{LSB}\right) \\ =& \frac{3}{4}Q\left(\sqrt{\frac{2\left(\alpha_1^2+\alpha_2^2+\alpha_3^2+\alpha_4^2\right)d^2}{\sigma_w^2}}\right)+\frac{1}{2}Q\left(\sqrt{\frac{18\left(\alpha_1^2+\alpha_2^2+\alpha_3^2+\alpha_4^2\right)d^2}{\sigma_w^2}}\right) \\ & -\frac{1}{4}Q\left(\sqrt{\frac{50\left(\alpha_1^2+\alpha_2^2+\alpha_3^2+\alpha_4^2\right)d^2}{\sigma_w^2}}\right) \end{aligned} \tag{7.33}$$

Consequently, the unconditional BER, denoted as P_{BER} is given by

$$P_{BER} = \int_0^\infty\int_0^\infty\int_0^\infty\int_0^\infty P_{BER|\alpha_1,\alpha_2,\alpha_3,\alpha_4}p(\alpha_1)p(\alpha_2)p(\alpha_3)p(\alpha_4)d\alpha_1 d\alpha_2 d\alpha_3 d\alpha_4 \tag{7.34}$$

where $p(\alpha_1)$, $p(\alpha_2)$, $p(\alpha_3)$ and $p(\alpha_4)$ are PDFs of α_1, α_2, α_3 and α_4, respectively. In addition, they are given by

$$\begin{aligned} p(\alpha_1) &= \frac{\alpha_1}{\sigma_{H_1}^2}e^{\frac{-\alpha_1^2}{2\sigma_{H_1}^2}} & p(\alpha_2) &= \frac{\alpha_2}{\sigma_{H_2}^2}e^{\frac{-\alpha_2^2}{2\sigma_{H_2}^2}} \\ p(\alpha_3) &= \frac{\alpha_3}{\sigma_{H_3}^2}e^{\frac{-\alpha_3^2}{2\sigma_{H_3}^2}} & p(\alpha_4) &= \frac{\alpha_4}{\sigma_{H_4}^2}e^{\frac{-\alpha_4^2}{2\sigma_{H_4}^2}} \end{aligned} \tag{7.35}$$

With the aid of (7.21), (7.34) is simplified further and becomes

$$\begin{aligned}P_{BER} =&\frac{3}{4\pi}\int_0^{\frac{\pi}{2}}\left[1+\frac{2\sigma_{H_1}^2 d^2}{\sigma_w^2\sin^2\theta}\right]^{-1}\left[1+\frac{2\sigma_{H_2}^2 d^2}{\sigma_w^2\sin^2\theta}\right]^{-1}\left[1+\frac{2\sigma_{H_3}^2 d^2}{\sigma_w^2\sin^2\theta}\right]^{-1}\left[1+\frac{2\sigma_{H_4}^2 d^2}{\sigma_w^2\sin^2\theta}\right]^{-1}d\theta\\ &+\frac{1}{2\pi}\int_0^{\frac{\pi}{2}}\left[1+\frac{18\sigma_{H_1}^2 d^2}{\sigma_w^2\sin^2\theta}\right]^{-1}\left[1+\frac{18\sigma_{H_2}^2 d^2}{\sigma_w^2\sin^2\theta}\right]^{-1}\left[1+\frac{18\sigma_{H_3}^2 d^2}{\sigma_w^2\sin^2\theta}\right]^{-1}\left[1+\frac{18\sigma_{H_4}^2 d^2}{\sigma_w^2\sin^2\theta}\right]^{-1}d\theta\\ &-\frac{1}{4\pi}\int_0^{\frac{\pi}{2}}\left[1+\frac{50\sigma_{H_1}^2 d^2}{\sigma_w^2\sin^2\theta}\right]^{-1}\left[1+\frac{50\sigma_{H_2}^2 d^2}{\sigma_w^2\sin^2\theta}\right]^{-1}\left[1+\frac{50\sigma_{H_3}^2 d^2}{\sigma_w^2\sin^2\theta}\right]^{-1}\left[1+\frac{50\sigma_{H_4}^2 d^2}{\sigma_w^2\sin^2\theta}\right]^{-1}d\theta\end{aligned} \tag{7.36}$$

7.5.2 Normalization in Transmit Power

In the case where the transmit power is normalized by the number of transmit antennas, the received signal in time domain is given by

$$\underbrace{\begin{bmatrix} r_1\\ r_2\\ r_3\\ r_4\\ r_5^*\\ r_6^*\\ r_7^*\\ r_8^*\end{bmatrix}}_{\mathbf{r}} = \frac{1}{\sqrt{4}}\underbrace{\begin{bmatrix} h_1(n) & h_2(n) & h_3(n) & h_4(n)\\ -h_2(n) & h_1(n) & -h_4(n) & h_3(n)\\ -h_3(n) & h_4(n) & h_1(n) & -h_2(n)\\ -h_4(n) & -h_3(n) & h_2(n) & h_1(n)\\ h_1^*(n) & h_2^*(n) & h_3^*(n) & h_4^*(n)\\ -h_2^*(n) & h_1^*(n) & -h_4^*(n) & h_3^*(n)\\ -h_3^*(n) & h_4^*(n) & h_1^*(n) & -h_2^*(n)\\ -h_4^*(n) & -h_3^*(n) & h_2^*(n) & h_1^*(n)\end{bmatrix}}_{\mathbf{h}}\underbrace{\begin{bmatrix} x_1\\ x_2\\ x_3\\ x_4\end{bmatrix}}_{\mathbf{x}} + \underbrace{\begin{bmatrix} w_1\\ w_2\\ w_3\\ w_4\\ w_5^*\\ w_6^*\\ w_7^*\\ w_8^*\end{bmatrix}}_{\mathbf{w}}$$

$$\mathbf{r} = \frac{1}{\sqrt{4}}\mathbf{h}\mathbf{x} + \mathbf{w} \tag{7.37}$$

Consequently, the received signal in frequency domain is given by

$$\underbrace{\begin{bmatrix} R_1\\ R_2\\ R_3\\ R_4\\ R_5^*\\ R_6^*\\ R_7^*\\ R_8^*\end{bmatrix}}_{\mathbf{R}} = \frac{1}{\sqrt{4}}\underbrace{\begin{bmatrix} H_1 & H_2 & H_3 & H_4\\ -H_2 & H_1 & -H_4 & H_3\\ -H_3 & H_4 & H_1 & -H_2\\ -H_4 & -H_3 & H_2 & H_1\\ H_1^* & H_2^* & H_3^* & H_4^*\\ -H_2^* & H_1^* & -H_4^* & H_3^*\\ -H_3^* & H_4^* & H_1^* & -H_2^*\\ -H_4^* & -H_3^* & H_2^* & H_1^*\end{bmatrix}}_{\mathbf{H}}\underbrace{\begin{bmatrix} X_1\\ X_2\\ X_3\\ X_4\end{bmatrix}}_{\mathbf{X}} + \underbrace{\begin{bmatrix} W_1\\ W_2\\ W_3\\ W_4\\ W_5^*\\ W_6^*\\ W_7^*\\ W_8^*\end{bmatrix}}_{\mathbf{W}}$$

$$\mathbf{R} = \frac{1}{\sqrt{4}}\mathbf{H}\mathbf{X} + \mathbf{W} \tag{7.38}$$

Let $\mathbf{Y}$ be the signal at the output of FFT, then $\mathbf{Y}$ is expressed as

$$\begin{aligned}\mathbf{Y} =&\mathbf{H}^H\mathbf{H}\mathbf{X} + \mathbf{H}^H\mathbf{W}\\ =&\frac{2\left(\alpha_1^2+\alpha_2^2+\alpha_3^2+\alpha_4^2\right)}{\sqrt{4}}\mathbb{I}_{4\times4}\mathbf{X}+\mathbf{W}^{''}\\ =&\left(\alpha_1^2+\alpha_2^2+\alpha_3^2+\alpha_4^2\right)\mathbb{I}_{4\times4}\mathbf{X}+\mathbf{W}^{''}\end{aligned} \tag{7.39}$$

where $\mathbf{W}^{''}$ is the noise component and is defined as (7.31). In addition, its variance is defined as (7.32).

We assume that the 16-QAM modulation is utilized to modulate signals. Like in previous cases, we make no distinction between four OFDM symbols and we assume that the average power of X_1, X_2, X_3 and X_4 are the same, namely $E\{X_1^2\} = E\{X_2^2\} = E\{X_3^2\} = E\{X_4^2\} = E\{X^2\}$. Denote $P^N_{BER|\alpha_1^2,\alpha_2^2,\alpha_3^2,\alpha_4^2}$ as the conditional BER of 16-QAM symbols conditioned on α_1^2, α_2^2, α_3^2 and α_4^2 for the case where the transmit power is normalized by the number of transmit antennas, then $P^N_{BER|\alpha_1^2,\alpha_2^2,\alpha_3^2,\alpha_4^2}$ is given by

$$\begin{aligned}P^N_{BER|\alpha_1,\alpha_2,\alpha_3,\alpha_4} =&\frac{1}{2}\left(P_{MSB}+P_{LSB}\right)\\ =&\frac{3}{4}Q\left(\sqrt{\frac{\left(\alpha_1^2+\alpha_2^2+\alpha_3^2+\alpha_4^2\right)d^2}{\sigma_w^2}}\right)+\frac{1}{2}Q\left(\sqrt{\frac{9\left(\alpha_1^2+\alpha_2^2+\alpha_3^2+\alpha_4^2\right)d^2}{\sigma_w^2}}\right)\\ &-\frac{1}{4}Q\left(\sqrt{\frac{25\left(\alpha_1^2+\alpha_2^2+\alpha_3^2+\alpha_4^2\right)d^2}{\sigma_w^2}}\right)\end{aligned} \tag{7.40}$$

Subsequently, to obtain the unconditional BER, (7.40) is integrated over four PDFs, namely

$$P^N_{BER} = \int_0^\infty\int_0^\infty\int_0^\infty\int_0^\infty P^N_{BER|\alpha_1,\alpha_2,\alpha_3,\alpha_4}p(\alpha_1)p(\alpha_2)p(\alpha_3)p(\alpha_4)d\alpha_1 d\alpha_2 d\alpha_3 d\alpha_4 \tag{7.41}$$

where $p(\alpha_1)$, $p(\alpha_3)$, $p(\alpha_2)$ and $p(\alpha_4)$ are defined as (7.35). Finally, rewriting $Q(\cdot)$ function as (7.21), (7.41) is simplified to

$$\begin{aligned}P^N_{BER} =&\frac{3}{4\pi}\int_0^{\frac{\pi}{2}}\left[1+\frac{\sigma_{H_1}^2d^2}{2\sigma_w^2\sin^2\theta}\right]^{-1}\left[1+\frac{\sigma_{H_2}^2d^2}{2\sigma_w^2\sin^2\theta}\right]^{-1}\left[1+\frac{\sigma_{H_3}^2d^2}{2\sigma_w^2\sin^2\theta}\right]^{-1}\left[1+\frac{\sigma_{H_4}^2d^2}{2\sigma_w^2\sin^2\theta}\right]^{-1}d\theta\\ &+\frac{1}{2\pi}\int_0^{\frac{\pi}{2}}\left[1+\frac{9\sigma_{H_1}^2d^2}{2\sigma_w^2\sin^2\theta}\right]^{-1}\left[1+\frac{9\sigma_{H_2}^2d^2}{2\sigma_w^2\sin^2\theta}\right]^{-1}\left[1+\frac{9\sigma_{H_3}^2d^2}{2\sigma_w^2\sin^2\theta}\right]^{-1}\left[1+\frac{9\sigma_{H_4}^2d^2}{2\sigma_w^2\sin^2\theta}\right]^{-1}d\theta\\ &-\frac{1}{4\pi}\int_0^{\frac{\pi}{2}}\left[1+\frac{25\sigma_{H_1}^2d^2}{2\sigma_w^2\sin^2\theta}\right]^{-1}\left[1+\frac{25\sigma_{H_2}^2d^2}{2\sigma_w^2\sin^2\theta}\right]^{-1}\left[1+\frac{25\sigma_{H_3}^2d^2}{2\sigma_w^2\sin^2\theta}\right]^{-1}\left[1+\frac{25\sigma_{H_4}^2d^2}{2\sigma_w^2\sin^2\theta}\right]^{-1}d\theta\end{aligned} \tag{7.42}$$

As one can see that (7.42) is much simpler and easier to evaluate since the BER expression contains a sum of three single integrals instead of a sum of three quadruple integrals.

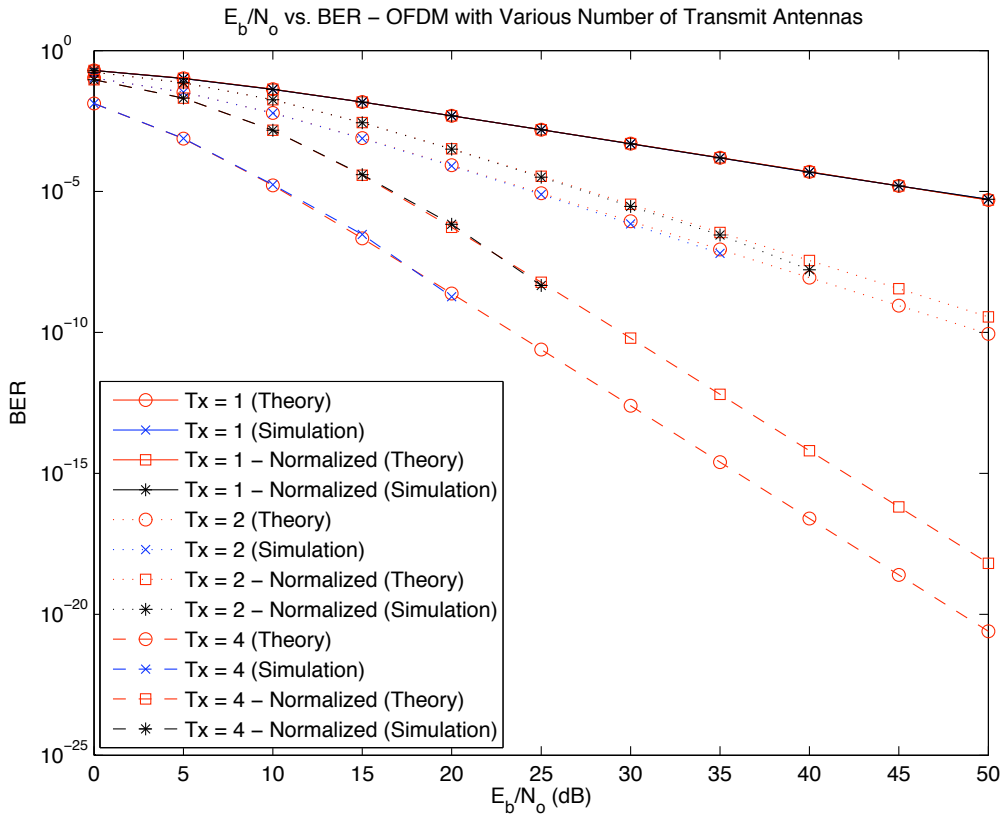

Figure 7.7 BER performance of a 16-QAM MIMO-OFDM system in Rayleigh fading channels for various number of transmit antennas with and without transmit power being normalized by the number of transmit antennas. In all cases, there is only a single receive antenna and simulations are performed under the assumption of perfect channel estimation.

7.6 Simulation Model and Simulation Results

The simulation models are implemented as described in Section 7.2 and 7.3. The input binary bits are modulated with the 16-QAM modulation and are processed by a 64-point IFFT. The resulting OFDM symbols are encoded by the STBC encoder based on the number of transmit antennas before transmissions. At the receiver, the received signal is decoupled and the BER performance is measured. In addition, without loss of generality, the means and variances of all Rayleigh fading channels are set to zero and one, respectively. Fig. 7.7 shows the simulation and theoretical results for a 16-QAM MIMO-OFDM system in Rayleigh fading channels for various number of transmit antennas with and without the normalization in transmit power. In the case where there is only one transmit antenna, the theoretical result is obtained from (Eq:(5.6)) in [43].

In general, for a given number of transmit antennas, the BER performance is worse when the transmit power is normalized by the number of transmit antennas. This is due to the reason

that the transmit power per antenna is smaller in value when compared with the case where the transmit power is not normalized. Subsequently, when under the same amount of noise, the BER performance for the case where the transmit power is normalized is worse than the case where the transmit power is not normalized. There is one exception which is in the case where the number of transmit antenna is one. In this case, all the transmit power is concentrated in a single antenna regardless of whether there is a normalization. In addition, for a given signal to noise (SNR) value, the performance improves as more transmit antennas are utilized for transmissions. Even though, utilizing the four transmit antennas for data transmissions can offer better performance than in the case where only two transmit antennas are being used, the transmission rate in the case of four transmit antennas is less than in the case where two transmit antennas are utilized in the system. This is because two different OFDM symbols are transmitted in two different time slots in the case of two transmit antennas, however, in the case of four transmit antennas, four different OFDM symbols are transmitted in eight different time slots. As a consequence, the transmission rate in the case where there are two transmit antennas is twice as much as in the case where there are four transmit antennas.

7.7 Conclusion

In this chapter, we first presented the performance analysis of a M-QAM MIMO-OFDM system with the Alamouti code and two transmit antennas in Rayleigh fading channels. Furthermore, the performance analysis of the MIMO-OFDM system with two transmit antennas was analyzed both with and without the normalization in transmit power. The BER expressions for both cases where there are two transmit antennas are simplified further by rewriting the $Q(\cdot)$ function as its alternate form. The final BER expression is a sum of three single integrals and is easier to evaluate compared to conventional results where the BER expression is a sum of three double integrals. Next, we analyzed another M-QAM MIMO-OFDM system which has four transmit antennas in Rayleigh fading channels. In this case, the performance analysis is also presented with and without the transmit power being normalized by the number of transmit antennas. Furthermore, the complexity of the BER expression presented for the case of four transmit antennas is significantly reduced to a sum of three single integrals. We then presented simulation results along with the theoretical values for 16-QAM MIMO-OFDM systems with various number of transmit antennas in Rayleigh fading channels with and without the normalization in transmit power. In addition, we briefly discuss the advantages and disadvantages of utilizing more than one transmit antennas for transmission.

8

Effects of Nonlinear Amplifier and Narrowband Interference on the Performance of MIMO-OFDM

8.1 Introduction

As mentioned already in previous chapters, Orthogonal Frequency Division Multiplexing (OFDM) has several technical advantages. Furthermore, due to the technical superiorities such as high bandwidth efficiency and robustness in fading channels, OFDM has been adapted in IEEE standards such as IEEE 802.11a/g/n [2–4]. Despite its technical superiorities, one of major drawbacks associated with OFDM is high peak to average power ratio (PAPR) which is due to the superimposition of multi-carrier signals. When the multi-carrier signals are added coherently in IFFT and FFT processes, the output signal would have peak power that is L times larger than the average power where L is the number of signals in the multi-carrier signal. In practice, this signal which has a high peak to average power ratio often force practical high power amplifiers (HPAs) to operate at their nonlinear region when it is amplified. As a consequence, HPAs often introduce nonlinear distortion such as clipping and spectral regrowth which subsequently degrade the system performance [24, 25].

Until recently, a Single Input Single Output (SISO) antenna configuration has always been the mainstream implementation in wireless communication systems. As technology advances toward the Fourth Generation (4G), the demand for high data rate which is needed in communication applications has increased dramatically. To satisfy the acute demand for high data rate, Multiple Input Multiple Output (MIMO) antenna configuration and Space Time coding (STC), more specifically Space Time Block Code (STBC), have been proposed to increase the data rate in literature. A simple technique that explores the diversity of the system was first proposed by Alamouti [21]

and was later applied to OFDM systems [36] which are generally referred to as MIMO-OFDM or STBC-OFDM systems in literature. Furthermore, the performance of such MIMO-OFDM systems with various sources of impairments has been studied and reported [38, 41, 44].

While there are some papers dealing with the performance of STBC-OFDM systems in Rayleigh fading channels, very few address the combined effect of nonlinear HPA and narrowband interference (NBI) on the performance of STBC-OFDM systems with and without channel estimation error. In [41], the authors presented the performance analysis of STBC-OFDM in selective fading channels without considering the effects of nonlinear HPA, NBI and channel estimation error. Diao *et. al* [38] analyzed the performance of a STBC-OFDM system that is subject to channel estimation error only. In [44], only simulation results of a Space-Frequency Block Code (SFBC) OFDM and a SFBC-OFDM with carrier interferometry systems which were only subject to either nonlinear HPAs or NBI were presented. In addition, the performance of a SFBC-OFDM system under those impairments was not analyzed analytically in the paper. In addition, the authors in [44] assumed that the source of NBI was close to the receiver; hence, NBI did not experience any channel effects. This particular assumption does not provide useful insights to the performance of a STBC-OFDM system in the presence of NBI because in many cases, the sources of NBI are usually located in several city blocks away. Therefore, it is more reasonable and practical to assume that the NBI signal experiences another separate channel response.

In Chapters 4 and 5 [45, 46], we analyzed the performance of a Single Input Single Output (SISO) M-ary Quadrature Amplitude Modulation (M-QAM) OFDM system that was subject to a nonlinear HPA, channel estimation error, and jamming in a Rayleigh fading channel. In contrast to the NBI model presented in [44], we assumed that the NBI by itself experienced a separate channel response. The theoretical and simulation results of the performance of the OFDM system were presented for various combination of impairments with and without channel estimation error in the previous work. In this chapter, we extend our previously studied OFDM systems with multiple antennas while subjecting the system to nonlinear HPAs, a NBI and channel estimation error. Then, we create a simulation model that is an extension to the analytical model such that it conforms to the IEEE 802.11n specification. The simulation results are validated with the theoretical analysis.

The chapter is organized as follows. In Section 8.2, a system block diagram is presented and each component is discussed in detail. Section 8.3 contains the performance analysis of the analytical system. Section 8.4 discusses the simulation setup. Section 8.5 provides simulation results of the system described in Section 8.4. Finally, Section 8.6 summarizes the chapter.

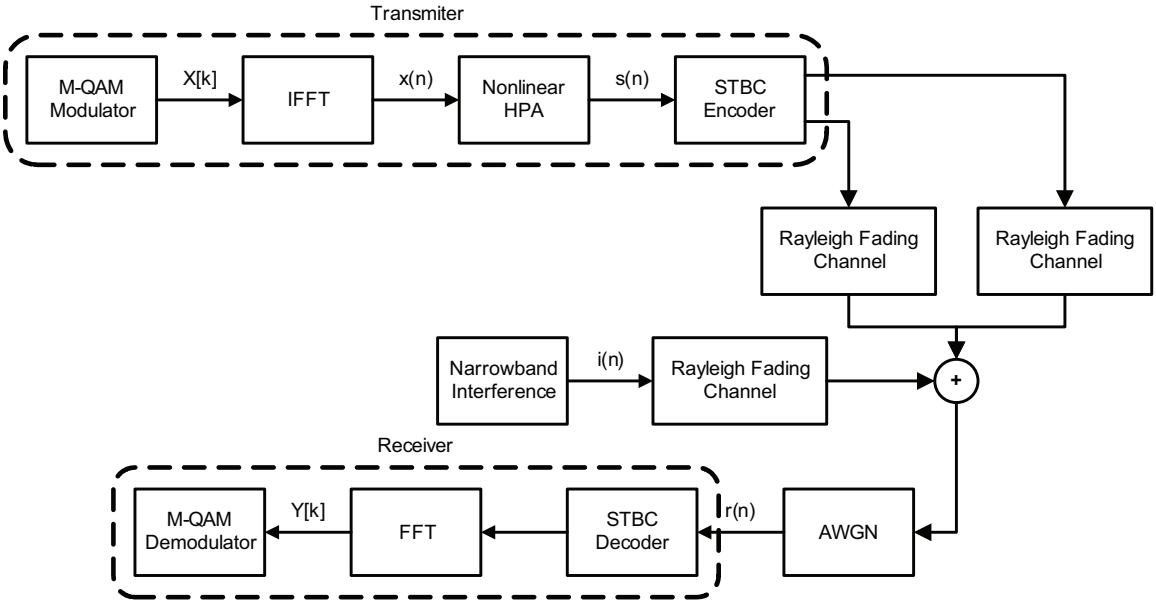

Figure 8.1 The system block diagram of a M-QAM STBC-OFDM system which is subject to nonlinear HPAs, narrowband interference and channel estimation error in Rayleigh fading channels.

8.2 System Description

The block diagram of an analytical system which has two transmit antennas and one receive antenna is shown in Fig. 8.1. Each block in the system is discussed in more detail in following subsections.

8.2.1 Transmitter

The transmitter is composed of a M-QAM modulator, IFFT, Nonlinear HPA and STBC encoder. The binary input to the M-QAM modulator is assumed to be statistically equiprobable and independent. They are subsequently grouped into a block size of $log_2 M$ and mapped into M-QAM symbols, $X[k]$, according to the alphabet, $A = \{(2m - 1 - \sqrt{M}) + j(2n - 1 - \sqrt{M})\}$ where $m, n = 1, 2, ...\sqrt{M}$ and M is the signal constellation size. At appropriate sampling time, the signal at the output of the IFFT which is denoted as $x(n)$ is given by

$$x(n) = \frac{1}{N} \sum_{k=0}^{N-1} X[k] e^{j\frac{2\pi nk}{N}} \qquad 0 \leq n \leq N-1 \tag{8.1}$$

where N is the total number of subcarriers.

8.2.2 HPA Model

The nonlinear HPA model in the transmitter represents the nonlinear distortion imposed on the signal. In this chapter, the nonlinear HPA model follows the Saleh model which has been

described in Chapter 2, Section 2.3.

8.2.3 STBC Encoder

In this chapter, the STBC, or Alamouti code, for two transmit antennas and one receive antenna is utilized to encode OFDM symbols. The encoding process of Alamouti code has been described in Chapter 7, Section 7.2.2.

8.2.4 Narrowband Interference Model, Channel Model and AWGN

The NBI signal in time domain, $i(n)$, is expressed as

$$i(n) = \frac{1}{N} \sum_{k=0}^{N-1} I[k] e^{j \frac{2\pi n k}{N}} \tag{8.2}$$

where $I[k]$ represents the NBI signal for the k^{th} subcarrier and has power equal to $\frac{|I[k]|^2}{2}$.

Denote $h_1(n)$ as the impulse response of the channel between the first transmit antenna and the receive antenna. The in-phase and quadrature components of $h_1(n)$ are assumed to be Gaussian random variables with zero mean and $\sigma^2_{H_1}$ variance. Let $h_2(n)$ be the channel impulse response between the second transmit antenna and the receive antenna and its in-phase and quadrature components are assumed to be Gaussian random variables with zero mean and $\sigma^2_{H_2}$ variance. Finally, let $h_3(n)$ be the channel impulse response between the source of NBI and the receiver. The in-phase and quadrature components of $h_3(n)$ are Gaussian random variables with zero mean and $\sigma^2_{H_3}$ variance. All three Rayleigh fading channels and their in-phase and quadrature components are assumed to be statistically independent of each other and are static for the duration of two OFDM symbols transmissions. The additive white Gaussian noise (AWGN) which is denoted as $w(n)$ represents the thermal noise and is modeled as an AWGN process which has zero mean and $2\sigma^2_w$ variance.

8.2.5 Receiver

The receiver consists of a STBC decoder, a FFT and a M-QAM demodulator. For the simplicity of notations, we will drop the time and frequency indices in the rest of chapter. Assuming perfect synchronization, $r_t(n)$ which denotes the received signal in time domain at transmission time index t is given by

$$r_t = \begin{cases} h_1 s_o + h_2 s_e + h_3 i + w_o & t = odd \\ -h_1 s_e^* + h_2 s_o^* + h_3 i + w_e & t = even \end{cases} \tag{8.3}$$

where the variables s_o and s_e represent the odd and even number of OFDM symbols, respectively. In addition, $(\cdot)^*$ implies the complex conjugate operation of the signal in the argument. After rewriting

(8.3) in the matrix format, $r_t(n)$ and its FFT are given by

$$\underbrace{\begin{bmatrix} r_o \\ r_e^* \end{bmatrix}}_{\mathbf{r}} = \underbrace{\begin{bmatrix} h_1 & h_2 \\ h_2^* & -h_1^* \end{bmatrix}}_{\mathbf{h_D}} \underbrace{\begin{bmatrix} s_o \\ s_e \end{bmatrix}}_{\mathbf{s}} + \underbrace{\begin{bmatrix} h_3 & 0 \\ 0 & h_3^* \end{bmatrix}}_{\mathbf{h_N}} \underbrace{\begin{bmatrix} i \\ i \end{bmatrix}}_{\mathbf{i}} + \underbrace{\begin{bmatrix} w_o \\ w_e^* \end{bmatrix}}_{\mathbf{w}}$$

$$\mathbf{r} = \mathbf{h_D s} + \mathbf{h_N i} + \mathbf{w} \overset{FFT}{\longleftrightarrow} \mathbf{R} = \mathbf{H_D S} + \mathbf{H_N I} + \mathbf{W} \tag{8.4}$$

where the bold face letters represent either matrices or vectors.

To accurately demodulate the received signal, estimating the channel responses are necessary and can be obtained with the aid of pilots in frequency domain. Let $\hat{\mathbf{H}}_\mathbf{D}$ be the estimate of the channel response matrix, $\mathbf{H_D}$, then $\hat{\mathbf{H}}_\mathbf{D}$ is often expressed as [38]

$$\hat{\mathbf{H}}_\mathbf{D} = \begin{bmatrix} \hat{H}_1 & \hat{H}_2 \\ \hat{H}_2^* & -\hat{H}_1^* \end{bmatrix} = \begin{bmatrix} H_1 + \epsilon_1 & H_2 + \epsilon_2 \\ H_2^* + \epsilon_2^* & -H_1^* - \epsilon_1^* \end{bmatrix} \tag{8.5}$$

where $\hat{H}_1$ and $\hat{H}_2$ are the channel estimates for channels, H_1 and H_2, respectively. The variable ϵ_1 in (8.5) represents the error in estimating the channel, H_1, and is modeled as a complex Gaussian random process with zero mean and $2\sigma_{\epsilon_1}^2$ variance. The variable ϵ_2 denotes the error in estimating the channel, H_2, and is assumed to be a complex Gaussian random process with zero mean and $2\sigma_{\epsilon_2}^2$ variance. In addition, both ϵ_1 and ϵ_2 are statistically independent of all three channels and are statistically independent of each other as well.

Fig. 8.2 shows the scenario where only one subcarrier in the OFDM signal is under the influence of NBI. As shown in Fig. 8.2, the NBI does not have impact on the subcarriers, other than the one that it is present. For the situation where the NBI only affects some subcarriers in the received signal, this suggests that the received signal can be broken down into two cases. Let $\mathbf{Y}$ be the signal matrix at the output of the FFT, then for the case where the NBI is present in the subcarrier, $\mathbf{Y}$ is found to be

$$\begin{aligned} \mathbf{Y} =& \hat{\mathbf{H}}_\mathbf{D}^H \mathbf{R} \\ =& \hat{\mathbf{H}}_\mathbf{D}^H \mathbf{H_D S} + \hat{\mathbf{H}}_\mathbf{D}^H \mathbf{H_N I} + \hat{\mathbf{H}}_\mathbf{D}^H \mathbf{W} \end{aligned} \tag{8.6}$$

where $(\cdot)^H$ denotes the Hermitian operation of the matrix. For the other case where the subcarrier is not affected by the NBI, $\mathbf{Y}$ is obtained by setting $\mathbf{I}$ in (8.6) to zero, namely

$$\mathbf{Y} = \hat{\mathbf{H}}_\mathbf{D}^H \mathbf{H_D S} + \hat{\mathbf{H}}_\mathbf{D}^H \mathbf{W} \tag{8.7}$$

8.3 Performance Analysis

In this section, the bit error rate (BER) of the analytical model shown in Fig. 8.1 is derived and will later be used to measure the performance of the system. The performance analysis

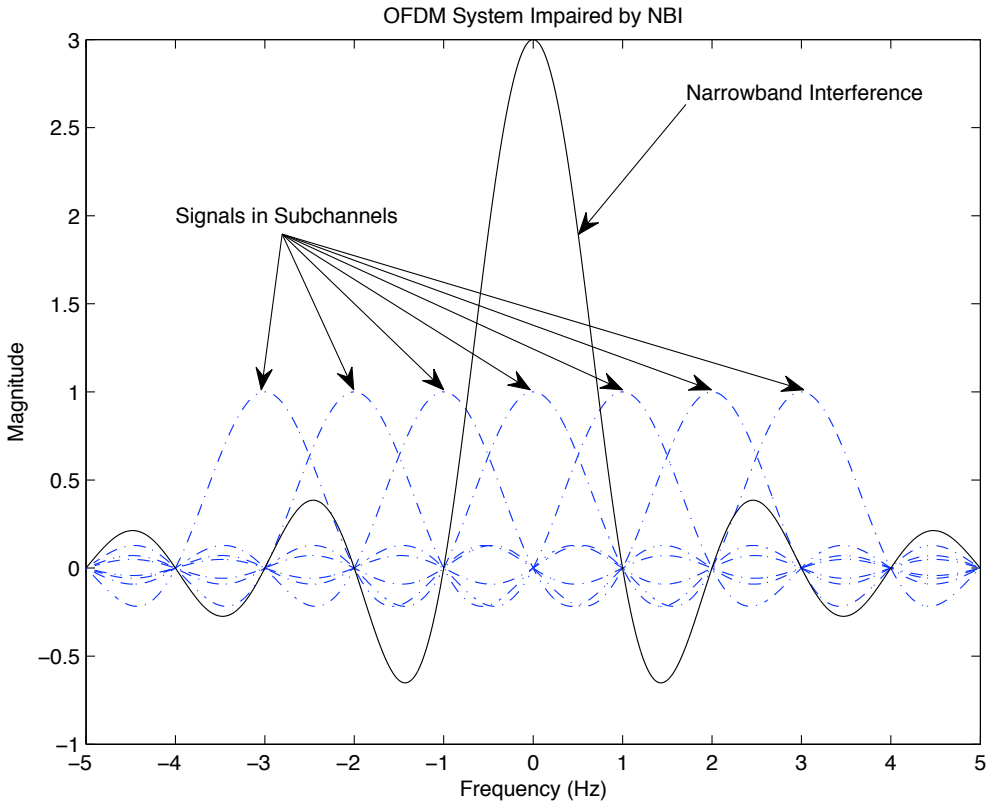

Figure 8.2 An illustration of effect of narrowband interference (NBI) on the OFDM signals

of the system starts with the characterization of $x(n)$. Under the assumption that N is large, by the *Central Limit Theorem*, $x(n)$ is said to be Gaussian distributed with zero mean [19]. With that assumption, Banelli, *et al.* [20] had shown that $s(n)$ can be written as a product of a complex gain, α_G, and the input signal, $x(n)$, added with noise distortion, $d_G(n)$. The transmitted signal, $s(n)$, and its FFT are then given by

$$s(n) = \alpha_G x(n) + d_G(n) \overset{FFT}{\longleftrightarrow} S[k] = \alpha_G X[k] + D_G[k] \tag{8.8}$$

where $D_G[k]$ was shown to be a complex Gaussian random variable with zero mean and $2\sigma^2_{D_G}$ variance. The numerical value of σ^2_D can be obtained by following steps outlined in Section 2.4 of Chapter 2.

For two different subcarriers, k_1 and k_2, $D_G[k_1]$ and $D_G[k_2]$ are mutually independent. Furthermore, the in-phase and quadrature phase components of $D_G[k]$ were shown to be mutually independent and identically distributed (i.i.d) [15]. The multiplicative coefficient α_G in (8.8) is given

by

$$\alpha_G = \frac{E\{s(n)^* x(n)\}}{2\sigma^2_{x(n)}} = \alpha_{G_I} + j\alpha_{G_Q} \tag{8.9}$$

where $E\{\cdot\}$ is the expected value [20] and $(\cdot)^*$ denotes the complex conjugate of the signal. In addition, the subscripts I and Q represent the in-phase and quadrature components.

As mentioned before in Section 8.2.5, the received signal at the output of the FFT depends on whether the particular subcarrier is under the influence of NBI. Since the received signal at the output of FFT for the case where the subcarrier is free from NBI can be obtained from the other case where the NBI is present in the subcarrier, we will continue the derivation for the case where the subcarrier is affected by the NBI. Once the derivation for this case is completed, the performance analysis for the other case where the subcarrier is free from NBI can be found by setting appropriate terms that are in the case where the subcarriers are interfered by NBI to zero.

After some mathematical simplification, (8.6) becomes

$$\begin{aligned}\begin{bmatrix} Y_o \\ Y_e \end{bmatrix} =& (\alpha_1^2 + \alpha_2^2)\mathbb{I}_{2\times 2} \begin{bmatrix} S_o \\ S_e \end{bmatrix} + \begin{bmatrix} H_1\epsilon_1^* + H_2^*\epsilon_2 & H_2\epsilon_1^* - H_1^*\epsilon_2 \\ H_1\epsilon_2^* - H_2^*\epsilon_1 & H_1^*\epsilon_1 + H_2\epsilon_2^* \end{bmatrix} \begin{bmatrix} S_o \\ S_e \end{bmatrix} \\ &+ \begin{bmatrix} H_3(H_1^* + \epsilon_1^*) & H_3^*(H_2 + \epsilon_2) \\ H_3(H_2^* + \epsilon_2^*) & H_3^*(-H_1 - \epsilon_1) \end{bmatrix} \begin{bmatrix} I \\ I \end{bmatrix} + \begin{bmatrix} H_1^* + \epsilon_1^* & H_2 + \epsilon_2 \\ H_2^* + \epsilon_2^* & -H_1 - \epsilon_1 \end{bmatrix} \begin{bmatrix} W_o \\ W_e^* \end{bmatrix}\end{aligned} \tag{8.10}$$

where α_1 and α_2 are the magnitudes of H_1 and H_2, respectively. In addition, $\mathbb{I}_{2\times 2}$ represents a 2 by 2 identity matrix. Substituting (8.8) into (8.10), the received signal matrix, denoted as $\mathbf{Y}$, is expressed as

$$\begin{bmatrix} Y_o \\ Y_e^* \end{bmatrix} = (\alpha_1^2 + \alpha_2^2)\mathbb{I}_{2\times 2} \begin{bmatrix} \alpha_G X_o \\ \alpha_G X_e \end{bmatrix} + \mathbf{\Xi} + \mathbf{\Upsilon} + \mathbf{\Psi} + \mathbf{\Phi} + \mathbf{\Omega} \tag{8.11}$$

where

$$\begin{aligned}\mathbf{\Xi} =& (\alpha_1^2 + \alpha_2^2)\mathbb{I}_{2\times 2} \begin{bmatrix} D_{G_o} \\ D_{G_e} \end{bmatrix} \\ \mathbf{\Upsilon} =& \begin{bmatrix} H_1\epsilon_1^* + H_2^*\epsilon_2 & H_2\epsilon_1^* - H_1^*\epsilon_2 \\ H_1\epsilon_2^* - H_2^*\epsilon_1 & H_1^*\epsilon_1 + H_2\epsilon_2^* \end{bmatrix} \begin{bmatrix} \alpha_G X_o \\ \alpha_G X_e \end{bmatrix} \\ \mathbf{\Psi} =& \begin{bmatrix} H_1\epsilon_1^* + H_2^*\epsilon_2 & H_2\epsilon_1^* - H_1^*\epsilon_2 \\ H_1\epsilon_2^* - H_2^*\epsilon_1 & H_1^*\epsilon_1 + H_2\epsilon_2^* \end{bmatrix} \begin{bmatrix} D_{G_o} \\ D_{G_e} \end{bmatrix} \\ \mathbf{\Phi} =& \begin{bmatrix} H_3(H_1^* + \epsilon_1^*) & H_3^*(H_2 + \epsilon_2) \\ H_3(H_2^* + \epsilon_2^*) & H_3^*(-H_1 - \epsilon_1) \end{bmatrix} \begin{bmatrix} I \\ I \end{bmatrix} \\ \mathbf{\Omega} =& \begin{bmatrix} H_1^* + \epsilon_1^* & H_2 + \epsilon_2 \\ H_2^* + \epsilon_2^* & -H_1 - \epsilon_1 \end{bmatrix} \begin{bmatrix} W_o \\ W_e^* \end{bmatrix}\end{aligned} \tag{8.12}$$

Since $\mathbf{\Xi}$, $\mathbf{\Upsilon}$, $\mathbf{\Psi}$, $\mathbf{\Phi}$, and $\mathbf{\Omega}$ are noise with zero mean, finding the conditional variance for each term is required in order to evaluate the performance of the system.

Let σ^2_{Ξ} be the conditional variance for the in-phase or quadrature component of $\mathbf{\Xi}$, then σ^2_{Ξ} is given as

$$\sigma^2_{\Xi} = E\left\{\mathbf{\Xi}\mathbf{\Xi}^H\right\} = (\alpha_1^2 + \alpha_2^2)^2\sigma^2_{D_G}\mathbb{I}_{2\times 2} \tag{8.13}$$

Denote σ^2_{Υ} as the conditional variance for the in-phase or quadrature component of $\mathbf{\Upsilon}$, then σ^2_{Υ} is expressed as

$$\sigma^2_{\Upsilon} = E\left\{\mathbf{\Upsilon}\mathbf{\Upsilon}^H\right\} = |\alpha_G|^2 E\left\{|X|^2\right\}(\alpha_1^2 + \alpha_2^2)(\sigma^2_{\epsilon_1} + \sigma^2_{\epsilon_2})\mathbb{I}_{2\times 2} \tag{8.14}$$

One observation about (8.14) is the dependency of σ^2_{Υ} on the choices of data modulation scheme, more specifically, the signal constellation of the modulation. As already mentioned in Section 6.3 of Chapter 6, the expression for σ^2_{Υ} which is defined as (8.14) would yield the same numerical values if the signal constellation is circular. However, in the situation where the signal constellation is not circular, one should pay more attention to the calculation of σ^2_{Υ} since the numerical values of $E\{|X|^2\}$ would vary according to the symbols in the constellation. To explicitly show the dependency on modulated symbols, we rewrite (8.14) as

$$\sigma^2_{\Upsilon_i} = |\alpha_G|^2 E\left\{|X_i|^2\right\}(\alpha_1^2 + \alpha_2^2)(\sigma^2_{\epsilon_1} + \sigma^2_{\epsilon_2})\mathbb{I}_{2\times 2} \tag{8.15}$$

where the subscript i in X_i represents the i^{th} modulated symbol in the constellation.

Denote σ^2_{Ψ} as the conditional variance for the in-phase or quadrature component of $\mathbf{\Psi}$, then σ^2_{Ψ} is found to be

$$\sigma^2_{\Psi} = E\left\{\mathbf{\Psi}\mathbf{\Psi}^H\right\} = \sigma^2_{D_G}(\alpha_1^2 + \alpha_2^2)(\sigma^2_{\epsilon_1} + \sigma^2_{\epsilon_2})\mathbb{I}_{2\times 2} \tag{8.16}$$

Without loss of generality, it is assumed that $E\left\{X_o^2\right\} = E\left\{X_e^2\right\} = E\left\{X^2\right\}$ and $\sigma^2_{D_{G_o}} = \sigma^2_{D_{G_e}} = \sigma^2_{D_G}$ when calculating (8.13), (8.14), and (8.16),. Denote σ^2_{Φ} as the conditional variance for the in-phase or quadrature component of $\mathbf{\Phi}$, then σ^2_{Φ} is found to be

$$\sigma^2_{\Phi} = E\left\{\mathbf{\Phi}\mathbf{\Phi}^H\right\} = \frac{|I[k]|^2}{2}\begin{bmatrix} \phi_{11} & \phi_{12} \\ \phi_{21} & \phi_{22} \end{bmatrix} \tag{8.17}$$

where

$$\begin{aligned} \phi_{11} =& \alpha_3^2(\alpha_1^2 + \sigma^2_{\epsilon_1} + \alpha_2^2 + \sigma^2_{\epsilon_2}), \qquad \phi_{21} = \sigma^2_{H_3}(\sigma^2_{H_2} + \sigma^2_{\epsilon_2} - \sigma^2_{H_1} - \sigma^2_{\epsilon_1}) \\ \phi_{12} =& \sigma^2_{H_3}(-\sigma^2_{H_1} - \sigma^2_{\epsilon_1} + \sigma^2_{H_2} + \sigma^2_{\epsilon_2}), \qquad \phi_{22} = \alpha_3^2(\alpha_2^2 + \sigma^2_{\epsilon_2} + \alpha_1^2 + \sigma^2_{\epsilon_1}) \end{aligned} \tag{8.18}$$

where α_3 is the magnitude of the channel, H_3. Finally, let σ^2_{Ω} be the conditional variance for the in-phase or quadrature component of $\mathbf{\Omega}$, then σ^2_{Ω} is

$$\sigma^2_{\Omega} = E\left\{\mathbf{\Omega}\mathbf{\Omega}^H\right\} = \sigma^2_w(\alpha_1^2 + \alpha_2^2 + \sigma^2_{\epsilon_1} + \sigma^2_{\epsilon_2})\mathbb{I}_{2\times 2} \tag{8.19}$$

Table 8.1 Numerical Values of Variables in Conditional BER for MSB

Index i	X_{I_i}	X_{Q_i}	$E\{\|X_i\|^2\}$	Index i	X_{I_i}	X_{Q_i}	$E\{\|X_i\|^2\}$
1	d	$3d$	$10d^2$	5	$3d$	$3d$	$18d^2$
2	d	d	$2d^2$	6	$3d$	d	$10d^2$
3	d	$-d$	$2d^2$	7	$3d$	$-d$	$10d^2$
4	d	$-3d$	$10d^2$	8	$3d$	$-3d$	$18d^2$

Since $E\left\{X_o^2\right\} = E\left\{X_e^2\right\} = E\left\{X^2\right\}$, (8.11) can be further reduced to

$$\begin{aligned} Y =& \left\{(\alpha_1^2+\alpha_2^2)\left(\alpha_{G_I}X_I - \alpha_{G_Q}X_Q\right) + \boldsymbol{\Xi}_I + \boldsymbol{\Upsilon}_I + \boldsymbol{\Psi}_I + \boldsymbol{\Phi}_I + \boldsymbol{\Omega}_I\right\} \\ &+ j\left\{(\alpha_1^2+\alpha_2^2)(\alpha_{G_I}X_Q + \alpha_{G_Q}X_I) + \boldsymbol{\Xi}_Q + \boldsymbol{\Upsilon}_Q + \boldsymbol{\Psi}_Q + \boldsymbol{\Phi}_Q + \boldsymbol{\Omega}_Q\right\} \\ =& Y_I + jY_Q \end{aligned} \tag{8.20}$$

where $\boldsymbol{\Xi}_I$, $\boldsymbol{\Upsilon}_I$, $\boldsymbol{\Psi}_I$, $\boldsymbol{\Phi}_I$ and $\boldsymbol{\Omega}_I$ represent the in-phase component of $\boldsymbol{\Xi}$, $\boldsymbol{\Upsilon}$, $\boldsymbol{\Psi}$, $\boldsymbol{\Phi}$ and $\boldsymbol{\Omega}$, respectively. Furthermore, $\boldsymbol{\Xi}_Q$, $\boldsymbol{\Upsilon}_Q$, $\boldsymbol{\Psi}_Q$, $\boldsymbol{\Phi}_Q$ and $\boldsymbol{\Omega}_Q$ represent the quadrature component of $\boldsymbol{\Xi}$, $\boldsymbol{\Upsilon}$, $\boldsymbol{\Psi}$, $\boldsymbol{\Phi}$ and $\boldsymbol{\Omega}$, respectively.

To continue the derivation, we assume that 16-QAM modulation is utilized to modulate data bits in the system. Nevertheless, other rectangular QAM constellations can be derived in the similar fashion if they are chosen to modulate signals. For the case where the subcarrier is affected by NBI and conditioned on α_1, α_2, and α_3, the conditional BER, denoted as $P^I_{BER|\alpha_1,\alpha_2,\alpha_3}$, is

$$P^I_{BER|\alpha_1,\alpha_2,\alpha_3} = \frac{1}{2}(P^I_{MSB} + P^I_{LSB}) \tag{8.21}$$

where P^I_{MSB} and P^I_{LSB} are the conditional BER of most significant bits (MSB) and least significant bits (LSB) of 16-QAM symbols, respectively. Based on the decision boundaries, P^I_{MSB} is given by

$$P^I_{MSB} = \frac{1}{8}\sum_{i=1}^{8} Q\left(\sqrt{\frac{\Lambda_i^2}{\sigma^2_{\Xi} + \sigma^2_{\Upsilon_i} + \sigma^2_{\Psi} + \sigma^2_{\Phi} + \sigma^2_{\Omega}}}\right) \tag{8.22}$$

where $\Lambda_i = (\alpha_1^2+\alpha_2^2)(\alpha_{G_I}X_{I_i} - \alpha_{G_Q}X_{Q_i})$ and $Q(\nu) = \int_{\nu}^{\infty}\frac{1}{\sqrt{2\pi}}e^{\frac{-t^2}{2}}dt, \nu \geq 0$. In addition, σ^2_{Ξ}, $\sigma^2_{\Upsilon_i}$, σ^2_{Ψ}, σ^2_{Φ} and σ^2_{Ω} are defined in (8.13), (8.15), (8.16), (8.17) and (8.19), respectively. The numerical values for X_{I_i}, X_{Q_i} and $E\{|X_i|^2\}$ in (8.22) are listed in Table 8.1. For the case where the subcarriers are affected by NBI, the conditional BER of LSB can be found in a similar way and it is found to be

$$P^I_{LSB} = \frac{1}{8}\sum_{i=1}^{16} \lambda_i Q\left(\sqrt{\frac{(\kappa_i 2(\alpha_1^2+\alpha_2^2)d + \zeta_i\Lambda_i)^2}{\sigma^2_{\Xi} + \sigma^2_{\Upsilon_i} + \sigma^2_{\Psi} + \sigma^2_{\Phi} + \sigma^2_{\Omega}}}\right) \tag{8.23}$$

where λ_i, κ_i, and ζ_i are signs of the values for the i^{th} quantity and are listed along with values for X_{I_i}, X_{Q_i} and $E\{|X_i|^2\}$ in Table 8.2. In both Tables 8.1 and 8.2, $d^2 = \frac{2E_b}{5}$ where E_b is the energy per bit. For the case where the subcarrier is free from NBI, the conditional BER, denoted as $P^F_{BER|\alpha_1,\alpha_2}$, is expressed as

$$P^F_{BER|\alpha_1,\alpha_2} = \frac{1}{2}(P^F_{MSB} + P^F_{LSB}) \tag{8.24}$$

Table 8.2 Numerical Values and Signs of Variables in Conditional BER for LSB

Index i	λ_i	κ_i	ζ_i	X_{I_i}	X_{Q_i}	$E\{\|X_i\|^2\}$
1	+	+	+	d	$3d$	$10d^2$
2	+	+	-	d	$3d$	$10d^2$
3	+	+	+	d	d	$2d^2$
4	+	+	-	d	d	$2d^2$
5	+	+	+	d	$-d$	$2d^2$
6	+	+	-	d	$-d$	$2d^2$
7	+	+	+	d	$-3d$	$10d^2$
8	+	+	-	d	$-3d$	$10d^2$
9	+	-	-	$-3d$	$3d$	$18d^2$
10	-	+	-	$-3d$	$3d$	$18d^2$
11	+	-	-	$-3d$	d	$10d^2$
12	-	+	-	$-3d$	d	$10d^2$
13	+	-	-	$-3d$	$-d$	$10d^2$
14	-	+	-	$-3d$	$-d$	$10d^2$
15	+	-	-	$-3d$	$-3d$	$18d^2$
16	-	+	-	$-3d$	$-3d$	$18d^2$

where P^F_{MSB} and P^F_{LSB} can be obtained from (8.22) and (8.23) by setting σ^2_Φ to 0.

Finally, since some of data subcarriers in the signal are affected by NBI while some of them are not, the unconditional BER is obtained by averaging of unconditional BER of the two cases. Let N^I be the number of data subcarriers which are affected by the NBI and $N^F = N - N^I$ be the number of data subcarriers which are free from NBI. Then, unconditional BER, denoted as P_{BER}, is given by

$$\begin{aligned} P_{BER} =& \frac{N^I}{N} \int_0^\infty \int_0^\infty \int_0^\infty P^I_{BER|\alpha_1,\alpha_2,\alpha_3} p(\alpha_1)p(\alpha_2)p(\alpha_3)d\alpha_1 d\alpha_2 d\alpha_3 \\ &+ \frac{N^F}{N} \int_0^\infty \int_0^\infty P^F_{BER|\alpha_1,\alpha_2} p(\alpha_1)p(\alpha_2)d\alpha_1 d\alpha_2 \end{aligned} \tag{8.25}$$

where $p(\alpha_i)$ is the probability density function (PDF) of α_i and is given by [47]

$$p(\alpha_i) = \frac{\alpha_i}{\sigma^2_{H_i}} e^{\frac{-\alpha_i^2}{2\sigma^2_{H_i}}} \qquad i = 1, 2, 3 \tag{8.26}$$

Notice that in (8.25), the first term represents the BER contribution from the case where the subcarriers are affected by the NBI while the second term represents the BER contribution from the case where the subcarriers are free from NBI. If we further assume that the NBI is not present in the channel, i.e. $N^I = 0$, (8.25) is further reduced to

$$P_{BER} = \int_0^\infty \int_0^\infty P^F_{BER|\alpha_1,\alpha_2} p(\alpha_1)p(\alpha_2)d\alpha_1 d\alpha_2 \tag{8.27}$$

Table 8.3 Summary of Simulation Cases

Case Number	NBI Power	HPA	Subcarriers	$2\sigma_\epsilon^2$
1	0	Varying	0	0
2	Varying	Constant	1	0
3	Constant	Constant	Varying	0
4	Constant	Constant	1	Varying

Table 8.4 Simulation Parameters for Nonlinear HPA Model

Case Number	α_{AM}	β_{AM}	α_{PM}	β_{PM}
1-A	1	0	0	0
1-B	1	0.25	π	0.25
1-C	1	0.25	1.2π	0.01
1-D	1	0.25	1.5π	0.01

8.4 Simulation Model and Parameters

The simulation model is an extension of the analytical model such as it complies with the IEEE 802.11n standard ([4], Clause 10.4.4.2 rate code 118); except the convolutional encoder, interleaver/deinterleaver and Viterbi decoder are omitted from the model. After pre-appending 16-bit Service Field and padding enough bits to ensure the transmission from each antenna are multiples of whole OFDM symbols, the resulting signal is scrambled with a scrambler that is based on the IEEE 802.11a standard. The data is modulated with the 16-QAM modulation and processed with the 64-point IFFT, of which subcarriers, ± 21, are designated for pilots. The OFDM symbols are then cyclically extended and passed through the nonlinear HPAs. The resulting OFDM symbols are encoded using STBC encoding scheme as described in Section 8.2.3 and pre-appended with the preamble sequences as specified in [4] before transmission. To recover the data, the corresponding receiver reverses the encoding procedure in the transmitter.

The simulations are performed based on the extended model for four cases which are summarized in Table 8.3. In case 1, the transmitted signal is subjected to various degrees of nonlinear distortion introduced by the nonlinear HPAs while the power of NBI is assumed to be zero. The numerical values for parameters used in the nonlinear HPA model are listed in Table 8.4. Notice in case 1-A where α_{AM} is set to one while the rest of parameters are set to zero, the HPA becomes a perfectly linear HPA which has an unity gain with no phase distortion. Instead of varying the nonlinearity, in case 2, we vary the power of NBI. Furthermore, we assume that only one subcarrier is interfered by the NBI. As for case 3, we let the total power of NBI be a constant which is equal to $\frac{5^2}{2}$. We then vary the number of subcarriers that are affected by the NBI. For the first three cases, we assume that the channel estimation is perfect. For case 4, we simulate the system which is impaired by NBI and nonlinear HPAs for various levels of the channel estimation error. In the cases 2, 3, and 4, the parameters for nonlinear HPA model for the case 1-C are used in simulations. Finally, we assume the Rayleigh channels have unity variances. In addition, we let the variances

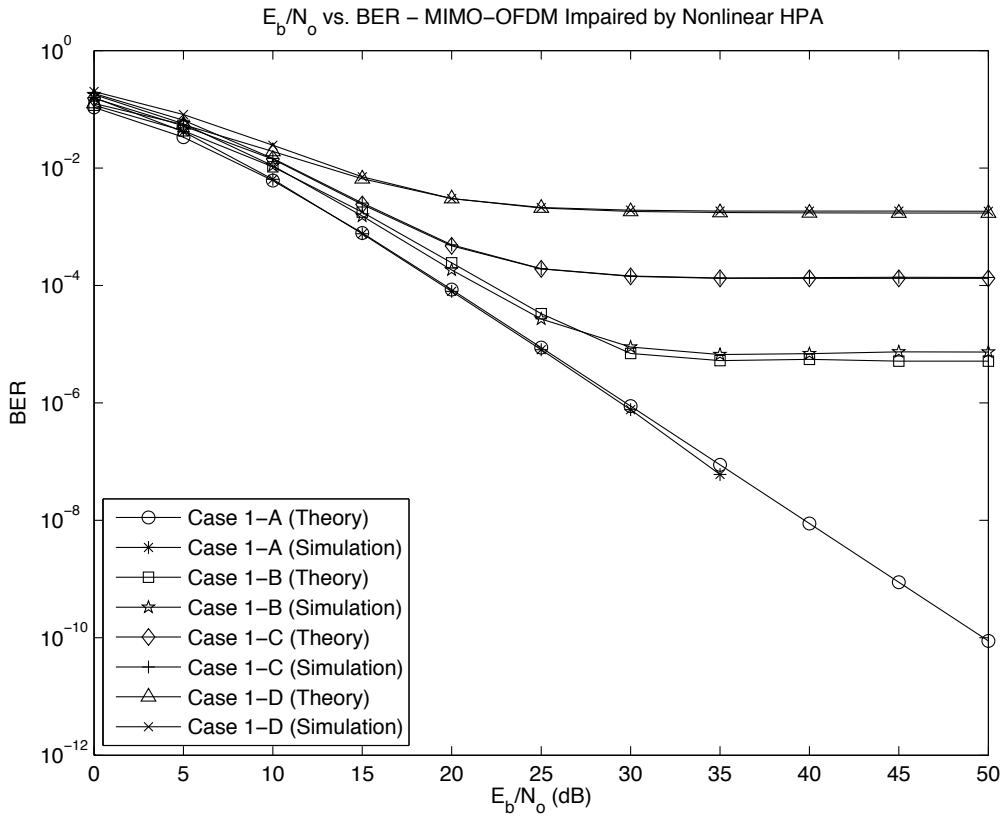

Figure 8.3 BER performance of a MIMO-OFDM system that is subject to nonlinear distortion which is produced by nonlinear HPAs.

of the channel estimation error when estimating both channels, H_1 and H_2, to be the same, i.e. $\sigma^2_{\epsilon_1} = \sigma^2_{\epsilon_2} = \sigma^2_{\epsilon}$.

8.5 Simulation Results

In case 1 where we assume the only source of degradation aside from AWGN is nonlinear distortion introduced by nonlinear HPAs, the simulation and theoretical results are shown in Fig. 8.3. As one can observe from Fig. 8.3, the BER performance degrades as more nonlinear distortion is introduced by the nonlinear HPAs to the system. This is due to the reason that as the system is subject to more nonlinear distortion, the power of nonlinear distortion or overall noise power increases for a given SNR value. As a result, the BER performance gets worse. For case 2, the amplitude of NBI varies from 0 to 1.5 with an increment of 0.5. The simulation results are plotted against the theoretical values obtained from (8.25) and are shown in Fig. 8.3. Depending on how much degradation there is in the system, the error floor in the performance might occur at higher signal to noise ratio (SNR) than the other case. In both cases, the error floor generally occurs at

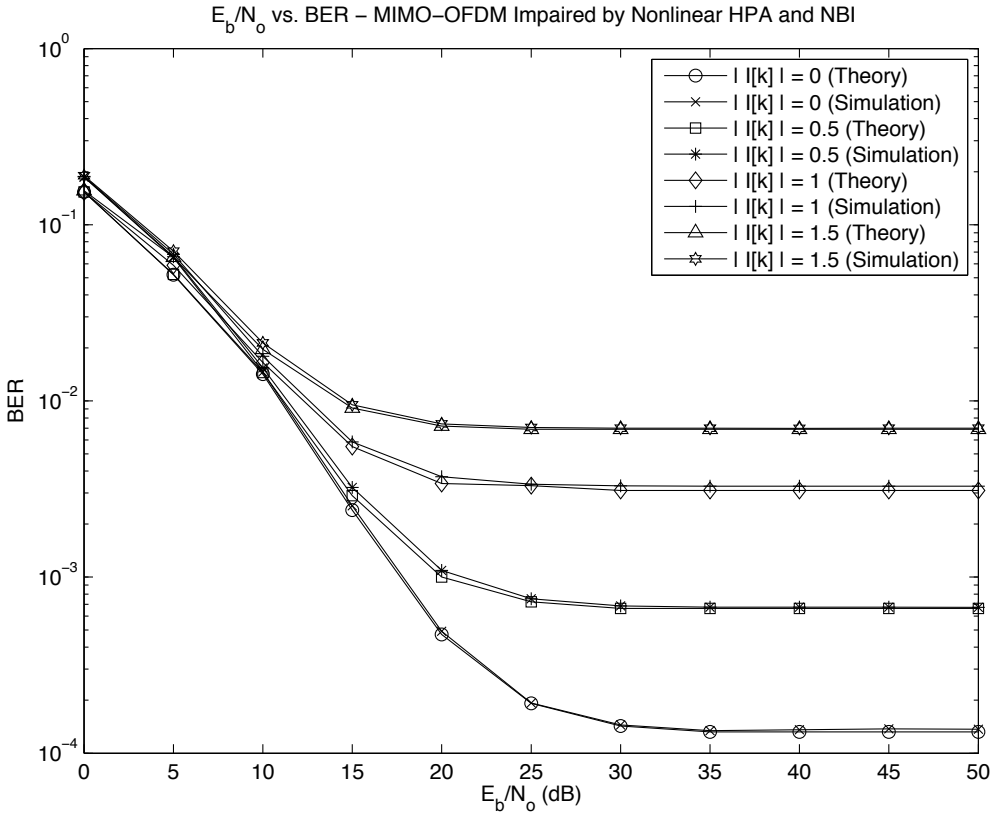

Figure 8.4 BER performance of a MIMO-OFDM system that is impaired by nonlinear HPAs and NBI for various amplitude. In addition, it is assumed that there is only one subcarrier which is interfered by the NBI.

around 25 dB. The occurrence of the error floor can be explained by the SNR of either the MSB or LSB probabilities. For example, at the high SNR, the effect of σ_w^2 is negligible compared to σ_Ξ^2 and σ_Φ^2. As a result, the SNR for MSB BER becomes

$$SNR_{MSB} \simeq \frac{(\alpha_1^2 + \alpha_2^2)^2 (\alpha_{G_I} X_{I_i} - \alpha_{G_Q} X_{Q_i})^2}{\sigma_\Xi^2 + \sigma_\Phi^2} \tag{8.28}$$

where SNR_{MSB} is only a function of E_b, α_G, σ_Ξ^2, and σ_Φ^2 of which α_G and σ_Ξ^2 are constants for a given set of parameters used in the nonlinear HPA model. In addition, σ_Φ^2 only depends on the power of NBI. Therefore, at high SNR, the system still has the same amount of degradation and subsequently produces an error floor in BER performance.

In case 3, the total power of NBI is held constant; however, the number of data subcarriers that are affected by the NBI are set to 0, 1, 5 and 10. Both simulation and theoretical results are shown in Fig. 8.5. As one can see from Fig. 8.5, the NBI that has all its energy concentrated in one data subcarrier causes the most degradation in the system performance as compared to other

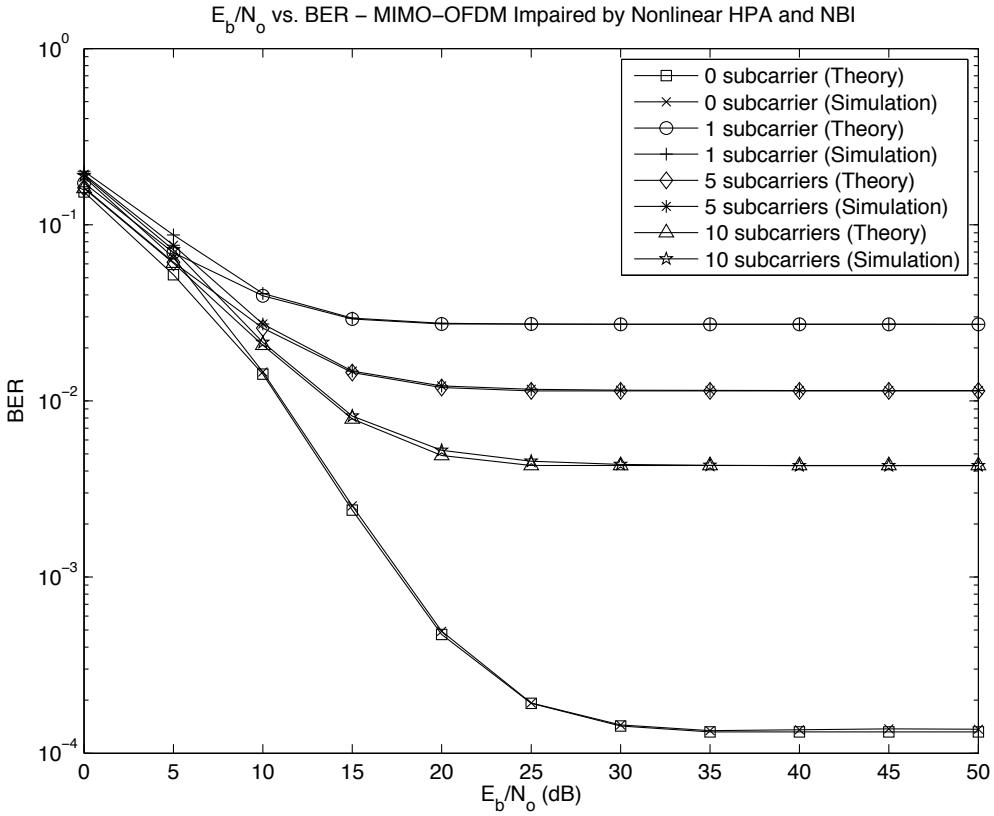

Figure 8.5 BER performance of a MIMO-OFDM system that is impaired by nonlinear HPAs and NBI for various number of subcarriers that are interfered by NBI. The total power of NBI is assumed to be constant.

cases where the number of data subcarriers that are affected by NBI is greater than one subcarrier. This is because as the number of subcarriers that are affected by NBI increases, the power of NBI per subcarrier has to decrease in order to preserve the condition that the total NBI power is held constant. As a result, σ_Φ^2 becomes smaller in value and has less impact on the system performance.

By looking at the results in Fig. 8.5, one might be inclined to use a NBI who has all its energy concentrated in one data subcarrier when it comes to designing a NBI. Even though, this particular approach causes the most degradation in the system performance, it is not practical in real situations for two main reasons. The first main reason is, in order for this type of NBI to be effective and causes sever degradation in system performance, the NBI must have the perfect knowledge of the center frequency of the transmitted signal. Otherwise, the system is completely free from the NBI interference. Another reason is the system can simply turn off the particular subcarrier's frequency at which the NBI interferes. By doing so, the BER performance can improve greatly at the expenses of decreased in data rate.

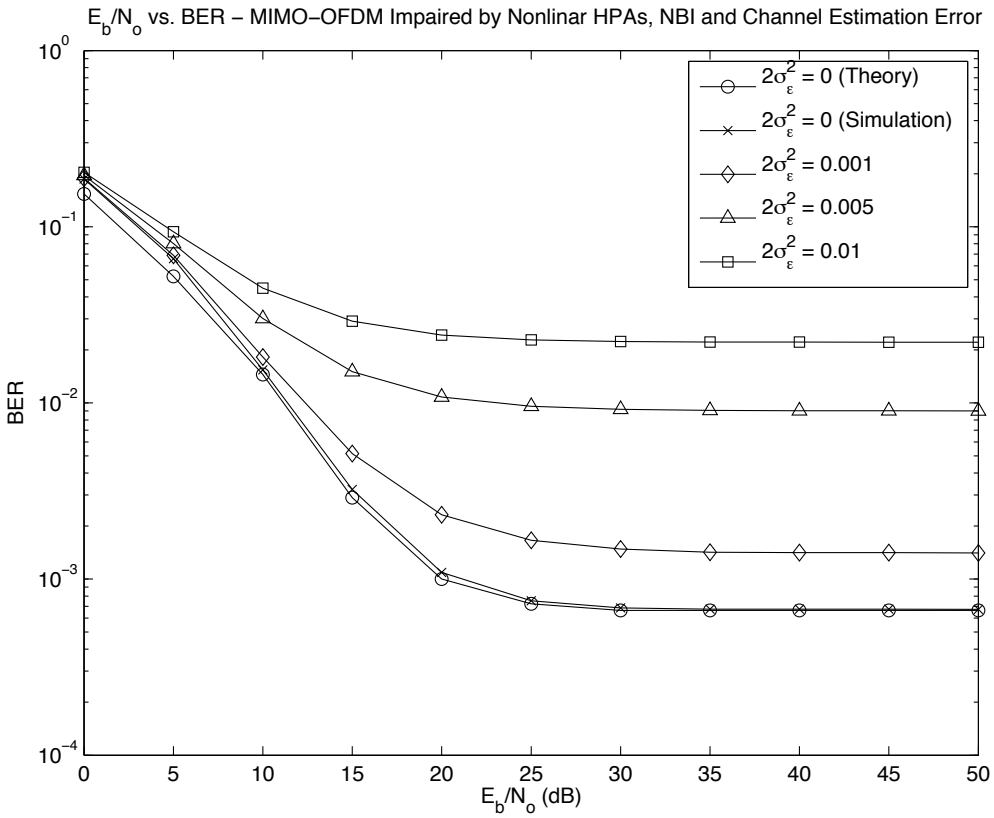

Figure 8.6 BER performance of a MIMO-OFDM system that is impaired by nonlinear HPAs and NBI for various values of $2\sigma_\epsilon^2$.

Finally, the BER performance further degrades when there are errors in estimating channel responses. Fig. 8.6. shows the effect of channel estimation error on the performance of a MIMO-OFDM system that is subject to nonlinear HPAs and NBI.

8.6 Conclusion

In this chapter, we analyzed the performance of a MIMO-OFDM system that was subject to nonlinear HPAs, NBI and channel estimation error in Rayleigh fading channels. The model for the NBI presented in this chapter was more realistic compared to the other models in previous studies because it experienced a separate channel response. Since the NBI was only affecting some of the data subcarriers, the received signal in frequency domain can be separated into two cases. One of which is for the situation where the subcarriers are interfered by the NBI. The other case represents the scenario which the subcarriers are free from the interference of NBI. In this chapter, we derived the BER expressions for the two cases and showed how the BER expression of the case

where the subcarriers were free from the interference of NBI can be obtained from the other case where the subcarriers are affected by NBI by setting appropriate terms in the SNR expression to zero. For the purpose of simulation, we also extended the analytical model such that it conforms to a MIMO-OFDM WLAN system as specified in the IEEE 802.11n specification. We also discussed the effectiveness of NBI with various bandwidth on the BER performance of the MIMO-OFDM system under the condition that the total NBI power was held constant. Finally, we presented both simulation and theoretical results for various sets of degradation with and without channel estimation error.

The text in Chapter 8 is based on the material as it appears in:

David W. Chi and Pankaj Das, "Effects of Nonlinear Amplifier and Narrowband Interference in MIMO-OFDM with Application to 802.11n WLAN", 2008 IEEE Global Communications Conference (Submitted).

The dissertation author was the primary researcher and author, and the co-author listed in the publication directed and supervised the research which forms the basis for this chapter.

9

Effects of Jammer with Normalized Frequency Offset and Nonlinear Amplifier on the Performance of MIMO-OFDM

9.1 Introduction

In Orthogonal Frequency Division Multiplexing (OFDM), the broadband channel is divided into several orthogonal and narrowband subchannels which are known as subcarriers. The bandwidth of a subcarrier is often smaller than the channel coherence bandwidth; therefore, OFDM systems are able to deliver high data rates with high bandwidth efficiency and lower receiver complexity. Due to those technical advantages mentioned previously, OFDM has been adopted in IEEE standards such as IEEE 802.11a/g/n [2–4]. In addition, it is currently being considered for the fourth generation (4G) mobile and Wireless Local Area Network (WLAN) communication systems.

In the past, the Single Input Single Output (SISO) has always been a main configuration for antenna implementation in wireless communication systems. However, the SISO antenna implementation can no longer satisfy the demands of high data rate and superior performance as wireless technology moves toward 4G. To further enhance the system performance, a simple coding scheme which encodes transmitted symbols in time and across space domain, then transmits multiple encoded symbols through multiple antennas was first proposed by Alamouti [21]. This simple coding technique which is generally referred to as Space Time Block Code (STBC) or Alamouti code was later applied in OFDM systems and its system performance was first presented in [36]. Since

then, OFDM systems with multiple antennas configuration and STBC are generally referred to as Multiple Input Multiple Output (MIMO)-OFDM or STBC-OFDM systems in literature.

Even though, OFDM has abilities to deliver high data rate and offer robustness in performance in fading channels, by itself, OFDM is also known to have some disadvantages such as high peak to average power ratio (PAPR) and high sensitivity to frequency offset or phase noise. The phenomenon of high PAPR is a direct consequence of the superimposition of multi-carrier signals. Practical high power amplifiers (HPAs) have difficulty reproducing such high PAPR signals and often introduce nonlinear distortion such as clipping and spectral regrowth which subsequently degrade the system's performance [24, 25]. In general, the frequency offset is caused by the frequency deviation between the transmitter and receiver, or by Doppler shift. Unlike the frequency offset, the phase noise is usually a random process because the phase noise is often caused by the fluctuation of the transmitter and receiver oscillators. When either the frequency offset or phase noise is present in the system, the orthogonality between subcarriers is no longer valid. As a result, the inter-carrier interference (ICI) will occur and the system performance degrades [5]. The performance of MIMO-OFDM systems with various degradation sources has been studied extensively and reported [38, 40, 41, 44].

While there are some papers dealing with the effect of nonlinear distortion and channel estimation error in MIMO-OFDM systems, very few adequately address the joint effect of nonlinear HPAs and jammer on the performance of MIMO-OFDM systems in Rayleigh fading channels. Mudulodu, *et al.* presented the performance of a MIMO-OFDM system in the selective fading channel without considering the effects of either nonlinear HPAs, jammer or channel estimation error [41]. In [38, 40], the authors only considered the effect of channel estimation error on the performance of MIMO-OFDM systems. In [44], simulation results of a Space-Frequency Block Code (SFBC)-OFDM and a SFBC-OFDM with carrier interferometry systems which were only subject to either nonlinear distortion or narrowband interference (NBI) were presented. Nevertheless, the performance of a SFBC-OFDM system under those impairments was not analyzed analytically in the paper. In addition, the authors assumed that the source of NBI was close to the receiver; hence, NBI did not experience any channel effects. This particular assumption does not provide useful insights to the performance of a MIMO-OFDM system in the presence of jammer because in most cases, the sources of jamming are often located in remote areas such as satellites in orbit or battleships at sea. Therefore, it is more reasonable and practical to assume that the jamming signal experiences another separate channel response.

In previous chapter [45, 46], we analyzed the joint effect of nonlinear HPA and jammer on the performance of OFDM systems with and without channel estimation error. In contrast to the jammer model presented in [44], we assumed that the jammer by itself experienced a separated

channel response. We then extended our work to the case where multiple antennas were included in the system [48]. In this chapter, we further extend the jamming model that was presented in our previous work to include the situations where the jammer has an offset in frequency with respect to the desired signal. This assumption is generally valid because the jammer usually does not have prior knowledge of which frequency the desired signal is being transmitted. As a consequence, the jammer, in most cases, transmits at a frequency which is slightly offset from the frequency that the receiver has locked onto and introduces varying amounts of interference to the system. Using this proposed jammer model, we present the performance analysis of a MIMO-OFDM system which is also impaired by nonlinear HPAs. Furthermore, the analytical model is extended to be in compliance with the IEEE 802.11n standard for the purpose of simulation.

The chapter is organized as follows. In Section 9.2, the block diagram of analytical system is presented and each component is discussed in detail. Section 9.3 contains the performance analysis of the analytical model. Section 9.4 discusses the simulation setup and parameters for extended model. Section 9.5 provides simulation results of the model described in Section 9.4. Finally, Section 9.6 summarizes the chapter.

9.2 System Description

The block diagram of an analytical system which has two transmit antennas and one receive antenna is shown in Fig. 9.1. Each block in the system is discussed in more detail in following subsections.

9.2.1 Transmitter

The transmitter is composed of a M-ary Quadrature Amplitude Modulation (M-QAM) modulator, a IFFT, a nonlinear HPA and a STBC encoder. The binary input to the M-QAM modulator is assumed to be equiprobable and independent. They are subsequently grouped into a block size of $log_2 M$ and mapped into M-QAM symbols, $X[k]$, according to alphabet, $A = \{(2m - 1 - \sqrt{M}) + j(2n - 1 - \sqrt{M})\}$ where $\{m, n = 1, 2, ...\sqrt{M}\}$ and M is the signal constellation size. At appropriate sampling time, the signal at the output of the IFFT, denoted as $x(n)$, is expressed as

$$x(n) = \frac{1}{N} \sum_{k=0}^{N-1} X[k] e^{j\frac{2\pi nk}{N}} \qquad 0 \leq n \leq N-1 \tag{9.1}$$

where N is the total number of subcarriers.

9.2.2 HPA Model

The nonlinear HPA model in the transmitter represents the nonlinear distortion imposed on the signal. In this chapter, the nonlinear HPA model follows the Saleh model which has been

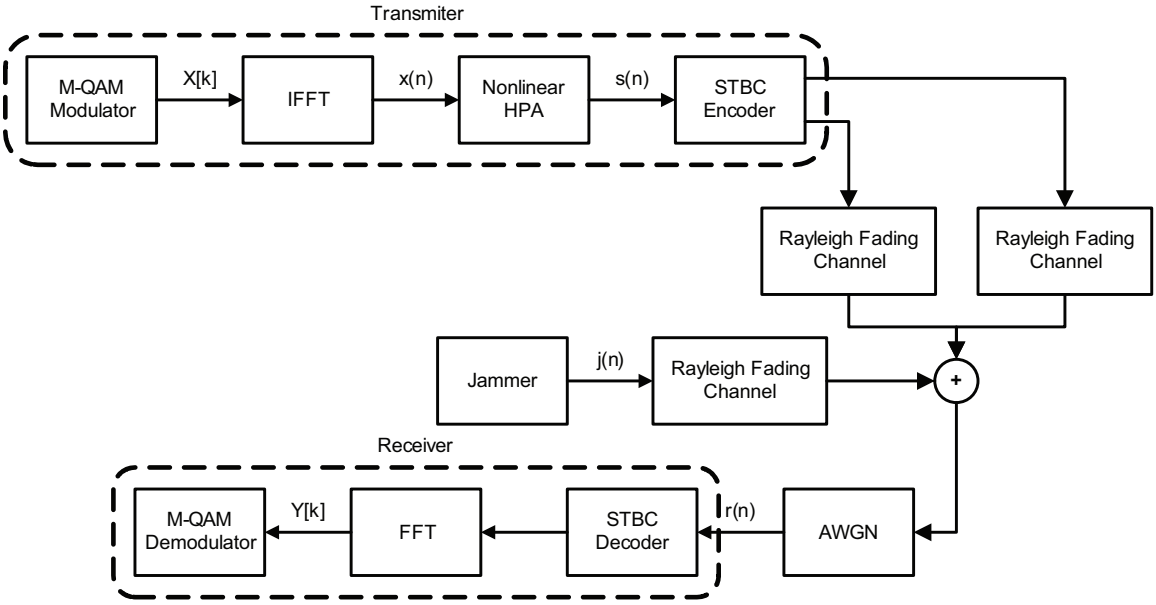

Figure 9.1 The system block diagram of a M-QAM MIMO-OFDM system which is subject to nonlinear HPAs, jammer and channel estimation error in Rayleigh fading channels.

described in Chapter 2, Section 2.3.

9.2.3 STBC Encoder

In this chapter, the STBC, or Alamouti code, for two transmit antennas and one receive antenna is utilized to encode OFDM symbols. The encoding process of Alamouti code has been described in Chapter 7, Section 7.2.2.

9.2.4 Jammer Model, Channel Model and AWGN

The jamming signal in time domain, denoted as $j(n)$, is expressed as

$$j(n) = \frac{1}{N} \sum_{k=0}^{N-1} J[k] e^{j \frac{2\pi n(k+f)}{N}} \tag{9.2}$$

where $J[k]$ represents the jamming signal for the k^{th} subcarrier and has power equal to $\frac{|J[k]|^2}{2}$. Furthermore, f in (9.2) represents the normalized frequency offset between the jamming and transmitted signals.

Denote $h_1(n)$ as the impulse response of the Rayleigh fading channel between the first transmit antenna and the receive antenna. The in-phase and quadrature components of $h_1(n)$ are assumed to be Gaussian random variables with zero mean and $\sigma^2_{H_1}$ variance. Let $h_2(n)$ be the channel impulse response between the second transmit antenna and the receive antenna and its in-phase

and quadrature components are assumed to be Gaussian random variables with zero mean and $\sigma^2_{H_2}$ variance. Finally, let $h_3(n)$ be the channel impulse response between the jammer and the receiver. The in-phase and quadrature components of $h_3(n)$ are Gaussian random variables with zero mean and $\sigma^2_{H_3}$ variance. All three Rayleigh fading channels and their in-phase and quadrature components are assumed to be statistically independent of each other and the channel impulse responses are static for the duration of two OFDM symbols transmissions. The additive white Gaussian noise (AWGN), denoted as $w(n)$, represents the thermal noise and is modeled as an AWGN process which has zero mean and $2\sigma^2_w$ variance.

9.2.5 Receiver

For the simplicity of notation, we will drop the time and frequency indices. Let $r_t(n)$ be the received signal in time domain for the transmission time index t, under the assumption of perfect synchronization, $r_t(n)$ is then given by

$$r_t = \begin{cases} h_1 s_o + h_2 s_e + h_3 j + w_o & t = odd \\ -h_1 s_e^* + h_2 s_o^* + h_3 j + w_e & t = even \end{cases} \tag{9.3}$$

The odd and even number of OFDM symbols are denoted as s_o and s_e, respectively. In addition, $(\cdot)^*$ implies the complex conjugate operation of the signal in the argument. Representing (9.3) in the matrix format, $r(n)$ becomes

$$\underbrace{\begin{bmatrix} r_o \\ r_e^* \end{bmatrix}}_{\mathbf{r}} = \underbrace{\begin{bmatrix} h_1 & h_2 \\ h_2^* & -h_1^* \end{bmatrix}}_{\mathbf{h_D}} \underbrace{\begin{bmatrix} s_o \\ s_e \end{bmatrix}}_{\mathbf{s}} + \underbrace{\begin{bmatrix} h_3 & 0 \\ 0 & h_3^* \end{bmatrix}}_{\mathbf{h_N}} \underbrace{\begin{bmatrix} j \\ j \end{bmatrix}}_{\mathbf{j}} + \underbrace{\begin{bmatrix} w_o \\ w_e^* \end{bmatrix}}_{\mathbf{w}}$$

$$\mathbf{r} = \mathbf{h_D s} + \mathbf{h_N j} + \mathbf{w} \tag{9.4}$$

where the bold face letters represent matrices or vectors.

To accurately demodulate the received signal, estimating the channel responses are necessary and can be obtained with the aid of pilots in frequency domain. Let $\hat{\mathbf{H}}_\mathbf{D}$ be the matrix which presents the estimate of channel matrix, then $\hat{\mathbf{H}}_\mathbf{D}$ is often expressed as [38]

$$\hat{\mathbf{H}}_\mathbf{D} = \begin{bmatrix} \hat{H}_1 & \hat{H}_2 \\ \hat{H}_2^* & -\hat{H}_1^* \end{bmatrix} = \begin{bmatrix} H_1 + \epsilon_1 & H_2 + \epsilon_2 \\ H_2^* + \epsilon_2^* & -H_1^* - \epsilon_1^* \end{bmatrix} \tag{9.5}$$

where $\hat{H}_1$ and $\hat{H}_2$ are channel estimates for channels, H_1 and H_2, respectively. In addition, H_1 and H_2 are the Fast Fourier Transform (FFT) of $h_1(n)$ and $h_2(n)$. The variable ϵ_1 in (9.5) represents the error in estimating the channel, H_1, and is modeled as a complex Gaussian random process with zero mean and $2\sigma^2_{\epsilon_1}$ variance. Furthermore, ϵ_2 denotes the error in estimating the channel, H_2, and is assumed to be a complex Gaussian random process with zero mean and $2\sigma^2_{\epsilon_2}$ variance. In addition, both the in-phase and quadrature components of ϵ_1 and ϵ_2 are statistically independent of

all three channels and are statistically independent of each other.

Denote $\mathbf{Y}$ as the signal matrix at the output of FFT, then $\mathbf{Y}$ is found to be

$$\mathbf{Y} = \begin{bmatrix} Y_o \\ Y_e \end{bmatrix} = \hat{\mathbf{H}}_{\mathbf{D}}^{H}\mathbf{R} \tag{9.6}$$

where $\mathbf{R}$ is the FFT of $\mathbf{r}$ which is defined as (9.4). In addition, $(\cdot)^H$ implies the Hermitian operation of the matrix.

9.3 Performance Analysis

In this section, the bit error rate (BER) of the analytical model shown in Fig. 9.1 is derived and will later be used to measure the performance of the system. The performance analysis of the system starts with the characterization of $x(n)$. Under the assumption that N is large, by the *Central Limit Theorem*, $x(n)$ is said to be Gaussian distributed with zero mean [19]. With that assumption, Banelli, *et al.* [20] had shown that $s(n)$ can be written as a product of a complex gain, α_G, and the input signal, $x(n)$, added with noise distortion $d_G(n)$. The transmitted signal, denoted as $s(n)$, and its FFT are given by

$$s(n) = \alpha_G x(n) + d_G(n) \overset{FFT}{\longleftrightarrow} S[k] = \alpha_G X[k] + D_G[k] \tag{9.7}$$

where $D_G[k]$ was shown to be a complex Gaussian random variable with zero mean and $2\sigma_{D_G}^2$ variance which can be obtained by following the steps outlined in [20].

For two different subcarriers, k_1 and k_2, $D_G[k_1]$ and $D_G[k_2]$ are mutually independent of each other. Furthermore, the in-phase and quadrature components of $D_G[k]$ were shown to be mutually independent and identically distributed (i.i.d) [15]. The multiplicative coefficient α_G in (9.7) is given by

$$\alpha_G = \frac{E\{s(n)^* x(n)\}}{2\sigma_{x(n)}^2} = \alpha_{G_I} + j\alpha_{G_Q} \tag{9.8}$$

where $E\{\cdot\}$ is the expected value [20]. The subscripts I and Q represent the in-phase and quadrature components.

After some mathematical simplification, (9.6) becomes

$$\begin{aligned}
\begin{bmatrix} Y_o \\ Y_e \end{bmatrix} =& (\alpha_1^2 + \alpha_2^2)\mathbb{I}_{2\times 2} \begin{bmatrix} S_o \\ S_e \end{bmatrix} + \begin{bmatrix} H_1\epsilon_1^* + H_2^*\epsilon_2 & H_2\epsilon_1^* - H_1^*\epsilon_2 \\ H_1\epsilon_2^* - H_2^*\epsilon_1 & H_1^*\epsilon_1 + H_2\epsilon_2^* \end{bmatrix} \begin{bmatrix} S_o \\ S_e \end{bmatrix} \\
&+ \begin{bmatrix} H_3(H_1^* + \epsilon_1^*) & H_3^*(H_2 + \epsilon_2) \\ H_3(H_2^* + \epsilon_2^*) & H_3^*(-H_1 - \epsilon_1) \end{bmatrix} \begin{bmatrix} J_D \\ J_D \end{bmatrix} + \begin{bmatrix} H_3(H_1^* + \epsilon_1^*) & H_3^*(H_2 + \epsilon_2) \\ H_3(H_2^* + \epsilon_2^*) & H_3^*(-H_1 - \epsilon_1) \end{bmatrix} \begin{bmatrix} J_O \\ J_O \end{bmatrix} \\
&+ \begin{bmatrix} H_1^* + \epsilon_1^* & H_2 + \epsilon_2 \\ H_2^* + \epsilon_2^* & -H_1 - \epsilon_1 \end{bmatrix} \begin{bmatrix} W_o \\ W_e^* \end{bmatrix}
\end{aligned} \tag{9.9}$$

where α_1 and α_2 are the magnitudes of H_1 and H_2, respectively. In addition, $\mathbb{I}_{2\times 2}$ represents a 2 by 2 identity matrix. J_D and J_O in (9.9) are defined as

$$\begin{aligned} J_D[k] =& J[k]\frac{1}{N}\sum_{n=0}^{N-1} e^{j2\pi\frac{fn}{N}} \\ J_O[k] =& \sum_{n=0}^{N-1}\frac{1}{N}\sum_{\substack{l=0\\ l\neq k}}^{N-1} J[l]e^{j2\pi\frac{(l+f-k)n}{N}} \end{aligned} \tag{9.10}$$

As shown in Fig. 5.2 in Section 5.3 of Chapter 5, when the normalized frequency offset is nonzero, the jammer will affect all the subcarriers in the received signal with varying amount of jamming power. This can also be seen from (9.9). One can observe the effect of the frequency offset that is due to the mismatch between the frequencies of jamming and desired signals. When the jammer has prior knowledge about the frequency of the desired signal, i.e. the frequency offset is zero, $J_D[k]$ which is due to the jammer in the channel is the only source of interference present in the received signal aside from nonlinear distortion caused by HPAs and AWGN. In the case where the frequency offset is nonzero, not only is $J_D[k]$ present in the received signal, but the jammer produces an additional interference, $J_O[k]$, which behaves like ICI and causes further degradation in the BER performance.

Substituting $S[k]$ in (9.7) into (9.9), the received signal, $\mathbf{Y}$, is expressed as

$$\begin{bmatrix} Y_o \\ Y_e^* \end{bmatrix} = (\alpha_1^2+\alpha_2^2)\mathbb{I}_{2\times 2}\begin{bmatrix} \alpha_G X_o \\ \alpha_G X_e \end{bmatrix} + \mathbf{\Xi} + \mathbf{\Upsilon} + \mathbf{\Psi} + \mathbf{\Phi_D} + \mathbf{\Phi_O} + \mathbf{\Omega} \tag{9.11}$$

where

$$\begin{aligned} \mathbf{\Xi} =& (\alpha_1^2+\alpha_2^2)\mathbb{I}_{2\times 2}\begin{bmatrix} D_{G_o} \\ D_{G_e} \end{bmatrix} \\ \mathbf{\Upsilon} =& \begin{bmatrix} H_1\epsilon_1^* + H_2^*\epsilon_2 & H_2\epsilon_1^* - H_1^*\epsilon_2 \\ H_1\epsilon_2^* - H_2^*\epsilon_1 & H_1^*\epsilon_1 + H_2\epsilon_2^* \end{bmatrix}\begin{bmatrix} \alpha_G X_o \\ \alpha_G X_e \end{bmatrix} \\ \mathbf{\Psi} =& \begin{bmatrix} H_1\epsilon_1^* + H_2^*\epsilon_2 & H_2\epsilon_1^* - H_1^*\epsilon_2 \\ H_1\epsilon_2^* - H_2^*\epsilon_1 & H_1^*\epsilon_1 + H_2\epsilon_2^* \end{bmatrix}\begin{bmatrix} D_{G_o} \\ D_{G_e} \end{bmatrix} \\ \mathbf{\Phi_D} =& \begin{bmatrix} H_3(H_1^*+\epsilon_1^*) & H_3^*(H_2+\epsilon_2) \\ H_3(H_2^*+\epsilon_2^*) & H_3^*(-H_1-\epsilon_1) \end{bmatrix}\begin{bmatrix} J_D \\ J_D \end{bmatrix} \\ \mathbf{\Phi_O} =& \begin{bmatrix} H_3(H_1^*+\epsilon_1^*) & H_3^*(H_2+\epsilon_2) \\ H_3(H_2^*+\epsilon_2^*) & H_3^*(-H_1-\epsilon_1) \end{bmatrix}\begin{bmatrix} J_O \\ J_O \end{bmatrix} \\ \mathbf{\Omega} =& \begin{bmatrix} H_1^*+\epsilon_1^* & H_2+\epsilon_2 \\ H_2^*+\epsilon_2^* & -H_1-\epsilon_1 \end{bmatrix}\begin{bmatrix} W_o \\ W_e^* \end{bmatrix} \end{aligned} \tag{9.12}$$

Since $\mathbf{\Xi}$, $\mathbf{\Upsilon}$, $\mathbf{\Psi}$, $\mathbf{\Phi_D}$, $\mathbf{\Phi_O}$ and $\mathbf{\Omega}$ are noise with zero mean, obtaining the conditional variance for each term is required in order to evaluate the system performance.

Let σ^2_{Ξ} be the conditional variance for the in-phase or quadrature component of $\mathbf{\Xi}$, then σ^2_{Ξ} is given by

$$\sigma^2_{\Xi} = E\left\{\mathbf{\Xi}\mathbf{\Xi}^H\right\} = (\alpha_1^2 + \alpha_2^2)^2\sigma^2_{D_G}\mathbb{I}_{2\times 2} \tag{9.13}$$

Denote σ^2_{Υ} as the conditional variance for the in-phase or quadrature component of $\mathbf{\Upsilon}$, then σ^2_{Υ} is expressed as

$$\sigma^2_{\Upsilon} = E\left\{\mathbf{\Upsilon}\mathbf{\Upsilon}^H\right\} = |\alpha_G|^2 E\left\{|X|^2\right\}(\alpha_1^2 + \alpha_2^2)(\sigma^2_{\epsilon_1} + \sigma^2_{\epsilon_2})\mathbb{I}_{2\times 2} \tag{9.14}$$

Looking at (9.14), one might notice the dependency on modulated symbols, X, in the expression for σ^2_{Υ}. As mentioned in previous chapters, the numerical values for σ^2_{Υ} significantly depends on the shape of the signal constellation. For M-ary Phase Shift Keying (M-PSK) modulations which have circular signal constellations, $E\{|X|^2\}$ are the same for all M-PSK symbols. However, the numerical values of $E\{|X|^2\}$ are different when the modulation does not have a circular signal constellation. Therefore, one shall pay more attention to the calculation of σ^2_{Υ}. To include all possible signal constellations, we will rewrite (9.14) as

$$\sigma^2_{\Upsilon_i} = |\alpha_G|^2 E\left\{|X_i|^2\right\}(\alpha_1^2 + \alpha_2^2)(\sigma^2_{\epsilon_1} + \sigma^2_{\epsilon_2})\mathbb{I}_{2\times 2} \tag{9.15}$$

where the subscript i in X_i represents the i^{th} modulated symbol in the constellation.

Denote σ^2_{Ψ} as the conditional variance for the in-phase or quadrature component of $\mathbf{\Psi}$, then σ^2_{Ψ} is found to be

$$\sigma^2_{\Psi} = E\left\{\mathbf{\Psi}\mathbf{\Psi}^H\right\} = \sigma^2_{D_G}(\alpha_1^2 + \alpha_2^2)(\sigma^2_{\epsilon_1} + \sigma^2_{\epsilon_2})\mathbb{I}_{2\times 2} \tag{9.16}$$

Without loss of generality, it is assumed that $E\left\{X_o^2\right\} = E\left\{X_e^2\right\} = E\left\{X^2\right\}$ and $\sigma^2_{D_{G_o}} = \sigma^2_{D_{G_e}} = \sigma^2_{D_G}$ when obtaining (9.13), (9.14), and (9.16). Denote $\sigma^2_{\Phi_D}$ as the conditional variance for the in-phase or quadrature component of $\mathbf{\Phi_D}$, then $\sigma^2_{\Phi_D}$ is found to be

$$\sigma^2_{\Phi_D} = E\left\{\mathbf{\Phi_D}\mathbf{\Phi_D}^H\right\} = \sigma^2_{J_D}\begin{bmatrix} \phi_{11} & \phi_{12} \\ \phi_{21} & \phi_{22} \end{bmatrix} \tag{9.17}$$

where

$$\begin{aligned} \phi_{11} =& \alpha_3^2(\alpha_1^2 + \sigma^2_{\epsilon_1} + \alpha_2^2 + \sigma^2_{\epsilon_2}), \qquad \phi_{21} = \sigma^2_{H_3}(\sigma^2_{H_2} + \sigma^2_{\epsilon_2} - \sigma^2_{H_1} - \sigma^2_{\epsilon_1}) \\ \phi_{12} =& \sigma^2_{H_3}(-\sigma^2_{H_1} - \sigma^2_{\epsilon_1} + \sigma^2_{H_2} + \sigma^2_{\epsilon_2}), \qquad \phi_{22} = \alpha_3^2(\alpha_2^2 + \sigma^2_{\epsilon_2} + \alpha_1^2 + \sigma^2_{\epsilon_1}) \end{aligned} \tag{9.18}$$

and $\sigma^2_{J_D}$ can be found by first expanding $J_D[k]$ using Geometric series which is defined as [29]

$$\sum_{i=0}^{N-1}\alpha^i = \frac{1-\alpha^N}{1-\alpha} \qquad\qquad |\alpha| < 1 \tag{9.19}$$

After expansion, $\sigma^2_{J_D}$ is found to be

$$\sigma^2_{J_D} = E\{J_D[k]J^*_D[k]\} = \frac{1}{N^2}\left(\frac{\sin^2(\pi f)}{\sin^2\left(\frac{\pi f}{N}\right)}\right)\frac{|J[k]|^2}{2} \tag{9.20}$$

Let $\sigma^2_{\Phi_O}$ be the conditional variance for the in-phase or quadrature component of Φ_O, then $\sigma^2_{\Phi_O}$ can be found in similar fashion, namely

$$\sigma^2_{\Phi_O} = E\left\{\mathbf{\Phi_O}\mathbf{\Phi_O}^H\right\} = \sigma^2_{J_O}\begin{bmatrix}\phi_{11} & \phi_{12}\\ \phi_{21} & \phi_{22}\end{bmatrix} \tag{9.21}$$

where ϕ_{11}, ϕ_{12}, ϕ_{21}, and ϕ_{22} are defined as (9.18). Applying the same approach, namely expanding $J_O[k]$ using the Geometric series, then $\sigma^2_{J_O}$ is found to be

$$\begin{aligned}\sigma^2_{J_O} =& E\{J_O[k]J^*_O[k]\}\\ =& \frac{1}{N^2}\sum_{l=0}^{N-1}\frac{|J[l]|^2}{2}\left[\frac{\sin^2(\pi(l+f-k))}{\sin^2\left(\frac{\pi(l+f-k)}{N}\right)}\right]\\ &-\frac{1}{N^2}\left[\frac{\sin(\pi f)}{\sin\left(\frac{\pi f}{N}\right)}\right]\sum_{l=0}^{N-1}E\{J[l]J^*[k]\}e^{j\pi(l-k)(1-\frac{1}{N})}\left[\frac{\sin(\pi(l+f-k))}{\sin\left(\frac{\pi(l+f-k)}{N}\right)}\right]\\ &-\frac{1}{N^2}\left[\frac{\sin(\pi f)}{\sin\left(\frac{\pi f}{N}\right)}\right]\sum_{l=0}^{N-1}E\{J^*[l]J[k]\}e^{-j\pi(l-k)(1-\frac{1}{N})}\left[\frac{\sin(\pi(l+f-k))}{\sin\left(\frac{\pi(l+f-k)}{N}\right)}\right]\\ &+\frac{1}{N^2}\frac{|J[k]|^2}{2}\left[\frac{\sin^2(\pi f)}{\sin^2\left(\frac{\pi f}{N}\right)}\right]\end{aligned} \tag{9.22}$$

Finally, let σ^2_Ω be the conditional variance for the in-phase or quadrature component of $\mathbf{\Omega}$, then σ^2_Ω is found to be

$$\sigma^2_\Omega = E\left\{\mathbf{\Omega}\mathbf{\Omega}^H\right\} = \sigma^2_w(\alpha_1^2+\alpha_2^2+\sigma^2_{\epsilon_1}+\sigma^2_{\epsilon_2})\mathbb{I}_{2\times 2} \tag{9.23}$$

Since $E\left\{X_o^2\right\} = E\left\{X_e^2\right\} = E\left\{X^2\right\}$, (9.11) can further be reduced to

$$\begin{aligned}Y =& \left\{(\alpha_1^2+\alpha_2^2)\left(\alpha_{G_I}X_I - \alpha_{G_Q}X_Q\right) + \mathbf{\Xi}_I + \mathbf{\Upsilon}_I + \mathbf{\Psi}_I + \mathbf{\Phi_D}_I + \mathbf{\Phi_O}_I + \mathbf{\Omega}_I\right\}\\ &+ j\left\{(\alpha_1^2+\alpha_2^2)(\alpha_{G_I}X_Q + \alpha_{G_Q}X_I) + \mathbf{\Xi}_Q + \mathbf{\Upsilon}_Q + \mathbf{\Psi}_Q + \mathbf{\Phi_D}_Q + \mathbf{\Phi_O}_Q + \mathbf{\Omega}_Q\right\}\\ =& Y_I + jY_Q\end{aligned} \tag{9.24}$$

where $\mathbf{\Xi}_I$, $\mathbf{\Upsilon}_I$, $\mathbf{\Psi}_I$, $\mathbf{\Phi_D}_I$, $\mathbf{\Phi_O}_I$ and $\mathbf{\Omega}_I$ represent the in-phase component of $\mathbf{\Xi}$, $\mathbf{\Upsilon}$, $\mathbf{\Psi}$, $\mathbf{\Phi_D}$, $\mathbf{\Phi_O}$ and $\mathbf{\Omega}$, respectively. Furthermore, $\mathbf{\Xi}_Q$, $\mathbf{\Upsilon}_Q$, $\mathbf{\Psi}_Q$, $\mathbf{\Phi_D}_Q$, $\mathbf{\Phi_O}_Q$ and $\mathbf{\Omega}_Q$ represent the quadrature component of $\mathbf{\Xi}$, $\mathbf{\Upsilon}$, $\mathbf{\Psi}$, $\mathbf{\Phi_D}$, $\mathbf{\Phi_O}$ and $\mathbf{\Omega}$, respectively.

To continue the derivation, we assume that 16-QAM modulation is utilized in the system. Nevertheless, other rectangular QAM constellations can be derived in the similar fashion if

Table 9.1 Numerical Values of Variables in Conditional BER for MSB

Index i	X_{I_i}	X_{Q_i}	$E\{\|X_i\|^2\}$	Index i	X_{I_i}	X_{Q_i}	$E\{\|X_i\|^2\}$
1	d	$3d$	$10d^2$	5	$3d$	$3d$	$18d^2$
2	d	d	$2d^2$	6	$3d$	d	$10d^2$
3	d	$-d$	$2d^2$	7	$3d$	$-d$	$10d^2$
4	d	$-3d$	$10d^2$	8	$3d$	$-3d$	$18d^2$

they are chosen for modulating signals. Since all the subcarriers are affected by the jammer with various degrees of jamming power, we need to calculate the BER for each individual subcarrier. Next, the conditional BER is obtained by averaging over all subcarriers. Finally, we can obtain the unconditional BER by integrating the conditional BER over the probability density functions (PDFs) of α_1, α_2, and α_3. Let $P^k_{BER|\alpha_1,\alpha_2,\alpha_3}$ be the conditional BER for the k^{th} subcarrier, conditioned on α_1, α_2, and α_3, then $P^k_{BER|\alpha_1,\alpha_2,\alpha_3}$ is given by

$$P^k_{BER|\alpha_1,\alpha_2,\alpha_3} = \frac{1}{2}\left(P^k_{MSB} + P^k_{LSB}\right) \tag{9.25}$$

where P^k_{MSB} and P^k_{LSB} are the conditional BER of most significant bits (MSB) and least significant bits (LSB) of 16-QAM symbols conditioned on α_1, α_2, and α_3 for the k^{th} subcarrier. Based on the decision boundaries, P^k_{MSB} is expressed as

$$\begin{aligned} P^k_{MSB} =& P(Y_I < 0|\alpha_1,\alpha_2,\alpha_3) \\ =& \frac{1}{8}\sum_{i=1}^{8} Q\left(\sqrt{\frac{\Lambda_i^2}{\sigma^2_\Xi + \sigma^2_{\Upsilon_i} + \sigma^2_\Psi + \sigma^2_{\Phi_D} + \sigma^2_{\Phi_O} + \sigma^2_\Omega}}\right) \end{aligned} \tag{9.26}$$

where $\Lambda_i = (\alpha_1^2+\alpha_2^2)(\alpha_{G_I}X_{I_i} - \alpha_{G_Q}X_{Q_i})$ and $Q(\nu) = \int_\nu^\infty \frac{1}{\sqrt{2\pi}} e^{\frac{-t^2}{2}} dt, \nu \geq 0$. Furthermore, σ^2_Ξ, $\sigma^2_{\Upsilon_i}$, σ^2_Ψ, $\sigma^2_{\Phi_D}$, $\sigma^2_{\Phi_O}$, and σ^2_Ω are defined as (9.13), (9.15), (9.16), (9.17), (9.21), and (9.23), respectively. The numerical values for X_{I_i}, X_{Q_i} and $E\{|X_i|^2\}$ in (9.26) are listed in Table 9.1. The conditional BER of LSB can be found in the similar way and it is found to be

$$P^k_{LSB} = \frac{1}{8}\sum_{i=1}^{16} \lambda_i Q\left(\sqrt{\frac{(\kappa_i 2(\alpha_1^2+\alpha_2^2)d + \zeta_i\Lambda_i)^2}{\sigma^2_\Xi + \sigma^2_{\Upsilon_i} + \sigma^2_\Psi + \sigma^2_{\Phi_D} + \sigma^2_{\Phi_O} + \sigma^2_\Omega}}\right) \tag{9.27}$$

where λ_i, κ_i, and ζ_i are signs of the values for i^{th} quantity and are listed along with values for X_{I_i}, X_{Q_i} and $E\{|X_i|^2\}$ in Table 9.2. In both Tables 9.1 and 9.2, $d^2 = \frac{2E_b}{5}$ where E_b is the energy per bit.

With (9.25), (9.26) and (9.27), the unconditional BER is given as

$$P_{BER} = \frac{1}{N}\sum_{k=0}^{N-1}\int_0^\infty\int_0^\infty\int_0^\infty P^k_{BER|\alpha_1,\alpha_2,\alpha_3} p(\alpha_1)p(\alpha_2)p(\alpha_3)d\alpha_1 d\alpha_2 d\alpha_3 \tag{9.28}$$

where $p(\alpha_i)$ is the PDF of α_i and is given by

$$p(\alpha_i) = \frac{\alpha_i}{\sigma^2_{H_i}} e^{\frac{-\alpha_i^2}{2\sigma^2_{H_i}}} \qquad i = 1,2,3 \tag{9.29}$$

Table 9.2 Numerical Values and Signs of Variables in Conditional BER for LSB

Index i	λ_i	κ_i	ζ_i	X_{I_i}	X_{Q_i}	$E\{\|X_i\|^2\}$
1	+	+	+	d	$3d$	$10d^2$
2	+	+	-	d	$3d$	$10d^2$
3	+	+	+	d	d	$2d^2$
4	+	+	-	d	d	$2d^2$
5	+	+	+	d	$-d$	$2d^2$
6	+	+	-	d	$-d$	$2d^2$
7	+	+	+	d	$-3d$	$10d^2$
8	+	+	-	d	$-3d$	$10d^2$
9	+	-	-	$-3d$	$3d$	$18d^2$
10	-	+	-	$-3d$	$3d$	$18d^2$
11	+	-	-	$-3d$	d	$10d^2$
12	-	+	-	$-3d$	d	$10d^2$
13	+	-	-	$-3d$	$-d$	$10d^2$
14	-	+	-	$-3d$	$-d$	$10d^2$
15	+	-	-	$-3d$	$-3d$	$18d^2$
16	-	+	-	$-3d$	$-3d$	$18d^2$

Table 9.3 Summary of Simulation Cases

Case Number	HPA	$\|J[k]\|$	f	Jamming Tones	$2\sigma_\epsilon^2$
1	Vary	0	0	0	0
2	0	Vary	Vary	1	0
3	Constant	Vary	0.5	1	0
4	Constant	Constant	0.5	Vary	0
5	Constant	Constant	0.5	1	Vary

9.4 Simulation Model and Parameters

We extend the analytical model to a WLAN system based on the IEEE 802.11n standard ([4], Clause 10.4.4.2 rate code 118); except the convolutional encoder, interleaver/deinterleaver and Viterbi decoder are omitted. After pre-appending 16-bit Service Field and padding enough bits to ensure the transmission from each antenna are multiples of whole OFDM symbols, the resulting signal is scrambled with a scrambler which is based on the IEEE 802.11a standard. The data is modulated with the 16-QAM modulation and processed with the 64-point IFFT, of which subcarriers, ± 21, are designated for pilots. The OFDM symbols are then cyclically extended and passed through the nonlinear HPAs. The resulting OFDM symbols are encoded by following STBC coding scheme as described in Section 9.2.3 and pre-appended with the preamble sequences as specified in [4] before transmission. To recover the data, the corresponding receiver reverses the encoding procedure in the transmitter.

The extended model is simulated with several different sets of parameters. The parameters for each case are summarized in Table 9.3. In Case 1, the jammer is assumed to be absent from the system. We vary the severity of nonlinear distortion introduced by the nonlinear HPAs. The

Table 9.4 Simulation Parameters for Nonlinear HPA Model

Case Number	α_{AM}	β_{AM}	α_{PM}	β_{PM}
1-A	1	0	0	0
1-B	1	0.25	π	0.25
1-C	1	0.25	1.2π	0.01
1-D	1	0.25	1.5π	0.01

numerical values for parameters used in the HPA model for Case 1 are listed in Table 9.4. Notice that in Case 1-A when α_{AM} is set to 1 while the rest of parameters are set to zero, the nonlinear HPA model becomes an ideal HPA which has an unity gain and no phase distortion. In Case 2, the system is only subject to the effect of a single tone jammer, aside from the effect of AWGN. The jammer amplitude is varied from 10, 15 to 20. Furthermore, for each jamming amplitude, the normalized frequency offset is varied from 0 to 1 with an increment of 0.1. For Case 3, we simulate the system under the influence of nonlinear HPAs and a single tone jammer. In this case, the jamming amplitude is varied from 0, 0.5, 1 to 1.5 while the normalized frequency offset is fixed at 0.5. Next, in Case 4, instead of varying the jamming amplitude, we assume that the total jamming power is held constant at $\frac{|5|^2}{2}$ while we vary the number of jamming tones in the jammer. For Case 5, in addition to nonlinear distortion, a single tone jamming, we introduce various degrees of the channel estimation error to the system. In Cases 3, 4, and 5, the parameters for Case 1-C are used in the HPA model. In addition, we assume perfect channel estimation for the first four cases. Finally, without loss of generality, we set the variances of all three Rayleigh fading channels to unity, i.e. $\sigma^2_{H_1} = \sigma^2_{H_2} = \sigma^2_{H_3} = 1$. In addition, we let the variances of the channel estimation error when estimating both channels, H_1 and H_2, to be the same, i.e. $\sigma^2_{\epsilon_1} = \sigma^2_{\epsilon_2} = \sigma^2_{\epsilon}$.

9.5 Simulation Results

In Case 1, we assume the only source of degradation aside from AWGN is the nonlinear distortion caused by nonlinear HPAs. The theoretical results can be obtained by evaluating (9.28) with $\sigma^2_{\Phi_D}$ and $\sigma^2_{\Phi_O}$ set to zero. The theoretical and simulation results in this case are shown in Fig. 9.2. As one can see, the BER performance gets worse as more nonlinear distortion is introduced to the system. This is due to the fact that the numerical values of $\sigma^2_{D_G}$ and σ^2_{Ψ} increase as more nonlinear distortion is being introduced. As a result, the BER performance degrades.

For Case 2, instead of varying nonlinearity, we vary the normalized frequency offset, f, in (9.2) from 0 to 1 with an increment of 0.1 for three different jamming amplitudes. Then, we plot the BER performance as a function of normalized frequency offset when E_b/N_o equals to 40 dB. The theoretical and simulation results for Case 2 are shown in Fig. 9.3.

As one can observe from Fig. 9.3, for a given jamming amplitude, the BER performance

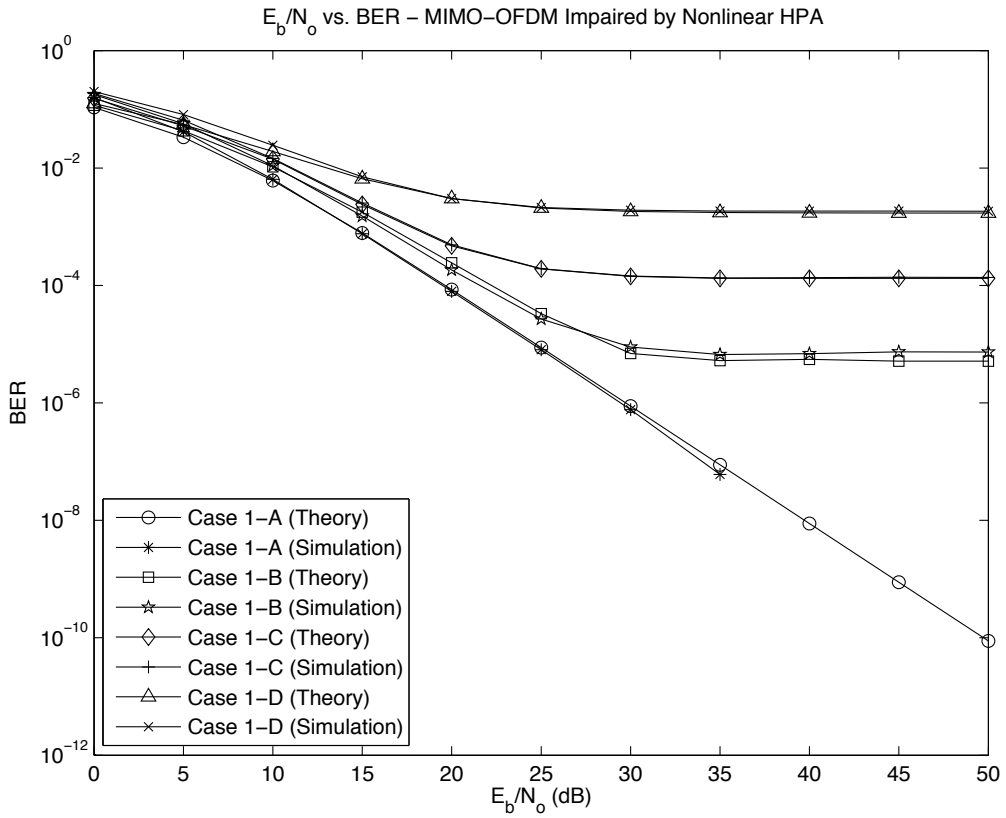

Figure 9.2 BER performance of a 16-QAM MIMO-OFDM system for various degrees of nonlinear distortion introduced by nonlinear HPAs.

gets worse as the normalized frequency offset increases. However, the BER performance starts to improve once the normalized frequency offset is greater than 0.5. The reason that the BER performance improves is due to the fact that the orthogonality between subcarriers is lost when normalized frequency offset is nonzero. As a result, the jamming magnitude due to the k^{th} frequency is nonzero at the other subcarriers. As normalized frequency offset increases, the magnitude at all subcarriers, other than k^{th} subcarrier, increases. Since the jamming signal in the time domain is a sinc function, the magnitude will be at its highest when the normalized frequency offset is at 0.5. Once the normalized frequency offset is greater than 0.5, the magnitude of the jamming signal at all subcarriers, other than k^{th} subcarrier, starts to decrease. Hence, for a given jamming amplitude, the BER performance is at its worst when the normalized frequency offset is equal to 0.5.

In Case 3, the system is subject to not only jamming but also nonlinear distortion produced by HPAs. The theoretical results are shown in Fig. 9.4 along with simulation results. In addition, Fig. 9.4 shows that as jamming amplitude increases, the BER performance degrades. When the jamming amplitude increases, $\sigma^2_{\Phi_D}$ and $\sigma^2_{\Phi_O}$ also increase in value which implies the increase in the

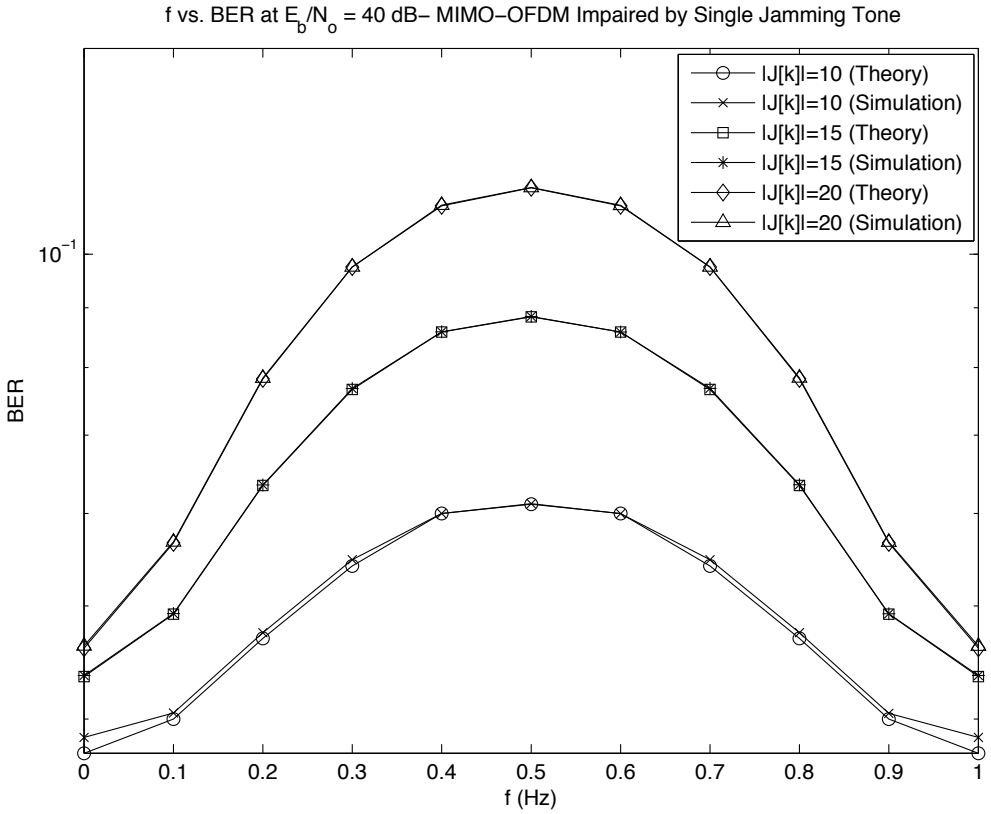

Figure 9.3 The effect of normalized frequency offset, f, on the BER performance of a 16-QAM MIMO-OFDM system impaired by a single tone jammer for various jamming amplitudes at E_b/N_o = 40 dB.

denominator of the Signal to Noise Ratio (SNR) and degradation in BER performance. In Cases 1 and 3, the error floor in the BER performance occurs at around 30 dB and the occurrence of the error floor can be explained by examining SNR for MSB or LSB probabilities. For example, at high SNR, the effect of σ_w^2 is negligible compared to σ_Ξ^2, σ_Υ^2, σ_Ψ^2, $\sigma_{\Phi_D}^2$ and $\sigma_{\Phi_O}^2$. As a consequence, the SNR for MSB probability, denoted as SNR_{MSB}, becomes

$$SNR_{MSB} \simeq \frac{\Lambda_i^2}{\sigma_\Xi^2 + \sigma_{\Phi_D}^2 + \sigma_{\Phi_O}^2} \tag{9.30}$$

where Λ_i is defined in (9.26). Furthermore, SNR_{MSB} is only a function of Λ_i, σ_Ξ^2, $\sigma_{\Phi_D}^2$ and $\sigma_{\Phi_O}^2$ of which σ_Ξ^2 is a constant for a given set of parameters used in the HPA model. $\sigma_{\Phi_D}^2$ and $\sigma_{\Phi_O}^2$ only depend on the jamming power and are not functions of SNR. Therefore, at high SNR, the system is still being affected by the same amount of degradation and subsequently produces an error floor in the BER performance. The same conclusion can be drawn if one examines the SNR for LSB probability.

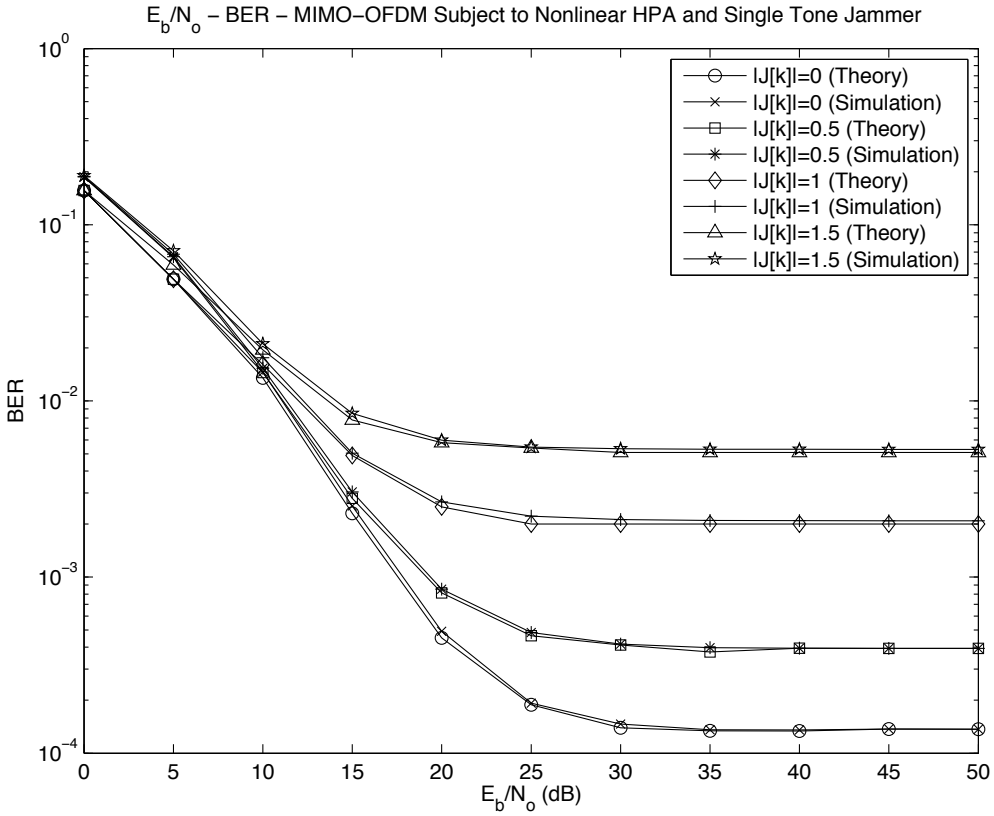

Figure 9.4 BER performance of a 16-QAM MIMO-OFDM system that is impaired by nonlinear HPAs and a single tone jammer in Rayleigh fading channels.

In Case 4, the amplitude of the jammer or the total of jamming power is held constant while the number of jamming tones in the jammer varies. The theoretical and simulation results are shown in Fig. 9.5. As one can see from Fig. 9.5 , a single tone jammer causes the most the degradation in the BER performance as compared to a jammer that is composed of more than one frequency tone. This is because as the number of jamming tones increases, the jamming power per frequency tone has to decrease in order to preserve the condition that the total jamming power is held constant. As a consequence, $\sigma^2_{\Phi_D}$ and $\sigma^2_{\Phi_O}$ become smaller in values and have less impact in the BER performance.

By looking at the results in Fig. 9.5, a single tone jammer seems to be the best choice for designing the most effective jammer. Nonetheless, a single tone jammer is not a practical solution in real situations for two reasons when the most important design criterion is the effectiveness of jammer on the performance of the system. The first reason is the jammer does not usually have the perfect knowledge of the center frequency of the desired transmitted signal. Consequently, the jamming signal often does not appear within the frequency spectrum of the desired signal. When that is the case, only the ICI-like interference which is due to the jammer can affect the system and

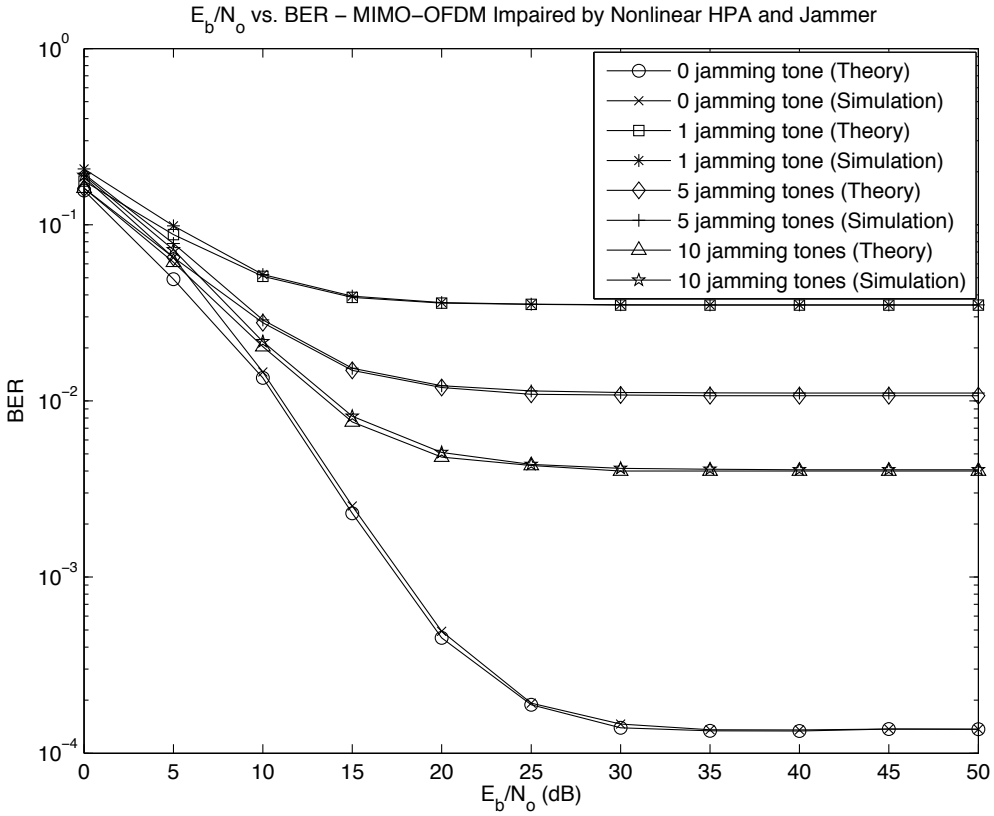

Figure 9.5 BER performance of a 16-QAM MIMO-OFDM system that is impaired by nonlinear HPAs and a jammer in Rayleigh fading channels for various number of jamming tones in the jammer. The total jamming power is held constant.

cause degradation in BER performance. Furthermore, the effect of the ICI-like interference on the BER performance solely depends on the location of the jamming signal with respect to the desired signal in the frequency spectrum. The further away the jamming signal is in the frequency spectrum, the less impact that ICI-like interference has on the BER performance. Another reason is that the system can simply turn off the subcarrier's frequency at which the jammer interferes. By doing so, the BER performance can improve since only the ICI-like interference is present in the received signal. However, the cost of not using a particular subcarrier's frequency is the decrease in data rate. Based on those two reasons mentioned above, a jammer that has all its energy concentrated in a one single subcarrier might not be the best design choice, especially in the case where the jammer does not have the prior knowledge of the center frequency of the desired signal.

Finally, when the channel responses are not perfectly known at the receiver, the error between the channel estimates and the true channel responses further degrades the BER performance. Fig. 9.6 shows the effect of channel estimation error on the BER performance of a 16-QAM

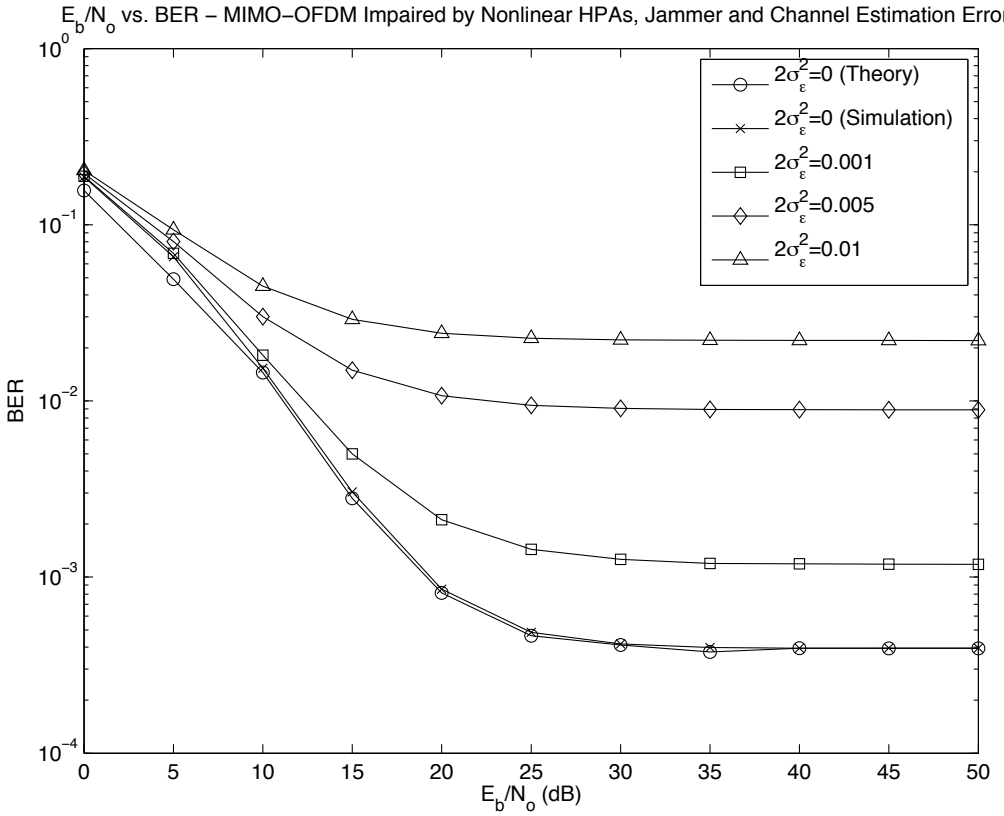

Figure 9.6 BER performance of a 16-QAM MIMO-OFDM system that is impaired by nonlinear HPAs and a jammer in Rayleigh fading channels for various values of $2\sigma_\epsilon^2$.

MIMO-OFDM system that is subject to nonlinear HPAs, and jamming. From Fig. 9.6, one can conclude that as the quality of channel estimates worsens, the BER performance degrades. This is because as the quality of channel estimates decreases, power of the channel estimation error increases which would increase the numerical values of noise variances, $\sigma_{\Upsilon_i}^2$, σ_{Ψ}^2, $\sigma_{\Phi_D}^2$, $\sigma_{\Phi_O}^2$ and σ_{Ω}^2. Subsequently, the BER performance will worsen due to the increases in the noise variances.

9.6 Conclusion

In this chapter, we analyzed the performance of a M-QAM MIMO-OFDM system that was subject to nonlinear HPAs, jammer and channel estimation error in the Rayleigh fading channels. Different from the jammer models presented in previous studies, we presented a more realistic jammer model by adding two distinct assumptions. The first assumption which would simulate more realistic situations was the jammer experienced a separate channel impulse response. Second, we assumed that the jammer did not have perfect knowledge of the frequency which the desired signal was being transmitted on. This particular assumption of the frequency offset between the jamming

and transmitted signals caused the occurrence of an ICI-like interference which was due to the presence of the jammer in the received signal and further degraded the BER performance. In addition, an analytical expression for BER performance of such a system that was under combination of these impairments was presented in the chapter. We also extended the analytical system to be in compliance with IEEE 802.11n standard for the purpose of simulation. Based a design criterion and under the assumption that the total jamming power was held constant, we discussed the effectiveness of jamming on the performance of the system when the jammer had one or more than one frequency tones. Finally, we presented the theoretical and simulation results for different scenarios such as under the influence of nonlinear distortion or effect of jamming tones with the condition of constant jamming power with and without channel estimation error.

The text in Chapter 9 is based on the material as it appears in:

David W. Chi and Pankaj Das, "Effects of Jammer and Nonlinear Amplifier in MIMO-OFDM with Application to 802.11n WLAN", 2008 IEEE Military Communications Conference (Submitted).

The dissertation author was the primary researcher and author, and the co-author listed in the publication directed and supervised the research which forms the basis for this chapter.

10

PAPR Reduction Techniques Review

10.1 Introduction

As mentioned in previous chapters, Orthogonal Frequency Division Multiplexing (OFDM) is known for its high bandwidth efficiency and outstanding performance in fading channels, however, it suffers from peak to average power ratio (PAPR) problem. The phenomenon of PAPR generally arises when the wireless communication systems utilize multicarrier modulations such as OFDM. In the OFDM modulation process, a number of independent signals are added up to produce an output signal which could potentially give a large peak to average power ratio if all the phases of independent signals are aligned. This would produce a peak power that is L times larger than average power where L is the number of the signals. An example of PAPR has been presented in Fig. 2.1 in Section 2.1, Chapter 2.

Those large PAPR signals bring an increased complexity in designing Radio Frequency (RF) components such as high power amplifiers (HPAs) due to the fact that the large magnitude signals saturate HPAs. As a consequence, the HPAs operate at their nonlinear region. When HPAs are operating in the nonlinear region, the effects of HPAs on the system performance has been presented and discussed in previous chapters. One obvious approach to solving the PAPR problem is to employ highly linear HPAs which provide a larger range of linear region for HPAs to operate and tolerate the large magnitudes of modulated signals before HPAs are saturated. However, those highly linear HPAs are usually very complicated to build and even if hardware implementation is feasible, they are often too expensive for massive commercial productions.

Another possible solution is to have a large input backoff (IBO) for HPAs. The IBO

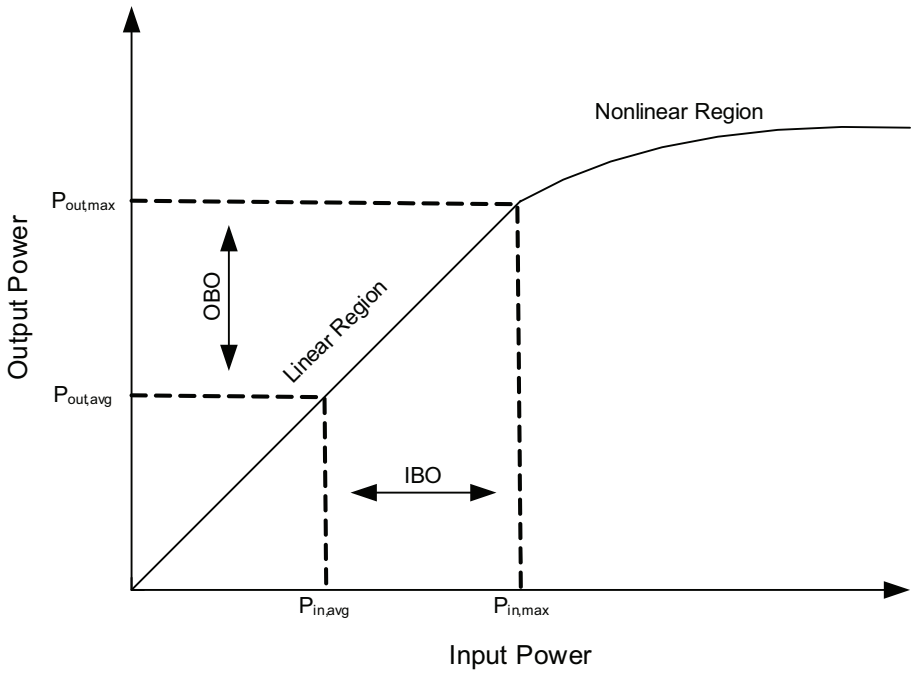

Figure 10.1 The relationship between $P_{in,max}$, $P_{in,avg}$, input backoff (IBO), $P_{out,max}$, $P_{out,avg}$ and output backoff (OBO).

is defined as [49–51]

$$IBO = \frac{P_{in,max}}{P_{in,avg}} \tag{10.1}$$

where $P_{in,max}$ represents the maximum input power at which the output power saturation occurs, and sometimes, it is referred to as input saturation power. $P_{in,avg}$ denotes the average power of an input signal. Another term which is proportionally related to IBO is output backoff (OBO) which is defined as [51]

$$OBO = \frac{P_{out,max}}{P_{out,avg}} \tag{10.2}$$

where $P_{out,max}$ is the output saturation power and $P_{out,avg}$ is the average output power. The relationship between IBO and OBO is shown in Fig. 10.1[1] based on the input and output responses of HPAs.

As one can see from (10.1) and (10.2), when there is an increase in IBO, it implies that $P_{in,avg}$ becomes smaller in value since the input saturation power is normally fixed for a certain type of HPA. In addition, this means that the HPA can operate within the linear region, therefore, less nonlinear distortion would be produced by the HPA. However, a smaller $P_{in,avg}$ translates to a smaller $P_{out,avg}$ and a larger OBO as shown in Fig. 10.1. This is due to the fact that the output

[1]The figure is drawn based on Fig. 4.12 in [51] with the notations used in (10.1) and (10.2).

saturation power of a particular class of HPA is also a constant. Operating HPAs with high IBO results in reduction in the power efficiency of the HPA which is detrimental to the battery life in mobile applications. Furthermore, the range of transmission is reduced as a consequence of the lower transmit power.

Since battery life and production cost often dictate engineering designs for wireless communication systems, several other PAPR reduction techniques such as direct clipping [11], selective mapping (SLM) [52] and partial transmit sequences (PTS) [9] have been proposed and their effectiveness have been reported in literature. In this chapter, we will first give a detail description of PAPR and its statistical distribution. Then, we present a brief review of some of the most popular PAPR reduction techniques in literature. This chapter is organized as follows. In Section 10.2, a discussion of PAPR and its signal distribution is given in detail. Section 10.3 provides a discussion of some PAPR reduction techniques. Section 10.4 summaries the chapter.

10.2 Distribution of PAPR

In this section, we will present the concepts of PAPR and OFDM signal distribution through mathematical definitions. Let $x(t)$ be the continuous time OFDM signal in time domain, then $x(t)$ is given by [53]

$$x(t) = \frac{1}{N}\sum_{k=0}^{N-1} X(k)e^{j2\pi f_k t} \qquad 0 \le t < T_s \tag{10.3}$$

where $X(k)$ represents the data signal which is modulated onto the k^{th} frequency. N is the number of subcarriers. Furthermore, f_k is the k^{th} frequency and T_s is the OFDM symbol duration. Then, PAPR is expressed as

$$PAPR = \frac{\underset{0\le t<T_s}{max} \; |x(t)|^2}{E\left\{|x(t)|^2\right\}} \tag{10.4}$$

From (10.4), we can see that for any input signal, the PAPR is upper bounded by N. For example, if $x(t)$ is

$$x(t) = [\underbrace{1\ 1\ 1\ ...\ 1}_{N\ times}] \tag{10.5}$$

then, by the definition of PAPR given in (10.4), the PAPR of $x(t)$ is found to be

$$PAPR = \frac{1}{1/N} = N \tag{10.6}$$

Hence, the PAPR of any input signal is upper bounded by N.

In the discrete case, oversampling might be necessary if Nyquist-rate samples do not coincide with peaks of the continuous time signal. Denote L as the oversampling factor, the discrete

time OFDM signal is then sampled at $t = n\frac{T_s}{LN}$. As a result, the sampled OFDM signal in time domain, $x(n)$, is given by

$$x\left(\frac{n}{L}\right) = x\left(n\frac{T_s}{LN}\right) = \frac{1}{N}\sum_{k=0}^{N-1} X[k]e^{j\frac{2\pi nk}{N}} \qquad 0 \le n \le LN-1 \tag{10.7}$$

When $L = 1$, it is said that the sampling rate corresponds to the Nyquist sampling rate [53]. The PAPR in this case is defined as

$$PAPR = \frac{\underset{0\le n<NL-1}{max} \; |x\left(\frac{n}{L}\right)|^2}{E\left\{|x\left(\frac{n}{L}\right)|^2\right\}} \tag{10.8}$$

Even though, oversampling may yield a more accurate result for PAPR, however, the difference between the case where $L = 1$ and the case where $L \ge 1$ is less than 1 dB [53]. In the rest of thesis, we will use $L = 1$ to obtain the PAPR of the OFDM signal.

The distribution of PAPR is often measured by Complementary Cumulative Distribution Function (CCDF). Let $L = 1$ and since $x(n)$ can be assumed to be a complex Gaussian random process with zero mean based on *Central Limit Theorem*, the magnitude of $x(n)$ has a Rayleigh probability density function (PDF), namely

$$p(\alpha) = \frac{\alpha}{\sigma_\alpha^2} e^{\frac{-\alpha^2}{2\sigma_\alpha^2}} \tag{10.9}$$

where α represents the magnitude of $x(n)$ and $2\sigma_\alpha^2$ denotes the variance. The Cumulative Distribution Function (CDF) of the magnitude is then given by

$$\begin{aligned} CDF =& \int_0^\alpha \frac{r}{\sigma_\alpha^2} e^{\frac{-r^2}{2\sigma_\alpha^2}} dr \\ =& 1 - e^{\frac{-\alpha^2}{2\sigma_\alpha^2}} \\ =& 1 - e^{-PAPR_o} \end{aligned} \tag{10.10}$$

where $PAPR_o$ is a particular PAPR threshold value. For an OFDM symbol with no oversampling, the CDF is found to be

$$CDF = P(PAPR \le PAPR_o) = \left(1 - e^{-PAPR_o}\right)^N \tag{10.11}$$

In the case where we oversample by a factor of L, the CDF is given by [10]

$$CDF = P(PAPR \le PAPR_o) = \left(1 - e^{-PAPR_o}\right)^{LN} \tag{10.12}$$

Subsequently, the CCDFs for these two cases are

$$\begin{aligned} CCDF =& 1 - CDF \\ =& \begin{cases} 1 - \left(1 - e^{-PAPR_o}\right)^N & \text{L = 1} \\ 1 - \left(1 - e^{-PAPR_o}\right)^{LN} & \text{L > 1} \end{cases} \end{aligned} \tag{10.13}$$

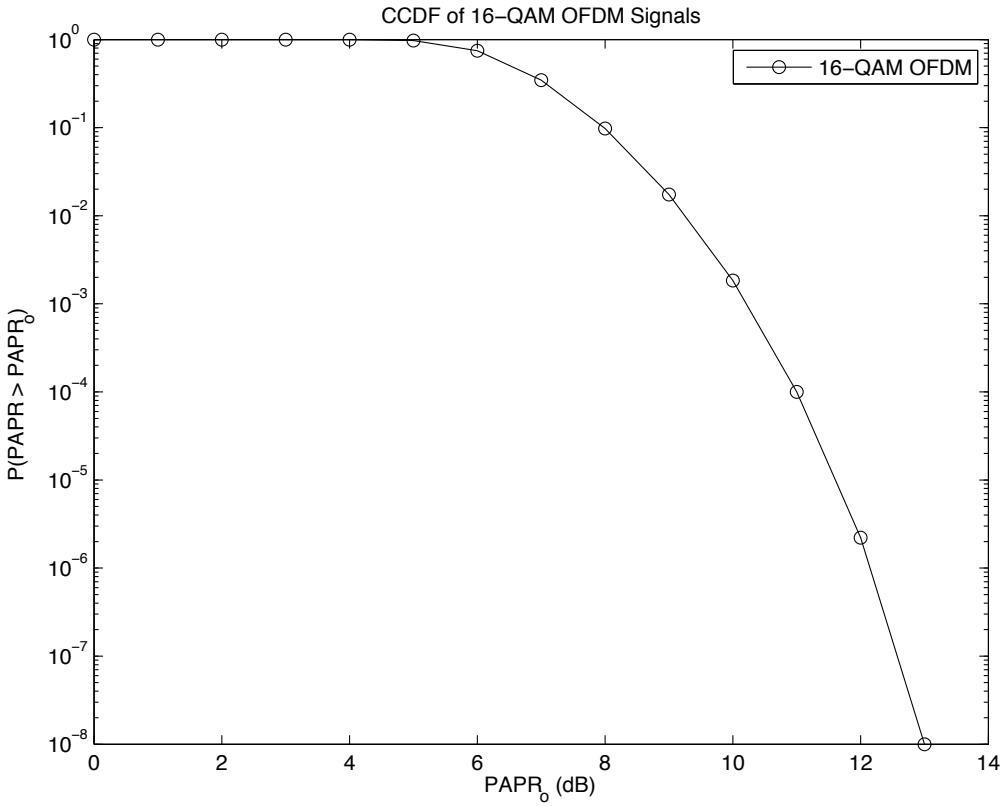

Figure 10.2 The Complementary Cumulative Distribution Function (CCDF) of 16-QAM OFDM signals.

In this thesis, we will use the CCDF with $L = 1$ as a measure of PAPR performance.

To obtain the CCDF of OFDM signals in discrete time with any signal modulation through simulations, one can follow the steps outlined below,

1. Generate K number of statistically independent OFDM symbols with any signal modulation
2. For each OFDM symbol, calculate PAPR as defined in (10.8)
3. Next, calculate the CCDF of OFDM symbols and save the results
4. Repeat previous steps for I times where the product of K and I has to be sufficiently large to yield an accurate CCDF result

We simulate $KI = 10^8$ 16-QAM OFDM symbols which are statistically independent of each other. Subsequently, the result of CCDF is calculated and shown in Fig. 10.2. As one can see from Fig. 10.2, 10% of PAPR is at around 7.9 dB. Assuming the nonlinear HPAs are operating in the nonlinear region when PAPR is greater than 6 dB, having 10% of the PAPR at around 7.9 dB implies that

10% of the time, the signal amplitude is large enough to force the HPAs to operate in the nonlinear region, thereby producing nonlinear distortion in the system. To resolve this problem, one can utilize one of PAPR reduction techniques which are discussed in detail in the next section to reduce the maximum amplitude of OFDM signals. By reducing the PAPR, the nonlinear HPAs would have less chance of operating in the nonlinear region. As a consequence, less amount of nonlinear distortion is introduced to the system and the system performance is improved.

10.3 PAPR Reduction Techniques

Over the years, there are several algorithms that are proposed for PAPR reduction. Those techniques can be categorized as follow,

- Clipping [11, 54–57]
- Coding [12, 58–61]
- Interleaving [62–64]
- Partial Transmit Sequences (PTS) [8, 9, 65–67]
- Selective Mapping (SLM) [13, 52, 68–71]
- Predistortion [72–75]
- Companding [76–79]

Each of techniques will be then discussed in the following subsections.

10.3.1 Clipping

The Clipping is the simplest, yet effective, technique to reduce the PAPR. It is done by limiting the amplitude of the Inverse Fast Fourier Transform (IFFT) output sequences to a predetermined threshold. Denote $x(n)$ as the output sequence of the IFFT, then the clipped signal , $x^{'}(n)$, is given by

$$x^{'}(n) = \begin{cases} -Ae^{j\theta}, & \text{if } |x(n)| < -A \\ x(n), & \text{if } -A \leq |x(n)| \leq A \\ Ae^{j\theta}, & \text{if } |x(n)| > A \end{cases} \tag{10.14}$$

where θ is the phase of $x(n)$ and A represents the maximum amplitude allowed before HPAs operate at the nonlinear region [11].

Even though, clipping is the simplest method, however, it should be utilized with care since it is a nonlinear process. By deliberately clipping the signal, another source of distortion

which is generally referred to as clipping noise is introduced to the system. As a consequence, the system performance degrades. Depending on the sampling rate of the signal, clipping would create more in-band distortion if the sampling rate of the signal equals to Nyquist rate. If clipping was performed on an oversampled signal, there would be less in-band noise while there would be an increase in the out-of-band radiation. This increase in out-of-band radiation leads to a reduction of the spectral efficiency [54, 55]. The in-band distortion can not be reduced by filtering and subsequently causes degradation in performance. To remove the out-of-band radiation, the authors in [11, 54] proposed to use an bandpass finite-impulse response (FIR) filter to filter out the out-of-band noise. Nevertheless, the price for the out-of-band noise reduction is the possibility of peak regrowth. So, after clipping and filtering, the resulting signal can sometimes exceed the predetermined threshold level, A.

More advanced techniques have been developed to reduce PAPR. In [56], authors proposed to regenerate the clipping noise and use it to cancel the clipping noise samples in frequency domain. The proposed iterative process begins by first detecting the received signal to yield estimated data bits. The estimated data signal branches out in two paths. The estimated data signal in one path is used to generate the attenuated frequency domain signal by multiplying with the constant, α_G. In another path, the estimated data signal is then transformed to time domain and clipped by the same clipping process at the transmitter. After transforming the new clipped signal back to frequency domain, the attenuated frequency domain signal is subtracted from this new generated clipped signal. The difference between two signals would be the nonlinear distortion. The resulting nonlinear distortion is then passed through the same channel impulse response and is later used to subtract the received signal in frequency domain at the next iteration.

This particular method brings two disadvantages to the system. The first disadvantage is a moderate increase in the complexity of the receiver structure since a pair of IFFT and Fast Fourier Transform (FFT) is required at the iterative process. Another assumption that the authors make is the receiver has perfect knowledge about the channel impulse response, hence, the channel impulse response for the nonlinear distortion signal at the receiver is the same channel impulse response as the one that is for the transmitted signal. In practice, this particular assumption in general might not be valid due to the reason that the receiver can not estimate the channel perfectly, especially in time varying channels. Therefore, the error in channel estimation would further degrade the performance. This suggests that the proposed method might not be suitable for mobile applications in time varying channels.

The authors in [55] presented an alternative method which is based on the iterative decision-aided reconstruction. In this algorithm, the received signal is equalized in frequency domain. After equalization, the signal path is separated into two different paths. In one path, the equalized sig-

nal is transformed back to time domain and is stored in memory for later use. In another path, the equalized signal is utilized by the demodulator to yield data bits. The estimated data bits are transformed back to time domain and are used to generated a new time domain sequence. Denote $r^{'}(n)$ as the new time domain sequence, then $r^{'}(n)$ is generated in the following fashion

$$r^{'}(n) = \begin{cases} z^{m}(n) & |\hat{x}(n)| \leq A \\ \hat{x}(n) & |\hat{x}(n)| > A \end{cases} \tag{10.15}$$

where $z^{m}(n)$ represents the equalized signal that is previously stored in the memory and $\hat{x}(n)$ denotes the estimated data bits in time domain. Next, $r^{'}(n)$ is converted to the frequency domain and is used by the demodulator to yield the estimate of data bits for the next iteration. One disadvantage is the possible errors in generating $r^{'}(n)$. When there is an error in estimating data bits, this error would be carried over to its time domain signal. In generating a new time domain signal, the inaccuracy in data estimation leads to a few clipped samples that do not get replaced by the algorithm mentioned above. As a consequence, the improvement that the proposed algorithm offers diminishes and the system performance will degrade.

One assumption that both algorithms proposed in [55, 56] share is that the receiver has perfect knowledge about the clipping threshold, A and is able to use it in the reconstruction or regeneration process. In practice, the clipping threshold might not be known for all wireless communication applications, hence, an estimation algorithm is required to obtain the numerical value of A. In [57], the authors proposed to create a lookup table for clipping ratio and clipping noise to signal ratio (CNSR) and utilize the one to one relationship between them to obtain the clipping threshold, A. The clipping ratio, γ, is defined as

$$\gamma = \frac{A}{\sqrt{\sigma^{2}_{x(n)}}} \tag{10.16}$$

where $\sigma^{2}_{x(n)}$ represents the transmit power. The CNSR is defined as

$$CNSR = \frac{\sigma^{2}_{D_G}}{\sigma^{2}_{X}} \tag{10.17}$$

where $\sigma^{2}_{D_G}$ and σ^{2}_{X} are the power of nonlinear distortion and data symbols, respectively.

By estimating CNSR, the numerical value of A can be obtained through the lookup table. To estimate CNSR, the authors proposed to find the nonlinear distortion after channel impulse response, namely

$$H[p]D_G[p] = Y[p] - \alpha_G H[p]P[p] \tag{10.18}$$

where $H[p]$ and $D_G[p]$ are the channel impulse response and nonlinear distortion at the p^{th} pilot, respectively. α_G denotes the complex gain that is due to the nonlinear HPA. $Y[p]$ is the received

signal at the p^{th} pilot in frequency domain and is given by

$$Y[p] = \alpha_G H[p]P[p] + H[p]D_G[p] \tag{10.19}$$

In addition, $P[p]$ represents the pilot signal. The next step is to take (10.18) and divide it by $\alpha_G H[p]$ to obtain $\frac{\sigma^2_{D_G}}{\alpha^2_G}$ where $\frac{\sigma^2_{D_G}}{\alpha^2_G}$ is given by

$$\frac{\sigma^2_{D_G}}{\alpha^2_G} = \frac{|Y[p]|^2 - \alpha^2_G|H[p]|^2|P[p]|^2}{\alpha^2_G|H[p]|^2} \tag{10.20}$$

Once (10.20) is found, then CNSR can be obtained since σ^2_X is known to the receiver. Subsequently, clipping ratio, γ, and the clipping threshold, A, can both be found through the lookup table.

However, this proposed algorithm has two disadvantages. One disadvantage is that (10.20) only yields the estimation at the pilot subcarriers, not at the data subcarriers. In which case, possible other techniques such as interpolation may be required to obtain the values of $\sigma^2_{D_G}$ at the data subcarriers. Another problem associated with this technique is the memory required for the lookup table. To have the most improvement in the system performance, a large memory size is required to store all the possible values of CNSR and clipping ratio. This might be not be feasible in real practice. Furthermore, either the error in the estimation of $\sigma^2_{D_G}$ or the lack of large memory size for storing CNSR and clipping ratio would degrade the system performance.

10.3.2 Coding

Coding can also be used to reduce PAPR in OFDM systems. Wilkinson *et al.* [58] analyzed the effect of a block code on the PAPR reduction of a Binary Phase Shift Keying (BPSK) OFDM system. The authors noticed that certain data sequences could produce a very high PAPR and proposed to use a block code to encode data bits in such way that a data symbol with three bits was mapped onto a four-bit codeword. In this particular coding scheme, the set of possible codewords follows after an odd parity code. The simulation results in [58] showed that for a BPSK OFDM system with 8 subcarriers and a code rate[2], $R = 3/4$, the PAPR was 3.01 dB compared to an uncoded case where the PAPR was 9.03 dB, a reduction of 6.02 dB. However, the authors also pointed out that the reduction of PAPR was achieved at the expense of an increase in the bandwidth for the same data rate and a reduction in energy per transmitted bit for the same transmission power.

To further improve the system performance, the authors in [59–61] utilized the block coding that is based on complementary sequences to suppress high PAPR in OFDM systems. The simulation results showed that the M-ary Phase Shift Keying (M-PSK) OFDM system with 8 subcarriers and complementary sequences generated PAPR at most 3 dB. In addition to the superior capability

[2]The code rate is defined as a ratio of the number of information bits to the length of a corresponding codeword [80]. For example, 5 information bits are encoded into a codeword whose length is 8, then the code rate in this case is $\frac{5}{8}$.

in PAPR reduction, the complementary sequences also provides the benefits of error correction code and improvements in bit error rate (BER) performance. Both superior ability of suppressing PAPR and moderate improvement in performance that are both due to the coding suggest that coding may be a very attractive and effective feature for suppressing high PAPR in OFDM systems. However, the proposed coding schemes in [58–61] all share one disadvantage which is significant PAPR reduction only limited to small number of subcarriers. For example, 8 subcarriers with PAPR equals to 3 dB was reported in [60]. The number of subcarriers is too small for any practical uses today since 64 subcarriers are required in IEEE 802.11a/n [2, 4]. Authors in [12] proposed to break up a large frame size into M disjoint frames and applied the complementary sequence to each frame in M frames. Although, good PAPR reduction is achieved, the number of subcarriers that is used in the paper is still too small to be considered for current wireless communication applications today.

10.3.3 Interleaving

Interleaving is also another simple method that can be used in PAPR reduction. The technique is based on the idea that highly correlated data sequences produce a large PAPR. By breaking down the long correlation pattern in the data sequences, the PAPR then can be reduced. Due to the fact that interleaving is a deterministic process, i.e. an one to one mapping function whose mapping is predetermined, the permutation pattern has to be carefully selected to be the most effective in PAPR reduction. In [62], the authors analyzed the effects that interleaving had on reducing PAPR in Quadrature Phase Shift Keying (QPSK) OFDM systems with 256 subcarriers. In the paper, the authors proposed a pseudo random interleaver which would generate $K-1$ completely different sequences. In each sequence, it would contain a different order of permutation indices which ranges from 0 to $N-1$ where N is the number of subcarriers. The order of the original signal is then rearranged to yield the new sequence based on the permutation indices. After FFT, the new sequence that has the lowest PAPR among the K different sequences including the original signal will be chosen for transmission. The simulation results in [62] show that as K increases, the PAPR statistic improves, for example, for $K = 4$, 0.1% PAPR is reduced by 2.2 dB and for $K = 16$, the reduction is about 3 dB.

To further improve PAPR reduction and BER, the authors in [63] proposed to reduce PAPR by employing both interleaving and clipping. The structure of the interleaver utilized in the paper is the same as the one proposed in [62] where $K-1$ different versions of an original signal are generated. In addition, the sequence that has the lowest PAPR after FFT is chosen for transmission. However, different from [62], the amplitude of the new sequence is clipped at the threshold, A, and filtered at the frequency domain to avoid spectral regrowth. The resulting signal is then repeatedly clipped in time domain and filtered in frequency domain for M times before the transmission. Utilizing only interleaving, the authors reported that 10% PAPR was reduced by about 2.7 dB for $K = 16$ comparing the original sequence. The simulation result cited in the paper showed about

the same improvement that was reported by [62]. When employing both interleaving and clipping, an additional improvement can be gained. For $K = 16$, $M = 3$ and $A = 3$ dB, the authors reported that 10% PAPR was further reduced by about 1 dB.

Even though interleaving is simple and effective, there are some disadvantages associated with this technique. One disadvantage is a total of K IFFTs are required to compute PAPR for $K-1$ different versions of the original sequences. Not only there is an increase in hardware complexity, having a large number of IFFTs places a limit on the battery life of a mobile unit as well. Another disadvantage is the memory size that is required to store those permutation indices. The memory size which grows linearly with the number of IFFTs, K, can soon become too large and costly to build. In addition to these two disadvantages, a side information regarding which permutation indices are used at the transmitter has to be transmitted to the receiver in order to deinterleave the received signal correctly. To correctly identify which interleaver is used at the transmitter, $\lfloor log_2(K) \rfloor$ number of bits are required for side information [64]. As a consequence, there is a decrease in data rate.

To solve the problem of loss in data rate due to the side information, the authors in [64] proposed to use pilots to identify which interleaver is used at the transmitter. The idea behind this approach is to assign special pilot symbols for each interleaver and insert those pilot symbols among data subcarriers after interleaving. After IFFT, the sequence with the lowest PAPR is chosen for transmission. For example, for $K = 4$, the pilot symbols are

- pilot symbols = [+1 +1] are assigned to Interleaver # 1
- pilot symbols = [+1 -1] are assigned to Interleaver # 2
- pilot symbols = [-1 +1] are assigned to Interleaver # 3
- pilot symbols = [-1 -1] are assigned to Interleaver # 4

Upon receiving, the values at the pilot subcarriers are evaluated to determine which interleaver is used at the transmitter to randomize the original signal. Even though, there is no transmission of the side information, this approach might not be practical in real practice. The receiver might make the wrong decision on the interleaver when pilot symbols are severely corrupted by the channel. In which case, the information is lost and the BER performance is severely degraded. In addition, the proposed approach still requires K number of IFFTs for computing PAPR and a large memory size for storing permutation indices for a large number of subcarriers.

10.3.4 Partial Transmit Sequences (PTS)

Reducing PAPR by utilizing partial transmit sequences (PTS) was first proposed by Muller *et al.* [65]. The block diagram of an OFDM system with PTS implementation is shown in Fig.

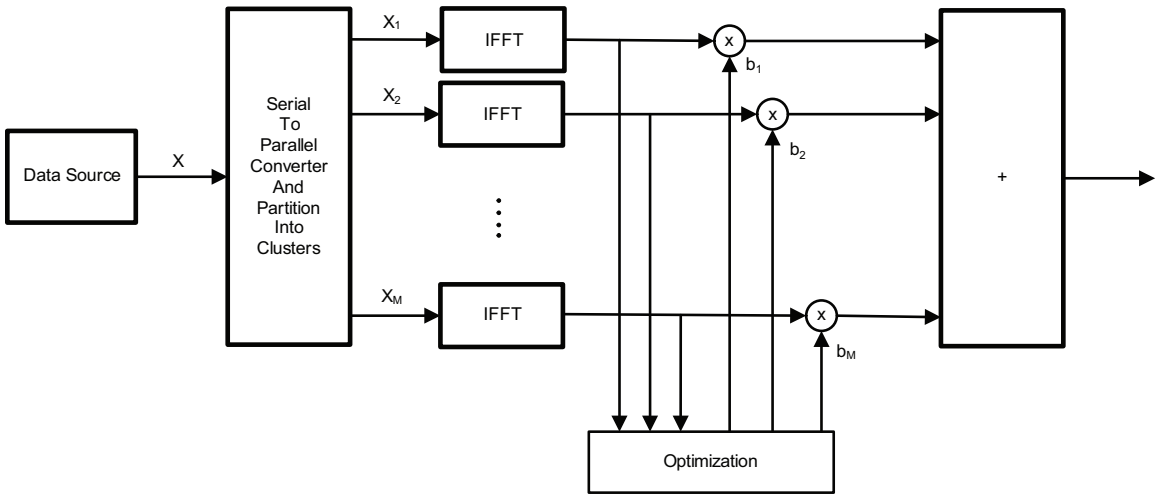

Figure 10.3 A block diagram of OFDM systems with partial transmit sequences (PTS) implementation for PAPR reduction.

10.3 [9]. In the PTS scheme, the data block, denoted as X, is partitioned into M disjoint subblocks such that

$$X = \sum_{m=1}^{M} X_m \tag{10.21}$$

where X_m represents the m^{th} subblock. Subsequently, for each subcarrier in each subblock is weighted with a vector of phase factors, denoted as b_m. After IFFT, the output in time domain is given by

$$x^{'} = \sum_{m=1}^{M} b_m x_m \tag{10.22}$$

where b_m is expressed as

$$b_m = e^{j\phi_m} \qquad\qquad m = 1, 2, ..., M \tag{10.23}$$

x_m in (10.22) is generally referred to as the partial transmit sequence and is defined as IFFT of X_m. The phase factors, b_m, are chosen in such a way that the PAPR of $x^{'}$ is minimized. Before obtaining the optimal phase factors, the algorithm has to search W^{M-1} different possible sets of phase factors where W represents the possible values that ϕ_m can take on. In general, the search for the optimal b_m that can significantly reduce PAPR is usually complicated and the complexity increases exponentially as the number of subblocks increases.

In [9], the authors analyzed the effects of PTS that had on reducing PAPR in OFDM systems that were modulated with QPSK or 16 Quadrature Amplitude Modulation (16-QAM) modulations and 256 subcarriers. To reduce the complexity of the search for the optimal phase factors,

the authors proposed a simple method of generating sub-optimal phase factors. For example, if only binary phase factors such as $+1$ and -1 are considered, this simple method begins by initialing all $b_m = 1$ for all m. The PAPR is then computed and retained as a reference. The next step is to invert the first phase factor, i.e. $b_1 = -1$ while the rest of phase factors stay the same. After inversion, the new PAPR is computed and compared to the previous case. If the new phase factor sequence produces a lower PAPR compared to the previous case, then $b_1 = -1$ is saved as a part of final phase factor. If the new phase factor sequence does not produce a lower PAPR, then b_1 is changed back to $+1$. This process of flipping the values of phase factors between $+1$ and -1 continues until all M phase factors have been explored. Comparing to the original search method, the complexity of the proposed algorithm which is proportional to $(M-1)W$ is greatly reduced.

In the simulation results that are presented in [9], it shows that for an QPSK OFDM system with 256 subcarriers and optimal phase factors, 10% PAPR is reduced to about 6.5 dB, a 3 dB gain in PAPR reduction for the same QPSK OFDM system that is without PTS. When employing the binary phase factor and the proposed algorithm described above to search for the sub-optimal phase factors, 10% PAPR is about 7.5 dB which is only 1 dB loss in performance. However, by utilizing this method to generate sub-optimal phase factors, the time that is often required for the search of optimal phase factors can be greatly reduced. In addition, simulation results have also shown that the numerical value of M is a factor in how much of PAPR reduction is achieved for a given set of parameters. In general, the more reduction in PAPR, the larger M has to be.

Instead of flipping one phase factor and multiplying x_m with an entire new phase factor each time, the authors in [66] proposed an alternative method to represent $x^{'}$ in each iteration of flipping. Since only the l^{th} phase factor in b_m is flipped at any given time, we can conclude that

$$b_l^i = -b_l^{i+1} \qquad\qquad 1 \le l \le M \tag{10.24}$$

where i implies the i^{th} flipping. Furthermore, for $l \neq m$ where $m = 1, 2, ..., M$, we know that

$$b_m^i = b_m^{i+1} \tag{10.25}$$

With (10.24) and (10.25), $x^{'}$ at the $(i+1)^{th}$ flipping can be expressed as a function of $x^{'}$ at the i^{th} flipping, namely

$$\begin{aligned} x^{',i+1} &= \sum_{m=1}^{M} b_m^{i+1} x_m = \sum_{\substack{m=1 \\ m\neq l}}^{M} b_m^{i+1} x_m + b_l^{i+1} x_l \\ &= \sum_{\substack{m=1 \\ m\neq l}}^{M} b_m^{i} x_m + b_l^{i+1} x_l + b_l^i x_l - b_l^i x_l = \sum_{m=1}^{M} b_m^i x_m - 2 b_l^i x_l \\ &= x^{',i} - 2 b_l^i x_l \end{aligned} \tag{10.26}$$

where $x^{'},^{i}$ and $x^{'},^{i+1}$ are $x^{'}$ at the i^{th} and $(i+1)^{th}$ flips, respectively. The algorithm proposed in [66] works in exactly the same way as the one described in [9]. The only thing that is different is the calculation of $x^{'}$ after the first iteration. Instead of using (10.22), the new $x^{'}$ is calculated based on (10.26) for the rest of iterations until $i > M$. Even though, the performance gain based on this approach is minimal compared to the algorithm which is proposed by Cimini *et al.*, the complexity in computation is greatly reduced by utilizing (10.26).

Another simple method of generating $x^{'}$ which is defined as (10.22) is to cyclically shift x_m by δ samples, namely

$$x_{cs}^{'} = \sum_{m=1}^{M} b_m x_{(m+\delta)} \tag{10.27}$$

where $x_{(m+\delta)}$ implies the partial transmit sequence that is obtained by cyclically shifting x_m [8]. In simulations, 10% PAPR is reduced further by 0.1 dB to 0.2 dB which is minimal compared to the case where the original search method is utilized. Even though this method of generating $x^{'}$ is simple, the simplicity in the algorithm does not offset the possibility that there can be a degradation in the BER performance. The degradation in the system performance might occur when there is a linear phase shift in X_m which is due to the time shift in $x_{(m+\delta)}$ by δ samples. If this linear phase shift is not completely removed, it might cause additional degradation in the system performance.

Han *et al.* [67] proposed a more advanced search technique for finding a set of suitable phase factors that would significantly reduce PAPR. The search technique is based on the iterative gradient search which begins by initializing b_m to an all one vector whose length is M. The PAPR is then computed and stored in memory for comparison later. Next, find another set of phase factors which has a Hamming weight[3] that is less than r compared to the previous set of phase factors. r in this case is a predetermined parameter chosen by engineers. The PAPR when utilizing the new set of phase factors is computed and compared to the previous PAPR value that is stored in memory. If the PAPR value that is based on the previous set of phase factors is less than the new PAPR value, then the algorithm terminates. Otherwise, the algorithm updates the phase factors and its PAPR value for the next iteration. When the number of iteration has reached to predetermined value, denoted as I, then the algorithm will stop. The process can be summarized as follows.

1. Initialize $b_m^{i=1} = \underbrace{[1, 1, 1, ..., 1]}_{M\ elements}$ for iteration counter, $i = 1$.
2. Compute PAPR based on the phase factors $b_m^{i=1}$ and store the result in a memory.
3. Find another set of phase factors, $b_m^{'}$, where the Hamming weight between $b_m^{'}$ and $b_m^{i=1}$ is less than r.

[3]Hamming Weight is defined as the number of elements in which the two sequences differ [81, 82].

4. Compute PAPR based on the phase factors $b_m^{'}$ and compare the result with the PAPR value obtained in 2. The next step is determined as follows.

   (a) If the new PAPR result obtained based on the phase factors $b_m^{'}$ is less than the PAPR result obtained from 2, then update $b_m^{i=1}$ with $b_m^{'}$ and go to 5.

   (b) Otherwise, terminate the algorithm

5. If iteration counter, i, is less than the maximum allowed number of iterations, denoted as I, then increment i by 1 and go to 3. Otherwise, terminate the search.

The complexity of search in this case is ${}_{M-1}C_r W^r$ where ${}_aC_b$ is defined as [67]

$$ {}_aC_b = \binom{a}{b} = \frac{a!}{(a-b)!b!} \tag{10.28}$$

For the same specification, namely $N = 64$, $M = 8$ and $W = 4$, the simulation results show that 10% PAPR is reduced to about 6.1 dB based on the proposed algorithm with $r = 1$ and $I = 3$. This is about 0.3 dB better than employing the algorithm proposed in [9]. When $r = 2$ and $I = 3$, the performance in PAPR reduction improves, more specifically, 10% PAPR is reduced to about 5.6 dB, about 0.8 dB gain in performance when comparing with the algorithm in [9]. In addition, the simulation results show that the amount of reduction in PAPR is a dependent of r and I. In general, the larger r or I is, the more reduction in PAPR is achieved.

All the algorithms that are described in [8, 9, 66, 67] share some major drawbacks. One of them is the complexity in searching for the optimal phase factor that would greatly reduce PAPR. Although, some alternatives with various levels of complexity for searching phase factors have been proposed, the performance of PAPR reduction is still not as good as optimal phase factor. Another disadvantage is the required memory sizes for storing b_m at both transmitter and receiver. As M increases, the memory sizes that are required to store b_m can grow to be too large for implementation in hardware. Another disadvantage is the number of IFFT operations which are required to find a sequence that would produce the lowest PAPR. When using the original PTS, W^{M-1} IFFT operations are performed before determining which set of phase factors yields the lowest PAPR. In the case of flipping, $(M-1)W$ IFFT operations are performed before the decision. Nonetheless, this could have a significant impact on the battery life of the mobile units and might be impractical for mobile applications. The last problem associated with PTS is the required side information at the receiver. In order to reconstruct the original OFDM signal without any error, the side information such as the index of which phase factors is used to generate the lower PAPR has to be transmitted to the receiver. As a consequence, the transmission of side information will cause a loss in data rate of the OFDM system.

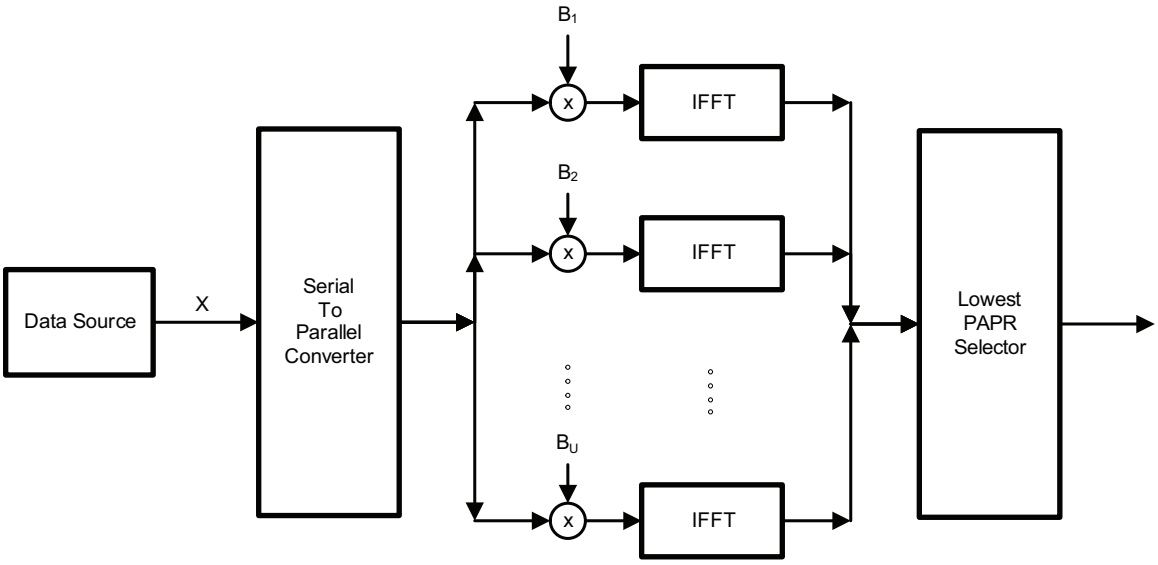

Figure 10.4 A block diagram of OFDM systems with selective mapping (SLM) implementation for PAPR reduction.

10.3.5 Selective Mapping (SLM)

The selective mapping (SLM) was first proposed in 1996 to reduce PAPR in OFDM systems [68]. The system block diagram of an OFDM system with SLM is shown in Fig. 10.4 [52]. In the SLM algorithm, the data source, denoted as X, is multiplied by the U different sets of phase factors element-wise to produce U different copies of X, namely

$$X_u = B_u X \qquad\qquad u = 1, 2, ..., U \tag{10.29}$$

where U is the design parameter in SLM. In general, more reduction in PAPR is likely to achieved when U increases. In addition, B_u is defined as

$$B_u = \left[\begin{array}{ccccc} B_{u,1} & B_{u,2} & B_{u,3} & ... & B_{u,(N-1)} \end{array} \right] \tag{10.30}$$

where N represents the number of subcarriers in IFFT and $B_{u,k}$ is given by

$$B_{u,k} = e^{j\phi_{u,k}} \qquad\qquad k = 0, 1, 2, ..., N-1 \tag{10.31}$$

After multiplying X with the phase factors, each X_u is processed by IFFTs and its PAPR is then computed and compared with the others. The resulting signal that yields the lowest PAPR is subsequently chosen for transmission. In addition, the B_{opt} which implies the optimal B_u that produces the lowest PAPR has to be transmitted to receiver as a side information. The receiver will then use B_{opt} to recover the data source, X.

The SLM technique works in the similar way which PTS operates. The commonalities between SLM and PTS are the requirement of a set of vectors of weighting factors in both schemes

and only one modified data sequence which has lowest PAPR is chosen for transmission. However, there are two noticeable differences between the PTS and SLM schemes. The first difference is there is no subblocks partitioning in the SLM method, i.e. the entire information bearing signal is processed by IFFT. Another difference is that the phase vector operates differently on data signal. In PTS, the phase factor, b_m, operates on the modulated OFDM symbols while B_u operates on the subcarrier level in SLM. Since phase factors are also utilized in SLM to reduce PAPR, SLM too suffers from the same drawbacks such as the high complexity in search for the optimal phase factors that the conventional PTS has.

The issue related to the complexity in search for optimal phase factors has been discussed in Section 10.3.4 of this chapter. In addition, alternative search methods have also been presented and some of search methods such as flipping method described in [9] can be modified and applied to SLM. In this section, we will focus on another disadvantage that both SLM and PTS share which is the loss in data rate. The decrease in data rate is due to the transmission of side information which is required at the receiver to correctly recover the original OFDM signals. Not only the transmission of side information is required, the integrity of the side information also has a significant impact on the BER performance.

To avoid a decrease in data rate, Han *et al.* [13] proposed to estimate the phase factors at receiver. In this case, the authors considered the linear block code which can be produced by using systematic encoders with a code rate, $R = \frac{l}{m}$. In a codeword, the first l will be exactly the same as the information data bits and the rest of $(m - l)$ bits are redundancy which are generally referred to as parity bits. The data bits and parity bits in the codewords are then modulated separately and after modulation, are concatenated into a sequence with N symbols. As the authors pointed out that the coding in this algorithm was intended to be used for error correction and did not have effects on the PAPR reduction.

The resulting coded data signal is then processed according to the SLM scheme. However, the design of the phase factors in the proposed method is different from the ordinary SLM algorithm. In the ordinary SLM algorithm, there is no restriction on the design of the phase factors, as long as each set of phase factors is different enough from each other. In this case, B_u is designed as

$$B_u = \begin{cases} B_{u,k} = 1 & k = \text{data subcarriers} \\ B_{u,k} = e^{j\phi_{u,k}} & \text{Otherwise} \end{cases} \tag{10.32}$$

for all u. Fig. 10.5 demonstrates the concept of the proposed design for B_u where elements in B_u takes on either $\{\pm 1, \pm j\}$.

At the receiver, authors exploited the fact that only subcarriers that have parity bits were

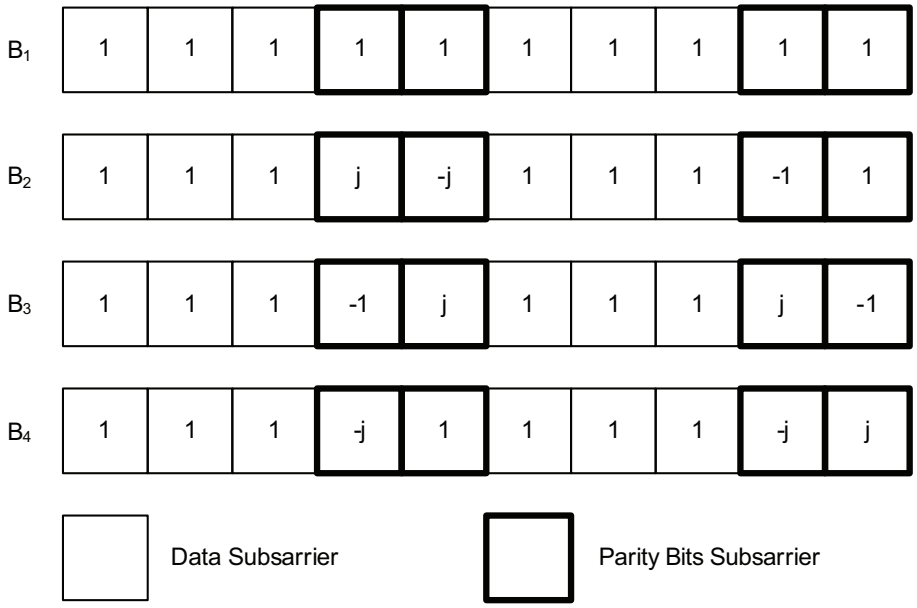

Figure 10.5 An example of design of B_u proposed by Han *et al.* for $N = 10$, $l = 3$, $m = 5$ and $U = 4$.

phase rotated in the transmitter during the process of extracting phase factors. After transforming the received signal back to frequency domain and removing the channel impulse response, the first l subcarriers in the received signal are the data bits and the rest of $(m - l)$ subcarriers are parity bits with unknown phase rotations. To estimate the phase factors, the authors proposed to encode the data bits in the data subcarriers in the received signal by using the same systematic encoder that was used at the transmitter. This would produce another sequence whose first l bits are data bits followed by $(m - l)$ parity bits. Even though, these parity bits are estimates, they are not phase rotated and can be used to extract phase factors on the received signal. Denoted $Y_{u,k}$ as the received parity bit in the k^{th} subcarrier which is rotated by the u^{th} set of phase factors and let $\hat{Y}_{u,k}$ be the estimates of the parity bits which are produced by encoding the data bits in the received signal, subsequently the phase factor at the k^{th} subcarrier is expressed as

$$\hat{B}_{u,k} = \frac{Y_{u,k}}{\hat{Y}_{u,k}} \qquad k = \text{Parity bits subcarriers} \tag{10.33}$$

Of course, (10.33) will most likely produce a phase factor with some errors that are due to either the additive white Gaussian noise (AWGN) or the residual of removal of the channel impulse response. However, one can compare the estimate of phase factors with all available phase factors in the memory in the receiver. In addition, the phase factors in the memory that the estimate is closest to is chosen to recover parity bits. Afterward, either a MAP or a Viterbi decoder can be used to decode codewords and recover data source. In simulations, the proposed algorithm produces 10% PAPR at 6.7 dB which is almost the same performance as ordinary SLM can offer. However, 0.1% PAPR is reduced by 0.3 dB when utilizing the proposed method. Although, it is not required to transmit side

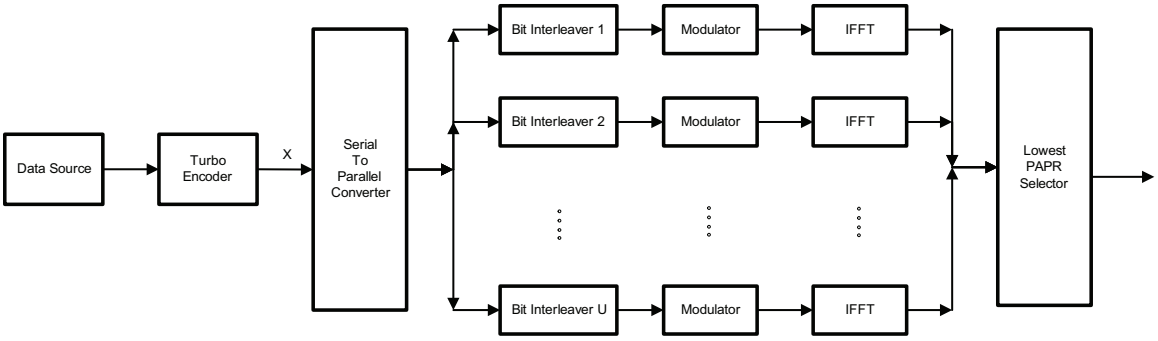

Figure 10.6 A block diagram of turbo coded OFDM transmitters with modified selective mapping (SLM) implementation for PAPR reduction proposed by Lin *et al.*.

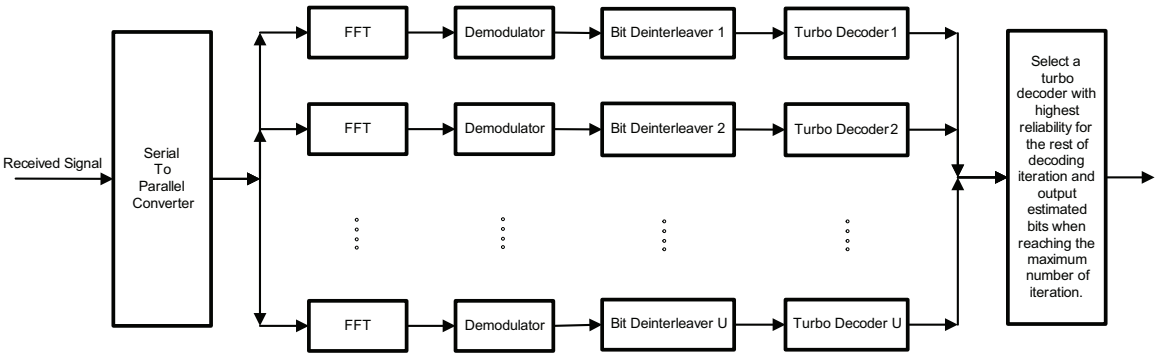

Figure 10.7 A block diagram of turbo coded OFDM receivers with modified selective mapping (SLM) implementation for PAPR reduction proposed by Lin *et al.*.

information in this case, the error in estimating phase factors may indirectly cause a degradation in BER performance through the process of decoding codewords.

In [69], another technique was proposed to replace the search for the optimal phase factors and to avoid the side information transmission. A block diagram of a turbo coded OFDM transmitter with modified SLM proposed by Lin *et al.* is shown in Fig. 10.6. The data source is first encoded by a turbo encoder and then interleaved by U different bit interleavers. Each bit interleaver will rearrange the input bits differently. The output of a bit interleaver is modulated by any modulation scheme such as BPSK, QPSK or QAM and processed by the IFFT. After PAPR is computed for each resulting time domain signal, the one which has the lowest PAPR is chosen for transmission.

A block diagram of the receiver structure is shown in Fig. 10.7 [69]. At the receiver, the received signal is first transformed back to frequency domain and demodulated. The output of the demodulator is then deinterleaved by U different deinterleavers which have the inverse mappings of the interleavers at the transmitter. The deinterleaved signals are subsequently processed by turbo decoder. At the i^{th} decoding iteration, the reliability of the bits in the message for the u^{th} turbo

decoder, denoted as $\mathfrak{R}_u^i$, is computed as

$$\mathfrak{R}_u^i = \sum_{l=1}^{L} log\left[\frac{p(d_l = 1)}{p(d_l = 0)}\right] \tag{10.34}$$

where L denotes the number of bits in the message [69]. The j^{th} turbo decoder is selected to continue for the rest of the decoding iteration when $\mathfrak{R}_j^i$ is greater than $\mathfrak{R}_u^i$ for $u = 1, 2, ..., U$ and $u \neq j$. The decoding process is terminated when i has reached to the maximum allowed iterations.

Based on the simulation results, 10% PAPR is reduced to about 7.1 dB and 0.1% PAPR is reduced to about 10.1 dB for a turbo coded OFDM system with BPSK modulation and coding rate, $R = \frac{1}{2}$. In this case, the transmission of the side information is avoided, however, the proposed scheme offers very little gain in the performance of PAPR reduction. In addition, there is a significant increase in the complexity of the receiver structure and an increase in time delay due to the array of turbo decoders.

To avoid using multiple turbo decoders at the receiver and the transmission of side information at the same time, both authors in [70, 71] independently proposed this new technique that relies on convolutional encoders to generate U different copies of same information bearing signal. In [70], for each frame of data, the dummy sequence, denoted as d_u where $u = 1, 2, ..., U$, is inserted at the beginning of the data frame to yield U different representations of the same information bearing signal. In addition, each d_u has ν number of bits where $\nu = log_2(U)$. The resulting signal is then encoded by the convolutional encoder with code rate, R. The encoded signal is subsequently processed by the BPSK modulator and IFFTs. After computing PAPR for each copy, the one that has the lowest PAPR is chosen for transmission.

At the receiver, the received signal is transformed back to frequency domain and subsequently processed by the BPSK demodulator. Instead of multiple convolutional decoders, only one convolutional decoder is needed to decode the encoded signal and yield the estimate of data sequence. The dummy bits in the data sequence is then expunged. For $N = 120$ subcarriers and $U = 4$, 10% PAPR is reduced to 6.4 dB from 8.2 dB which is for the same system that is without dummy bits insertion. In [71], the authors proposed a technique that is similar to the one proposed in [70], except 8 Amplitude Shift Keying (8-ASK) is used instead of BPSK. The performance of PAPR reduction in this case is quite similar to the performance reported in [70]. Nonetheless, the transmission of side information can be avoided in both algorithms proposed in [70, 71], at the same time with a reduction in complexity of the receiver structure.

In all the algorithms presented in this subsection, the transmission of the side information such as which set of phase factors is used to reduce PAPR is not required; hence, there is no loss in data rate in time domain. Nonetheless, the data rate in the frequency domain is cut by

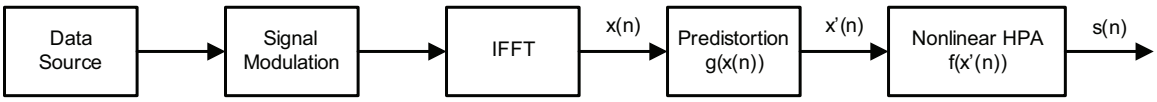

Figure 10.8 A block diagram of an OFDM system with predistortion.

the code rate, R, which is due to either the turbo encoders or the convolutional encoders. This implies that the highest data rate that is achievable is 50% which corresponds to the cases where $R = \frac{1}{2}$. In addition, a high code rate and superior performance in PAPR reduction usually do not coexist together, therefore, often this is a tradeoff between the code rate and performance in PAPR reduction. In addition, the increase in the complexity of the receiver is also an issue since in some cases, multiple decoders are required at the receiver. The last disadvantage that is associated with proposed algorithms in [13, 69–71] is the delay in time. The delay in time can increase dramatically due to the relationship between accuracy of the estimated data bits and the number of iterations in the decoding process since running more iterations implies yielding more accurate estimates.

10.3.6 Predistortion

In general, techniques related to predistortion are not covered under the topic of PAPR reduction since the predistorted signals do not usually yield better performance in PAPR reduction than the signals that have not been predistorted. However, it is included in this chapter because predistortion can be used in offsetting the nonlinearity in practical HPAs which is also the purpose of reducing PAPR. Fig. 10.8 shows OFDM systems with predistortion. The general idea of predistortion is by using a predistorter in front of a nonlinear HPA, then the desired output of the nonlinear HPA is the same as the input to the predistorter. In other words, let $g(x(n))$ represents the nonlinear function which is implemented in the predistorter and $f(x^{'}(n))$ be the nonlinear function that is used in nonlinear HPAs, then $g(x(n))$ is a nonlinear function that satisfies the following

$$\begin{aligned} g(x(n)) &= \min_{g(x(n))} |x(n) - s(n)| \\ &= \min_{g(x(n))} \left| x(n) - f(x^{'}(n)) \right| \end{aligned} \tag{10.35}$$

where $x(n)$ is the input signal to the predistorter and $s(n)$ is the output of the nonlinear HPA. Furthermore, the ideal predistortion function in this case is just the inverse of the nonlinear function, i.e. $g(x(n)) = f^{-1}(x^{'}(n))$. When $g(x(n))$ is the implemented based on the ideal predistortion function, this would lead to $s(n) = x(n)$.

In [72], the authors analyzed effects of predistortion on the total degradation in an OFDM system that is impaired by a nonlinear HPA. The nonlinear HPA in this case is modeled as the Saleh

model and is given by

$$\begin{aligned} A(r) =& A_{sat}^2 \frac{r}{r^2 + A_{sat}^2} \\ \Phi(r) =& \frac{\pi}{3} \frac{r^2}{r^2 + A_{sat}^2} \end{aligned} \tag{10.36}$$

where r is the magnitude of the input signal, $x(n)$ and A_{sat} is the input saturation voltage. Notice that the AM/AM and AM/PM definitions given in (10.36) are different from the definitions given in (2.6) in Section 2.3 of Chapter 2. However, $A(r)$ in (10.36) can be obtained by setting α_{AM} and β_{AM} in (2.6) to 1 and $\frac{1}{A_{sat}^2}$, respectively. For $\Phi(r)$ in (10.36), it is obtained by setting α_{PM} to $\frac{\pi}{3A_{sat}^2}$ and β_{PM} to $\frac{1}{A_{sat}^2}$ in (2.6).

To reduce the nonlinearity, the authors proposed to utilize the inverse functions of (10.36) in predistorter. As pointed out in the paper, $A(r)$ is not a one to one function for all r, hence, the inversion is only possible when $r \leq \frac{A_{sat}}{2}$ and for $r > A_{sat}$, the amplitude of the predistorter output is set at A_{sat}. However, such a problem does not exit when inverting the AM/PM function. The maximum value that $\Phi(r)$ takes on is $\frac{\pi}{6}$ which is obtained by evaluating $\Phi(r)$ with $r = A_{sat}$. Then, the inverse functions of (10.36) are given by

$$\begin{aligned} |g(x(n))| =& A^{-1}(r) = \begin{cases} \frac{A_{sat}^2}{2r} \left[1 - \sqrt{1 - \left(\frac{2r}{A_{sat}} \right)^2} \right] & r \leq \frac{A_{sat}}{2} \\ A_{sat} & r > \frac{A_{sat}}{2} \end{cases} \\ \angle g(x(n)) =& \Phi^{-1}(r) = \begin{cases} \theta(n) - \frac{\pi}{6} \left[1 - \sqrt{1 - \left(\frac{2r}{A_{sat}} \right)^2} \right] & r \leq \frac{A_{sat}}{2} \\ \theta(n) - \frac{\pi}{6} & r > \frac{A_{sat}}{2} \end{cases} \end{aligned} \tag{10.37}$$

where $|g(x(n))|$ and $\angle g(x(n))$ represent the magnitude and phase of $g(x(n))$, respectively. $\theta(n)$ denotes the phase of the input signal, $x(n)$.

Instead of measuring the system performance based on the BER, the performance of the system is measured based on the amount of total degradation in the system which is given by [72]

$$Total\ Degradation = SNR - SNR_{HPA} + Backoff \tag{10.38}$$

where the unit is in dB. SNR represents the signal to noise ratio (SNR) and SNR_{HPA} represents the SNR of the signal at the output of the nonlinear HPA. $Backoff$ implies the IBO in the nonlinear HPA. Through simulations, it is shown that an OFDM system with predistortion has a gain about 3.5 dB in total degradation compared with an OFDM system without predistortion when both OFDM systems are subject to nonlinear HPAs.

For Solid State Power Amplifier (SSPA), Lee *et al.* [73] also proposed to predistort signals by using the inverting the nonlinear HPA. The AM/AM and AM/PM conversions for SSPAs

are given by

$$A(r) = \frac{r}{\left(1 + \left(\frac{r}{A_O}\right)^{2p}\right)^{\frac{1}{2p}}}$$
$$\Phi(r) \approx 0 \tag{10.39}$$

where A_O is the maximum output amplitude and p is the parameter that controls the smoothness of the transition. Since $\Phi(r) \approx 0$ and maximum amplitude of the signal at the output of nonlinear HPA is A_O, subsequently, the inverse of $A(r)$ is found to be

$$|g(x(n))| = A^{-1}(r) = \begin{cases} \frac{r}{\left(1-\left(\frac{r}{A_O}\right)^{2p}\right)^{\frac{1}{2p}}} & r < A_O \\ A_O & r \geq A_O \end{cases} \tag{10.40}$$

For $A_O = 1.5$ and $p = 1.5$, the simulation results show that the OFDM system with predistortion has a gain about 1.8 dB in SNR compare with the system that is without predistortion for BER $= 10^{-3}$. In addition, the simulation shows that the BER performance improves when the IBO is increased which is what one could expect from an increase in IBO. Even though changing IBO does not implies a change in the characteristics of the nonlinear function that nonlinear HPAs retain, with an increase in the numerical value of IBO, the HPA becomes more linear in a sense that now, the HPA operates in the linear region. This implies that less nonlinear distortion will be introduced to the system, therefore, the BER performance will improve. However, as it has been mentioned already, by increasing IBO, the efficiency of the HPA decreases. In addition, the decrease in the efficiency of the HPA leads to a detrimental effect on battery life. Both inversion techniques proposed in [72, 73] share one disadvantage which is the requirement of knowing the parameters such as A_O, p and A_{sat} that are used in the nonlinear HPA models. If a predistorter does not have prior knowledge about the numerical values of those parameters, it can not predistort the signal perfectly. As a result, the signal at the output of the nonlinear HPA would still contain various degrees of nonlinear distortion which causes a degradation in the BER performance.

To predistort signal without knowing the parameters used in the HPA model, Yoshimi *et al.* [74] proposed a technique that was based the combination of PTS and modified predistortion. The implementation of PTS follows the description given in the subsection 10.3.4 of this chapter. The flipping technique proposed by Cimini *et al.* [9] is utilized to obtain the sub-optimal phase factors. The output of the PTS, $x^{'}(n)$, is then processed by the envelope peak detector where the symbol that has the maximum magnitude, denoted as $x^{'}_{max}(n)$, is obtained. $x^{'}(n)$ is then normalized in the following fashion.

$$x^{''}(n) = x^{'}(n)\frac{A_{sat}}{x^{'}_{max}(n)} \tag{10.41}$$

where $x^{''}(n)$ is the normalized signal and A_{sat} denotes the input saturation voltage. The magnitude of $x^{''}(n)$ would correspond to a predistorted magnitude and phase in the lookup table. The

predistorted magnitude and phase are passed on to the nonlinear HPA and the resulting signal is subsequently transmitted.

In a BPSK OFDM system that is subject a nonlinear HPA in AWGN channel, about 2.5 dB can be gained in BER performance at BER = 10^{-2} when using only predistortion. One more dB can be gained in BER performance if PTS is used in addition to predistortion. Since PTS is utilized, the proposed technique also suffers from the common drawback that most PTS methods have which is the loss in data rate. In this proposed algorithm, the side information is still required to be transmitted to the receiver to recover the original data sequence without any error. Another disadvantage is the memory size for the lookup table. To perfectly predistort the signal, all possible numerical values of input magnitudes and predistorted magnitudes and phases have to be stored in the memory. Furthermore, the size of memory that is required for information storage might not be feasible to implement in actual hardware as the accuracy of predistortion becomes an important design criterion.

To reduce the size of required memory for storing all possible input magnitudes, Wesolowski *et al.* [75] proposed to quantize the magnitude of the input signal to the predistorter and through an iterative process, the output of the predistorter can be fine tuned in such a way that the output of nonlinear HPAs does not contain nonlinear distortion. Denote the signal at the input of the predistorter as $x(n)$, then $x(n)$ is given by

$$x(n) = re^{j\theta} \tag{10.42}$$

where r and θ are the magnitude and phase of $x(n)$, respectively. Let $y_i(n)$ be the signal at the output of the predistorter at the i^{th} iteration, then $y_i(n)$ is given by

$$\begin{aligned} y_i(n) =& A_i^{-1}(\hat{r}) r e^{j(\theta + \Phi_i^{-1}(\hat{r}))} \\ =& r_i^{'} e^{j\theta_i^{'}} \end{aligned} \tag{10.43}$$

where $\hat{r}$ represents the magnitude of the signal after quantization. $A_i^{-1}(\hat{r})$ is the predistorted magnitude based on the quantized magnitude, $\hat{r}$, at the i^{th} iteration while $\Phi_i^{-1}(\hat{r})$ denotes the predistorted phase. Furthermore, $r_i^{'}$ and $\theta_i^{'}$ are the magnitude and the phase of $y_i(n)$, respectively.

Denote $s(n)$ as the output of the nonlinear HPA, then $s(n)$ is given by

$$s(n) = A(r_i^{'}) e^{j(\Phi(r_i^{'}) + \theta_i^{'})} \tag{10.44}$$

Ideally, it is desired to have the output of the nonlinear HPA equal to the input signal to the predistorter, namely, $s(n) = x(n)$. To achieve this, Wesolowski *et al.* proposed to update $A_i^{-1}(\hat{r})$ and $\Phi_i^{-1}(\hat{r})$ in (10.43) through a gradient adaptation algorithm which can be described by the

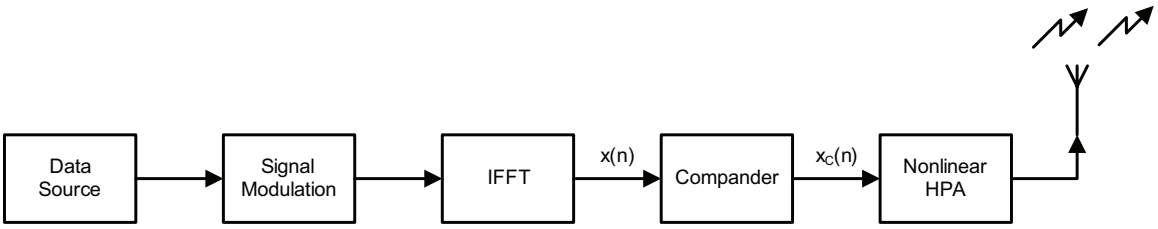

Figure 10.9 A block diagram of an OFDM transmitter with compander that is subject to a nonlinear HPA.

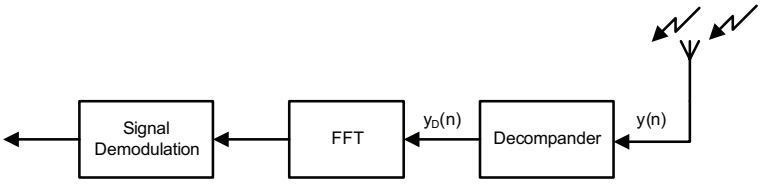

Figure 10.10 A block diagram of an OFDM receiver for the transmitter shown in Fig. 10.9.

following two equations, namely

$$\begin{aligned} A_{i+1}^{-1}(\hat{r}) =& A_i^{-1}(\hat{r}) - c_A \left(\frac{A(r_i^{'})}{r} - 1 \right) \\ \Phi_{i+1}^{-1}(\hat{r}) =& \Phi_i^{-1}(\hat{r}) - c_\Phi \left(\Phi(r_i^{'}) + \theta_i^{'} - \theta \right) \end{aligned} \tag{10.45}$$

where c_A and c_Φ are the step sizes for $A^{-1}(\hat{r})$ and $\Phi^{-1}(\hat{r})$, respectively. Not only reducing a small amount of memory size through quantization, the proposed algorithm updates the predistorted signal through a simple gradient adaptation process to improve the accuracy of predistorted signal.

10.3.7 Companding

In general, the companding techniques are similar to predistortion in a way that both types of techniques alter the magnitudes of OFDM signals in such way that nonlinear HPAs are not forced to operate at the nonlinear region. However, the difference between companding techniques and predistortion is when utilizing companding techniques, the compensation for companding is required at receivers while it is not needed in the case where predistortion is employed. Fig. 10.9 shows a block diagram of an OFDM transmitter with compander that is subject to a nonlinear HPA. The block diagram of corresponding receiver is shown in Fig. 10.10. Let $x(n)$ be the signal at the input of compander, then the output of compander, denoted as $x_C(n)$, is expressed as

$$x_C(n) = u(|x(n)|)e^{j\theta} \tag{10.46}$$

where $u(|x(n)|)$ represents the companding function which is a function of magnitude of $x(n)$. In addition, θ denotes the phase of the $x(n)$. Subsequently, $x_C(n)$ is subject to nonlinear distortion in the HPA and transmitted from an antenna.

Let $y(n)$ be the received signal and $y_D(n)$ be the signal at the output of the decompander, then $y_D(n)$ is found to be

$$y_D(n) = q(|y(n)|)e^{j\phi} \tag{10.47}$$

where $q(|y(n)|)$ is the decompanding function which is a function of magnitude of $y(n)$. Furthermore, ϕ is the phase of $y(n)$. Subsequently, $y_D(n)$ is processed by the FFT and demodulated to yield estimated data bits. In most cases, it is desired to implement the decompander as inverse of the compander, namely

$$|x(n)| = q(u(|x(n)|)) \tag{10.48}$$

However, it is most likely that (10.48) will not hold in practice since $y(n)$ contains various sources of noise that arise from transmissions through wireless channels. Since the decompander is inverse of the compander, one of the criteria for designing a compander is the companding function has to be an one to one function or an invertible function, so the inverse function exists and then can be implemented in the decompander.

In 1999, Wang *et al.* [76] proposed to use a μ-Law companding to reduce PAPR of OFDM signals. For the μ-Law compander, the proposed companding function which is parameterized by μ and A_N is given by

$$u(r) = \frac{A_\mu ln\left(1 + \mu\frac{r}{A_N}\right)}{ln\,(1+\mu)} \tag{10.49}$$

where A_μ is the normalization constant and is defined as the maximum of r such that $0 \leq \frac{r}{A_\mu} \leq 1$ where r represents the magnitude of $x(n)$. Furthermore, the optimal value for μ is given as

$$\mu = \sqrt{N-2} \tag{10.50}$$

where N is the number of subcarriers. The decompanding function is subsequently given by

$$q(r^{'}) = \frac{A_\mu\left(e^{\frac{r^{'} ln(1+\mu)}{A}} - 1\right)}{\mu} \tag{10.51}$$

where $r^{'}$ denotes the magnitude of the received signal, $y(n)$. Through simulation, it was shown that the μ-Law companding technique increases the amplitude of small signals while keeping the large signals unchanged after companding. As a result, the PAPR of OFDM signals is reduced due to the increase in the average power.

In [77, 78], authors proposed to reduce PAPR of OFDM signals by utilizing an exponential companding function. The exponential companding function is given as

$$u(r) = \sqrt[d]{A_e\left(1 - e^{\frac{-r^2}{\sigma^2_{x(n)}}}\right)} \tag{10.52}$$

where d is a constant parameter which can be chosen to optimize the PAPR reduction result. A_e is a normalization constant which keeps the average power of input and output signals of the exponential compander at the same level. Furthermore, A_e is defined as

$$A_e = \left(\frac{E\{r^2\}}{E\left\{ \sqrt[d]{\left(1 - e^{\frac{-r^2}{\sigma^2_{x(n)}}}\right)^2} \right\}} \right)^{d/2} \tag{10.53}$$

In addition, $\sigma^2_{x(n)}$ in both (10.52) and (10.53) represents the power of input signal, $x(n)$. At the receiver, the decompanding function is utilized to decompress the received signal and the function is given by

$$q(r^{'}) = \sqrt{-\sigma^2_{x(n)} ln\left(1 - \frac{r^d}{A_e}\right)} \tag{10.54}$$

Different from the μ-Law companding where small signals are boosted while keeping the large signals unchanged, the exponential compander adjusts both small and large signals by various scales. As a consequence, the PDF of the companded signal is transformed from the Rayleigh distribution to uniform distribution. The simulation results show that the amount of reduction in PAPR asymptotically decreases when d is greater than 2.

Kumar *et al.* [79] modified the existing exponential compander by introducing two more parameters in the companding function. The modified companding function is then given by

$$u(r) = B_e^{\frac{1}{d}} \left(1 - e^{\frac{-c_1 r^2}{2\sigma^2_{x(n)}}}\right)^{c_2/d} \tag{10.55}$$

where B_e is a constant parameter that keeps the average power of input and output signals of the compander constant. In addition, B_e is given by

$$B_e = \left(\frac{E\{r^2\}}{E\left\{ \left(1 - e^{\frac{-c_1 r^2}{2\sigma^2_{x(n)}}}\right)^{2c_2/d} \right\}} \right)^{d/2} \tag{10.56}$$

c_1 and c_2 in both (10.55) and (10.56) are two additional constant parameters that are introduced by Kumar *et al.*. Finally, d is still defined as (10.52).The corresponding decompander is implemented as the inverse of companding function which is given by

$$q(r^{'}) = \sqrt{\frac{-2\sigma^2_{x(n)} ln\left(1 - \left(\frac{r'^d}{B_e}\right)^{1/c_2}\right)}{c_1}} \tag{10.57}$$

The simulation results show that as c_1 increases, the amount of reduction in PAPR also increases for fixed d and c_2. This is due to the fact that as c_1 increases, the peak power becomes equal to the average power, in which case, the PAPR is reduced to 1. However, the BER performance worsens as c_1 increases. This suggests that there is a tradeoff between the choice of c_1 that can significantly reduce PAPR and the BER performance.

With minimum increase in the complexity of the receiver structure, it seems that PAPR of OFDM signals can be effectively reduced by choosing an appropriate companding function that has an one to one mapping and is invertible. Another advantage is that there is no loss in data rate which makes companding techniques even more attractive. However, from these papers reviewed here, there might be a disadvantage which is the OFDM system with a compander might not perform well in Rayleigh fading channels. This is based on the fact that none of simulation results in the papers that were presented was simulated with Rayleigh fading channels.

10.4 Conclusion

In this chapter, we first discussed the concept of PAPR by defining PAPR for the continuous time OFDM signals. To derive the PAPR definition for the discrete case, we introduced the idea of oversampling continuous time OFDM signals because the peaks of continuous time OFDM signals may not be picked up when using the Nyquist sampling rate. Next, we represented the PAPR distribution of OFDM signals by using CCDF. The CCDFs of PAPR were given with and without oversampling the continuous time OFDM signals. We also introduced the easiest way to avoid the introduction of nonlinear distortion which was caused by the OFDM signals through practical HPAs. This was done by increasing IBO of HPAs; however, this led to the problem of efficiency of power conversion in HPAs. To resolve this problem, we presented several alternatives such as clipping, coding, interleaving, PTS, SLM, predistortion and companding which were some of the most popular techniques for PAPR reduction in literature. Finally, Table 10.1 provides a brief summary of all methods.

Table 10.1 Summary of PAPR Reduction Techniques

Techniques	Advantages	Disadvantages
Clipping	▶ Simplest technique ▶ No loss in data rate ▶ Can be combined with other techniques	▶ In-band distortion ▶ Out-of-band radiation ▶ Possible peak regrowth after filtering
Coding	▶ Moderate effective method ▶ Can be used to improve BER	▶ Requires good codes with good code rates ▶ Possible large memory size required for look-up tables ▶ Limited to small number of subcarriers
Interleaving	▶ Least effective technique ▶ Can be combined with other techniques	▶ Require side information transmission ▶ Loss in data rate
PTS	▶ Very effective for PAPR reduction	▶ Searching for optimal phase factors is complicated ▶ Needs M IFFTs ▶ Require side information transmission ▶ Loss in data rate
SLM	▶ Same as PTS	▶ Same as PTS
Predistortion	▶ Effective for PAPR reduction ▶ No side information required	▶ Need to invert nonlinear functions ▶ Require knowledge of parameters in nonlinear functions
Companding	▶ Very effective for PAPR reduction ▶ No side information required ▶ No loss in data rate	▶ Require invertible functions, i.e. one to one mapping ▶ Minimal increase in complexity of receiver structure ▶ Might not work in fading channels

11

Effects of Narrowband Interference and Nonlinear Amplifier on the Performance of Companded OFDM

11.1 Introduction

Due to its capability of delivering high data rate and superior performance in fading channels, Orthogonal Frequency Division Multiplexing (OFDM) has become a primary candidate to be considered in the Fourth Generation (4G) mobile and Wireless Local Area Network (WLAN) communication systems [4]. However, one of disadvantages that OFDM has is high peak to average power ratio (PAPR) which is due to the superimposition of multi-carrier signals. Practical high power amplifiers (HPAs) have difficulty reproducing such high PAPR signals and often introduce nonlinear distortion such as clipping and spectral regrowth [24, 25]. Subsequently, the system performance will degrade.

To reduce PAPR or minimizing the nonlinear distortion produced by the OFDM signals through practical HPAs, authors in [76] proposed a companding technique for reducing PAPR. The proposed μ-Law compander which is placed before the nonlinear HPAs compresses the magnitude of OFDM signals while leaving the phase of the OFDM signals unaltered [76]. By compressing the magnitude of OFDM signals, we can ensure that the nonlinear HPAs will operate in its linear region. Therefore, less amount of nonlinear distortion caused by HPAs is introduced to the system and as a result, the bit error rate (BER) performance is improved. To recover the original uncompressed

OFDM signals at the receiver, the decompander which is the inverse of a compander decompresses the received signals. In [77], the authors proposed another compander that utilized the exponential function. The proposed exponential compander worked in the same way as the μ-Law compander in reducing the PAPR of OFDM signals. In both PAPR reduction schemes, the companding technique shows some advantages such as requiring no additional Inverse Fast Fourier Transform (IFFT) operations and transmissions of side information when compared to Selective Mapping (SLM) and Partial Transmit Sequences (PTS) [9, 83]. Nonetheless, both authors in [76, 77] only presented simulation results of companded OFDM systems in Additive White Gaussian Noise (AWGN) channels, and not in Rayleigh fading channels.

Since the bandwidth of available frequency spectrum is limited, it is inevitable that an OFDM system finds itself operating in coexistence with interference such as narrowband interference (NBI). While there are some papers dealing with the effects of nonlinear HPAs on the performance of OFDM systems in AWGN channels, very few analyze the combined effect of NBI together with nonlinear distortion caused by nonlinear HPAs in OFDM systems through Rayleigh fading channels. Costa, *et al.* [15] presented the performance analysis of a M-ary Quadrature Amplitude Modulation (M-QAM) OFDM system with impairment from a nonlinear HPA and phase noise in AWGN channel only. In [26], the authors analyzed an equalized OFDM system in a Rayleigh fading channel for various modulations; however, the nonlinear HPAs and NBI were not considered in the performance analysis. In [27], an OFDM system with carrier interferometry spreading codes and NBI in a Rayleigh fading channel was analyzed without considering the effect of nonlinear distortion produced by nonlinear HPAs. In addition, the authors in the paper assumed that the source of NBI was very close to the receiver; hence, the NBI did not experience any channel effect. This particular assumption does not provide useful insights to the performance of an OFDM system in the presence of NBI because in many cases, the sources of NBI are usually located in several city blocks away. Therefore, it is more reasonable and practical to assume that the NBI signal experiences another separate channel response.

In the previous work [45, 46], we presented the performance analysis of a M-QAM OFDM system that was subject to a nonlinear HPA, channel estimation error and NBI in a Rayleigh fading channel. In contrast to the NBI model presented in [27], we assumed that the NBI by itself experienced a separate channel response. In this chapter, we extend the previous work and analyze the combined effect of NBI and a nonlinear HPA on the performance of a M-QAM OFDM system with a compander in a Rayleigh fading channel. In addition, we propose a new companding function for the compander and a novel receiver structure which minimizes the degradation effects caused by the decompander when the OFDM systems operate in a Rayleigh fading channel. For the purpose of simulation, we extend our analytical model to an 802.11n WLAN system based on IEEE 802.11n specification . The simulation and theoretical results will be presented for various combined sources

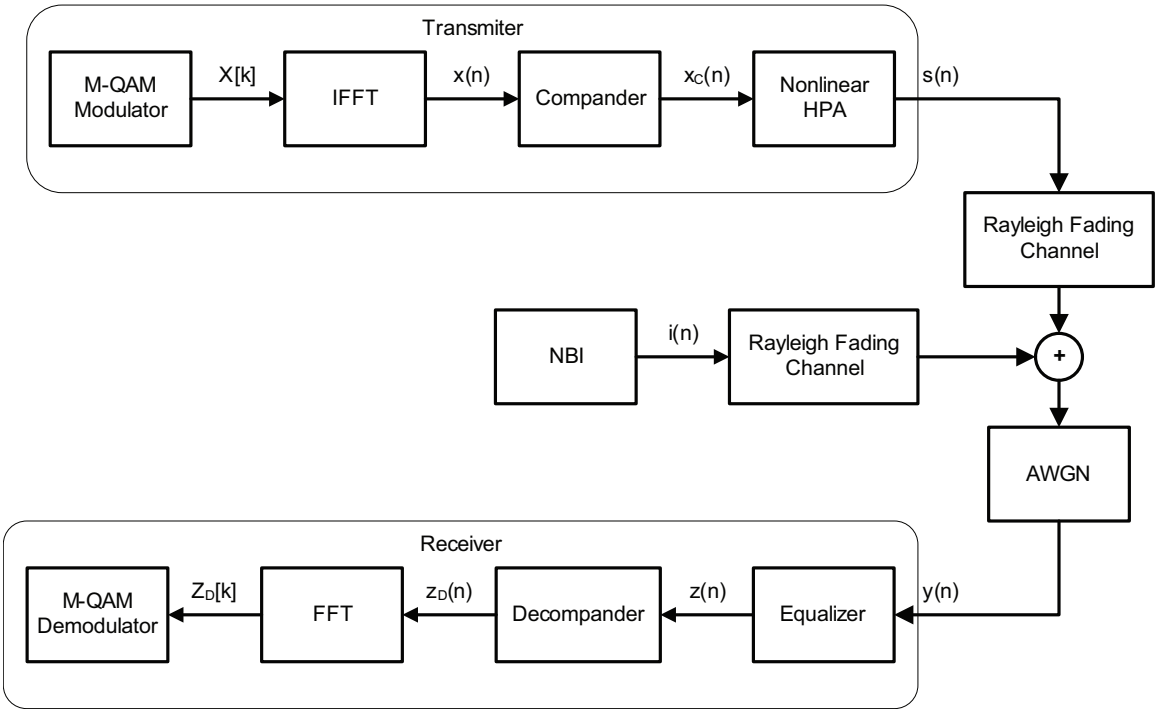

Figure 11.1 The system block diagram of a M-QAM companded OFDM system which is subject to a nonlinear HPA, channel estimation error and NBI in a Rayleigh fading channel.

of degradation.

The chapter is organized as follows. In Section 11.2, the analytical model is presented and each component is discussed in detail. Section 11.3 presents the performance analysis of the analytical model. Section 11.4 discusses the simulation setup. Section 11.5 contains the theoretical and simulation results of the system described in Section 11.4. Finally, Section 11.6 summarizes the chapter.

11.2 System Description

Fig. 11.1 shows the block diagram of an analytical model which consists of a transmitter, a NBI in a wireless channel and a receiver. Each block in Fig. 11.1 is discussed in the following subsections.

11.2.1 Transmitter

The transmitter consists of a M-QAM modulator, an IFFT, a compander and a nonlinear HPA. The input to the M-QAM modulator is assumed to be binary bits and the values of the bits are equiprobable and statically independent of each other. The stream of binary data bits are then

mapped to M-QAM symbols, denoted as $X[k]$. The output of the modulator is subsequently fed into and processed by IFFT. Denote $x(n)$ as the signal at the output of the IFFT, then at appropriate sampling time, $x(n)$ is given by

$$x(n) = \frac{1}{N} \sum_{k=0}^{N-1} X[k] e^{j\frac{2\pi nk}{N}} \qquad 0 \leq n \leq N-1 \tag{11.1}$$

where N is the number of subcarriers.

11.2.2 Compander

In this subsection, we propose a new nonlinear companding technique which is used to eliminate the nonlinear distortion caused by a nonlinear HPA. Denote $x_C(n)$ as the companded OFDM signals at the output of the compander, then $x_C(n)$ is expressed as

$$x_C(n) = u(r) e^{j\angle x(n)} \tag{11.2}$$

where r is the magnitude of the input signal, $x(n)$, and $\angle x(n)$ represent the phase of $x(n)$. In addition, $u(r)$ is defined as

$$u(r) = \frac{A_N r}{(1 + (\frac{r}{A_O})^{2p})^{\frac{1}{2p}}} \tag{11.3}$$

where A_O represents the maximum output magnitude allowed and p is the smoothness controller. Furthermore, A_N is the normalization factor that ensures the average power of $x(n)$ and $x_C(n)$ are equal and is found as

$$A_N = \left(\frac{E\{r^2\}}{E\left\{ \frac{r^2}{(1+(\frac{r}{A_O})^{2p})^{\frac{1}{p}}} \right\}} \right)^{1/2} \tag{11.4}$$

where $E\{\cdot\}$ is the expected value.

11.2.3 HPA Model

The nonlinear HPA model in the transmitter represents the nonlinear distortion imposed on the signal. In this chapter, the nonlinear HPA model follows the Saleh model which has been described in Chapter 2, Section 2.3.

11.2.4 Narrowband Interference Model, Channel Model and AWGN

The NBI signal in time domain, denoted as $i(n)$, is expressed as

$$i(n) = \frac{1}{N} \sum_{k=0}^{N-1} I[k] e^{j\frac{2\pi nk}{N}} \tag{11.5}$$

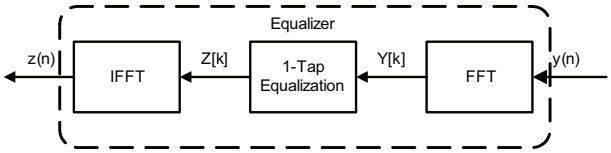

Figure 11.2 A detail block diagram of an equalizer shown in Fig. 11.1.

where $I[k]$ represents the NBI signal for the k^{th} subcarrier and has power equal to $\frac{|I[k]|^2}{2}$.

Denote $h_1(n)$ as the channel impulse response of the Rayleigh fading channel for the transmitted signal, $s(n)$. The in-phase and quadrature components of $h_1(n)$ are modeled as zero mean and $\sigma^2_{H_1}$ variance Gaussian random variables. In addition, in-phase and quadrature components are assumed to be statistically independent of each other. Let $h_2(n)$ be the channel impulse response between the NBI and the receiver and is assumed to be a separate Rayleigh fading channel with zero mean and $2\sigma^2_{H_2}$ variance. Furthermore, the in-phase and quadrature components of the channel impulse response, $h_2(n)$, are assumed to be independent of each other. The thermal noise, denoted as $w(n)$, is modeled as an independent AWGN process which has zero mean and $2\sigma^2_w$ variance.

11.2.5 Receiver

In this section, we propose the new receiver structure, shown in Fig. 11.1, consisting of an equalizer, a decompander, a Fast Fourier Transform (FFT) and a M-QAM demodulator. Each block is also discussed in detail in following subsections. Denote $y(n)$ as the received signal in time domain, then $y(n)$ is given by

$$y(n) = h_1(n)s(n) + h_2(n)i(n) + w(n) \tag{11.6}$$

where $s(n)$ represents the transmitted signal.

11.2.6 Equalizer

In conventional OFDM systems, the equalization is usually done in the frequency domain since the transmitted signal after channel impulse response is a multiplication of two signals in frequency domain. However, when a decompander is preceded by the equalizer, the magnitude of $y(n)$ after decompander can be enormous due to the decompression in the decompander. Subsequently, it leads to an unexpected increase in BER even under the assumption of perfect channel estimation. Therefore, we propose a new equalizer which equalizes the received signal before the decompander. By equalizing the signal before the decompander, the effect of channel response on the magnitude of decompanded signal can be greatly reduced. Fig. 11.2 shows the structure of the new proposed equalizer in detail.

Since NBI does not affect all the subcarriers in the transmitted signal, the received signal in frequency domain can be separated into two cases. Let the subcarrier index k represents the case where the subcarrier is under the influence of NBI. Then, the received signal in frequency domain, denoted as $Y[i]$, is expressed as

$$Y[i] = \begin{cases} H_1[k]S[k] + H_2[k]I[k] + W[k] & \text{i = k} \\ H_1[l]S[l] + W[l] & \text{Otherwise} \end{cases} \tag{11.7}$$

where $H_1[k]$, $H_2[k]$, $S[k]$ and $W[k]$ are the FFT of $h_1(n)$, $h_2(n)$, $s(n)$ and $w(n)$, respectively.

One of the most attractive features of OFDM systems is the simplicity in the equalization process which is adequately done by utilizing a one-tap equalizer in the frequency domain. Among many available algorithms, we choose the Zero Forcing algorithm because of its simplicity in implementation. Before equalization, obtaining the channel estimate is necessary and can be done with the aid of pilots and interpolation. After obtaining the channel estimate, the equalized signal, denoted as $Z[i]$, is given by

$$Z[i] = \frac{Y[i]}{\hat{H}_1[i]} = \begin{cases} \frac{H_1[k]}{\hat{H}_1[k]}S[k] + \frac{H_2[k]}{\hat{H}_1[k]}I[k] + \frac{W[k]}{\hat{H}_1[k]} & \text{i = k} \\ \frac{H_1[l]}{\hat{H}_1[l]}S[l] + \frac{W[l]}{\hat{H}_1[l]} & \text{Otherwise} \end{cases} \tag{11.8}$$

where $\hat{H}_1[i]$ is the estimate of $H_1[i]$ and is expressed as

$$\hat{H}_1[i] = H_1[i] + \epsilon[i] \tag{11.9}$$

where $\epsilon[i]$ represents the error in estimating the channel, $H_1[i]$, and is modeled as a complex Gaussian random process with zero mean and $2\sigma_\epsilon^2$ variance. At the output of the equalizer, the equalized signal is converted back to the time domain signal which is denoted as $z(n)$.

11.2.7 Decompander

Let $z_D(n)$ be the decompressed signal at the output of the decompander, then $z_D(n)$ is given by

$$z_D(n) = q(r^{'})e^{j\angle z(n)} \tag{11.10}$$

where $q(r^{'})$ is the inverse function of $u(r)$ and is defined as

$$q(r^{'}) = \frac{r^{'}}{(A_N^{2p} - (\frac{r^{'}}{A_O})^{2p})^{\frac{1}{2p}}} \tag{11.11}$$

where $r^{'}$ represents the magnitude of $z(n)$. Next, the $z_D(n)$ is fed into and processed by the FFT and the M-QAM demodulator.

11.3 Performance Analysis

In this section, we will derive the BER for the analytical model. The BER will later be used as a measure of the performance. In addition, for the sake of simplicity in the mathematical notation, we will drop the time and frequency indices in the derivation. The performance analysis starts with the characterization of $x(n)$. Under the assumption that N is large and by the *Central Limit Theorem*, $x(n)$ is said to be Gaussian distributed with zero mean [19]. With that assumption, Banelli, *et al.* [20] had shown that $x_C(n)$ can be written as a product of a complex gain, α_{G_1}, and the input signal, $x(n)$, added with noise distortion, $d_{G_1}(n)$. The compressed signal, $x_C(n)$, and its FFT are given by

$$x_C = \alpha_{G_1} x + d_{G_1} \overset{FFT}{\longleftrightarrow} X_C = \alpha_{G_1} X + D_{G_1} \tag{11.12}$$

where D_{G_1} was shown to be a complex Gaussian random variable with zero mean and $2\sigma^2_{D_{G_1}}$ variance. In addition, the numerical value of σ^2_D can be obtained by following steps outlined in Section 2.4 of Chapter 2.

For two different subcarriers, k_1 and k_2, $D_{G_1}[k_1]$ and $D_{G_1}[k_2]$ are mutually independent. Furthermore, the in-phase and quadrature phase components of D_{G_1} were shown to be mutually independent and identically distributed (i.i.d) [15]. The multiplicative coefficient α_{G_1} in (11.12) is given by

$$\alpha_{G_1} = \frac{E\{x_C^* x\}}{2\sigma_x^2} = \alpha_{G_{1_I}} + j\alpha_{G_{1_Q}} \tag{11.13}$$

where $(\cdot)^*$ implies the complex conjugate [20]. The subscripts I and Q represent the in-phase and quadrature components. The resulting companded OFDM signal is then subject to a nonlinear HPA. At the output of the nonlinear HPA, $s(n)$ and its FFT are expressed as

$$s = \alpha_{G_2} x_C + d_{G_2} \overset{FFT}{\longleftrightarrow} S = \alpha_{G_2} X_C + D_{G_2} \tag{11.14}$$

where α_{G_2} is defined as

$$\alpha_{G_2} = \frac{E\{s^* x_C\}}{2\sigma^2_{x_C}} = \alpha_{G_{2_I}} + j\alpha_{G_{2_Q}} \tag{11.15}$$

and the numerical value of $2\sigma^2_{D_{G_2}}$ can be obtained by following steps outlined in Section 2.4 of Chapter 2. After equalizing and decompressing the received signal, the output of the decompander, denoted as z_D, and its FFT are given by

$$z_D = \alpha_{G_3} z + d_{G_3} \overset{FFT}{\longleftrightarrow} Z_D = \alpha_{G_3} Z + D_{G_3} \tag{11.16}$$

where the value of $2\sigma^2_{D_{G_3}}$ can be obtained by following steps outlined in Section 2.4 of Chapter 2. Furthermore, α_{G_3} is defined as

$$\alpha_{G_3} = \frac{E\{z_D^* z\}}{2\sigma_z^2} = \alpha_{G_{3_I}} + j\alpha_{G_{3_Q}} \tag{11.17}$$

Since the equalized signal for the case where the subcarriers are free from NBI can be obtained from the other case where the subcarriers are under the influence of NBI by setting the power of NBI to zero, we will continue to derive the performance for the case where the subcarriers are affected by the NBI. Once the derivation is completed, the performance analysis for the other case is found by setting $I[k]$ to zero. Substituting (11.8), (11.12) and (11.14) into (11.16), then Z_D becomes

$$\begin{aligned} Z_D =& \frac{H_1}{\hat{H}_1}\alpha_{G_1}\alpha_{G_2}\alpha_{G_3}X + \underbrace{\frac{H_1}{\hat{H}_1}\alpha_{G_2}\alpha_{G_3}D_{G_1}}_{\beta_1} + \underbrace{\frac{H_1}{\hat{H}_1}\alpha_{G_3}D_{G_2}}_{\beta_2} + \underbrace{\frac{H_2}{\hat{H}_1}\alpha_{G_3}I}_{\eta} + \underbrace{\alpha_{G_3}\frac{W}{\hat{H}_1}}_{\xi} + \underbrace{D_{G_3}}_{\beta_3} \\ =& \frac{\alpha_1}{\hat{\alpha}_1}e^{j\theta}\alpha_{G_1}\alpha_{G_2}\alpha_{G_3}X + \beta_1 + \beta_2 + \eta + \xi + \beta_3 \end{aligned} \tag{11.18}$$

where α_1 and $\hat{\alpha}_1$ are the magnitudes of H_1 and $\hat{H}_1$, respectively. θ represents the phase difference between H_1 and $\hat{H}_1$. Since β_1, β_2, η, ξ and β_3 are noise with zero mean, their conditional variances are required in analyzing the performance. Let $\sigma^2_{\beta_1}$, $\sigma^2_{\beta_2}$, σ^2_{η}, σ^2_{ξ} and $\sigma^2_{\beta_3}$ be the variances for the in-phase or quadrature component of β_1, β_2, η, ξ and β_3, respectively, then they are given by

$$\begin{aligned} \sigma^2_{\beta_1} =& E\left\{\beta_1\beta_1^*\right\} = \frac{\alpha_1^2}{\hat{\alpha}_1^2}\alpha^2_{G_2}\alpha^2_{G_3}\sigma^2_{D_{G_1}}, \qquad \sigma^2_{\beta_2} = E\left\{\beta_2\beta_2^*\right\} = \frac{\alpha_1^2}{\hat{\alpha}_1^2}\alpha^2_{G_3}\sigma^2_{D_{G_2}} \\ \sigma^2_{\eta} =& E\left\{\eta\eta^*\right\} = \frac{\alpha_2^2}{\hat{\alpha}_1^2}\alpha^2_{G_3}\frac{|I[k]|^2}{2}, \qquad \sigma^2_{\xi} = E\left\{\xi\xi^*\right\} = \frac{\sigma^2_w}{\hat{\alpha}_1^2}\alpha^2_{G_3} \\ \sigma^2_{\beta_3} =& E\left\{\beta_3\beta_3^*\right\} = \sigma^2_{D_{G_3}} \end{aligned} \tag{11.19}$$

After further expanding Z_D into in-phase and quadrature components, Z_D becomes

$$\begin{aligned} Z_D =& \underbrace{\left[\Lambda_I + \beta_{1_I} + \beta_{2_I} + \eta_I + \xi_I + \beta_{3_I}\right]}_{Z_{D_I}} + j\underbrace{\left[\Lambda_Q + \beta_{1_Q} + \beta_{2_Q} + \eta_Q + \xi_Q + \beta_{3_Q}\right]}_{Z_{D_Q}} \\ =& Z_{D_I} + jZ_{D_Q} \end{aligned} \tag{11.20}$$

where Λ_I and Λ_Q are defined as

$$\begin{aligned} \Lambda_I =& \frac{\alpha_1}{\hat{\alpha}_1}\left(\alpha_{G_I}X_I\cos\theta - \alpha_{G_Q}X_Q\cos\theta - \alpha_{G_Q}X_I\sin\theta - \alpha_{G_I}X_Q\sin\theta\right) \\ \Lambda_Q =& \frac{\alpha_1}{\hat{\alpha}_1}\left(\alpha_{G_Q}X_I\cos\theta + \alpha_{G_I}X_Q\cos\theta + \alpha_{G_I}X_I\sin\theta - \alpha_{G_Q}X_Q\sin\theta\right) \end{aligned} \tag{11.21}$$

In addition, α_{G_I} and α_{G_Q} are given by

$$\begin{aligned} \alpha_{G_I} =& \left(\alpha_{G_{1_I}}\alpha_{G_{2_I}}\alpha_{G_{3_I}} - \alpha_{G_{1_Q}}\alpha_{G_{2_Q}}\alpha_{G_{3_I}} - \alpha_{G_{1_I}}\alpha_{G_{2_Q}}\alpha_{G_{3_Q}} - \alpha_{G_{1_Q}}\alpha_{G_{2_I}}\alpha_{G_{3_Q}}\right) \\ \alpha_{G_Q} =& \left(\alpha_{G_{1_I}}\alpha_{G_{2_Q}}\alpha_{G_{3_I}} + \alpha_{G_{1_Q}}\alpha_{G_{2_I}}\alpha_{G_{3_I}} + \alpha_{G_{1_I}}\alpha_{G_{2_I}}\alpha_{G_{3_Q}} - \alpha_{G_{1_Q}}\alpha_{G_{2_Q}}\alpha_{G_{3_Q}}\right) \end{aligned} \tag{11.22}$$

Table 11.1 Numerical Values of Variables in Conditional BER for MSB

Index i	X_{I_i}	X_{Q_i}	Index i	X_{I_i}	X_{Q_i}
1	d	$3d$	5	$3d$	$3d$
2	d	d	6	$3d$	d
3	d	$-d$	7	$3d$	$-d$
4	d	$-3d$	8	$3d$	$-3d$

To continue the derivation, we assume that 16-QAM modulation scheme is utilized to modulate signal. However, the BER can be derived in the similar fashion if other rectangular QAM modulation schemes are chosen to modulate signal. The BER of 16-QAM conditioned on α_1, α_2, $\hat{\alpha}_1$ and θ for the case where the subcarriers are affected by NBI is expressed as

$$P^I_{BER|\alpha_1,\alpha_2,\hat{\alpha}_1,\theta} = \frac{1}{2}(P^I_{MSB} + P^I_{LSB}) \tag{11.23}$$

where P^I_{MSB} and P^I_{LSB} are the conditional BER of the most significant bits (MSB) and least significant bits (LSB) of 16-QAM symbols for the case where the subcarriers are affected by NBI. Based on the decision boundaries, P^I_{MSB} is found as

$$\begin{aligned} P^I_{MSB} =& P(Z_{D_I} < 0|\alpha_1,\alpha_2,\hat{\alpha}_1,\theta) \\ =& \frac{1}{8}\sum_{i=1}^{8} P(\Lambda_{I_i} + \beta_{1_I} + \beta_{2_I} + \eta_I + \xi_I + \beta_{3_I} < 0) \\ =& \frac{1}{8}\sum_{i=1}^{8} Q\left(\sqrt{\frac{(\Lambda_{I_i})^2}{\sigma^2_{\beta_1} + \sigma^2_{\beta_2} + \sigma^2_\eta + \sigma^2_\xi + \sigma^2_{\beta_3}}}\right) \end{aligned} \tag{11.24}$$

where $Q(\nu) = \int_\nu^\infty \frac{1}{\sqrt{2\pi}} e^{\frac{-t^2}{2}} dt, \nu \geq 0$. $\sigma^2_{\beta_1}$, $\sigma^2_{\beta_2}$, σ^2_η, σ^2_ξ and $\sigma^2_{\beta_3}$ are defined as (11.19) and $\Lambda_{I_i} = \frac{\alpha_1}{\hat{\alpha}_1}(\alpha_{G_I} X_{I_i}\cos\theta - \alpha_{G_Q} X_{Q_i}\cos\theta - \alpha_{G_Q} X_{I_i}\sin\theta - \alpha_{G_I} X_{Q_i}\sin\theta)$. In addition, the numerical values for X_{I_i} and X_{Q_i} are listed in Table 11.1. The conditional BER of LSB for the cases where the subcarriers are affected by NBI can be found in a similar fashion and P^I_{LSB} is given by

$$\begin{aligned} P^I_{LSB} =& \{P(Z_{D_I} < -2d|\alpha_1,\hat{\alpha}_1,\theta,\alpha_2) + P(Z_{D_I} > 2d|\alpha_1,\hat{\alpha}_1,\theta,\alpha_2)\}|_{LSB=0} \\ &+ \{P(-2d < Z_{D_I} < 2d|\alpha_1,\hat{\alpha}_1,\theta,\alpha_2)\}|_{LSB=1} \\ =& \frac{1}{8}\sum_{i=1}^{16} \lambda_i Q\left(\sqrt{\frac{(\kappa_i 2d + \zeta_i \Lambda_{I_i})^2}{\sigma^2_\Xi}}\right) \end{aligned} \tag{11.25}$$

where $|_{LSB=0}$ and $|_{LSB=1}$ represent the boundaries for LSB is zero and one, respectively. In (11.25), λ_i, κ_i, and ζ_i are signs of the values for i^{th} quantity and are listed along with values for X_{I_i} and X_{Q_i} in Table 11.2. In both Tables 11.1 and 11.2, $d^2 = \frac{2E_b}{5}$ where E_b is the energy per bit. Denoting $P^F_{BER|\alpha_1,\hat{\alpha}_1,\theta}$ as the conditional BER for the case where the subcarriers are free from NBI, then $P^F_{BER|\alpha_1,\hat{\alpha}_1,\theta}$ can be obtained by setting $|I[k]|$ or σ^2_η in (11.23) to zero, namely

$$P^F_{BER|\alpha_1,\hat{\alpha}_1,\theta} = P^I_{BER|\alpha_1,\alpha_2,\hat{\alpha}_1,\theta}|_{\sigma^2_\eta=0} \tag{11.26}$$

Table 11.2 Numerical Values and Signs of Variables in Conditional BER for LSB

Index i	λ_i	κ_i	ζ_i	X_{I_i}	X_{Q_i}	Index i	λ_i	κ_i	ζ_i	X_{I_i}	X_{Q_i}
1	+	+	+	d	$3d$	9	+	-	-	$-3d$	$3d$
2	+	+	-	d	$3d$	10	-	+	-	$-3d$	$3d$
3	+	+	+	d	d	11	+	-	-	$-3d$	d
4	+	+	-	d	d	12	-	+	-	$-3d$	d
5	+	+	+	d	$-d$	13	+	-	-	$-3d$	$-d$
6	+	+	-	d	$-d$	14	-	+	-	$-3d$	$-d$
7	+	+	+	d	$-3d$	15	+	-	-	$-3d$	$-3d$
8	+	+	-	d	$-3d$	16	-	+	-	$-3d$	$-3d$

Let N^I be the number of subcarriers that are under the influence of NBI and $N^F = N - N^I$ be the number of subcarriers that are free from NBI, the unconditional BER is subsequently given by

$$\begin{aligned} P_{BER} =& \frac{N^I}{N} \int_0^\infty \int_0^\infty \int_0^\infty \int_{-\pi}^{\pi} P^I_{BER|\alpha_1,\alpha_2,\hat{\alpha}_1,\theta} p(\alpha_2) p(\alpha_1, \hat{\alpha}_1, \theta) d\alpha_1 d\hat{\alpha}_1 d\theta d\alpha_2 \\ &+ \frac{N^F}{N} \int_0^\infty \int_0^\infty \int_{-\pi}^{\pi} P^F_{BER|\alpha_1,\hat{\alpha}_1,\theta} p(\alpha_1, \hat{\alpha}_1, \theta) d\alpha_1 d\hat{\alpha}_1 d\theta \end{aligned} \tag{11.27}$$

where $p(\alpha_2)$ is defined as

$$p(\alpha_2) = \frac{\alpha_2}{\sigma^2_{H_2}} e^{\frac{-\alpha_2^2}{2\sigma^2_{H_2}}} \tag{11.28}$$

In addition, $p(\alpha_1, \hat{\alpha}_1, \theta)$ is given by [28] as

$$p(\alpha_1, \hat{\alpha}_1, \theta) = \frac{\alpha_1 \hat{\alpha}_1}{2\pi |\Delta|^{\frac{1}{2}}} exp \left\{ - \frac{[\sigma^2_{\hat{H}_1} \alpha_1^2 + \sigma^2_{H_1} \hat{\alpha}_1^2 - 2R_c \alpha_1 \hat{\alpha}_1 \cos\theta - 2R_{cs} \alpha_1 \hat{\alpha}_1 \sin\theta]}{2|\Delta|^{\frac{1}{2}}} \right\} \tag{11.29}$$

where

$$\begin{aligned} &\sigma^2_{H_1} = E\{H^2_{1_I}\} = E\{H^2_{1_Q}\}, \qquad R_c = E\{H_{1_I} \hat{H}_{1_I}\} = E\{H_{1_Q} \hat{H}_{1_Q}\} \\ &\sigma^2_{\hat{H}_1} = E\{\hat{H}^2_{1_I}\} = E\{\hat{H}^2_{1_Q}\}, \qquad R_{cs} = E\{H_{1_I} \hat{H}_{1_Q}\} = -E\{H_{1_Q} \hat{H}_{1_I}\} \\ &|\Delta| = \left[\sigma^2_{H_1} \sigma^2_{\hat{H}_1} - R_c^2 - R_{cs}^2\right]^2 \end{aligned} \tag{11.30}$$

From (11.27), one can observe that the unconditional BER is composed of two sources. The first term of (11.27) represents the BER contribution that is due to the effect of NBI on parts of subcarriers, while the second term denotes the contribution from the subcarriers which are free from NBI. In the case where NBI is absent from the received signal, (11.27) is reduced to

$$P_{BER} = \int_0^\infty \int_0^\infty \int_{-\pi}^{\pi} P^F_{BER|\alpha_1,\hat{\alpha}_1,\theta} p(\alpha_1, \hat{\alpha}_1, \theta) d\alpha_1 d\hat{\alpha}_1 d\theta \tag{11.31}$$

Table 11.3 Summary of Simulation Cases

Case Number	HPA	Compander	$\|I[k]\|$	$2\sigma_\epsilon^2$
2	Varying	Yes	0	0
3	Varying	No	0	0
4	Nonlinear	Yes	Varying	0
5	Nonlinear	Yes	0.1	Varying

Table 11.4 Simulation Parameters for Nonlinear HPA Model

Case Number	α_{AM}	β_{AM}	α_{PM}	β_{PM}
2-A	1	0	0	0
2-B	1	0.25	π	0.25
2-C	1	0.25	1.2π	0.01
2-D	1	0.25	1.5π	0.01

11.4 Simulation Model and Parameters

The simulation model, constructed using Matlab Simulink, is an extension of the analytical model described in Section 11.2 in compliance with the IEEE 802.11n standard ([4], Clause 10.4.4.2 rate code 73); except the convolutional encoder, interleaver/deinterleaver and Viterbi decoder are omitted. After pre-appending 16-bit Service Field and padding enough bits to ensure the transmission from each antenna are multiples of whole OFDM symbols, the resulting signal is scrambled with a scrambler that is based on the IEEE 802.11a standard and subsequently demultiplexed alternately across the transmitter spatial streams. In each spatial stream, the data is modulated with the 16-QAM modulation and processed with the 64-point IFFT, of which subcarriers, $\pm$ 21, are designated for pilots. The OFDM symbol is then cyclically extended and pre-appended with the preamble sequences as specified in [4] before transmission. To recover the data, the corresponding receiver reverses the encoding procedure in the transmitter.

Without loss of generality, we set the mean of Rayleigh channels, H_1 and H_2 to zero and set $2\sigma_{H_1}^2 = 2\sigma_{H_2}^2 = 1$. In Case 1, we compare the effectiveness of PAPR reduction of the proposed compander with two other companders, namely the μ-Law and Exponential companders, based on the Complementary Cumulative Distribution Function (CCDF) of PAPR. In this case, we simulate 10^8 statistically independent 16-QAM OFDM symbols. Furthermore, we assume that the total number of subcarriers in IFFT is 64. For the rest of simulation cases, we measure and compare the BER performance of the system which is subject to different sources of impairments. The simulation parameters used for the rest of simulation cases are summarized in Table 11.3. In Case 2, we assume that the companded OFDM system is only subject to the nonlinear distortion caused by the nonlinear HPAs and AWGN. The severity of the nonlinearity in the HPAs is varied based on the parameters listed in Table 11.4. Notice in Case 2-A where α_{AM} is set to one and the rest of the parameters are set to zero, the nonlinear HPAs become perfectly linear HPAs which have an unity gain with no phase distortion. In Case 3, the system is also subject to the nonlinear

Table 11.5 A Comparison of PAPR Reduction

	Original	Exponential	μ-Law	Proposed
10% PAPR	8.2 dB	7.4 dB	6.4 dB	4.2 dB

distortion caused by the nonlinear HPAs. Different from Case 2, the compander and decompander are removed from the system in this case. In addition, the level of nonlinearity in the HPAs will be varied according to the same parameters listed in Table 11.4.

In Case 4, we assume that the system is impaired by both nonlinear HPAs and a NBI. In addition, we assume that there is only one subcarrier which is under the influence of a NBI. In this case, the amplitude of the NBI is varied from 0, 0.1, 0.3 to 0.5. In Cases 2, 3, and 4, we assume that there is no error in estimating the channel impulse response. In Case 5, we vary the power of channel estimation error in the system while subjecting the system to nonlinear distortion and a NBI whose amplitude is set to 0.1. In both Cases 4 and 5, the parameters used in Case 2-C are applied in the HPA model. Furthermore, through empirical analysis, A_O and p in the compander and decompander are found to be 0.5 and 1.5, respectively, for all cases.

11.5 Simulation Results

In Case 1, we compare the effectiveness of PAPR reduction of the proposed compander with μ-Law and Exponential companders by measuring the CCDFs. Furthermore, for the purpose of comparison, we also include the case where the compander is not present in the system. Before defining the CCDF, it is necessary to define PAPR and is given by

$$PAPR = \frac{\underset{0 \le k \le N}{max} |x_C[k]|^2}{E\{|x_C[k]|^2\}} \tag{11.32}$$

Then, the CCDF is defined as

$$\begin{aligned} CCDF =& P(PAPR > PAPR_o) \\ =& 1 - (1 - exp(-PAPR_o))^N \end{aligned} \tag{11.33}$$

where $PAPR_o$ implies the PAPR threshold [84]. The simulation result is shown in Fig. 11.3. As one can see from Fig. 11.3, the proposed compander has the best performance in PAPR reduction. When utilizing the Exponential compander, 10% PAPR is reduced to 7.4 dB while same percentage of PAPR can be reduced even further to around 6.4 dB when the compander is implemented based on the μ-Law technique. However, by using the proposed compander, 10% PAPR is reduced to around 4.2 dB which is 3.2 dB and 2.2 dB improvement when compared with PAPR reduction results from Exponential and μ-Law companders, respectively. Table 11.5 summarizes the results of PAPR reduction for Case 1.

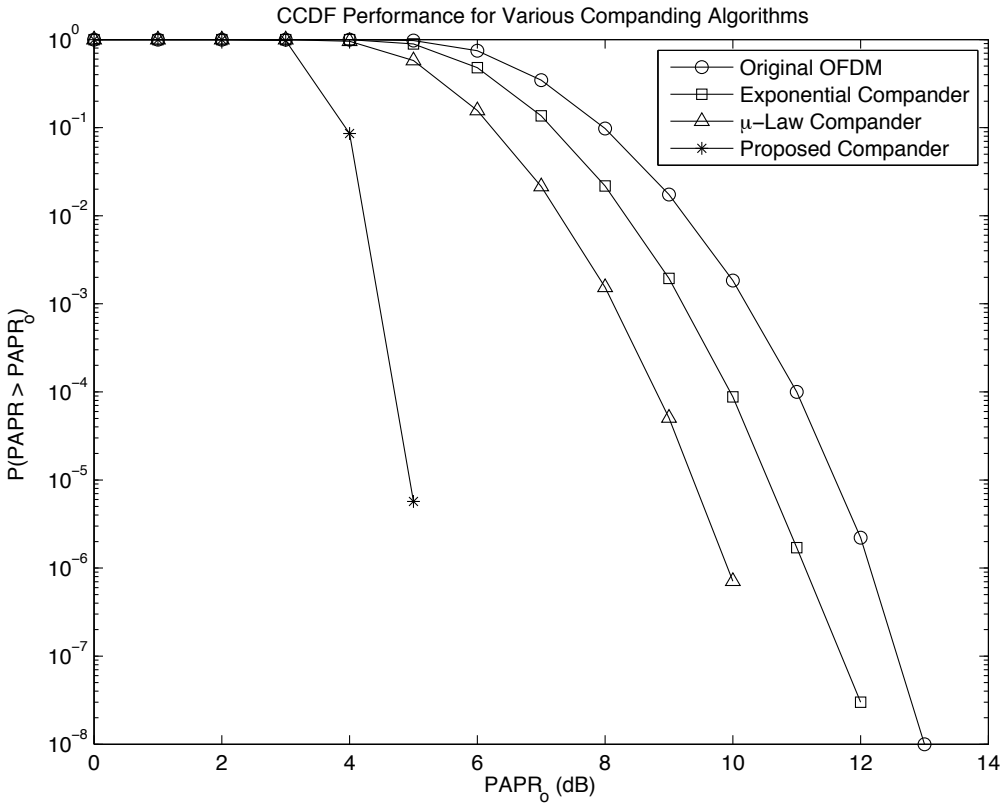

Figure 11.3 The comparison of CCDFs of the signals at the output of μ-Law, Exponential and proposed companders in a 16-QAM OFDM system.

In Case 2, the system is subject to only nonlinear distortion and AWGN while the level of nonlinearity in the HPA is varied. The theoretical results can be obtained from (11.27) by setting σ_η^2 to zero. The simulation results are plotted along with the theoretical results in Fig. 11.4. As one observes from Fig. 11.4, the BER performance gets worse as more nonlinear distortion is introduced to the system by the HPA. This is expected since an increase in nonlinear distortion implies an increase in the power of nonlinear distortion or overall noise power in the system for a given signal to noise ratio (SNR) value. As a result, the arguments of the Q functions become smaller in values and BER performance degrades.

Different from Case 2, the compander and decompander are removed from the system while the system is still subject to nonlinear distortion introduced by the nonlinear HPA in Case 3. For readers who are interested in theoretical results for Case 3, it can be found in [45, 46]. For the purpose of comparison, the simulation results for Case 2 and 3 are shown in Fig. 11.5. One can see from Fig. 11.5, the OFDM system which has a compander and a decompander outperforms the system that is without the compander and decompander for all levels of nonlinearity in the HPA. In

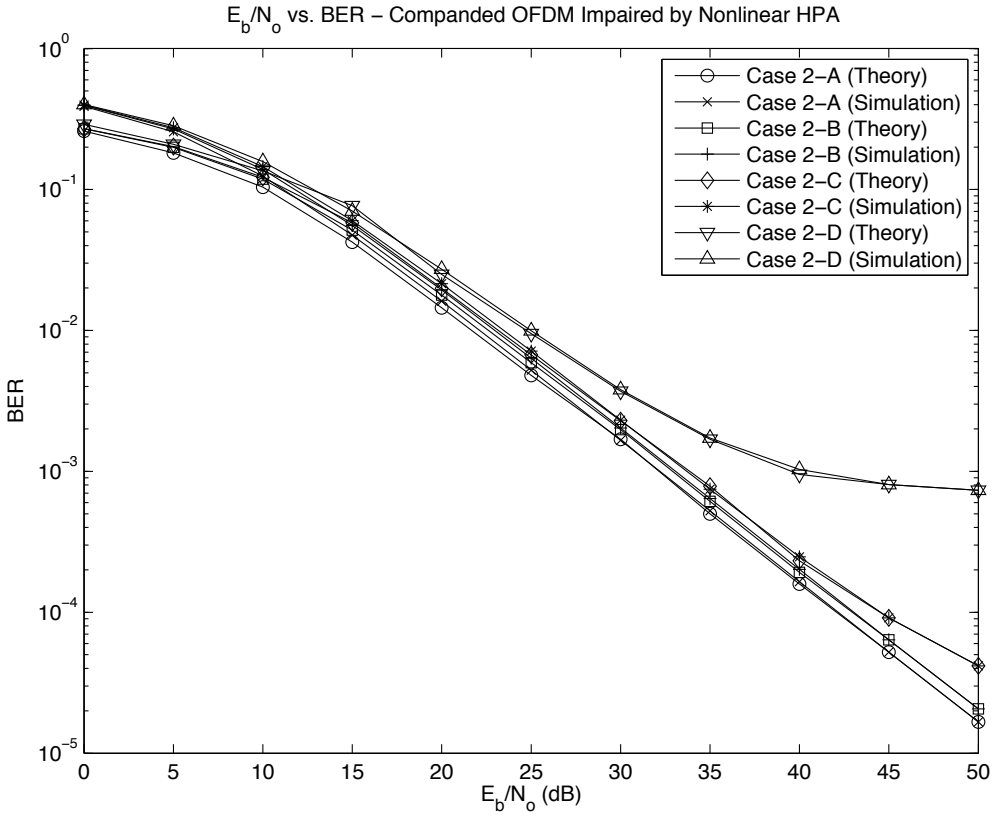

Figure 11.4 BER performance of a companded 16-QAM OFDM system in the Rayleigh fading channel for various levels of nonlinearity in the HPA.

addition, the BER performance improvement is most apparent when the HPA is highly nonlinear. This suggests that the proposed scheme can be implemented in OFDM systems to loosen the design criteria for the HPA and reduce the cost of production.

For Case 4, the system is impaired by both a nonlinear HPA and a NBI while we vary the amplitude of the NBI. This particular case simulates the situation where the system is operating in coexistence with a NBI. The simulation results are plotted along with the theoretical results obtained from (11.27) and shown in Fig. 11.6. As one would expect from the situation where the system is not only impaired by a nonlinear HPA but by a NBI as well, the BER performance degrades as more power of NBI is introduced to the system. Finally, when the channel impulse response is not perfectly known to the receiver, the error in estimating channel response further degrades the BER performance. Fig. 11.7 shows the BER performance of a 16-QAM OFDM system that is subject to a nonlinear HPA and a NBI in a Rayleigh fading channel for various values of $2\sigma_\epsilon^2$.

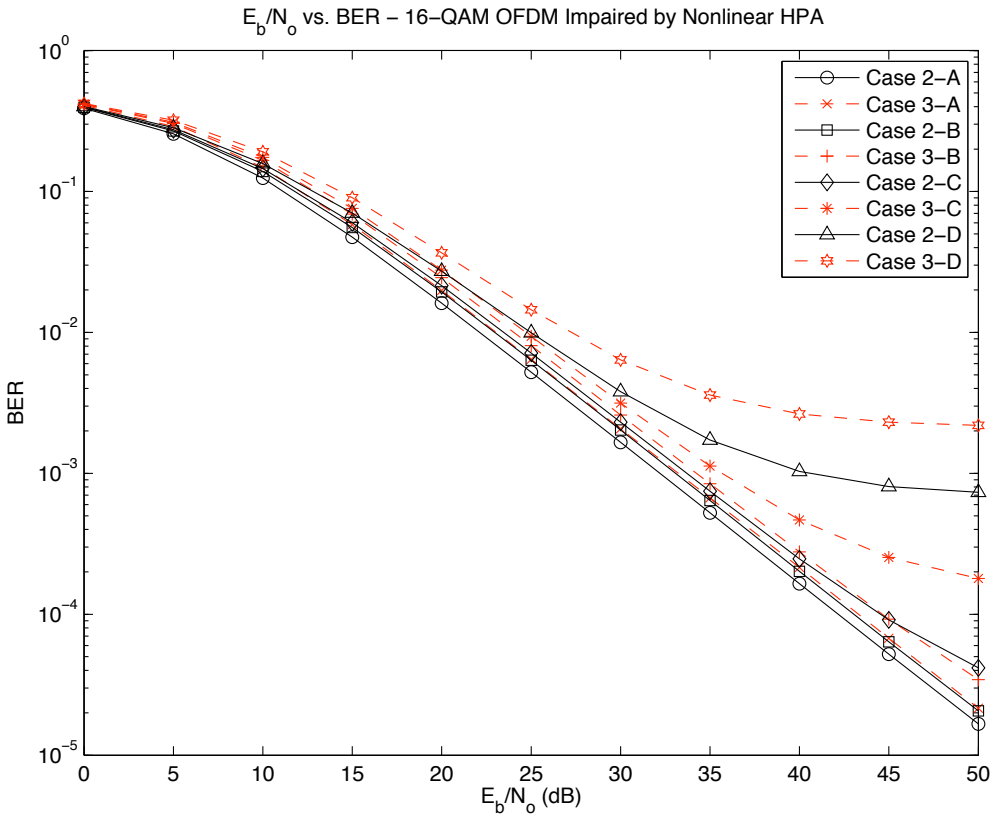

Figure 11.5 BER performance of a 16-QAM OFDM system which is subject to various degrees of nonlinearity in the HPA in the Rayleigh fading channel with and without a compander and a decompander.

11.6 Conclusion

In this chapter, we presented the performance analysis of a 16-QAM OFDM system which was subject to a nonlinear HPA, a NBI and channel estimation error in a Rayleigh fading channel. To simulate practical situations where the system was operating in coexistence with a NBI, we included a NBI in our channel model. Different from the NBI models presented in previous studies, we presented a more realistic NBI model by assuming the NBI experiences a separate channel impulse response. We presented a new compander which was utilized to reduce PAPR in the OFDM signal and a new receiver structure that would minimize the degradation effects due to the decompression in the decompander when the OFDM systems operated in a Rayleigh fading channel. We also extended the analytical system to be in compliance with IEEE 802.11n standard for the purpose of simulation. In addition, we showed the effectiveness of PAPR reduction of our proposed compander with the existing models through simulations. We also showed the effect of nonlinear distortion on the performance of a 16-QAM OFDM system with and without a compander and a

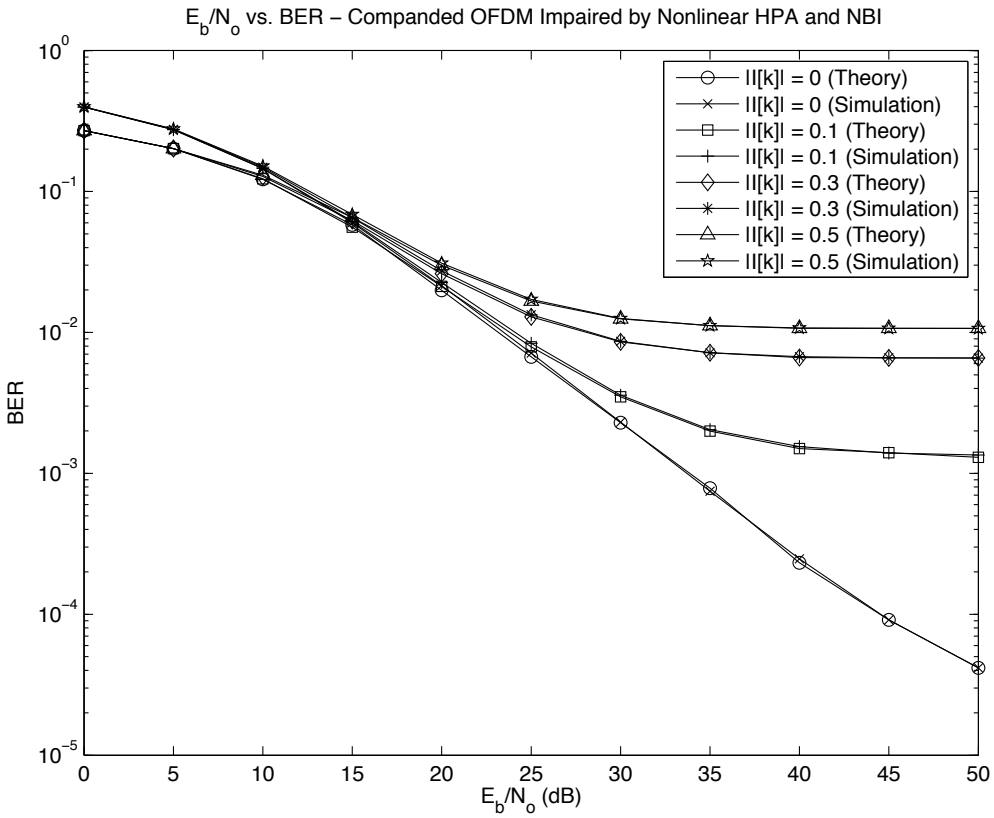

Figure 11.6 BER performance of a companded 16-QAM OFDM system which is impaired by a nonlinear HPA and a NBI in the Rayleigh fading channel.

decompander. The simulation results indicated that the proposed companding technique was highly effective in reducing PAPR and could be used to loosen the design criteria for the HPA and the cost of production. Finally, we presented the theoretical and simulation results for the system which is impaired by a nonlinear HPA and a NBI with and without channel estimation error.

The text in Chapter 11 is based on the material as it appears in:

David W. Chi and Pankaj Das, "Effects of Narrowband Interference and Nonlinear Amplifier in Companded OFDM with Application to 802.11n WLAN", 2009 IEEE International Conference on Communications (Submitted).

The dissertation author was the primary researcher and author, and the co-author listed in the publication directed and supervised the research which forms the basis for this chapter.

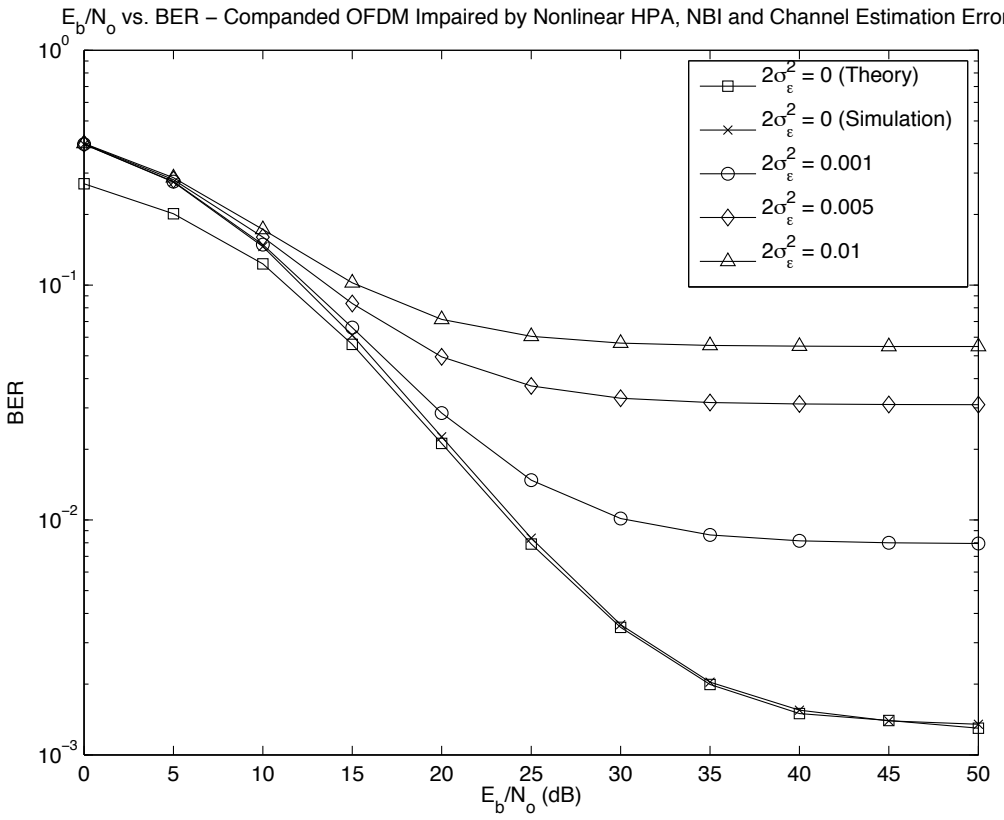

Figure 11.7 BER performance of a companded 16-QAM OFDM system which is impaired by a nonlinear HPA and a NBI in the Rayleigh fading channel for various values of $2\sigma_\epsilon^2$.

12

Conclusion and Contributions

In this thesis, we first presented the basic concept of Orthogonal Frequency Division Multiplexing (OFDM) and then we discussed briefly about its technical advantages such as superior performance in fading channels and disadvantages which include high peak to average power ratio (PAPR) and high sensitivity to frequency offset and phase noise. Next, we discussed the causes of the nonlinear distortion. The occurrence of the nonlinear distortion is due to the high PAPR in OFDM signals. As mentioned already, the high power amplifiers (HPAs) are often forced to operate in the nonlinear region due to the high PAPR in OFDM signals. To mathematically demonstrate the effect of nonlinear distortion on the system performance, we presented the performance analysis of a Binary Phase Shift Keying (BPSK) OFDM system that was subject to a nonlinear HPA in the additive white Gaussian noise (AWGN) channel. We also introduced two different HPA models which were a solid state power amplifier (SSPA) and a traveling wave tube amplifier (TWTA). The TWTA model which is also known as Saleh model was chosen for modeling a nonlinear HPA for the rest of thesis. We also presented a detail description of IEEE 802.11n WLAN which was given in Chapter 3. For the purpose of simulation, all analytical models presented in the thesis were extended to an 802.11n WLAN system based on the IEEE 802.11n specification. By simulating an actual WLAN system, it would provide valuable insights to the performance of a system when it is subject to impairments such as nonlinear HPAs, narrowband interference (NBI), and channel estimation error.

In Chapter 4, performance analysis of a M-ary Quadrature Amplitude Modulation (M-QAM) OFDM system that was subject to nonlinear HPAs, jammer and channel estimation error in a Rayleigh fading channel was presented. Different from other jammer models proposed in literature, we proposed a more realistic jammer model by introducing a separate channel impulse response between the source of jammer and the receiver. The theoretical and simulation results were presented for a M-QAM OFDM system that was subject to various combined sources of impairments with and without channel estimation error. Next, we analyzed a M-QAM OFDM system that was

subject to nonlinear HPAs, a partial band jammer and channel estimation error in a Rayleigh fading channel. In this case, we extended our work to include the situations where the partial band jammer transmitted jamming signal on a frequency that was slightly offset from the center frequency of the desired signal. By including this assumption, the jammer model became even closer to a jammer that systems might encounter in practice. In addition, we briefly discussed the effectiveness of partial band jammer on the system performance for various jamming subcarriers when total jamming power was held constant.

Based on simulation results, we found that a partial band jammer who had all its energy concentrated on a single subcarrier caused the most degradation to the performance. However, we also discussed the reasons of why this type of jammer was not practical in real situations. One of reasons is the partial band jammer did not have perfect knowledge of the center frequency at which the desired signal was being transmitted on. This would lead to the situation where the partial band jammer could only affect the system performance through its inter-carrier interference (ICI) like interference. In addition, the effect of the ICI-like interference on the system performance highly depended on the location of the frequencies of subcarriers in the jamming signal with respect to the desired signal in the frequency spectrum. The further away the partial band jammer was, the less effective the ICI-like interference on the system performance. Another reason was that the system could simply turn off the subcarrier's frequency if the partial band jammer appeared within the frequency spectrum of the transmitted signal. In which case, the performance could improve slightly at the cost of loss in data rate. In Chapter 6, the performance analysis of a M-QAM OFDM system that was subject to nonlinear HPAs and channel estimation error in a Rayleigh fading channel was presented. Following the conventional approach, the unconditional bit error rate (BER) was often obtained by integrating the conditional BER expression over a joint probability density function (PDF) of the magnitudes of the channel, its estimate and the phase difference between them. This inevitably led to the calculation of a triple integral. To facilitate the process of obtaining BER expression, we made use of the channel estimation error model which was proposed by Mishal *et al.* [31]. By utilizing the proposed channel estimation error model, we were able to simplify the BER expression from a triple integral to a single integral.

Next, we introduced the concepts of multiple input multiple output (MIMO) and Space Time Block Code (STBC). In addition, we presented performance analysis of a M-QAM MIMO-OFDM for two and four transmit antennas with one receiver antenna with and without the normalization in the total transmit power. Based on the conventional approach and under the assumption of perfect channel estimation, the BER expression for two transmit antennas was a sum of three double integrals while it was a sum of three quadruple integrals for the case of four transmit antennas. To simply the BER expressions, we represented the Q function in its alternative form. Through mathematical simplification, we were able to reduce the complexity of the BER expressions for both

two and four transmit antennas to a sum of three single integrals.

In Chapter 8, we extended our work to include multiple antennas and STBC. We analyzed the performance of a M-QAM MIMO-OFDM system that was subject to nonlinear HPAs, narrowband interference (NBI) and channel estimation error in Rayleigh fading channels. In this case, the Alamouti code was utilized since there were two transmit antennas. Furthermore, we continued to model the nonlinear HPA based on the Saleh model and utilized the jammer model that we proposed previously in the analysis. The simulations were performed for various sets of impairments and the simulation results were presented along with theoretical results with and without channel estimation error. Next, we extended the jammer model in the analysis which was under study in Chapter 8 to include the possibility of the frequency offset between the jamming and desired signals. Through simulations, we also found that the jammer which had all its energy concentrated in one subcarrier caused the most degradation to the system performance which had also been seen in the case of single antenna. In addition, we briefly discussed the advantages and disadvantages of implementing such jammer in practice.

In previous chapters, we had shown that the effect of nonlinear distortion caused by practical HPAs could be detrimental to the system performance. To address this problem, several algorithms such as clipping, coding, interleaving, partial transmit sequences (PTS), selective mapping (SLM), predistortion, and companding had been proposed in literature. A detail review of these existing techniques along with the definition of PAPR were given in Chapter 10. Next, we presented the performance analysis of a M-QAM OFDM system with a compander that was subject to nonlinear HPAs, NBI and channel estimation error in a Rayleigh fading channel. We also proposed a novel companding technique that was proved to be every effective in reducing PAPR and nonlinear distortion in the HPA. Due to the nature of highly dependency on the magnitude of the received signals, we also proposed a new receiver structure which would minimize the degradation effects due to the decompression process when the OFDM systems operated in fading channels. Through simulations, the proposed algorithm and the novel receiver structure yielded excellent results in reducing PAPR of OFDM signals and improving BER performance. This suggested that the design criteria of HPA could be less restrictive and the cost of production could be reduced when employing our proposed method.

Finally, the contributions of the thesis can be separated into three parts which are summarized as below,

1. Performance Analysis of OFDM Systems

   (a) The OFDM systems are subject to impairments such as nonlinear HPAs, jammer, and channel estimation error.

(b) We propose a more realistic jammer model by introducing

- Additional fading channel between the jammer and the receiver
- Normalized frequency offset that is between center frequencies of the jamming and desired signals

(c) We extend the analytical model based on IEEE 802.11n specification for the purpose of simulations and present simulation and theoretical results for various combined sources of impairments.

(d) We simplify the BER expressions from a triple integral to a single integral by making use a channel estimation error model proposed by Mishal *et al.* [31].

2. Performance Analysis of MIMO-OFDM Systems

(a) We extend our work to include the situations where OFDM systems have multiple transmit antennas, more specifically, an OFDM system that has two transmit antennas and one receive antenna.

(b) The MIMO-OFDM systems are subject to impairments such as nonlinear HPAs, jammer, and channel estimation error.

(c) In performance analysis, we utilize the proposed jammer model which is more practical compared to other models that are studied in literature.

(d) The analytical model is extended to a WLAN system based on the IEEE 802.11n standard and the simulation results are validated by the theoretical analysis for various combinations of impairments.

3. PAPR Reduction and Performance Enhancement of OFDM Systems

(a) We propose a new companding technique which has been shown to be extremely effective in reducing PAPR of OFDM signals and nonlinear distortion.

(b) We also propose a novel receiver structure which minimizes the BER that is due to the decompander when OFDM systems operate in fading channels.

(c) We utilize the proposed NBI model in deriving the performance.

(d) We extend the analytical model to be in compliance of IEEE 802.11n standard and present simulation results along with theoretical results for various sources of impairments.

(e) Through simulations, we show the potential benefits of proposed companding technique and receiver structure, i.e. less amount of nonlinear distortion produced by nonlinear HPAs and superior performance in fading channels.

13

Appendix

13.1 Derivation of b_m

In this section, we present the derivation of the coefficients of Bessel series expansion, b_m. From (2.18), $f(r)$ is given as

$$f(r) = \sum_{m=0}^{L} b_m J_1\left(\frac{(2m-1)\pi}{R_{max}} r\right) \tag{13.1}$$

After multiplying both sides of (13.1) by $rJ_1\left(\frac{(2n-1)\pi}{R_{max}} r\right)$ and integrating with respect to r from 0 to R_{max}, (13.1) becomes

$$\int_0^{R_{max}} rf(r) J_1\left(\frac{(2n-1)\pi}{R_{max}} r\right) dr = \sum_{m=0}^{L} b_m \int_0^{R_{max}} rJ_1\left(\frac{(2m-1)\pi}{R_{max}} r\right) J_1\left(\frac{(2n-1)\pi}{R_{max}} r\right) dr \tag{13.2}$$

However, the orthogonality of Bessel function gives [85]

$$\int_0^{R_{max}} rJ_1\left(\frac{(2m-1)\pi}{R_{max}} r\right) J_1\left(\frac{(2n-1)\pi}{R_{max}} r\right) dr = \frac{1}{2}\delta_{m,n} R_{max}^2 \left[J_2\left(\frac{(2n-1)\pi}{R_{max}} r\right)\right]^2 \tag{13.3}$$

Subsequently, (13.2) becomes

$$\int_0^{R_{max}} rf(r) J_1\left(\frac{(2n-1)\pi}{R_{max}} r\right) dr = \frac{b_n}{2} R_{max}^2 \left[J_2\left(\frac{(2n-1)\pi}{R_{max}} r\right)\right]^2 \tag{13.4}$$

Then b_n is given by

$$b_n = \frac{2\int_0^{R_{max}} rf(r) J_1\left(\frac{(2n-1)\pi}{R_{max}} r\right) dr}{R_{max}^2 \left[J_2\left(\frac{(2n-1)\pi}{R_{max}} r\right)\right]^2} \tag{13.5}$$

Changing the subscript, n, to m, (13.5) becomes

$$b_m = \frac{2\int_0^{R_{max}} rf(r) J_1\left(\frac{(2m-1)\pi}{R_{max}} r\right) dr}{R_{max}^2 \left[J_2\left(\frac{(2m-1)\pi}{R_{max}} r\right)\right]^2} \tag{13.6}$$

Bibliography

[1] R. W. Chang and R. A. Gibby, "A Theoretical Study of Performance of an Orthogonal Multiplexing Data Transmission Scheme," in *IEEE Transactions on Communications*, vol. 16, August 1968, pp. 529–540.

[2] IEEE, *Part 11: Wireless LAN Medium Access Control (MAC) and Physical Layer (PHY) specifictions High-speed Physical Layer in the 5 GHz Band*, June 2003.

[3] ——, *Part 11: Wireless LAN Medium Access Control (MAC) and Physical Layer (PHY) specifictions Amendment 4: Further Higher Data Rate Extensionn in the 2.4 GHz Band*, June 2003.

[4] C. Kose, B. Edwards, and etc., *WWiSE Proposal: High throughput extension to the 802.11 Standard*, January 2005.

[5] P. H. Moose, "A Technique for Orthogonal Frequency Division Multiplexing Frequency Offset Correction," in *IEEE Transactions on Communications*, vol. 42, no. 10, October 1994, pp. 2908–2914.

[6] H. A. Suraweera and J. Armstrong, "M-QAM OFDM and PCC-OFDM Performance in the Presence of Phase Noise," in *Australian Communication Theory Workshop*, February 2004, pp. 98–103.

[7] K. Sathananthan and C. Tellambura, "Performance Analysis of an OFDM System with Carrier Frequency Offset and Phase Noise," in *IEEE Vehicular Technology Conference*, vol. 4, October 2001, pp. 2329–2332.

[8] G. R. Hill, M. Faulkner, and J. Singh, "Reducing the Peak-to-Average Power Ratio in OFDM by Cyclically Shifting Partial Transmit Sequences," in *IEEE Electronic Letters*, vol. 36, no. 6, March 2000, pp. 560–561.

[9] L. J. C. Jr. and N. R. Sollenberger, "Peak-to-Average Power Ratio Reduction of an OFDM Signal Using Partial Transmit Sequenes," in *IEEE Communications Letters*, vol. 4, no. 3, March 2000, pp. 86–88.

[10] R. Prasad, *OFDM for Wireless Communications Systems*. Artech House Publishers, August 2004.

[11] X. Li and L. J. C. Jr., "Effects of Clipping and Filtering on the Performance of OFDM," in *IEEE Communications Letters*, vol. 2, May 1998, p. 131=133.

[12] T. Jiang and G. Zhu, "Complement Block Coding for Reduction in Peak-to-Average Power Ratio of OFDM Signals," in *IEEE Communications Magazine*, vol. 43, 2005, pp. S17–S22.

[13] S. Hee and J. H. Lee, "Modified Selected Mapping Technique for PAPR Reduction of Coded OFDM Signal," in *IEEE Transactions on Broadcasting*, vol. 50, no. 3, September 2004, pp. 335–341.

[14] C. Rapp, "Effects of HPA-Nonlinearity on a 4-DPSK/OFDM-Signal for a Digital Sound in Broadcasting Signal," in *ESA, Second European Conference on Satellite Communications (ECSC-2)*, October 1991, pp. 179–184.

[15] E. Costa and S. Pupolin, "M-QAM-OFDM System Performance in the Presence of a Nonlinear Amplifier and Phase Noise," in *IEEE Transactions on Communications*, vol. 50, no. 3, March 2002, pp. 462–472.

[16] C. Duda, A. T. Koc, and S. Koc, "Solid State Power Amplifier (SSPA) Nonlinearity Effects on Quadri-Phase Shift Keying Modulation," in *European Conference on Wireless Technology*, 2004, pp. 237–240.

[17] A. A. M. Saleh, "Frequency-Independent and Frequency-Dependent Nonlinear Models of TWT Amplifiers," in *IEEE Transactions on Communications*, vol. 29, no. 11, November 1981, pp. 1715–1720.

[18] G. Santella and F. Mazzenga, "A Hybrid Analytical-Simulation Procedure for Performance Evaluation in M-QAM-OFDM Schemes in Presence of Nonlinear Distortions," in *IEEE Transactions on Vehicular Technology*, vol. 47, February 1998, pp. 142–151.

[19] N. Ermolova, "Analysis of Nonlinear Effects in OFDM Communications Systems," in *IEEE VTC*, 2001, pp. 737–740.

[20] P. Banelli and S. Cacopardi, "Theoretical Analysis and Performance of OFDM Signals in Nonlinear AWGN Channels," in *IEEE Transactions on Communications*, vol. 48, no. 3, March 2000, pp. 430–441.

[21] S. M. Alamouti, "A Simple Transmit Diversity Technique for Wireless Communications," in *IEEE Journal on Select Areas in Communications*, vol. 16, no. 8, October 1998, pp. 1451–1458.

[22] T. Pollet, M. V. Bladel, and M. Moeneclaey, "BER Sensitivity of OFDM Systems to Carrier Frequency Offset and Wiener Phase Noise," in *IEEE Transactions on Communications*, vol. 43, no. 2/3/4, February/March/April 1995, pp. 191–193.

[23] L. Tomba, "On the Effect of Wiener Phase Noise in OFDM Systems," in *IEEE Transactions on Communications*, vol. 46, no. 5, May 1998, pp. 580–583.

[24] G. T. Zhou and R. Raich, "Spectral Analysis of Polynomial Nonlinearity with Applications to RF Power Amplifiers," *EURASIP Journal on Applied Signal Processing*, pp. 1831–1840, December 2004.

[25] K. G. Gard, H. M. Gutierrez, and M. B. Steer, "Characterization of Spectral Regrowth in Microwave Amplifiers Based on the Nonnlinear Transformation of a Complex Gaussian Process," in *IEEE Transactions on Microwave Theory and Techniques*, vol. 47, no. 7, July 1999, pp. 1059–1069.

[26] M.-X. Chang and Y. T. Su, "Performance Analysis of Equalized OFDM Systems in Rayleigh Fading," in *IEEE Transactions on Wireless Communications*, vol. 1, no. 4, October 2002, pp. 721–732.

[27] Z. Wu and C. R. Nassar, "Narrowband Interference Rejection in OFDM via Carrier Interferometry Spreading Codes," in *IEEE Transactions on Wireless Communications*, vol. 4, no. 4, July 2005, pp. 1491–1505.

[28] L. Cao and N. C. Beaulieu, "Exact Error-Rate Analysis of Diversity of 16-QAM With Channel Estimation Error," in *IEEE Transactions on Communications*, vol. 52, no. 6, June 2004, pp. 1019–1029.

[29] A. Ambardar, *Analog and Digital Signal Processing*, 2nd ed. Brooks/Cole Publishing Company, 1999.

[30] H. Sugimoto, D. Sasagawa, and Y. Suzuki, "Higher Data Rate Wireless LAN System Based on OFDM," in *IEEE International Symposium on Wireless Personal Multimedia Communications*, vol. 2, October 2002, pp. 734–737.

[31] M. Al-Gharabally and P. Das, "On the Performance of OFDM Systems in Time Varying Channels with Channel Estimation Error," in *IEEE International Conference on Communications*, vol. 11, June 2006, pp. 5180–5185.

[32] J. Kim, J. Park, and D. Hong, "Performance Analysis of Channel Estimation in OFDM Systems," in *IEEE Signal Processing Letters*, vol. 12, January 2005, pp. 60–62.

[33] X. Tang, M.-S. Alouini, and A. J. Goldsmith, "Effect of Channel Estimation Error on M-QAM BER Performance in Rayleigh Fading," in *IEEE Transactions on Communications*, vol. 47, no. 12, December 1999, pp. 1856–1864.

[34] V. Tarokh, H. Jafarkhani, and A. R. Calderbank, "Space-Time Block Codes from Orthogonal Designs," in *IEEE Transactions on Information Theory*, vol. 45, no. 5, July 1999, pp. 1456–1467.

[35] ——, "Space-Time Block Coding for Wireless Communications: Performance Results," in *IEEE Journal on Select Areas in Communications*, vol. 17, no. 3, March 1999, pp. 451–460.

[36] K. F. Lee and D. B. Williams, "A Space-Time Coded Transmitter Diversity Technique for Frequency Selective Fading Channels," in *IEEE Sensor Array and Multichannel Signal Processing Workshop*, March 2000, pp. 149–152.

[37] ——, "A Space-Frequency Transmitter Diversity Technique for OFDM Systems," in *IEEE Global Telecommunications Conference*, vol. 3, 2000, pp. 1473–1477.

[38] Z. Diao, D. Shen, and V. O. Li, "Performance Analysis of Space-Time Codes with Channel Information Errors," in *IEEE Vehicular Technology Conference*, vol. 4, September 2004, pp. 2399–2403.

[39] H. Cheon and D. Hong, "Performance Analysis of Space-Time Block Codes in Time-Varying Rayleigh Fading Channels," in *IEEE International Conference on Acoustics, Speech, and Signal Processing*, vol. 3, May 2002, pp. III–2357–III–2360.

[40] M. Stege, M. Bronzel, and G. Fettweis, "On the Performance of Space-Time-Blockcodes," in *IEEE Vehicular Technology Conference*, vol. 3, May 2001, pp. 2282–2286.

[41] S. Mudulodu and A. Paulraj, "A Transmit Diversity Scheme for Frequency Selective Fading Channels," in *IEEE Global Telecommunications Conference*, vol. 2, 2000, pp. 1089–1093.

[42] T. Z. Mingqian, A. B. Premkumar, and A. S. Madhukumar, "Performance investigation of STBC-OFDM systems with frequency offset and a semi-blind approach for the correction," in *IEEE Vehicular Technology Conference*, vol. 4, May 2004, pp. 1836–1839.

[43] M. K. Simon and M.-S. Alouini, *Digital Communication over Fading Channels*, 2nd ed., J. G. Proakis, Ed. Wiley - IEEE Press, December 2004.

[44] Y. Li, S.-W. Kim, J.-K. Chung, and H.-G. Ryu, "SFBC-based MIMO OFDM and MIMO CI-OFDM Systems in the Nonlinear and NBI Channel," in *IEEE International Conference on Communications, Circuits and Systems*, vol. 2, June 2006, pp. 898–901.

[45] D. W. Chi and P. Das, "Effect of Jammer on the Performance of OFDM In the Presence of Nonlinearity In Rayleigh Fading Channel with Application to 802.11n WLAN," in *IEEE Military Communications Conference*, October 2006, pp. 1–7.

[46] ——, "Effects of Nonlinear Amplifier and Partial Band Jammer in OFDM with Application to 802.11n WLAN," in *IEEE Military Communications Conference*, October 2007, pp. 1–8.

[47] J. G. Proakis, *Digital Communications*, 4th ed. McGraw-Hill, 2001.

[48] D. W. Chi and P. Das, "Effects of Nonlinear Amplifier and Narrowband Interference in MIMO-OFDM with Application to 802.11n WLAN," November 2008, To be published.

[49] H. Schulze and C. Lüders, *Theory and Applications of OFDM and CDMA - Wideband Wireless Communications*. Wiley - IEEE Press, September 2005.

[50] T. Itoh, G. Haddad, and J. Harvey, *RF Technologies for Low Power Wireless Communications*, 1st ed. Wiley - IEEE Press, August 2001.

[51] J. G. Andrews, A. Ghosh, and R. Muhamed, *Fundamentals of WiMAX - Understanding Broadband Wireless Networking*, 1st ed. Prentice Hall, March 2007.

[52] M. R. D. Rodrigues and I. J. Wassell, "SLM and PTS Based on an IMD Reduction Strategy to Improve the Error Probability Performance of Non-Linearly Distorted OFDM Signals," in *IEEE International Conference on Communications*, vol. 2, June 2004, pp. 857–861.

[53] Y. G. Li and G. L. Stüber, *Orthogonal Frequency Division Multiplexing for Wireless Communications*, 1st ed. Springer, February 2007.

[54] H. Ochiai and H. Imai, "On Clipping for Peak Power Reduction of OFDM Signals," in *IEEE Global Telecommunications Conference*, vol. 2, December 2000, pp. 731–735.

[55] D. Kim and G. L. Stüber, "Clipping Noise Mitigation for OFDM by Decision-Aided Reconstruction," in *IEEE Communications Letters*, vol. 3, no. 1, January 1999, pp. 4–6.

[56] H. Chen and A. M. Haimovich, "Iterative Estimation and Cancellation of Clipping Noise for OFDM Signals," in *IEEE Communications Letters*, vol. 7, no. 7, July 2003, pp. 305–307.

[57] C.-T. Lin and W.-R. Wu, "Clipping Ratio Estimation for OFDM Receivers," in *IEEE Vehicular Technology Conference*, vol. 2, June 2005, pp. 797–800.

[58] T. A. Wilkinson and A. E. Jones, "Minimisation of the Peak to Mean Envelope Power Ratio of Multicarrier Transmission Schemes by Block Coding," in *IEEE Vehicular Technology Conference*, vol. 2, July 1995, pp. 825–829.

[59] H. Ochiai and H. Imai, "Block Codes for Frequency Diversity and Peak Power Reduction in Multicarrier Systems," in *IEEE International Symposium on Information Theory*, August 1998, p. 192.

[60] ——, "Performance of Block Codes with Peak Power Reduction for Indoor Multicarrier Systems," in *IEEE Vehicular Technology Conference*, vol. 1, May 1998, pp. 338–342.

[61] ——, "MDPSK-OFDM with Highly Power-Efficient Block Codes for Frequency-Selective Fading Channels," in *IEEE Transactions on Vehicular Technology*, vol. 49, no. 1, January 2000, pp. 74–82.

[62] A. D. S. Jayalath and C. Tellambura, "Reducing the Peak-to-Average Power Ratio of Orthogonal Frequency Division Multiplexing Signal through Bit or Symbol Interleaving," in *IEEE Electronic Letters*, vol. 36, no. 13, June 2000, pp. 1161–1163.

[63] J. Urban and R. Marsalek, "OFDM PAPR Reduction by Combination of Interleaving with Repeated Clipping and Filtering," in *EURASIP Conference on Speech and Image Processing, Multimedia Communications and Services*, June 2007, pp. 249–252.

[64] H.-G. Ryu, S.-K. Kim, and S.-B. Ryu, "Interleaving Method without Side Information for the PAPR Reduction of OFDM System," in *IEEE International Symposium on Communications and Information Technology*, October 2007, pp. 72–76.

[65] S. H. Müller and J. B. Huber, "OFDM with Reduced Peak-to-Average Power Ratio by Optimum Combination of Partial Transmit Sequences," in *IEEE Electronic Letters*, vol. 33, no. 5, February 1997, pp. 368–369.

[66] L. Yang, R. S. Chen, Y. M. Siu, and K. K. Soo, "PAPR Reduction of an OFDM Signal by Use of PTS with Low Computational Complexity," in *IEEE Transactions on Broadcasting*, vol. 52, no. 1, March 2006, pp. 83–86.

[67] S. H. Han and J. H. Lee, "PAPR Reduction of OFDM Signals Using a Reduced Complexity PTS Technique," in *IEEE Signal Processing Letters*, vol. 11, no. 11, November 2004, pp. 887–890.

[68] R. W. Bäuml, R. F. H. Fischer, and J. B. Huber, "Reducing the Peak-to-Average Power Ratio of Multicarrier Modulation by Selected Mapping," in *IEEE Electronic Letters*, vol. 32, October 1996, pp. 2056–2057.

[69] M.-C. Lin, Y.-C. Tsai, and C.-J. Yang, "Selective-Mapping Type Peak Power Reduction Techniques For Turbo Coded OFDM," in *IEEE international Conference on Wireless Networks, Communications and Mobile Computing*, vol. 1, June 2005, pp. 119–122.

[70] S. Sumathi, "Peak to Average Power Ratio Reduction of OFDM Signal," in *IEEE Indicon*, December 2005, pp. 241–244.

[71] L. Sichao and Y. Dongfeng, "Reducing PAPR of OFDM with Convolutional Code and 8-ASK Mapping," in *IEEE International Conference on Wireless Communications, Networking and Mobile Computing*, vol. 1, no. 256, September 2005, p. 253.

[72] A. Brajal and A. Chouly, "Compensation of Nonlinear Distortions for Orthogonal Multicarrier Schemes Using Predistortion," in *IEEE Global Telecommunications Conference*, vol. 3, December 1994, pp. 1909–1914.

[73] B. M. Lee and R. J. P. de Figueiredo, "A Tunable Pre-Distorter for Linearization of Solid State Power Amplifier in Mobile Wireless OFDM," in *Emerging Technologies: Circuits and Systems for 4G Mobile Wireless Communications*, June 2005, pp. 84–87.

[74] H. Yoshimi and T. Ohtsuki, "An OFDM System with Modified Predistorter and MLS," in *IEEE Vehicular Technology Conference*, vol. 3, October 2001, pp. 1677–1681.

[75] K. Wesolowski and J. Pochmara, "Efficient Algorithm for Adjustment of Adaptive Predistorter in OFDM Transmitter," in *IEEE Vehicular Technology Conference*, vol. 5, September 2000, pp. 2491–2496.

[76] X. Wang, T. T. Tjhung, and C. S. Ng, "Reduction of Peak-to-Average Power Ratio of OFDM System using A Companding Technique," in *IEEE Transactions on Broadcasting*, vol. 45, September 1999, pp. 303–307.

[77] T. Jiang, Y. Yang, and Y.-H. Song, "Companding Technique for PAPR Reduction in OFDM Systems Based on An Exponential Function," in *IEEE Global Telecommunications Conference*, vol. 5, December 2005, pp. 2798–2801.

[78] ——, "Exponential Companding Technique for PAPR Reduction in OFDM Systems," in *IEEE Transactions on Broadcasting*, vol. 51, June 2005, pp. 244–248.

[79] N. S. L. P. Kumar, A. Banerjee, and P. Sircar, "Modified Exponential Companding for PAPR Reduction of OFDM Signals," in *IEEE Wireless Communications and Networking Conference*, March 2007, pp. 1344–1349.

[80] V. Pless, *Introduction to the Theory of Error-Correcting Codes*, 3rd ed. Wiley - Interscience, June 1998.

[81] C. Schlegel, *Trellis Coding*. IEEE, December 1997.

[82] R. E. Blahut, *Algebraic Codes for Data Transmission*, 1st ed. Cambridge University Press, July 2002.

[83] M. Saito, A. Okuda, M. Okada, and H. Yamamoto, "Distortionless PAPR Reduction Method for Existing OFDM Systems," in *IEEE International Symposium on Wireless Communication Systems*, September 2005, pp. 404–408.

[84] N. T. Hieu, S.-W. Kim, and H.-G. Ryu, "PAPR Reduction of the Low Complexity Phase Weighting Method in OFDM Communication System," in *IEEE Transactions on Consumer Electronics*, vol. 51, August 2005, pp. 776–782.

[85] F. Bowman, *Introduction to Bessel Functions*. Dover Publications, June 1958.